UNIVERSITAT DE BARCELONA

Deciphering the role of peripheral and central nervous system metabotropic glutamate receptors in neuropathic pain with photoactivable ligands

Joan Font Ingles

Deciphering the role of peripheral and central nervous system metabotropic glutamate receptors in neuropathic pain with photoactivable ligands

Tesi doctoral

Memòria presentada per Joan Font Ingles per optar al títol de doctor per la Universitat de Barcelona

Aquesta Tesi ha estat realitzada en el Programa de Doctorat en Química Orgànica de la Universitat de Barcelona, a les instal·lacions de l'Institut de Química Avançada de Catalunya (IQAC-CSIC)

Doctorant:
Joan Font Ingles

Director:
Dr. Amadeu Llebaria Soldevila
Investigador científic
Departament de Química Biomèdica (IQAC-CSIC)

Codirector:
Dr. Jesús Giraldo Arjonilla
Professor titular
Departament de pediatria, d'obstetrícia, ginecologia i medicina preventiva (UAB)

Tutor:
Dra. Anna Maria Costa Arnau
Professora agregada
Departament de Química Orgànica (UB)

Agraïments

M'agradaria agrair i dedicar aquesta tesi a molta gent que ha estat al meu costat i m'ha ajudat en el desenvolupament d'aquesta dia a dia, directe o indirectament, ja que sense l'aportació de cadascú no hagués pogut dur-la a terme.

Per començar m'agradaria agrair al meus directors de tesi Jesús Giraldo amb qui tot i no estar dia a dia en contacte, m'ha ajudat en tot el que he necessitat i s'ha preocupat sempre de la meva formació com a científic, i també a l'Amadeu Llebaria que m'ha tractat com un fill preocupant-se del meu benestar tant dins com fora del laboratori, per la confiança que sempre m'ha dipositat a pesar dels cops que el faig enfadar per voler anar ràpid, i per tot el que he après amb ell que ha estat moltíssim.

A part dels meus directors de tesi oficials, he tingut la sort de comptar amb gent que han exercit com a tal tot i no tenir-ne la necessitat real de fer-ho i espero no perdre'n mai el contacte, com la jefa suprema del grup la Carme Serra i el Juanlo Catena que han tingut massa paciència amb mi salvant-me sempre de les "liades" que he pogut fer, per els pinxos de truita dels divendres, les cerveses i lo bé que m'ho passo amb ells encara que el Juanlo hem busqui tot el dia.

A la meva gent del laboratori de Barcelona, especialment al meu post-doc Xavi Gomez que m'ha ensenyat tot desinteressadament i que va haver de viure amb mi a Montpellier (tot un repte), també agrair la festa de cada dia al laboratori amb la música de la jefa Roser (renova la llista de spotify si us plau), a la meva nena del lab Maria, que des de el dia 1 poc em necessitava, a la mañica (Silvia Cabello) que en poc ja serà mes catalana que la moreneta, a l'Isabel Masip, a en Xavier Gregori, i a tot el sector italià Alessia, Silvia Paranello, Ivan i Carlo, a la Ester per la seva paciència preguntant-li sempre per papers burocràtics de la tesi, a la Teresa, a la Lourdes que sempre l'estic molestant amb els meus HPLCs i que s'ha guanyat el cel, i a la gent del rubam Pol, Raquel i l'Anna Pou (ja ho tenim això Pou).

Un grand merci a mes amis de Montpellier pour leur hospitalité, surtout à Fanny Malhaire qui a été ma mère en France, Ludovic Fabre qui me manque énormément, à Charleine, à Michael, à Carmen pour me aider à Xavi et moi avec toute la bureaucratie, à Guillaume Lebon, et mon superviseur, ami, et père Français Cyril Goudet. Also thanks to my good friend Thor Møller for having lunch with me and all the catalan crew every day in Montpellier.

Agrair a tota la "catalan crew" de Montpellier, en especial a tres persones molt especials els quals espero no perdre'n mai el contacte, a en Xavi Rovira mestre absolut de tota la farmacologia que he après durant aquests anys de tesi i que segueixo aprenent dia a dia ara que ja el tinc a Barcelona, a en Miquel i les seves bromes (o no) de les arçons i de la jonquera, les cerveses dels divendres al bouchon catalan i perquè és una de les persones més nobles que conec, i a en David que ha estat com un germà gran, moltes gràcies pels partits de futbol i de tennis, per les paelles de l'alba, per invitar-me a dinar a casa teva quan no tenia tupper, per la viciada al clash of clans que teníem, per proporcionar-me tot el que

necessitava tant a la feina com fora, i encara que no tu creguis pels acudits tant dolents que tant m'indignen, saps que tot i que et tingui lluny sempre podràs comptar amb mi.

M'agradaria agrair també al grup de "bullers" que tinc com amics, a tot mini-goteles que en són uns quants, als 93 Pablo Otero, Martínez, Virgili, Yumin i Masdeu, a Escario, Somalo, als pica-flors de Sweetie i Ortega, al Palo i el seu "sin reglas", al tete Raul i el seu "gl i a comer choripan", als asobals Monty i Victor Saez, al excentricus d'Herranz, a sa Loti besis, a Julipan, Chinelo, al Padilla i els seus "trapis" de comunio, a Kike i les futures festes al camió, al meu DJ favorit Duran, al Tito i el seu bon dia família, al Mike i l'Assumpta i les discussions eternes de política, i al jefe de tots Guti, gràcies per totes les tardes a adagio o fogue que sense donar-se'n compte em feien oblidar dels problemes del dia a dia.

Moltes gràcies al meu gran amic i millor persona que m'ha aguantat tants anys Victor Aso, perquè sense tu, una de les millors parts de la vida no hagués estat el mateix, i per la Sonia Romero que espero que hem faci padrí algun dia. També al meu bon amic Ernest Muñoz, pels nostres sopars gourmet, per les nostres festes que acaben sempre amb algun que altre moble destrossat i per ajudar-me sempre desinteressadament quan pitjor estic.

Agrair també a dos persones que hem compartit moltíssim en molt poc temps, gràcies Fernando Otero i David Saez, per donar-me allotjament, els riures sobre el genocidi cel·lular del dia cada cop que tornava a casa, el "vicios" del Otero o el "por fin es viernes" del Saez, els sopars al burguer and co, les festes al panamà, perquè cada cop que marxava de Montpellier després de l'estada era un dia trist per mi, i tot i el poc temps des de la última, us trobo a faltar.

A la meva "casi" germana i pilar imprescindible en la meva vida des de fa ja molt temps Mireia Tarruella, i que les hem passat de tots colors, a la Nuria Segura que mai saps a quin lloc del món està i per molt que passi el temps, en realitat es com sinó hagués passat.

A la Yolanda, perquè poques persones m'aguanten i m'estimen com ella, per l'ajuda sobretot anímica que em proporciona dia a dia, aguantant poder la pitjor part de un doctorand que és quan ha descriure, aquesta tesi també es teva.

Gràcies a la meva família, als meus avis Joan, Carme, Gregori i Angelina, als meus tiets Jordi, Montserrat, Miquel i Conchita, als meus cosins que tant he compartit, Xavier, Jessica, Meritxell, Carlos, la petita Aina, Monica, Nacho, al bitxo del Biel, a l'Albert per ser un germà més que un cosí i perquè ell, més que ningú entén que és fer una tesi doctoral, la Marta (per aguantar-nos a l'Albert i a mi de tant en tant) i al nen dels meus ulls, el Nil.

A la meva segona mare més que germana Mireia, per cuidar-me i preocupar-se sempre més per mi que per ella mateixa des de que tinc ús de raó, i al meu germà més que cunyat David, per ser un sol de persona i una de les millors persones que tinc a la meva vida, així com els seus pares, aquesta tesi també es vostre.

Per últim agrair a les dues persones més importants de la meva vida, el meu pare Isidre i la meva mare Carme, per no donar-me mai per perdut, per haver-me donat tot el que he necessitat i no el que he volgut,

per fer-me créixer com el nen feliç que encara sóc, perquè la loteria m'ha tocat a mi per tenir els pares que he tingut, aquesta tesi us la dedico a vosaltres ja que és més vostre que meva. Gràcies.

Abbreviations

1PE	One photon excitation
2PE	Two photon excitation
7TM	Transmembrane domain
Å	Angstroms
Abs	Absorbance
AcN	Acetonitrile
AcOEt	Ethyl acetate
AcOH	Acetic acid
AMPA	α-amino-3- hydroxyl-5-methl-4-isoxazolepropionic acid
ATP	Adenosine triphosphate
CCI	Chronic Constriction Injury
CNS	Central Nervous System
CRD	Cysteine rich domain
DAD	Diodes array detector
DCM	Dichloromethane
DEACM	Diethylaminocoumarin
DIPEA	Diisopropylethylamine
DMF	Dimethyl formamide
DMEM	Dulbecco's modified Eagle's medium
DMSO	Dimethylsulphoxide
EC_{50}	Half maximal effective concentration
ECD	Extracellular domain
EDAM	Extracellular domain allosteric modulator
Eq	Equivalents
FRET	Förster resonance energy transfer
GPCR	G-protein coupled receptor
h	Hours
HEK293	Human Embrionic Kidney cell line
HPLC	High performance liquid chromatography
HRMS	High resolution mass spectrometry
HTRF	Homogeneous Time resolved Fluorescence

IC_{50}	Half maximal inhibitory concentration
iGluR	Ionotropic glutamate receptors
IP	Inositol phosphate
KA	Kainate
LED	Light Emitting Diodes
MeOH	Methanol
mGlu	metabotropic glutamate
mGluR	metabotropic glutamate receptor
min	Minutes
mM	Millimolar
Mp	Melting point
MS	Mass spectrometry
µM	Micromolar
nm	Nanometres
NAM	Negative Allosteric Modulator
NEt_3	Triethylamine
NMDA	*N*-methyl-D-Aspartate
NMR	Nuclear magnetic resonance
PAM	Positive Allosteric Modulator
PBS	Phosphate buffered saline
PDA	Photodiodes detector
PNS	Peripheral Nervous System
rt	Room temperature
s	Seconds
SAM	Silent Allosteric Modulator
SEM	Standard error of the mean
t	Time
THF	Tetrahydrofurane
TMD	Transmembrane domain
TOF	Time of flight detector
TR-FRET	Time resolved Förster resonance energy transfer
UPLC	Ultrahigh Performance Liquid Chromatography
UV	Ultra violet
VFT	Venus Fly Trap

Vis Visible

Table of contents

Introduction

General Introduction

G-Protein Coupled Receptors (GPCRs)

G-protein coupled receptors (GPCRs) are the largest family of membrane-bound receptors in mammalian genome. The cell surface of these superfamily receptors encodes more than 800 genes in human (4% of the human genome)[1]. GPCRs are involved in many physiological processes, from vision, smell, and taste to neurological, cardiovascular, endocrine and reproductive functions. Thus, it is not an overstatement to say that this family of receptors participates in all of the major functions of living organisms.

This family of receptors is also involved in many human diseases, including heart failure, hypertension, diabetes, prostate cancer and bronchial asthma, to mention a few[2]. It is estimated that 30%–40% of drugs[3] prescribed to treat these diseases target GPCRs[4] and, due to the large number of orphan receptors and tools for pharmacological screening, this number will probably increase[5] in the near future. Moreover, these receptors are still good targets for development of new drugs (25% of new molecular entities in FDA during 2005-2016)[6].

The endogenous ligands for the GPCRs have tremendous variation both at the structural and functional levels; ligands such as neurotransmitters, peptide and protein hormones are able to mediate their message through these proteins.

Generally, GPCRs are seven-transmembrane alpha helices (TMD domain) pass proteins that are activated by binding a stimulus (or ligand) in the extracellular space and then transduce that information to the inside of the cell through conformational changes *Figure 1.* The conformation changes activate heterotrimeric guanine nucleotide-binding proteins (G-proteins) in the cytosol face, which execute downstream signalling pathways through the recruitment and activation of cellular enzymes. The highly specific ligand-GPCR interaction prompts an efficient cellular response, which is vital for the health of the cell and organism[7].

Additionally, some GPCRs can incorporate also an allosteric site, where, the orthosteric ligands don't bind, but other substances, like ions, sterols, peptides, proteins or small molecules can bind, causing a change in the normal conformational response of the receptor. Furthermore, recent advances on crystallography made possible the solution of many crystal structures of GPCRs (172 according to Protein Data Bank until 2015)[8], which helps the scientific community to understand the structural features of these proteins and their binding with the corresponding

ligands. These advances are also of great importance for medicinal chemistry, facilitating the design and synthesis of more selective and potent drug-like compounds.

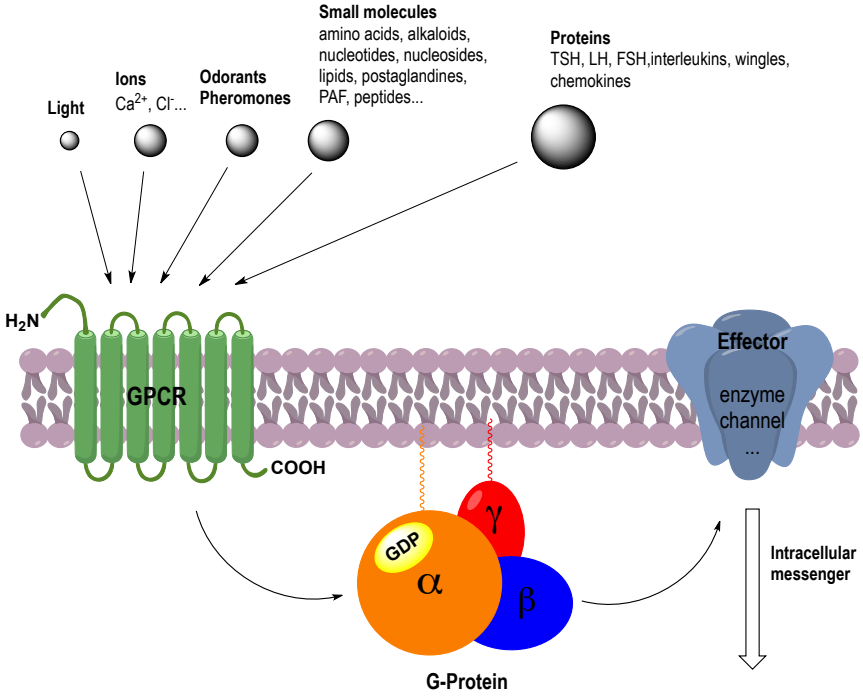

Figure 1: Topology of the signalling cascade of the GPCR and G-protein activation mechanism (Adapted from Bockaert & Pin[9])

Guanine nucleotide-binding proteins (G-protein)

As with the GPCRs, G-proteins represent an ancient and large protein family that has been highly conserved over evolution. G-proteins act as molecular switches inside the cell, transmitting signals from outside to the interior of the cells. These proteins which catalyse the hydrolysis of guanosine triphosphate (GTP) to guanosine diphosphate (GDP) by interacting with GPCRs are constituted by a heterotrimeric complex with three subunits: Gα (45KDa), which is the largest one and where the GTP binds, Gβ (35KDa) and Gγ (8KDa). The interaction with the active conformation of the GPCR induces a dissociation between Gα and Gβ subunits, releasing the Gα subunit which catalyses the exchange GDP->GTP. Then the signalling cascade begins with the interaction of Gα or Gβγ with the corresponding effectors *Table 1*. Once the reaction is finished, Gα is back-associated with Gβγ subunit.

Family	Subtype	Action
$G_s\alpha$	$G_s\alpha$	Activate adenylyl cyclases, Maxi K channel, Src tyrosine kinases and GTPases
	$G_{olf}\alpha$	Activate adenylyl cyclases from olfactory sensorial neurons
$G_{i/o}\alpha$	$G_i\alpha$, $G_o\alpha$, $G_z\alpha$	Inhibit adenylyl cyclases and Ca2+ channels; activates ERK/MAP kinases, K+ channels, GTPase of tubulin, Src tyrosine kinases and GRIN1-mediated activation of Cdc42
	$G_t\alpha$	Activate cGMP PDE (phospodiesterase) in the photoreceptors
	$G_{gust}\alpha$	Activate cGMP PDE in the gustative sensorial neurons
$G_q\alpha$	$G_q\alpha$, $G_{11}\alpha$	Activate PLC-β (Phospholipase C-β) isoforms, p63-RhoGEF (guanine nucleotide exchange factor), bruton's tyrosine kinase and K+ channels
	$G_{14}\alpha$, $G_{16}\alpha$	
$G_{12/13}\alpha$	$G_{12}\alpha$, $G_{13}\alpha$	Activate Phospholipase B and Cε, NHE-1, iNOS, E-cadherin-mediated cell adhesion, p115RhoGEF, PDZ-RhoGEF, LARG (Leukaemia-associated RhoGEF), Radixin, PP5 (Protein phosphatase 5), AKAP110-mediated activation of PKA, HSP90

Table 1: Summary of the human heterotrimeric G-Protein families and subtypes, with the main functions of each family (adapted from Miligan & Kostenis[10])

Classification of human GPCRs

Members of the GPCR superfamily are diverse in their primary structure, and this has been used for the phylogenetic classification of the family members. Attwood and Findlay made the first attempt to classify this family when they developed sequence-based fingerprints of the seven characteristic GPCR hydrophobic domains[11]. In 1994, Kolakowski presented an important overview of the GPCR superfamily: the well-known A-F classification system[12]. Kolakowski included all the receptors proteins that were proven to bind G-proteins, while the remaining seven transmembrane (7TM)-spanning proteins were assigned to the O (Other) family. This system is also used by the International Union of Pharmacology, Committee on Receptor Nomenclature and Classification (NC-IUPHAR).

Bockaert and Pin introduced a similar but extended nomenclature system for classifying GPCRs in 1999, in which the GPCRs were divided into family 1-5 on the basis of structural and ligand-binding criteria[11-12]. Simultaneously and independently from the first draft of the human genome in 2001, Fredriksson and collegues divided 802 (known and predicted) human GPCRs into families

on the basis of phylogenetic criteria, and they showed that most of the human GPCR can be found in five main families: Glutamate, Rhodopsin, Adhesion, Frizzled/Taste2 and Secretin[11-12]. Nevertheless, IUPHAR classifies GPCRs in class A (rhodopsin family), class B (secretin family), class C (glutamate family), class F (frizzled family), adhesion family and other non-classified 7TM proteins[11-12]. There also are two more families, D and E, which does not exist in human genome. Furthermore, there are some subfamilies of class A-F that neither exists in human; such as family IV in class A or archaebacterial opsins in class F.

Class A family of GPCRs

The *Rhodopsin* receptor family is the largest family of GPCRs and contains around 670 full-length human receptor proteins. The family can be divided into four groups: α, β, γ, and δ in which the largest cluster of members, the olfactory receptors, is found in the δ-group. The rhodopsin family of GPCRs is highly heterogeneous when both primary structure and ligand preference are considered. They can be activated from small molecules to proteins, as well as they can bind many different G-proteins, depending on the receptor subtype *Table 2.*

Group	Subgroup	Examples
α (Small molecules)	Prostaglandin	Prostaglandin and orphan receptors
	Amine	Serotonin (HTR/HT), dopamine (DRD/D), muscarinic (CHRM/M), histamine (HRH/H), adrenergic (ADR/a/b), trace amine (TAR/TA) and orphan receptors.
	Opsin	Rod visual pigments (RHO), cone visual pigments (OPN), peropisn (RRH), encephalopsin (OPN), melanopsin (OPN) and retinal GPCR (RGR)
	Melatonin	Melatonin (MTMR/MT) and orphan receptors
	MECA	Melanocortin (MCR/MC), endothenial differentiation GPCRs or Lysophospholipid (EDGR/LPA/S1P), cannabinoid (CNR/CB), adenosine (ADORA/A) and orphan receptors
β (Peptides)	-	Hypocretin (HCRTR/OX), neuropeptide FF(NPFFR/NPFF), neuropeptide Y (NPYR/Y), tachykinin (TACR/NK), cholecystokinin (CCKAR/CCK), endothelin-related (EDNR/ET), bombesin-like (GRPR/BB1 ; NMBR/BB2 ; BRS3/BB3), neurotensin (NTSR/NTS), growth hormone (TRHR), vasopressin (AVPR/V), gonadotropin-releasing hormone (GNRHR), oxytocin (OXTR) and orphan receptors
γ (Peptides-small proteins)	SOG	Galanin (GALR/GAL), kisspeptin (GPR54), somatostatin (SSTR/SST), neuropeptide B/W (NPBWR), opioid (OPR/∂, k, μ, NOP) receptors

	MCH	Melanin concentrating hormone receptor (MHCR/MHC-R)
	Chemokine	Classic chemokine (CCR, CXR / CC, CXC), angiotensin (AGTR), Bradykinin (BDKRB/B), chemerin (CMKLR) and orphan receptors
δ (Peptide, proteins, small molecules)	MAS	MAS1 oncogene (MAS) and MAS-related (MRG, MRGX) receptors
	Glycoprotein	Glycoprotein hormone receptors (FSHR, TSHR, LHCGR) and leucine-rich repeat containing GPCRs (LGR)
	Purinergic	Formyl peptide (FPR), nucleotide (P2RY/P2Y), Lysophosphatidic acid (LPAR/LPA), hydroxycarboxylic acid (HCAT/HCA), succinate (SUCNR), Oxoglutarate (OXGR), free fatty acids (FFAR/FFA) and orphan receptors

Table 2. Summary of the human class A or rhodopsin family GPCRs, with phylogenetic groups and subgroups classification. Find human gene symbol and IUPHAR receptor name in parentesis[12]

Class-A-GPCRs consist of a transmembrane domain (TMD), with seven helices forming a bundle with an eighth helix that runs in parallel to the membrane near the C-terminus. A few class-A-GPCRs have large extracellular domains (ECD) at the N-terminus, that bind ligands but, the orthosteric binding of the majority of class A GPCRs is located in the extracellular half of the bundle. These receptors can accommodate small molecules, peptides or proteins as ligands, depending on the group or subgroup of receptors to which they belong to (*Table 3*). Some small-molecule-binding class A receptors have a vestibule on the extracellular entrance of the binding site, just upper the binding site. The vestibule can act as an allosteric binding site or can accommodate parts of a long orthosteric ligand (*Figure* 2A) due to the large variety of Class-A-GPCRs[13].

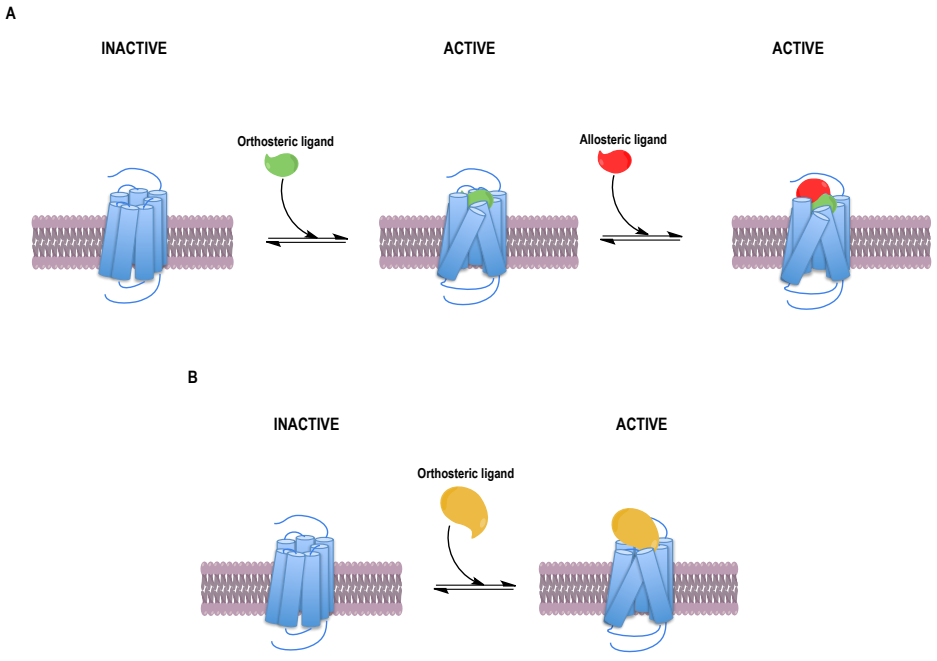

Figure 2. Topology of two class A GPCRs and general binding model: A) Model of binding to a class A GPCR of a small molecule and a possible allosteric modulator in a "vestibule" allosteric pocket. B) Model of binding of a peptide or a small protein to a class A GPCR (Adapted from Gómez-Santacana[13])

Class A GPCRs constitute a vast protein family that can bind several G-Proteins, depending on the receptors subtypes and encompasses a wide range of functions.

Nowadays, many receptor crystal structures have been elucidated. The first crystal structure isolated of class A GPCR was bovine rhodopsin[14]. Seven years after the β_2-adrenergic (β_2-AR) receptor crystal structure was solved in its inactive conformation with the co-crystallization of an antagonist[15]. From that day on, many other Class-A-GPCRs crystal structures have been solved[16] [17] (*Table 3*).

Group	Receptor (species)	Conformation (years of publication)
α	β_1A (turkey)	16 Crystal structures (2008-2014)
	β_2A (human)	20 Crystal structures (2007-2016)
	A_{2A} (human)	21 Crystal structures (2008-2016)
	D_3 (human)	1 Crystal structures (2010)
	H_1 (human)	1 Crystal structures (2011)
	M_1 (human)	2 Crystal structures (2016)
	M_2 (human)	3 Crystal structures (2012-2013)
	M_3 (human)	1 Crystal structures (2012)
	RHO (bovine)	26 Crystal structures (2000-2016)
	RHO (squid)	6 Crystal structures (2008-2016)
	$S1P_1$ (human)	2 Crystal structures (2012)
	$5\text{-}HT_{1B}$ (human)	2 Crystal structures (2013)
	$5\text{-}HT_{2B}$ (human)	2 Crystal structures (2013)
	ET_{B1} (human)	3 Crystal structures (2016)
	CB_1 (human)	1 Crystal structures (2016)
β	NTS_1	4 Crystal structures (2012-2014)
γ	CXC_4 (human)	5 Crystal structures (2010)
	CC_5 (human)	1 Crystal structures (2013)
	δ (mouse)	1 Crystal structures (2012)
	δ (human)	1 Crystal structures (2013)
	κ (human)	1 Crystal structures (2012)
	μ (mouse)	1 Crystal structures (2012)
	NOP (human)	1 Crystal structures (2012)
δ	PAR1 (human)	1 Crystal structures (2012)
	$P2Y_{12}$	3 Crystal structures (2014)
	FFA_1	1 Crystal structures (2014)

Table 3: Class A GPCRs with solved crystal structures before 2016[17]

Class B family of GPCRs

Class B GPCRs or secretin family is a small family of GPCRs whose members have an extracellular hormone-binding domain that can be activated by peptide of intermediate size (30-40 residues). This family comprises 15 members (*Table 4*) which share between 21 and 67% sequence identity and most of the variation is present in the *N*-terminal regions. However, all of the secretin family receptors contain conserved cysteine residues in the first and second extracellular loop of the TM regions, and almost all of them conserve cysteine residues that form a network of three cysteine bridges in the *N*-terminus. They mainly activate G_s, with lower predominance of G_q and G_i signalling pathways and are involved in biological and pathophysiological functions[18].

These receptors are characterized by the incorporation of an extracellular domain (ECD) of a moderate size (100-160 amino acid residues) in the *N*-terminus and a tail in the *C*-terminus. Peptides bind the receptor in a two domain model: the *C*-terminal portion of the peptide binds the ECD and the *N*-terminal portion, the TMD, with a consecutive activation mechanism of the receptor and the binding of the corresponding G-protein (*Figure 3*).

Subgroup	Examples
CPHRs/CALCRLs	Calcitonin (CALCR/CT) and corticotropin-releasing hormone (CPHR/CRH)
PTHRs	Parathyroid hormone receptors (PTHR)
GLPRs/GCGR/GIPR	Gastric inhibitory polypeptide (GIPR/GIP-R), glucagon (GCGR/GL-R) and glucagon-like peptide (GLPR/GLP-R) receptors
Secretin	Secretin (SCTR/SE), growth-hormone-releasing hormone receptor (GHRHR) vasoactive intestinal polypeptide (VIPR/VPAC), Pituitary adenylate cyclase activating polypeptide type I (ADCTAP1/PAC) receptors

Table 4: Summary of human class B or secretin family GPCRs, with a phylogenetic subgroups classification[12].

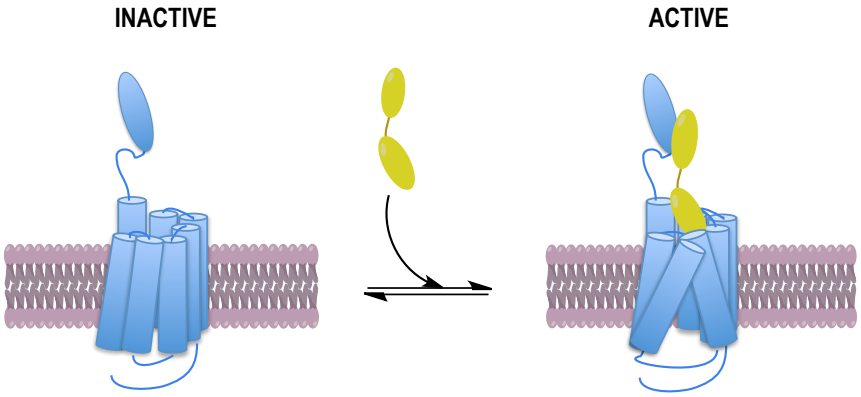

Figure 3: Topology of a class B GPCRs and general binding of a peptide interaction (adapted from Hoare[18])

Because class B GPCRs regulate a number of relevant biological processes, they constitute a potential targets for drug discovery. Nowadays, there are several peptide agonists of Class B GPCRs in the market as calcitonin, pramlintide, eduglutide, Lixisenatide or Tesamorelin, which are used to treat osteoporosis, diabetes, hypercalcaemia, Paget's disease or HIV-associated lipodystrophy.

The crystal structures of corticotoprin-releasing factor type 1 (CRF_1) and glucagon receptor (GL) were solved in 2013, both without ECD and co-crystallised with a non-peptidic antagonist[19]. These structures will be a very useful tool in the future for the development of new drug-like compounds.

Adhesion Class family of GPCRs

The adhesion class, are a new and peculiar family of GPCRs, which constitute the second largest family (33 members), is phylogenetically related to Class B GPCRs.

Group	Former name	Examples
Latrophilin (L)	I	Latrophilin receptors (LPHN/ADGRL) and 'epidermal growth factor (EGF) latrophilin and seven transmembrane domain-containing protein 1' (ELTD1/ADGRL4)
EGF-TM7 (E)	II	EGF-like module-containing much-like hormone receptors-like (EMR/ADGRE) and cluster of differentitation 97 receptor (CD97/ADGRES)
A	III	GPR123/ADGRA1, GPR1247ADGRA1 and GPR124/ADGRA1
CELSR (C)	IV	Cadherin EGF LAG seven-pass G-type receptors (CELSR/ADGRC)
D	V	GPR133/ADGRD1 AND GPR144/ADGRD2
F	VI	GPR110/ADGRF1, GPR111/ADGRF2, GPR113/ADGRF3,

		GPR115/ADGRF4 and GPR116(ADGRF5
BAI (B)	VII	Brain-specific angiogenesis inhibitors (BAI, ADGRB)
G	VIII	GPR56/ADGRG1, GPR64/ADGGRG2, GPR97/ADGRG3, GPR112/ADGRG4, GPR114/ADGRG5, GPR126/ADGRG6 and GPR128/ADGRG7

Table 5: Summary of the human Adhesion class family of GPCRs, with a phylogenetic subgroups classification[12]

These receptors bear the typical GPCR-like transmembrane-spanning regions fused together with one or several functional domains with adhesion-like motifs in the *N* terminus, such as EGF-like repeats, mucin-like regions, and conserved cysteine-rich motifs.

The *N*-terminus are variable in length, from about 200 to 2800 amino acids long, and are often rich in glycosylation sites and proline residues, forming what has been described as mucin-like stalks.

Two defining features of adhesion GPCRs are the highly conserved GPS and GAIN domain and its autoproteolysis. They are the units responsible for the cleavage of the receptor in the GPS, leading to two non-covalently bound subunits: an *N*-terminal-fragment (NTF) and a *C*-terminal fragment (CTF) but they both still keep an association after the cleavage. Moreover, adhesion GPCRs, after the cleavage, display promiscuity in NTF and CTF associations, leading to associations with other family members.

They can bind different Gα-protein subunits, depending on the subtypes, but they are also capable to activating non-G-protein signalling cascades[20]. However the difference in adhesion receptors between their active or inactive conformations is not well known due to the lack of known ligands.

There are two main hypotheses: 1) A segment of the ECD functions as an inverse agonist of the constitutive signalling of the TMD, which is removed upon agonist binding; 2) A segment of the ECD functions as an agonist and binds the TMD, like other ligands do with the rest of the GPCRs[20].

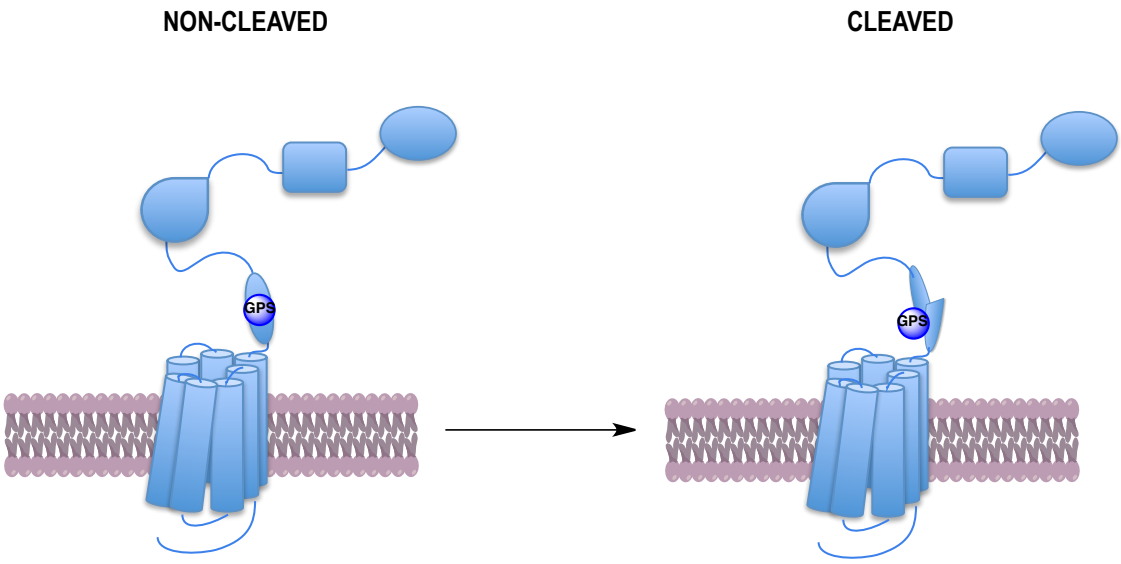

Figure 4: Topology of a Adhesion class GPCR model with GAIN domain and three additional motifs in the ECD and general cleavage model in the GAIN domain (adapted from publication[20])

Class C family of GPCRs

The glutamate family or Class C GPCRs consists of 22 human proteins[12] that can be activated by small molecules, such as amino acids or ions. They can bind several G-protein subtypes and are mainly expressed in the central nervous system ($GABA_B$ and mGlu), in the tongue (TAS1) or in multiple tissues (CaS).

Subgroup	Examples
GABA-B	Gamma amino butyric acid B receptors (GABBR/$GABA_B$)
TAS1/CASR	Taste1 (TAS1R), calcium sensing receptors (CASR/CaS)
Glutamate	Metabotropic glutamamte receptors (GRM/mGlu)
RAIG	Retinoic acid-inducible receptor (RAIG)

Table 6. Summary of the human class C or glutamate family GPCRs, with phylogenetic subgroups classification[12]

Class C GPCRs are dimeric (as homodimers or heterodimers) allosteric multidomain proteins composed of a large extracellular ligand-binding domain called “venus fly trap” (VFT), where orthosteric agonists bind, and heptahelical transmembrane domain (7TM), common to all GPCRs. In mGlu and other class C mGlu-like receptors, the ligand-binding domain is separated from the 7TM by the presence of a cysteine rich domain (CRD). In $GABA_B$, the CRD is absent in both subunits and the ligand-binding domain is directly linked to the 7TM.

The structural dynamics of the VFT is critical for class C receptor activation; early studies revealed that the VFT domain oscillates between an open and closed conformation in the absence of bound an agonist ligand and that ligand stabilizes the closed state, whereas antagonists stabilise the open one[21] [22] (*Figure 4*).

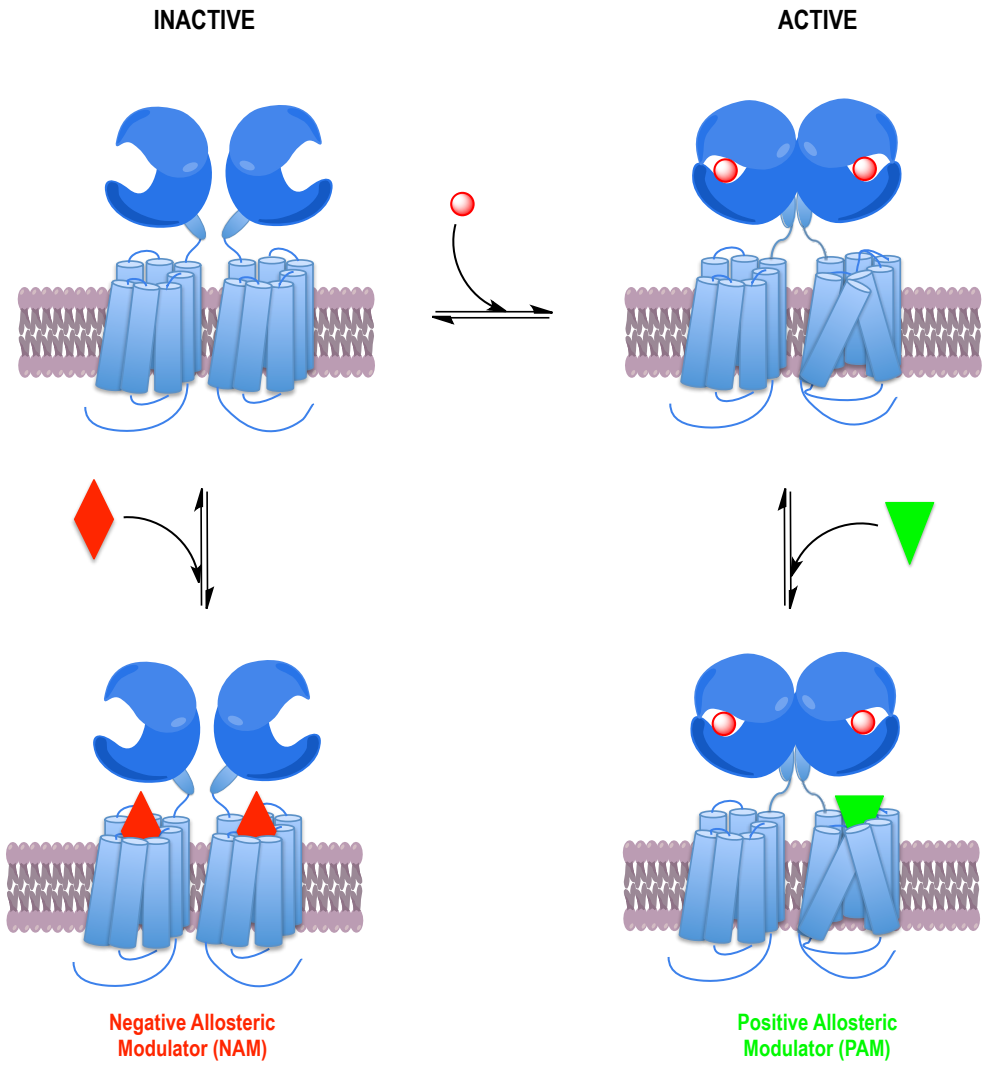

Figure 5: Topology of a class C GPCRs and general binding model of endogenous agonist and allosteric modulator (adapted from Rondard[23])

Class C GPCRs control a great variety of functions, mainly in the CNS for mGlu and $GABA_B$, while CaS controls calcium homeostasis by regulating the release of parathyroid hormone (PTH) and T1Rs sense the sweet and umami tastes in the tongue. Due to the importance of class C-GPCRs functions, its druggability is particularly appealing for drug discovery programs, both for orthosteric ligands and allosteric modulators. In 2014 two crystal structures of TMD of class C

GPCRs ($mGlu_1$ and $mGlu_5$) were solved in their inactive conformations bound with a negative allosteric modulators (NAM)[24]. Additionally, in 2015 two crystal structures of TMD $mGlu_5$ receptor were also solved with one NAM bound[25]. These crystal structures revealed that the allosteric binding site was positioned deeper than orthosteric site for class A GPCRs, but not as deep as the allosteric site of class B GPCRs. All these solved crystal structures constitute a new powerful tool for drug discovery.

Class F of GPCRs

Class F of GPCRs or the frizzled family, comprise 11 receptors, 10 frizzled (FZD) and 1 smoothened (SMO). The FZD are activated by lipoglycoproteins of the wingless/int1 (WNT) family, whereas SMO is indirectly activated by the Hedgehog (HH) family of proteins acting on the transmembrane protein patched (PTCHA).

According to the phylogenetic GRAFS classification, TAS2 receptors cluster together with the frizzled receptors, despite not having obvious similarities. Nevertheless, IUPHAR classify its 30 subtypes as Class A GPCRs[12].

FZDs family has an important function in cellular communication for proper embryonic development, stem cell differentiation, organogenesis and patterning[26].

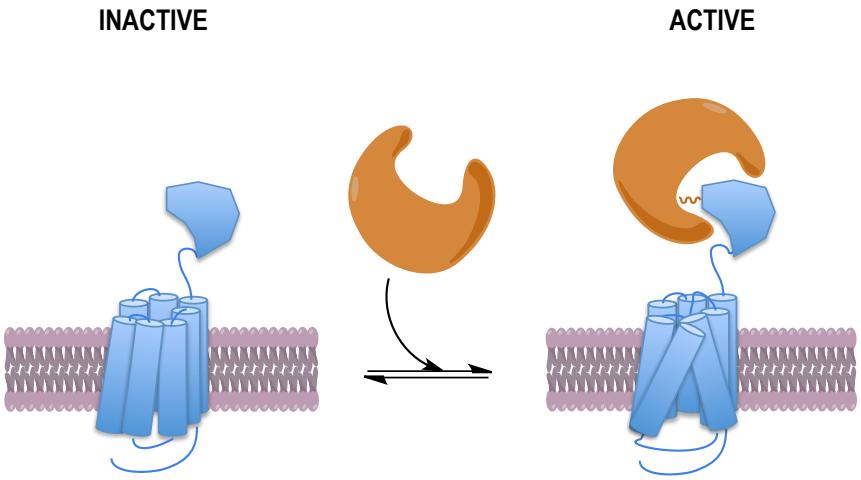

Figure 6: Topology of class F GPCRs and general binding model of Wnt-protein interaction (adapted from previous publications[27])

This family of receptors mainly binds to G_o-protein. Antagonists of class F GPCRs are specially interesting for the treatment of several types of cancer while agonists are relevant for regenerative medicine[28]. Furthermore, five crystal structures of SMO have recently been solved,

four of them co-crystallized with an antagonist in the inactive conformation and one co-crystallised with an agonist[27b, 29].

Glutamate Receptors

Glutamate (the conjugate base of the glutamic acid) is one of the twenty amino acids used to construct proteins and is found in high concentrations in every part of the body. It plays an additional role in the central nervous system (CNS) as a neurotransmitter. It's used by every major excitatory information-transmitting pathway in the vertebrate brain, accounting in total over 90% of the synaptic connections in the human brain.

In glutamic acid, the side chain carboxylic acid functional group has pK_a of 4.1 and therefore exists almost entirely in its negative charged deprotonated carboxylate form at pH values greater than 4.1; therefore, it is negatively charged at physiological pH ranging from 7.35 to 7.45.

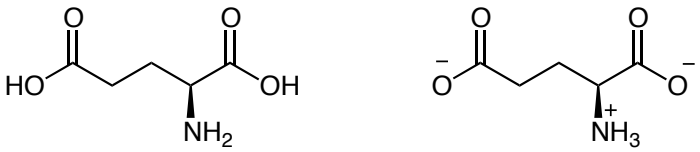

1a **1b**

Figure 7: Chemical structure of acid glutamic as a free base **1a** and **1b** with unprotonated chain carboxylic acid (at physiological pH).

Glutamatergic synapses convey most of the fast excitatory neurotransmission in the central nervous system, and intact glutamate signalling is thus critical for the majority of sensory processing and cognitive function.

In a functionally mature glutamatergic synapse, presynaptic compartments are enriched with glutamate-filled synaptic vesicles and specialized active zones that support the release of glutamate from the nerve terminal. A wide array of proteins function to transport glutamate into synaptic vesicles, localize filled vesicles to the active zone, and dock and prime vesicles for release. Scaffolding proteins coordinate voltage-gated calcium channels (VGCCs) and intracellular calcium sensors to orchestrate the rapid release of glutamate in response to a calcium influx triggered by action potentials. In addition, glutamate reuptake machinery on both neurons and neighbouring astrocytes regulates the concentration of glutamate in the synaptic cleft.

The postsynaptic compartment is primarily localized at specialized, actin-rich, dendritic protrusions called spines that often change their morphology and size with synaptic strength. The postsynaptic density (PSD), a compact network of scaffolding proteins, receptors, and signalling molecules in the spine head, concentrates postsynaptic machinery opposite the presynaptic terminal[30].

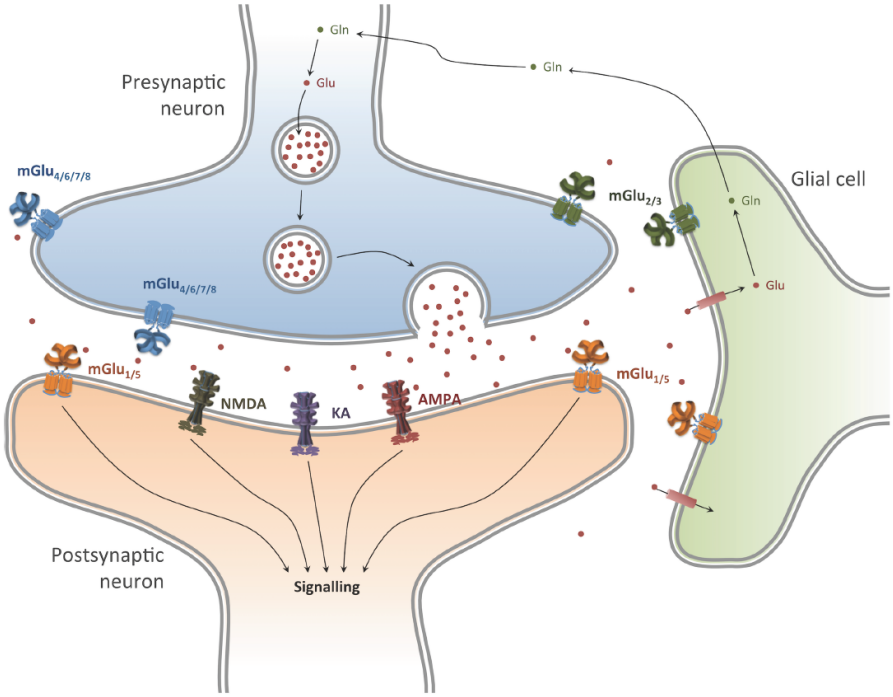

Figure 8: Glutamate synapse. Glutamate is accumulated in the vesicles in presynaptic compartments trough the vesicular glutamate receptors. In the synapse the vesicles are fused to the neuron membrane releasing glutamate, which is the responsible of activation of iGlu and mGlu (1 or 5) located to the postsynaptic terminal of a new neuron. The uptake glutamate is done by glial cells through glutamate transporters (EAAC), where it is converted to glutamine released to the presynaptic cell, where is converted to glutamate and stored in glutamate vesicles.

Glutamate confers its physiological actions through glutamate-gated ion channels, termed ionotropic glutamate receptors, and glutamate-activated G protein-coupled receptors, termed metabotropic glutamate receptors (mGluRs)[30].

Ionotropic glutamate receptors

Ionotropic glutamate receptors (iGluRs) are integral membrane proteins composed of four large subunits that form a central ion channel pore. They are split in three main subunits: the α-amino-3-hydroxy-5-methyl-4-isoxazolepropionic acid receptor (AMPA), kainate receptor (KA) and *N*-

Methyl-D-aspartate (NMDA). Glutamate receptors subunits are tetrameric modular structures that contain four discrete semiautonomous domains: the extracellular amino-terminal domain (ATD), the extracellular ligand-binding domain (LBD), the transmembrane domain (TMD), and an intracellular carboxyl-terminal domain (CTD)[31].

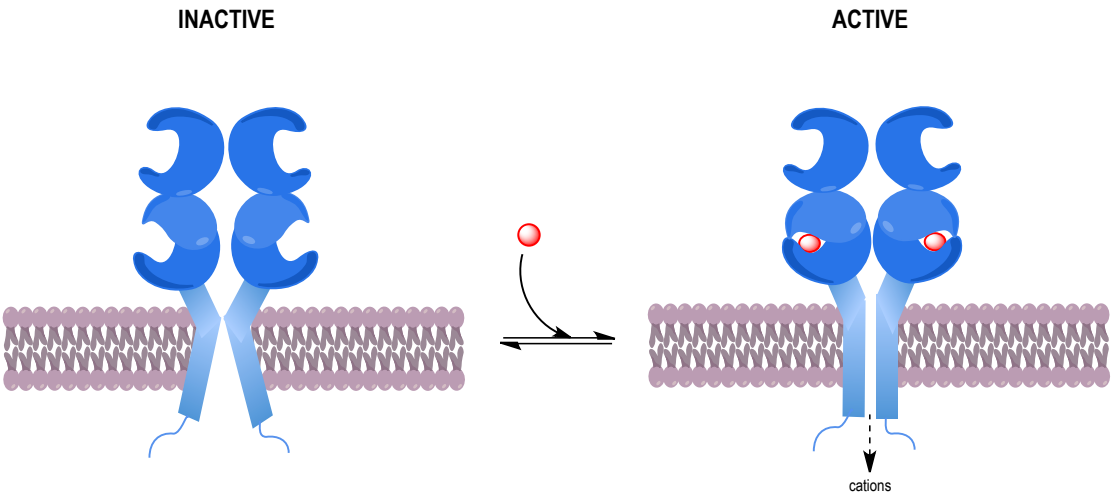

Figure 9: Topology of iGluR and general binding model of glutamate with the corresponding open of cation channels[31].

Ionotropic AMPA receptors are significantly involved in the post-synaptic excitatory potential due to their localization at the most active position in the postsynaptic density. These receptors are activated, opening the corresponding cation channels, when two of the four binding sites are occupied, increasing the current as more receptor sites are occupied by the agonist The presence of auxiliary proteins (TARPs) regulates de trafficking and are permeable to Na^+ and K^+, but not to Ca^{2+}, where this permeability depends on the presence of GluA2. The high activity in response to glutamate evidences that their activation only takes place upon a synaptic release of glutamate.

Ionotropic Kainate receptors are responsible for a minimal part of the postsynaptic currents and they have similar properties to AMPA receptors. They are also modulated by auxiliary proteins (Neto proteins) and mediate in the excitatory postsynaptic currents. The difference between them are the needle of extracellular Na^+ and Cl^- for the activation of Kainate receptors which are often slower respect to the AMPA receptors, and in addition they play a neuromodulatory role.

The ionotropic NMDA receptors are heterotetrameric systems involving two GluN1 subunits and two GluN2 or GluN3 subunits. Apart from glutamate acting as an agonist, glycine or D-serine

could act as co-agonists. The main functions of these receptors are regulatory and they play an important role in the synaptic plasticity[31].

Family	Gene/Subunit
AMPA	GRIA1/GluA1, GRIA2/GluA2, GRIA3/GluA3 and GRIA4/GluA4
Kainate	GRIK1/GluK1, GRIK2/GluK2, GRIK3/GluK3, GRIK4/GluK4 and GRIK5/GluK5
NMDA	GRIN1/GluN1, GRIN2A/GluN2A, GRIN2B/GluN2B, GRIN2C/GluN2C, GRIN2D/GluN2D, GRIN3A/GluN3A and GRIN3B/GluN3B
Orphan	GRID1/GluD1, GRID2/GluD2

Table 7: Classification of iGluRs with their subunits and human gens[32]

Metabotropic glutamate receptors

The metabotropic glutamate receptors (mGluRs) are key receptors in the modulation of excitatory synaptic transmission and they are widely distributed in the central nervous system (CNS) and the peripheral nervous system (PNS). They belong to class C GPCRs, and are activated by the major excitatory neurotransmitter: glutamate.

Structure and activation mechanisms

As previously described, mGluRs are constitutive dimers with each protomer composed of three subunits: a large extracellular domain (ECD) also called Venus Flytrap (VFT), where the glutamate binds, a cysteine rich domain (CRD) composed of about 70 amino acids residues which connects the extracellular domain to the heptahelical transmembrane domain (7TM) common to all GPCRs and responsible of the G-protein activation, and the 7TM itself.

The VFTs are bilobate proteins, each lobe being separated by a cleft where ligands bind. The VFTs exist in two major states: an open state in absence of ligand and stabilized by antagonists, and a closed state stabilized by agonists and required for receptor activation. The VFT dimer is in equilibrium between various conformations, depending on whether one or two VFTs are open or closed. In the absence of ligand or in the presence of antagonists, both VFTs are opened. The

binding of one or two agonists triggers the closure of one or two VFTs in the dimer, resulting in receptor activation.

Upon activation of the receptor, the closure of the VFTs in the dimer is associated with a large change in the relative orientation of the two VFTs, from resting to an active orientation. The major consequence of this reorientation is that the second lobes of the VFTs, which are distant in the resting state, become closer in the active conformation, stabilizing the active state of the transmembrane domain (*Figure 10*) [23, 33].

The cysteine rich domain (CRD) is a linker between the VFT and the TMD, with nine well-conserved cysteines, which afford four intradomain disulphide bridges and the ninth cysteine is linked to the VFT trough and additional disulphide bridge[23, 33]. The role of both CRD is crucial and they are likely contacting each other when the activation of the receptor takes place.

The TMDs can adopt different conformations and they are responsible for G-protein activation. Once the receptor is activated, the TMD of just one protomer changes from resting to an active conformation, while the other one remains in the resting conformation. This asymmetric active/inactive TMD dimeric state is the responsible for transducing the signal from the orthosteric site in the VFT to the G-protein. A full-length mGlu dimeric arrangement is required for G protein activation by the endogenous agonist glutamate, thus confirming that mGlu receptors signal through a dimeric structure in live systems[34]. However, in the presence of a positive allosteric modulator (PAM), monomeric mGlu receptors are able to activate a G protein either as full-length (VFT + CRD + TM) or in the form of truncated TM receptors[34].

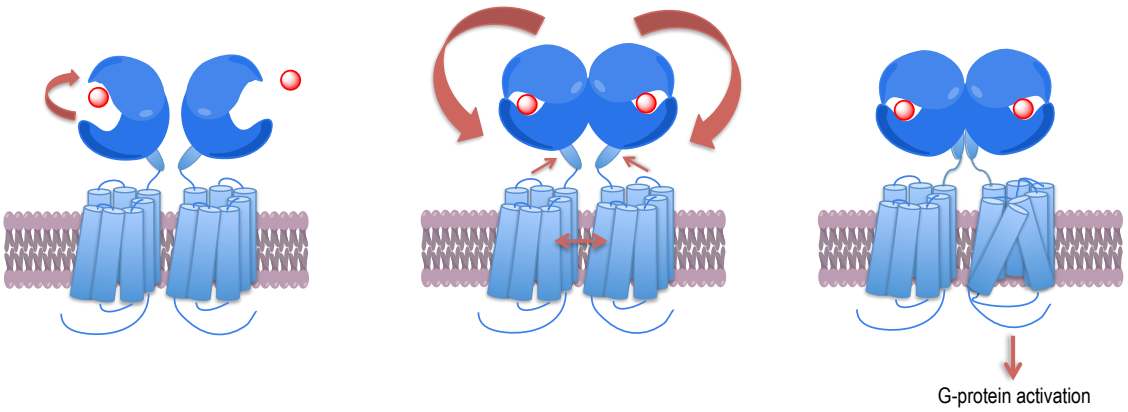

Figure 10: Activation steps of mGluRs. Adapted from Gomez[13]

Classification of Metabotropic glutamate receptors

Most of the actions produced by the major neurotransmitter glutamate within the central nervous system are mediated by activation of mGluRs. There are eight subtypes of mGluRs, which are expressed throughout the CNS except $mGlu_6$ that is only expressed in the retina. They are classified into three groups based on sequence homology and pharmacology: Group I includes $mGlu_1$ and $mGlu_5$; Group II, $mGlu_2$ and $mGlu_3$; and Group III, $mGlu_4$, $mGlu_6$, $mGlu_7$, $mGlu_8$ (*Table 8*). Group I mGluRs preferentially couple to the $G_{q/11}$ family of G proteins, activating phosphoinositide hydrolysis and calcium mobilization as their major signalling mechanism. In contrast, Group II and Group III mGluRs preferentially couple to $G_{i/o}$ and inhibit adenylyl cyclases.

Group	Subtype	Gene	Glu EC_{50}	Orth. ago	EC_{50}	G-Prot. (main signalling)
I	$mGlu_1$	GRM1	9-13	Quisqualic acid (**2**)	0.1-1	Gq (+IP3, + intracellular Ca^{2+}, +DAG, PKC activation)
	$mGlu_5$	GRM5	3-10		0.03-0.3	
II	$mGlu_2$	GRM2	4-20	LY 354740 (**3**)	0.005	Gi/o (-cAMP, inhibit voltage gated Ca^{2+} channels, activate K^+ channels, activate the MAPK and PtdIns-3-K pathways)
	$mGlu_3$	GRM3	4-5		0.0034	
III	$mGlu_4$	GRM4	3-20	L-AP_4 (**4**)	0.2-1.2	Gi/o (-cAMP, inhibit voltage gated Ca^{2+} channels, activate K^+ channels, activate the MAPK and PtdIns-3-K pathways)
	$mGlu_7$	GRM7	1000		0.9	
	$mGlu_8$	GRM8	16		160-500	
	$mGlu_6$	GRM6	2.5-11		0.06-0.6	Go (inhibits TrpM1 Ca^{2+} channel)

Table 8: Classification of mGlu receptors, with glutamate potency for every subtype (EC_{50}) in μM units[35]. The table also includes the most common orthosteric ligand for each group (*Figure 11*), with their corresponding potency as EC_{50} in μM units, the main G-protein and the main signalling pathway[36].

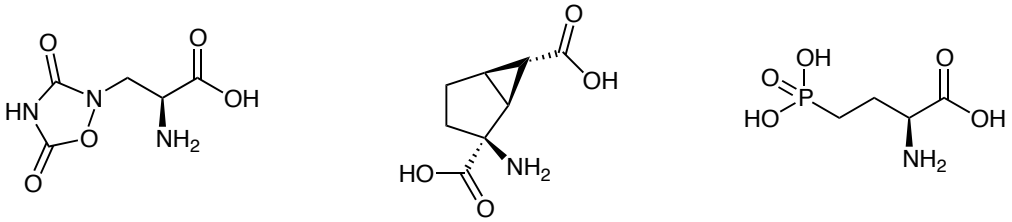

Quisqualic acid (**2**) LY 354740 (**3**) L-AP_4 (**4**)

Figure 11: Structure of common group-selective orthosteric ligands.

Group I mGluRs

Group I mGluRs, comprising $mGlu_1$ and $mGlu_5$, are extensively expressed throughout the CNS in neurons and they are predominantly found postsynaptically[37], where they increase neuronal excitability. It's important to note that the Group I mGluRs localized presynaptically can increase or decrease neurotransmitter release. In addition, they play important roles in synaptic plasticity by facilitating both long-term depression and potentiation of synaptic strength as well as inducing nonsynaptic conductance leading to enhance neuronal excitability.

$mGlu_1$ expression is most intense in Purkinje cells of the cerebellar cortex and the olfactory bulb with strong expression in neurons of the lateral septum, globus pallidus, ventral pallidum, most thalamic nuclei, as well as the substantia nigra. High levels of $mGlu_1$ are also found within the hippocampus, suggesting a potential role of this receptor in learning and memory.

Localization of $mGlu_5$ is greatest in corticolimbic areas responsible for controlling higher cognitive function including the striatum, hippocampus, cerebral cortex, septal nuclei as well as the thalamus, and olfactory bulb. Extensive studies using $mGlu_5$ KO mice implicate this receptor's role in cognition, addiction, anxiety, chronic pain and obesity[37].

Group II mGluRs

Group II mGluRs, $mGlu_2$ and $mGlu_3$, are widely distributed in the CNS and in the periphery[37]. Generally, $mGlu_2$ and $mGlu_3$ are expressed presynaptically where they modulate neurotransmitter release. In addition, they are also found at postsynaptic sites where they can induce hyperpolarization. Similarly to the Group I mGluRs, $mGlu_2$ and $mGlu_3$ KO mice have been heavily utilized in order to define the individual roles of the Group II mGluRs in a variety of physiologic processes.

$mGlu_2$ KO mice show a loss of Group II agonist-induced reversal of PCP-induced hyperlocomotion, an enhanced responsiveness to cocaine and alterations in synaptic transmission in a number of regions[38].

$mGlu_3$ KO mice also show decreased efficacy of Group II agonists in anxiolytic models, an increase in basal hippocampal c-Fos expression and a loss of Group II agonists-induced neuroprotection by astrocytes against NMDA excitotoxicity[38a].

Group III mGluRs

Group III mGluRs, ($mGlu_4$, $mGlu_6$, $mGlu_7$ and $mGlu_8$), with the exception of $mGlu_6$, which is localized postsynaptically on retinal ON bipolar cells, are mainly expressed presynaptically in neurons distributed throughout the CNS[37].

$mGlu_4$ is highly expressed in the cerebellum, with lower expression in the hippocampus, basal ganglia, and olfactory bulb and is also found peripherally in pancreatic islet cells and taste buds. Deletion of $mGlu_4$ gene results in mice with impaired cerebellar synaptic plasticity and deficits in learning of complicated motor tasks and spatial memory performance[39].

$mGlu_7$ and $mGlu_8$ are widely distributed throughout the brain. In particular, $mGlu_7$ is localized in active zones of synapses and has an extremely low affinity for glutamate, for this reason $mGlu_7$ is only activated in the presence of very high glutamate levels and thus serves to prevent overstimulation. $mGlu_7$ KO mice exhibits deficits in memory, learning and have been implicated in disorders such as anxiety and depression[40]. $mGlu_8$ KO mice displayed increased anxiety and weight gain. mGlu8 is also localized postsynaptically within the peripheral cells of the gut and pancreas and has been implicated in gastrointestinal motility and insulin secretion[41].

Unlike other Group III subtypes, the $mGlu_6$-signalling cascade has been shown to involve G_o protein subunit. $mGlu_6$ KO mice demonstrates deficits in ON response to light stimulation[42].

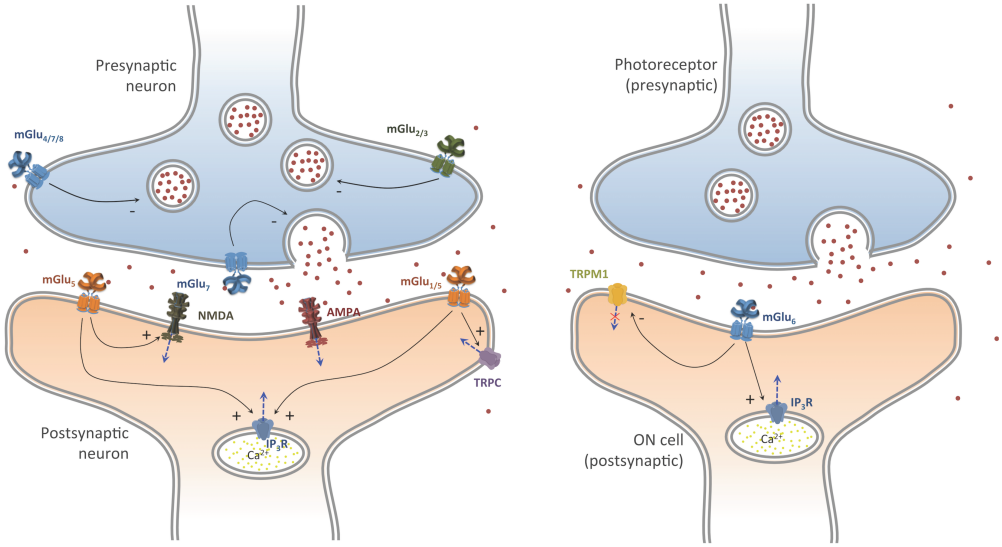

Figure 12: Glutamate synapse in glutamatergic neurons (left) and for photoreceptors ON (right), with the localization of all mGluRs subtypes[13]

Classification of ligands in Metabotropic glutamate receptors

Despite the innovative development of several tools to modulate the function of the mGluRs activity such as nanobodies or antibodies, one classical approach thas has been proved useful for receptor modulation is the addition of small molecules that bind to the receptor.

Ligands acting at mGluRs, depending where they bind to the receptor, can be classified in two main groups: Ligands acting at VFT (usually orthosteric ligands if they also bind at the same site as glutamate in which case they are competitive ligands) and ligands acting at TMD, called allosteric or non-competitive ligands.

Ligands acting at VFT

Based on glutamate (the endogenous ligand which binds at VFT), several studies of many compounds with similar scaffold have been designed and screened[43]. The ligands acting at the VFT could have different behaviours, including full agonists, partial agonists, antagonists or inverse agonist. All these compounds behave as competitors of glutamate for the orthosteric binding site. However there exists the possibility of allosteric compounds acting at the VFT (see below).

The need for compounds acting at the VFT and selective for every mGluR is an arduous task. However, some selective agonists for each group of mGluRs have been developed such as quisqualate (**2**) (group I), LY 354740 (**3**) (group II) and L-AP_4 (**4**) (group III) (*Table 8*, *Figure 11*). Also, extensive research has been performed for the quest of antagonist ligands at the VFT, that is, compounds that bind to the orthosteric site and prevent the VFT domain closure. We can mention for example LY 341495 (**5**), which has a slight selectivity for group II (*Figure 13*)[43].

Recently, an additional pocket at VFT was discovered due to a new group III agonist, LSP4-2022 (**6**), which bears a long chain that binds to the glutamate side and to a known chloride-binding site[44]. In fact, a chloride ion was reported to act as a positive allosteric modulator, binding at least at two different sites of the VFT[45]. Therefore, this discovery opens the possibility of finding new allosteric modulators that bind at the extracellular domain (EDAMs: Extracellular domain allosteric modulators) acting, for instance, at the chloride sites of the VFT, or long bitopic ligands that bind simultaneously to both the orthosteric and the allosteric sites of the VFT.

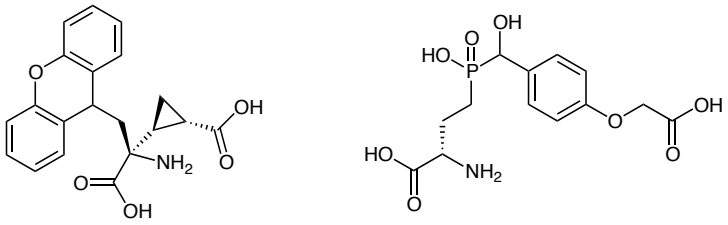

LY 341495 (**5**) LSP4-2022 (**6**)

Figure 13: Structures of antagonist LY 341495 and EDAM LSP4-2022

Ligands acting at TMD

Interestingly, CNS drug discovery efforts to target ligand-gated ion channels neurotransmitter receptors have focused primarily on developing ligands that interact with allosteric sites that are topographically distinct from the orthosteric neurotransmitter site. By binding to allosteric sites, such ligands could have the capacity of potentiate (positive allosteric modulators, PAMs) or inhibit (negative allosteric modulators, NAMs) the activation of the receptor by the endogenous agonist, affecting the intrinsic efficacy of the agonist to trigger the signalling response[46].

As mentioned above, PAMs potentiate the receptor responses to orthosteric agonists stabilising the active conformation of one TMD whereas, on the other hand, NAMs stabilise the inactive conformation of both TMDs. In addition, PAMs can have intrinsic efficacy and activate the receptor in the absence of an orthosteric agonist. PAMs that also possess intrinsic allosteric agonist activity in a given functional assay are referred to as ago-PAMs; however, the presence or absence of ago-PAM activity may depend on the assay system, the level of receptor expression or the efficiency of the receptor coupling with a given second messenger system[47].

Another class of ligands is that of those ligands that binds to allosteric sites but have no effect on receptor responses to orthosteric ligands. These allosteric compounds are called SAMs (silent allosteric modulators).

As previously mentioned, the TMD is located within the cellular membrane due to the hydrophobic residues that constitute the central part of this domain. Therefore, the polarity of the allosteric ligand designed to bind the TMD has to be low to afford the binding pocket at this receptor domain. This condition imposes several advantages and disadvantages with respect to the VFT ligands, which are highly hydrophilic.

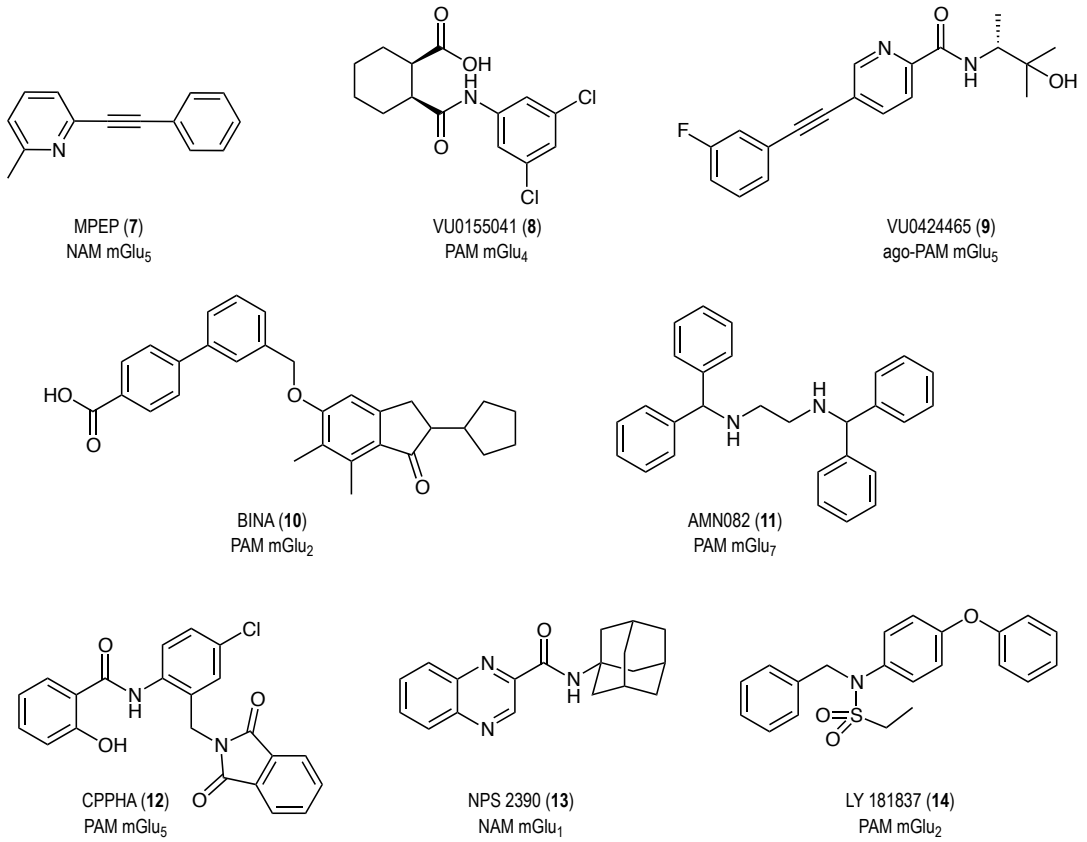

Figure 14: Examples of allosteric modulators for a single mGlu subtype[37 48]

An important drawback of TMD allosteric modulators is their lower solubility in water. However, due to their often-high potency, the usage of lower doses can compensate this issue, decreasing at the same time their side effects. In addition, the absorption of lipophilic molecules orally administrated is feasible and they usually tend to pass the blood-brain barrier, in comparison with orthosteric ligands that are more limited to cross the blood-brain barrier due to their high polarity[43].

An additional potential advantage of allosteric modulators is that they only inhibit or potentiate the activity of the receptor in presence of the orthosteric endogenous ligand in synapses. This is in contrast with orthosteric ligands which exert their effects independently of the neurotransmitter release.

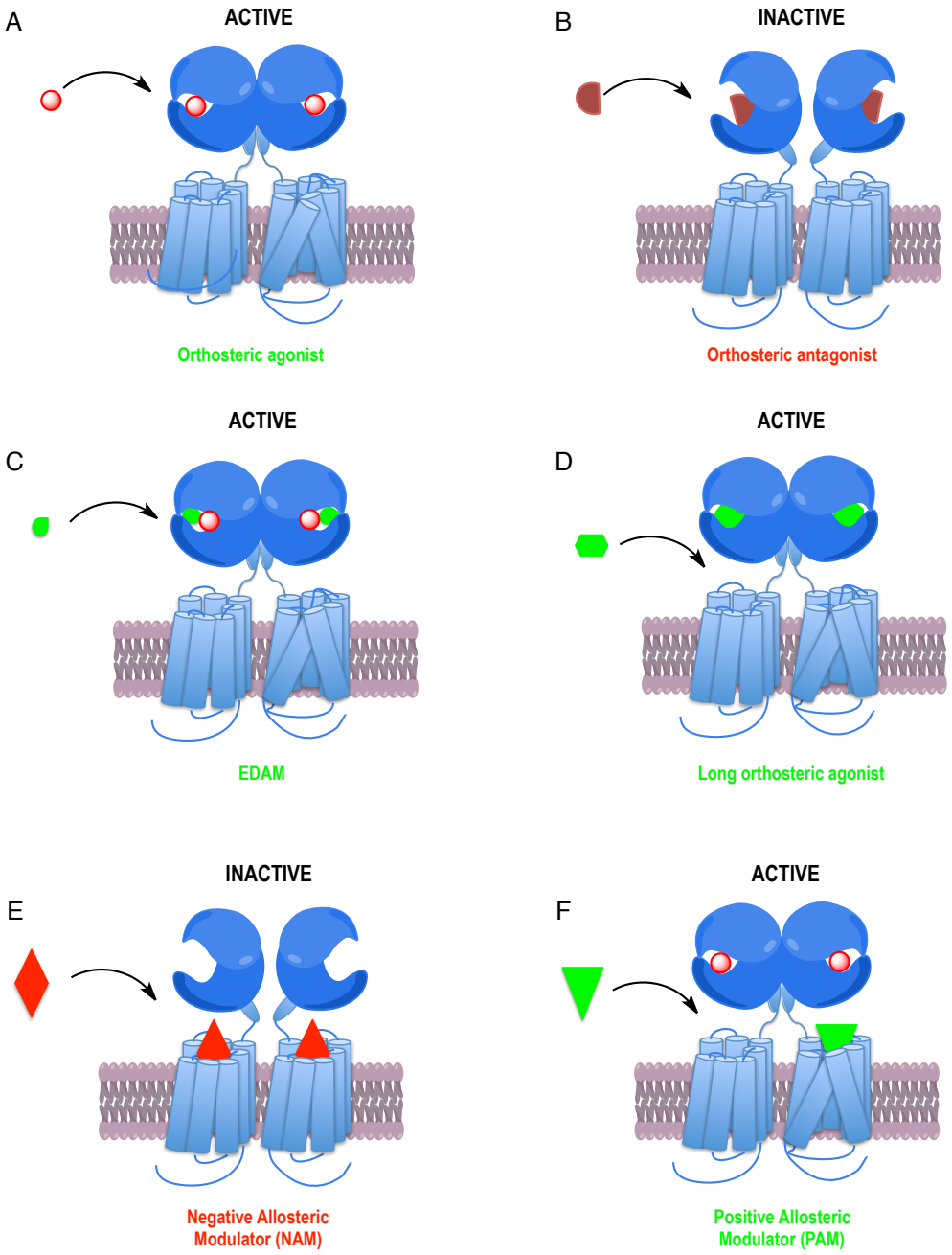

Figure 15: General binding model in mGluR: A) orthosteric agonist, B) orthosteric antagonist, C) extracellular domain allosteric modulators (EDAM), D) long orthosteric agonist, E) positive allosteric modulators (PAM), F) negative allosteric modulator (NAM) (adapated from Gomez[13])

Therapeutic potential of mGlu to treat human disorders

As we have summarized so far, mGlu receptors are widely distributed throughout the central and peripheral nervous systems and each subtype has singular a role. These receptors can be modulated to treat several human disorders by drug-like agonists, antagonists and allosteric modulators[37].

$mGlu_1$ and $mGlu_5$ NAMs for pain

Multiple studies have demonstrated the efficacy of $mGlu_1$ NAMs in model analgesia. For example, YM 298198 (**15**) NAM is analgesic in the streptozotocin-induced hyperalgesia mouse model[49], and FTIDC (**16**) displays analgesic effects in the formalin test[50]. In addition, the $mGlu_1$ NAM CPCCOEt (**17**) dose-dependently reversed capsaicin-induced sensitization in spinothalamic tract cells *in vivo* demonstrating the potential utility of $mGlu_1$-selective NAMs for the treatment of persistent pain associated with spinal sensitization[51].

Another target to treat pain is $mGlu_5$ by using NAMs. The inhibition of pain has been clearly demonstrated after $mGlu_5$ NAM Raseglurant (**18**) phase II trials for migraine, which was unfortunately discarded because of its hepatotoxic effects[52]. Other NAMs of $mGlu_5$ such as Fenobam (**19**) were used in phase I clinical trials to treat induced hyperalgesia in healthy volunteers[53].

$mGlu_5$ NAMs for anxiety, depression and fragile X syndrome

Several preclinical studies suggest a role for $mGlu_5$ NAMs as a therapeutic approach for the treatment of anxiety. MPEP (**7**) (*Figure 14*), a selective $mGlu_5$ NAM, has shown anxiolytic activity in several rodent behavioural models, elevated plus maze, fear-potentiated startle, social exploration, stress-induced hyperthermia, ultrasonic vocalizations, and the Vogel conflict test[54]. Furthermore, recent studies have also linked the antagonism of $mGlu_5$ with antidepressant activity. MPEP (**7**) and MTEP (**20**) exhibit antidepressant activity in multiple animal behavioural models of depression, including the tail suspension test and forced swim test in mice[55]. Although $mGlu_5$ NAM development has largely focused on anxiety disorders, additional studies suggest that $mGlu_5$ NAMs have therapeutic potential in the treatment of addiction, chronic pain, migraine, Alzheimer's disease, gastroesophogeal reflux as well as fragile X syndrome (FXS).

Particularly in FXS, multiple studies have demonstrated that increased $mGlu_5$ signalling occurs, where a reduction in $mGlu_5$ expression rescues FXS phenotypes[56], and a decrease in FXS phenotypes in mice when treated with MPEP (**7**)[57].

$mGlu_5$ PAMs for schizophrenia

Positive allosteric modulation of $mGlu_5$ has also emerged as a novel therapeutic target for the treatment of schizophrenia and cognitive disorders. Early clinical findings demonstrated that noncompetitive use-dependent NMDA receptor antagonists, such as phencyclidine and ketamine, produce a state of psychosis in humans that is not clinically distinguishable from that observed in schizophrenic patients[58].

Numerous studies suggest that $mGlu_5$ is a closely associated signalling partner with the NMDA receptor and may play an integral role in regulating NMDA receptor function in various forebrain regions implicated in the pathology of schizophrenia[59]. Consistently, activation of $mGlu_5$ receptor results in the potentiation of NMDA receptor currents in hippocampal pyramidal cells, suggesting a role of $mGlu_5$ in cognitive function. Therefore, selective activation of $mGlu_5$ and subsequent enhancement of NMDA receptor activity may provide a novel approach to the treatment of not only the positive symptoms but also the negative ones and cognitive deficits afflicting patients with schizophrenia [37].

Multiple $mGlu_5$ PAMs have been identified and potentiate $mGlu_5$-mediated electrophysiological responses in midbrain and forebrain circuits, such as CDPPB (**21**), ADX47273 (**22**) and VU0360172 (**23**) (*Figure 16*).

$mGlu_2$ PAMs for schizophrenia, anxiety disorders and drug dependence

There is a tremendous volume of clinical and preclinical evidence that Group II mGlu activators have potential as a novel approach for the treatment of schizophrenia and anxiety disorders. Many brain regions relevant to schizophrenia and anxiety express Group II mGlus, and their agonists reduce the neurotransmission in these regions[60]. Furthermore, the effects of psychotomimetics on thalamocortical glutamatergic neurotransmission, a region postulated to play a role in the pathophysiology of schizophrenia, are blocked by Group II mGlu agonists.

Numerous studies have further demonstrated that Group II agonists have activity in multiple animal models of anxiolytic and antipsychotic drug action[61].

The efficacy of Group II agonists in these models has paved the way for evaluation of mGu_2 selective PAMs as an alternative therapeutic route. Similarly to the Group II agonists, $mGlu_2$ PAMs have also been demonstrated to inhibit ketamine-induced neurotransmitter release in brain regions relevant for the antipsychotic action of Group II agonists, including norepinephrine and histamine[62]. Further, two distinct $mGlu_2$ PAMs, BINA (**10**) (*Figure 14*) and LY487379 (**24**), clinical studies with these compounds were disrupted in schizophrenic patients.

In addition, Group II agonists have also been suggested for the treatment of drug addiction and relapse. In animal models, agonists attenuate cocaine self administration[63], heroin seeking, food seeking and alcohol seeking implying that group II agonists decrease responses to both drug and natural rewards.

$mGlu_3$ PAMs for neuroprotection

mGlus have been suggested as a target for neurodegenerative disorders[64]. In particular, a number of studies have demonstrated that Group II mGlu agonists are neuroprotective when mixed cultures of cortical neurons and astrocytes are challenged with NMDA via glial-neuron mechanism involving transforming growth factor ß[65]. $mGlu_2$ and $mGlu_3$ KO mice have shown that $mGlu_3$ on the astrocytes are necessary for this effect and that, in absence of $mGlu_3$, the activation of neuronally expressed $mGlu_2$ may further contribute to excitotoxicity[66].

Recently, LY2389575 (**25**), a selective $mGlu_3$ NAM, was utilized in combination with $mGlu_3$ KO mice to further demonstrate that activation of glial $mGlu_3$ receptors was protective against amyloid ß neurotoxicity[67].

$mGlu_4$ PAMs for Parkinson's disease

$mGlu_4$ is expressed on GABAergic fibers within the indirect pathway of motor control in the basal ganglia circuit. Activation of these receptors decrease GABA release at the striatopallidal synapse, which is overactive after the loss of dopamine neurons in Parkinson's disease[68]. Disinhibition of thalamocortical neurons is believed to alleviate Parkinsonian symptoms and is the basis for targeting $mGlu_4$ for the treatment of Parkinson's disease. PHCCC (**26**), a selective $mGlu_4$ PAM, potentiates $mGlu_4$-mediated inhibition at the striatopallidal synapse[69]. In addition, PHCCC (**26**) as well as VU0155041 (**8**) (*Figure 14*), demonstrates antiparkinsonian effects in

preclinical models, such as reversal of haloperidol-induced catalepsy and reserpine-induced akinesia[69].

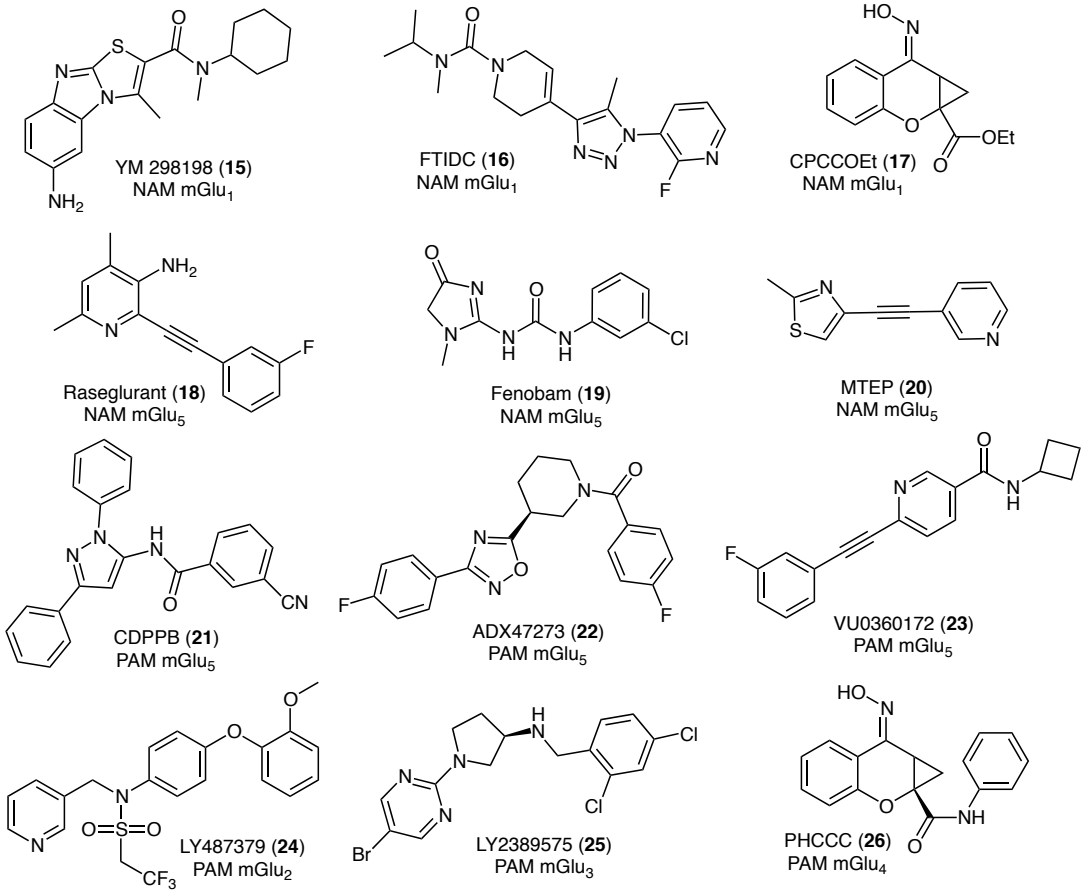

Figure 16: Chemical structures of PAMs and NAMs with therapeutic potential for the treatment of human disorders

Protein function assisted by light

Optogenetics approach

Photoisomerisables chromophores can be found in the nature and they switch a protein function by means of light, in a fast and precise manner. An example of such may be retinal in opsin proteins that can regulate the visual transduction (rhodopsin) (*figure 17A*), pump protons as a source of energy (bacteriopsins), or the trafficking of ions (channelrhodopsins and halorhodopsins)[70 71].

Optopharmacology approach

Conventional pharmacology has given us several drugs that affect many types of ion channels and neurotransmitter receptors, but this approach has some serious limitations.

First of all, the delivery of conventional drugs to intact neural structures is slow and imprecise and also, most of them are almost never fully specific for an individual subtype of a channel or receptor. Moreover, conventional drugs cannot distinguish between the same receptor expressed in different classes of neurons, especially if they are intertwined in a neural circuit.

The solution to these thorny problems lies in combining optics and chemistry in various ways. Optopharmacology refers to photosensitive reagents that act on channels and receptors (*Figure 17*). As they can be precisely regulated with light, these tools offer a potential solution to the problem of delivery. The optopharmacological tools that have been most widely used in neuroscience are caged agonists of neurotransmitter receptors, particularly glutamate receptors. The caged glutamate compounds give the opportunity to rapidly and locally release the agonists with spatial and temporal precision that rivals that of a real synaptic contact[72] (*Figure 17C*).

Chemical photoswitches (or photochromic ligands) are another type of optopharmacological tool[73]. These are compounds in which the ligand is attached to a photoisomerizable group that controls whether the ligand can fit properly into a binding site on a protein, either a channel or a receptor. One important advantage over caged compounds is the reversibility of azobenzene photoswitches. The compounds can repeatedly transition between the active versus the inactive photoisomeric states, either in response to different wavelengths of light or as a consequence of thermal relaxation[72] (*Figure 17D*).

Optogenetic pharmacology combines optics and chemistry and adds genetics to the mix, simultaneously solving both the subtype-specificity and cell-targeting problems. The idea is to attach a synthetic photosensitive ligand onto a genetically engineered protein to allow activation or inhibition of only that specific protein with light (*Figure 17B*).

The power of this approach is that it combines the absolute specificity that only genetics can provide with the unique precision that only light can provide to regulate function of targeted neurons at the molecular level. Nowadays, optogenetics pharmacology is technically demanding because it requires the introduction of two exogenous components, the chemical ligand and the gene encoding the target protein[72].

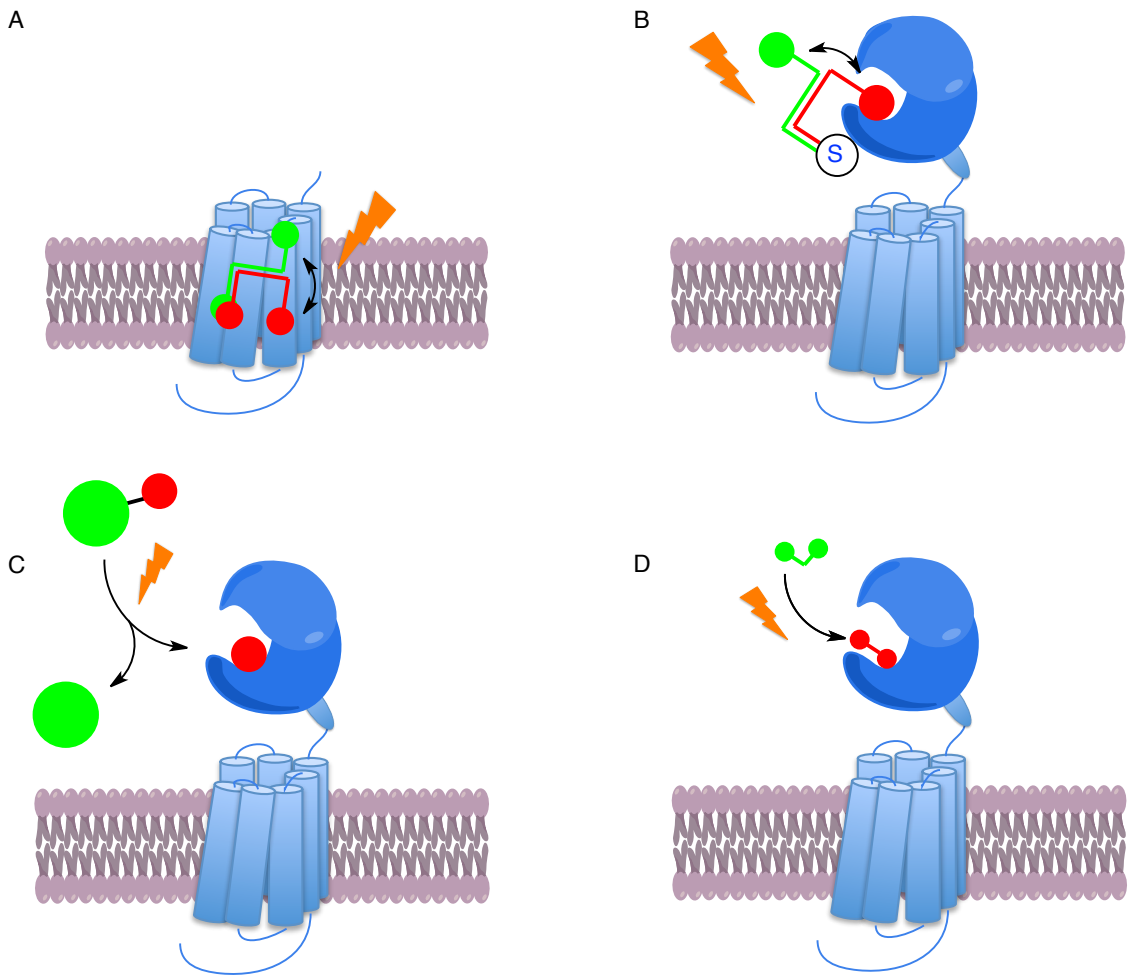

Figure 17: Representative approaches of protein function assisted by light: A) Optogenetics, B) Optogenetic pharmacology, C) Optopharmacology with caged compounds, D) Optopharmacology with photoswitchable compounds (adapted from Kramer[72] and Gomez[13].)

Optogenetic pharmacology

Optogenetics has revolutionized neuroscience by making it possible to use heterologously expressed light-proteins and pumps to stimulate or inhibit activity in genetically selected neurons and brain regions and thereby determine their roles in circuit function and behaviour[74].

While the production of pharmacological reagents targeted to membrane signalling proteins has been a major objective, many important membrane proteins are still without specific blockers. Moreover, where specific blockers exist, they often have high affinity and are selective only at low concentrations, so that the onset of their effect upon a exposure takes a long time develop and they bind so tightly that they are very difficult to remove. The development of photoswitched

tethered ligands (PTLs) that are targeted to an introduced cysteine near ligand binding sites of membrane proteins opened the door to the reversible control of membrane signalling, by using two wavelengths to photoisomerize the tether between one state that permits ligand binding and a second state, which prevents binding. Because specificity derives from the unique geometric relationship between the ligand binding site and the engineered anchoring site, rather than from tight binding, photoisomerization, to the nonbinding state rapidly removes the ligand. Moreover, the high effective concentration of the ligand near its binding site in the permissive state leads to rapid binding upon photoisomerization, itself a very rapid transition[74]. Together, these properties enable highly selective optical control of binding and unbinding on the millisecond timescale and micron space-scale[74].

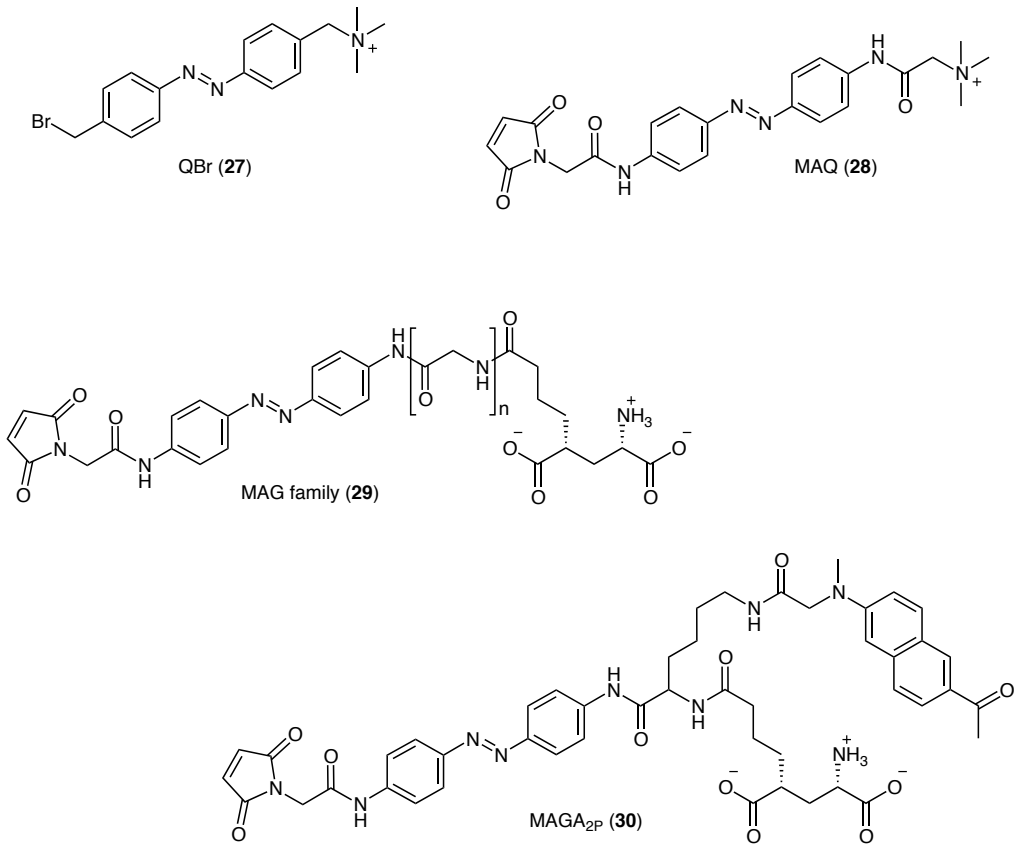

Figure 17: Chemical structures of PTLs examples

The first generation of PTLs were the nicotinic acetylcholine receptors (nAChR)[75], which natively include a cysteine-rich loop close to the binding site where the PTL (QBr **27**) can conjugate. Years after, new PTLs were designed with the corresponding mutation of the target proteins. Examples of such can be MAQ (**28**) family, as K^+ channel blockers[76], MAG (**29**) family, as GluK2

agonists or mGlu agonists[77] including $MAGA_{2P}$ (**30**), which is photoisomerisably illuminated with the two-photon technique[76].

Optopharmacology with photoisomerisable compounds

As explained above, photopharmacology have recently become a vibrant field for attempting to control biological function with synthetic photoswitches that act on native biopolymers or membranes.

The photoswitches used can either be covalently attached to their target like in the majority of the natural photoreceptors (photoswitchable tethered ligands PTLs) or be tightly bound through noncovalent interactions (photochromic ligands PCLs), which can be called simply photoswitchable ligands or photopharmaceuticals.

Today, they have been applied to a wide variety of biological targets such as ion channels, G-protein coupled receptors, transporters, enzymes and lipids[78 79].

Optopharmacology with photoisomerisable compounds (PCLs) adds a few extra dimensions to the drug design process. First of all, a suitable photoswitch needs to be chosen; the switching cannot be associated with phototoxicity and must take place reliably over many cycles. After initial photoisomerization by irradiation at certain wavelength, the reverse isomerization must also be considered. Depending on the biological question it might be more suitable to use thermally unstable photoswitch that spontaneously turns itself OFF after the irradiation is halted. Alternatively a bistable photoswitch, which requires light of one wavelength to turn ON and another one to turn OFF, could be more suitable toward the desired application.

Once the best photoswitch has been chosen, it need to be incorporated into the molecule of interest in such a way that the efficacy of the new ligand changes significantly upon photoswitching. Ideally, the ligand is active as an agonist, antagonist, blocker, etc. in one configuration and completely inactive in the other (*Figure 18*).

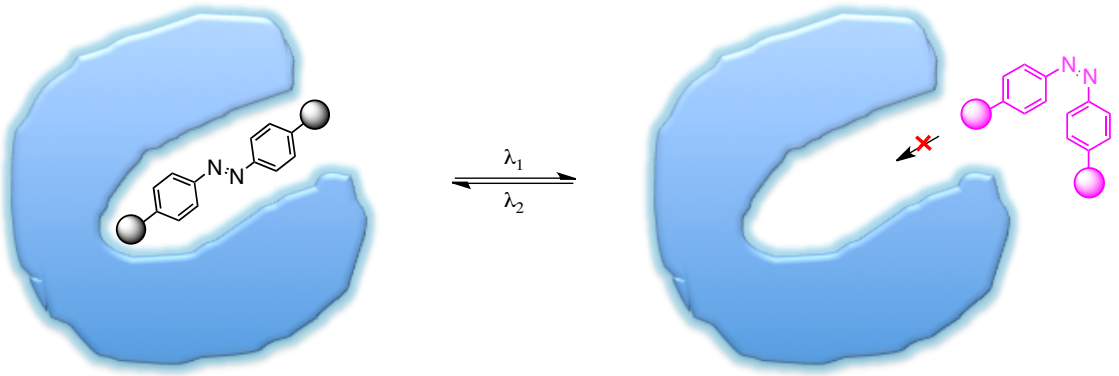

Figure 18: Representation of binding models for photoswitchable ligands (PCLs).

Apart from the non-tethered ligands (PTLs) described previously in optogenetics pharmacology, a previous known drug or drug-like bioactive can be modified to afford the photoswitchable compound, and it can be done by two main approaches: "Azo-extension" and "Azologization"[80]. Azologization approach consists in the mimetic structural motifs of certain isosteres of azobenzens commonly called "azosteres" such as stilbenes, *N*-aryl benzamides, benzyl phenyl (thio) ethers, benzyl anilines and 1,2-diaryl ethanes. One of the advantages of the azologization approach is that it can be pursued with a high level of confidence even in absence of X-ray structures. Several published photopharmaceuticals have been designed using the azologization approach (*Figure 19*)[80].

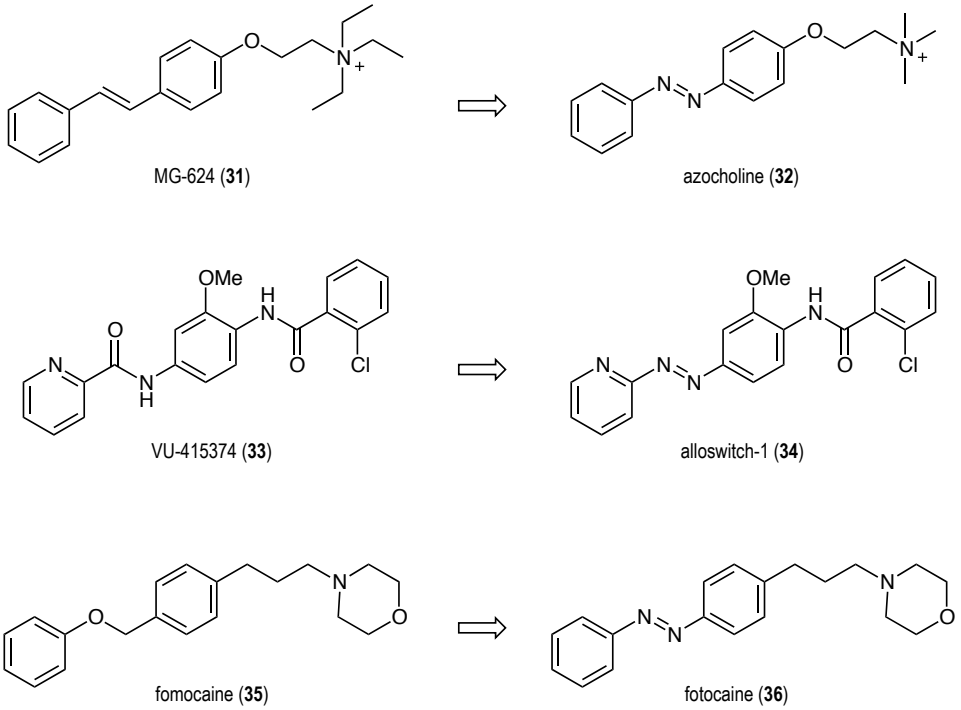

Figure 19: Structure examples of "Azologization" approach.

On the other hand, sometimes even in the absence of a clear azologization motif, photoswitchable ligands and drugs can be rationally developed with relative ease provided structure-activity tables. Often, these data have shown that certain substituents can be varied without completely abrogating the ligand's biological activity. This structural variation was called "azo-extension" strategy, which is usually associated with a change in efficacy and bodes well for a switchable substituent in the same position (*figure 20*)[80].

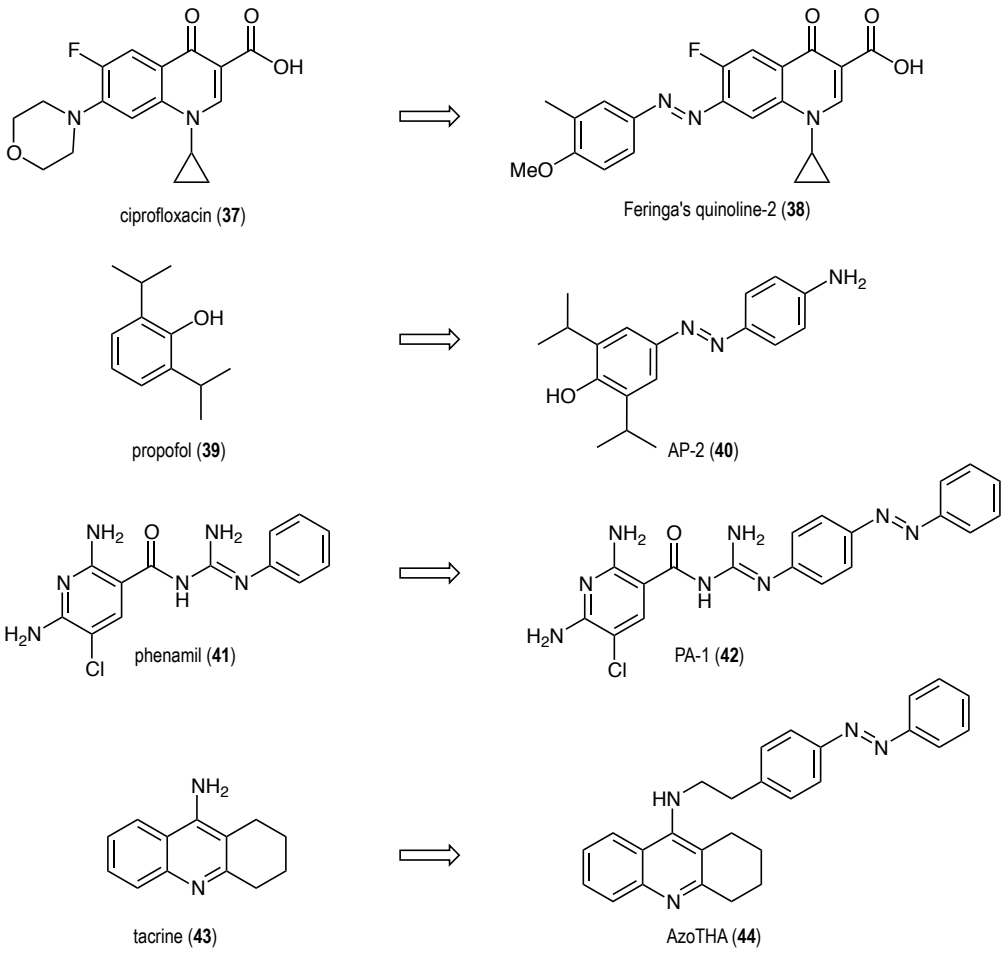

Figure 20: Structures examples of "Azo-extension" approach

Optopharmacology with cage compounds

Optopharmacology assisted by photoisomerisable compounds are reversible, and constitute a good technique for spatio-temporal control of the biological activity. Another approach in optopharmacology is based on the use of cage compounds which are constituted by

photoremovable groups that cage covalently with the active compound, preventing its biological activity and releasing it under exposure to light, broken the covalent bond in an irreversible way and losing the control after its release.

Many of this photoremovable (sometimes called photoreleasable, photocleavable or photoactivable) protecting groups (PPGs) can be used[81] and some of them have been designed for neuronal control, such as glutamate with DMNB[82], NI[82], MNI[82] or RuBi[83] for glutamate receptor, as well as GABA[84] concerning class C GPCRs, and L-enkephalin or dynorphin neurotransmitters with CNB[85] cage, for opiod receptors.

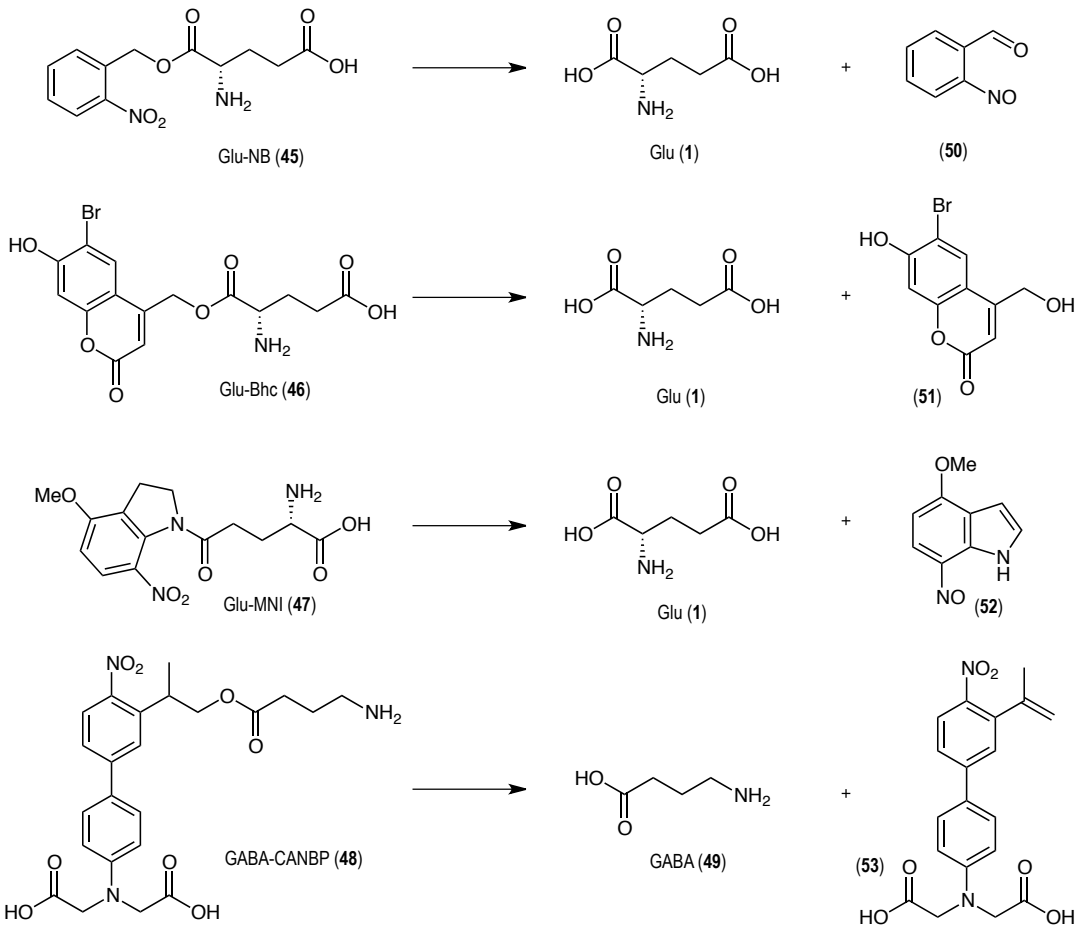

Figure 21: Examples of cage compounds for glutamate or GABA to control neuronal activity

Bibliography

1. Katritch, V.; Cherezov, V.; Stevens, R. C., Structure-function of the G protein-coupled receptor superfamily. *Annual review of pharmacology and toxicology* **2013,** *53*, 531-56.
2. Blumenthal, D. K. G., J.C. , Pharmacodynamics: Molecular mechanisms of drug action. In *The Pharmacological Basis of Therapeutics*, 12th ed.; Gilman's, G. a., Ed. Brunton, L., Ed.; McGraw Hill: New York, 2011; pp 47-72.
3. (a) Overington, J. P.; Al-Lazikani, B.; Hopkins, A. L., How many drug targets are there? *Nature reviews. Drug discovery* **2006,** *5* (12), 993-6; (b) Santos, R.; Ursu, O.; Gaulton, A.; Bento, A. P.; Donadi, R. S.; Bologa, C. G.; Karlsson, A.; Al-Lazikani, B.; Hersey, A.; Oprea, T. I.; Overington, J. P., A comprehensive map of molecular drug targets. *Nature reviews. Drug discovery* **2017,** *16* (1), 19-34.
4. Lefkowitz, R. J., A brief history of G-protein coupled receptors (Nobel Lecture). *Angewandte Chemie (International ed. in English)* **2013,** *52* (25), 6366-78.
5. Jacobson, K. A., New paradigms in GPCR drug discovery. *Biochemical pharmacology* **2015,** *98* (4), 541-55.
6. Garland, S. L., Are GPCRs still a source of new targets? *Journal of biomolecular screening* **2013,** *18* (9), 947-66.
7. Fredriksson, R.; Lagerstrom, M. C.; Lundin, L. G.; Schioth, H. B., The G-protein-coupled receptors in the human genome form five main families. Phylogenetic analysis, paralogon groups, and fingerprints. *Molecular pharmacology* **2003,** *63* (6), 1256-72.
8. GPCRs exp. crystal structures.
9. Bockaert, J.; Pin, J. P., Molecular tinkering of G protein-coupled receptors: an evolutionary success. *The EMBO journal* **1999,** *18* (7), 1723-9.
10. Milligan, G.; Kostenis, E., Heterotrimeric G-proteins: a short history. *British journal of pharmacology* **2006,** *147 Suppl 1*, S46-55.
11. Foord, S. M.; Bonner, T. I.; Neubig, R. R.; Rosser, E. M.; Pin, J. P.; Davenport, A. P.; Spedding, M.; Harmar, A. J., International Union of Pharmacology. XLVI. G protein-coupled receptor list. *Pharmacological reviews* **2005,** *57* (2), 279-88.
12. Davenport, A. P.; Alexander, S. P.; Sharman, J. L.; Pawson, A. J.; Benson, H. E.; Monaghan, A. E.; Liew, W. C.; Mpamhanga, C. P.; Bonner, T. I.; Neubig, R. R.; Pin, J. P.; Spedding, M.; Harmar, A. J., International Union of Basic and Clinical Pharmacology. LXXXVIII.

G protein-coupled receptor list: recommendations for new pairings with cognate ligands. *Pharmacological reviews* **2013,** *65* (3), 967-86.

13. Santacana, X. G. Design, synthesis and characterisation of photoswitchable allosteric modullators of metabotropic glutamate receptors. Universitat de Barcelona, 2016.

14. Palczewski, K.; Kumasaka, T.; Hori, T.; Behnke, C. A.; Motoshima, H.; Fox, B. A.; Le Trong, I.; Teller, D. C.; Okada, T.; Stenkamp, R. E.; Yamamoto, M.; Miyano, M., Crystal structure of rhodopsin: A G protein-coupled receptor. *Science (New York, N.Y.)* **2000,** *289* (5480), 739-45.

15. Cherezov, V.; Rosenbaum, D. M.; Hanson, M. A.; Rasmussen, S. G.; Thian, F. S.; Kobilka, T. S.; Choi, H. J.; Kuhn, P.; Weis, W. I.; Kobilka, B. K.; Stevens, R. C., High-resolution crystal structure of an engineered human beta2-adrenergic G protein-coupled receptor. *Science (New York, N.Y.)* **2007,** *318* (5854), 1258-65.

16. Rasmussen, S. G.; Choi, H. J.; Rosenbaum, D. M.; Kobilka, T. S.; Thian, F. S.; Edwards, P. C.; Burghammer, M.; Ratnala, V. R.; Sanishvili, R.; Fischetti, R. F.; Schertler, G. F.; Weis, W. I.; Kobilka, B. K., Crystal structure of the human beta2 adrenergic G-protein-coupled receptor. *Nature* **2007,** *450* (7168), 383-7.

17. Shonberg, J.; Kling, R. C.; Gmeiner, P.; Lober, S., GPCR crystal structures: Medicinal chemistry in the pocket. *Bioorganic & medicinal chemistry* **2015,** *23* (14), 3880-906.

18. Hoare, S. R., Mechanisms of peptide and nonpeptide ligand binding to Class B G-protein-coupled receptors. *Drug discovery today* **2005,** *10* (6), 417-27.

19. Bortolato, A.; Dore, A. S.; Hollenstein, K.; Tehan, B. G.; Mason, J. S.; Marshall, F. H., Structure of Class B GPCRs: new horizons for drug discovery. *British journal of pharmacology* **2014,** *171* (13), 3132-45.

20. Hamann, J.; Aust, G.; Arac, D.; Engel, F. B.; Formstone, C.; Fredriksson, R.; Hall, R. A.; Harty, B. L.; Kirchhoff, C.; Knapp, B.; Krishnan, A.; Liebscher, I.; Lin, H. H.; Martinelli, D. C.; Monk, K. R.; Peeters, M. C.; Piao, X.; Promel, S.; Schoneberg, T.; Schwartz, T. W.; Singer, K.; Stacey, M.; Ushkaryov, Y. A.; Vallon, M.; Wolfrum, U.; Wright, M. W.; Xu, L.; Langenhan, T.; Schioth, H. B., International Union of Basic and Clinical Pharmacology. XCIV. Adhesion G protein-coupled receptors. *Pharmacological reviews* **2015,** *67* (2), 338-67.

21. Kniazeff, J.; Prezeau, L.; Rondard, P.; Pin, J. P.; Goudet, C., Dimers and beyond: The functional puzzles of class C GPCRs. *Pharmacology & therapeutics* **2011,** *130* (1), 9-25.

22. Huang, S.; Cao, J.; Jiang, M.; Labesse, G.; Liu, J.; Pin, J. P.; Rondard, P., Interdomain movements in metabotropic glutamate receptor activation. *Proceedings of the National Academy of Sciences of the United States of America* **2011,** *108* (37), 15480-5.

23. Rondard, P.; Goudet, C.; Kniazeff, J.; Pin, J. P.; Prezeau, L., The complexity of their activation mechanism opens new possibilities for the modulation of mGlu and GABAB class C G protein-coupled receptors. *Neuropharmacology* **2011,** *60* (1), 82-92.

24. (a) Muto, T.; Tsuchiya, D.; Morikawa, K.; Jingami, H., Structures of the extracellular regions of the group II/III metabotropic glutamate receptors. *Proceedings of the National Academy of Sciences of the United States of America* **2007,** *104* (10), 3759-64; (b) Monn, J. A.; Prieto, L.; Taboada, L.; Pedregal, C.; Hao, J.; Reinhard, M. R.; Henry, S. S.; Goldsmith, P. J.; Beadle, C. D.; Walton, L.; Man, T.; Rudyk, H.; Clark, B.; Tupper, D.; Baker, S. R.; Lamas, C.; Montero, C.; Marcos, A.; Blanco, J.; Bures, M.; Clawson, D. K.; Atwell, S.; Lu, F.; Wang, J.; Russell, M.; Heinz, B. A.; Wang, X.; Carter, J. H.; Xiang, C.; Catlow, J. T.; Swanson, S.; Sanger, H.; Broad, L. M.; Johnson, M. P.; Knopp, K. L.; Simmons, R. M.; Johnson, B. G.; Shaw, D. B.; McKinzie, D. L., Synthesis and pharmacological characterization of C4-disubstituted analogs of 1S,2S,5R,6S-2-aminobicyclo[3.1.0]hexane-2,6-dicarboxylate: identification of a potent, selective metabotropic glutamate receptor agonist and determination of agonist-bound human mGlu2 and mGlu3 amino terminal domain structures. *Journal of medicinal chemistry* **2015,** *58* (4), 1776-94.

25. Christopher, J. A.; Aves, S. J.; Bennett, K. A.; Dore, A. S.; Errey, J. C.; Jazayeri, A.; Marshall, F. H.; Okrasa, K.; Serrano-Vega, M. J.; Tehan, B. G.; Wiggin, G. R.; Congreve, M., Fragment and Structure-Based Drug Discovery for a Class C GPCR: Discovery of the mGlu5 Negative Allosteric Modulator HTL14242 (3-Chloro-5-[6-(5-fluoropyridin-2-yl)pyrimidin-4-yl]benzonitrile). *Journal of medicinal chemistry* **2015,** *58* (16), 6653-64.

26. Dijksterhuis, J. P.; Petersen, J.; Schulte, G., WNT/Frizzled signalling: receptor-ligand selectivity with focus on FZD-G protein signalling and its physiological relevance: IUPHAR Review 3. *British journal of pharmacology* **2014,** *171* (5), 1195-209.

27. (a) Wu, H.; Wang, C.; Gregory, K. J.; Han, G. W.; Cho, H. P.; Xia, Y.; Niswender, C. M.; Katritch, V.; Meiler, J.; Cherezov, V.; Conn, P. J.; Stevens, R. C., Structure of a class C GPCR metabotropic glutamate receptor 1 bound to an allosteric modulator. *Science (New York, N.Y.)* **2014,** *344* (6179), 58-64; (b) Wang, C.; Wu, H.; Katritch, V.; Han, G. W.; Huang, X. P.; Liu, W.; Siu, F. Y.; Roth, B. L.; Cherezov, V.; Stevens, R. C., Structure of the human smoothened receptor bound to an antitumour agent. *Nature* **2013,** *497* (7449), 338-43.

28. Koval, A.; Purvanov, V.; Egger-Adam, D.; Katanaev, V. L., Yellow submarine of the Wnt/Frizzled signaling: submerging from the G protein harbor to the targets. *Biochemical pharmacology* **2011,** *82* (10), 1311-9.

29. Wang, C.; Wu, H.; Evron, T.; Vardy, E.; Han, G. W.; Huang, X. P.; Hufeisen, S. J.; Mangano, T. J.; Urban, D. J.; Katritch, V.; Cherezov, V.; Caron, M. G.; Roth, B. L.; Stevens, R. C., Structural basis for Smoothened receptor modulation and chemoresistance to anticancer drugs. *Nature communications* **2014,** *5*, 4355.

30. Volk, L.; Chiu, S. L.; Sharma, K.; Huganir, R. L., Glutamate synapses in human cognitive disorders. *Annual review of neuroscience* **2015,** *38*, 127-49.

31. Traynelis, S. F.; Wollmuth, L. P.; McBain, C. J.; Menniti, F. S.; Vance, K. M.; Ogden, K. K.; Hansen, K. B.; Yuan, H.; Myers, S. J.; Dingledine, R., Glutamate receptor ion channels: structure, regulation, and function. *Pharmacological reviews* **2010,** *62* (3), 405-96.

32. Collingridge, G. L.; Olsen, R. W.; Peters, J.; Spedding, M., A nomenclature for ligand-gated ion channels. *Neuropharmacology* **2009,** *56* (1), 2-5.

33. Doumazane, E.; Scholler, P.; Fabre, L.; Zwier, J. M.; Trinquet, E.; Pin, J. P.; Rondard, P., Illuminating the activation mechanisms and allosteric properties of metabotropic glutamate receptors. *Proceedings of the National Academy of Sciences of the United States of America* **2013,** *110* (15), E1416-25.

34. El Moustaine, D.; Granier, S.; Doumazane, E.; Scholler, P.; Rahmeh, R.; Bron, P.; Mouillac, B.; Baneres, J. L.; Rondard, P.; Pin, J. P., Distinct roles of metabotropic glutamate receptor dimerization in agonist activation and G-protein coupling. *Proceedings of the National Academy of Sciences of the United States of America* **2012,** *109* (40), 16342-7.

35. Pin, J. P.; De Colle, C.; Bessis, A. S.; Acher, F., New perspectives for the development of selective metabotropic glutamate receptor ligands. *European journal of pharmacology* **1999,** *375* (1-3), 277-94.

36. Nicoletti, F.; Bockaert, J.; Collingridge, G. L.; Conn, P. J.; Ferraguti, F.; Schoepp, D. D.; Wroblewski, J. T.; Pin, J. P., Metabotropic glutamate receptors: from the workbench to the bedside. *Neuropharmacology* **2011,** *60* (7-8), 1017-41.

37. Sheffler, D. J.; Gregory, K. J.; Rook, J. M.; Conn, P. J., Allosteric modulation of metabotropic glutamate receptors. *Advances in pharmacology (San Diego, Calif.)* **2011,** *62*, 37-77.

38. (a) Linden, A. M.; Shannon, H.; Baez, M.; Yu, J. L.; Koester, A.; Schoepp, D. D., Anxiolytic-like activity of the mGLU2/3 receptor agonist LY354740 in the elevated plus maze test is disrupted in metabotropic glutamate receptor 2 and 3 knock-out mice. *Psychopharmacology* **2005,** *179* (1), 284-91; (b) Morishima, Y.; Miyakawa, T.; Furuyashiki, T.; Tanaka, Y.; Mizuma, H.; Nakanishi, S., Enhanced cocaine responsiveness and impaired motor coordination in

metabotropic glutamate receptor subtype 2 knockout mice. *Proceedings of the National Academy of Sciences of the United States of America* **2005,** *102* (11), 4170-5.

39. Gerlai, R.; Roder, J. C.; Hampson, D. R., Altered spatial learning and memory in mice lacking the mGluR4 subtype of metabotropic glutamate receptor. *Behavioral neuroscience* **1998,** *112* (3), 525-32.

40. Cryan, J. F.; Kelly, P. H.; Neijt, H. C.; Sansig, G.; Flor, P. J.; van Der Putten, H., Antidepressant and anxiolytic-like effects in mice lacking the group III metabotropic glutamate receptor mGluR7. *The European journal of neuroscience* **2003,** *17* (11), 2409-17.

41. Tong, Q.; Kirchgessner, A. L., Localization and function of metabotropic glutamate receptor 8 in the enteric nervous system. *American journal of physiology. Gastrointestinal and liver physiology* **2003,** *285* (5), G992-g1003.

42. Sugihara, H.; Inoue, T.; Nakanishi, S.; Fukuda, Y., A late ON response remains in visual response of the mGluR6-deficient mouse. *Neuroscience letters* **1997,** *233* (2-3), 137-40.

43. Flor, P. J.; Acher, F. C., Orthosteric versus allosteric GPCR activation: the great challenge of group-III mGluRs. *Biochemical pharmacology* **2012,** *84* (4), 414-24.

44. Goudet, C.; Vilar, B.; Courtiol, T.; Deltheil, T.; Bessiron, T.; Brabet, I.; Oueslati, N.; Rigault, D.; Bertrand, H. O.; McLean, H.; Daniel, H.; Amalric, M.; Acher, F.; Pin, J. P., A novel selective metabotropic glutamate receptor 4 agonist reveals new possibilities for developing subtype selective ligands with therapeutic potential. *FASEB journal : official publication of the Federation of American Societies for Experimental Biology* **2012,** *26* (4), 1682-93.

45. Tora, A. S.; Rovira, X.; Dione, I.; Bertrand, H. O.; Brabet, I.; De Koninck, Y.; Doyon, N.; Pin, J. P.; Acher, F.; Goudet, C., Allosteric modulation of metabotropic glutamate receptors by chloride ions. *FASEB journal : official publication of the Federation of American Societies for Experimental Biology* **2015,** *29* (10), 4174-88.

46. Conn, P. J.; Lindsley, C. W.; Meiler, J.; Niswender, C. M., Opportunities and challenges in the discovery of allosteric modulators of GPCRs for treating CNS disorders. *Nature reviews. Drug discovery* **2014,** *13* (9), 692-708.

47. Conn, P. J.; Christopoulos, A.; Lindsley, C. W., Allosteric modulators of GPCRs: a novel approach for the treatment of CNS disorders. *Nature reviews. Drug discovery* **2009,** *8* (1), 41-54.

48. Maj, M.; Bruno, V.; Dragic, Z.; Yamamoto, R.; Battaglia, G.; Inderbitzin, W.; Stoehr, N.; Stein, T.; Gasparini, F.; Vranesic, I.; Kuhn, R.; Nicoletti, F.; Flor, P. J., (-)-PHCCC, a positive allosteric modulator of mGluR4: characterization, mechanism of action, and neuroprotection. *Neuropharmacology* **2003,** *45* (7), 895-906.

49. Kohara, A.; Toya, T.; Tamura, S.; Watabiki, T.; Nagakura, Y.; Shitaka, Y.; Hayashibe, S.; Kawabata, S.; Okada, M., Radioligand binding properties and pharmacological characterization of 6-amino-N-cyclohexyl-N,3-dimethylthiazolo[3,2-a]benzimidazole-2-carboxamide (YM-298198), a high-affinity, selective, and noncompetitive antagonist of metabotropic glutamate receptor type 1. *The Journal of pharmacology and experimental therapeutics* **2005,** *315* (1), 163-9.

50. Satow, A.; Maehara, S.; Ise, S.; Hikichi, H.; Fukushima, M.; Suzuki, G.; Kimura, T.; Tanak, T.; Ito, S.; Kawamoto, H.; Ohta, H., Pharmacological effects of the metabotropic glutamate receptor 1 antagonist compared with those of the metabotropic glutamate receptor 5 antagonist and metabotropic glutamate receptor 2/3 agonist in rodents: detailed investigations with a selective allosteric metabotropic glutamate receptor 1 antagonist, FTIDC [4-[1-(2-fluoropyridine-3-yl)-5-methyl-1H-1,2,3-triazol-4-yl]-N-isopropyl-N-methy l-3,6-dihydropyridine-1(2H)-carboxamide]. *The Journal of pharmacology and experimental therapeutics* **2008,** *326* (2), 577-86.

51. Neugebauer, V.; Chen, P. S.; Willis, W. D., Role of metabotropic glutamate receptor subtype mGluR1 in brief nociception and central sensitization of primate STT cells. *Journal of neurophysiology* **1999,** *82* (1), 272-82.

52. Marin, J. C.; Goadsby, P. J., Glutamatergic fine tuning with ADX-10059: a novel therapeutic approach for migraine? *Expert opinion on investigational drugs* **2010,** *19* (4), 555-61.

53. Cavallone, L., Fenobam on Heat/Capsaicin Induced Hyperalgesia in Healthy Volunteers.

54. Spooren, W.; Gasparini, F., mGlu5 receptor antagonists: a novel class of anxiolytics? *Drug news & perspectives* **2004,** *17* (4), 251-7.

55. Li, X.; Need, A. B.; Baez, M.; Witkin, J. M., Metabotropic glutamate 5 receptor antagonism is associated with antidepressant-like effects in mice. *The Journal of pharmacology and experimental therapeutics* **2006,** *319* (1), 254-9.

56. Dolen, G.; Carpenter, R. L.; Ocain, T. D.; Bear, M. F., Mechanism-based approaches to treating fragile X. *Pharmacology & therapeutics* **2010,** *127* (1), 78-93.

57. Yan, Q. J.; Rammal, M.; Tranfaglia, M.; Bauchwitz, R. P., Suppression of two major Fragile X Syndrome mouse model phenotypes by the mGluR5 antagonist MPEP. *Neuropharmacology* **2005,** *49* (7), 1053-66.

58. Luby, E. D.; Cohen, B. D.; Rosenbaum, G.; Gottlieb, J. S.; Kelley, R., Study of a new schizophrenomimetic drug; sernyl. *A.M.A. archives of neurology and psychiatry* **1959,** *81* (3), 363-9.

59. Homayoun, H.; Stefani, M. R.; Adams, B. W.; Tamagan, G. D.; Moghaddam, B., Functional Interaction Between NMDA and mGlu5 Receptors: Effects on Working Memory, Instrumental Learning, Motor Behaviors, and Dopamine Release. *Neuropsychopharmacology : official publication of the American College of Neuropsychopharmacology* **2004,** *29* (7), 1259-69.

60. Doherty, J. J.; Alagarsamy, S.; Bough, K. J.; Conn, P. J.; Dingledine, R.; Mott, D. D., Metabotropic glutamate receptors modulate feedback inhibition in a developmentally regulated manner in rat dentate gyrus. *The Journal of physiology* **2004,** *561* (Pt 2), 395-401.

61. Marek, G. J., Metabotropic glutamate2/3 (mGlu2/3) receptors, schizophrenia and cognition. *European journal of pharmacology* **2010,** *639* (1-3), 81-90.

62. Fell, M. J.; Katner, J. S.; Johnson, B. G.; Khilevich, A.; Schkeryantz, J. M.; Perry, K. W.; Svensson, K. A., Activation of metabotropic glutamate (mGlu)2 receptors suppresses histamine release in limbic brain regions following acute ketamine challenge. *Neuropharmacology* **2010,** *58* (3), 632-9.

63. Adewale, A. S.; Platt, D. M.; Spealman, R. D., Pharmacological stimulation of group ii metabotropic glutamate receptors reduces cocaine self-administration and cocaine-induced reinstatement of drug seeking in squirrel monkeys. *The Journal of pharmacology and experimental therapeutics* **2006,** *318* (2), 922-31.

64. Nicoletti, F.; Bruno, V.; Copani, A.; Casabona, G.; Knopfel, T., Metabotropic glutamate receptors: a new target for the therapy of neurodegenerative disorders? *Trends in neurosciences* **1996,** *19* (7), 267-71.

65. Bruno, V.; Battaglia, G.; Casabona, G.; Copani, A.; Caciagli, F.; Nicoletti, F., Neuroprotection by glial metabotropic glutamate receptors is mediated by transforming growth factor-beta. *The Journal of neuroscience : the official journal of the Society for Neuroscience* **1998,** *18* (23), 9594-600.

66. Corti, C.; Battaglia, G.; Molinaro, G.; Riozzi, B.; Pittaluga, A.; Corsi, M.; Mugnaini, M.; Nicoletti, F.; Bruno, V., The use of knock-out mice unravels distinct roles for mGlu2 and mGlu3 metabotropic glutamate receptors in mechanisms of neurodegeneration/neuroprotection. *The Journal of neuroscience : the official journal of the Society for Neuroscience* **2007,** *27* (31), 8297-308.

67. Caraci, F.; Molinaro, G.; Battaglia, G.; Giuffrida, M. L.; Riozzi, B.; Traficante, A.; Bruno, V.; Cannella, M.; Merlo, S.; Wang, X.; Heinz, B. A.; Nisenbaum, E. S.; Britton, T. C.; Drago, F.; Sortino, M. A.; Copani, A.; Nicoletti, F., Targeting group II metabotropic glutamate (mGlu) receptors for the treatment of psychosis associated with Alzheimer's disease: selective activation

of mGlu2 receptors amplifies beta-amyloid toxicity in cultured neurons, whereas dual activation of mGlu2 and mGlu3 receptors is neuroprotective. *Molecular pharmacology* **2011,** *79* (3), 618-26.

68. Macinnes, N.; Duty, S., Group III metabotropic glutamate receptors act as hetero-receptors modulating evoked GABA release in the globus pallidus in vivo. *European journal of pharmacology* **2008,** *580* (1-2), 95-9.

69. Marino, M. J.; Williams, D. L., Jr.; O'Brien, J. A.; Valenti, O.; McDonald, T. P.; Clements, M. K.; Wang, R.; DiLella, A. G.; Hess, J. F.; Kinney, G. G.; Conn, P. J., Allosteric modulation of group III metabotropic glutamate receptor 4: a potential approach to Parkinson's disease treatment. *Proceedings of the National Academy of Sciences of the United States of America* **2003,** *100* (23), 13668-73.

70. Kleinlogel, S.; Terpitz, U.; Legrum, B.; Gokbuget, D.; Boyden, E. S.; Bamann, C.; Wood, P. G.; Bamberg, E., A gene-fusion strategy for stoichiometric and co-localized expression of light-gated membrane proteins. *Nature methods* **2011,** *8* (12), 1083-8.

71. Boyden, E. S.; Zhang, F.; Bamberg, E.; Nagel, G.; Deisseroth, K., Millisecond-timescale, genetically targeted optical control of neural activity. *Nature neuroscience* **2005,** *8* (9), 1263-8.

72. Kramer, R. H.; Mourot, A.; Adesnik, H., Optogenetic pharmacology for control of native neuronal signaling proteins. *Nature neuroscience* **2013,** *16* (7), 816-23.

73. Fehrentz, T.; Schonberger, M.; Trauner, D., Optochemical genetics. *Angewandte Chemie (International ed. in English)* **2011,** *50* (51), 12156-82.

74. Levitz, J.; Pantoja, C.; Gaub, B.; Janovjak, H.; Reiner, A.; Hoagland, A.; Schoppik, D.; Kane, B.; Stawski, P.; Schier, A. F.; Trauner, D.; Isacoff, E. Y., Optical control of metabotropic glutamate receptors. *Nature neuroscience* **2013,** *16* (4), 507-16.

75. Bartels, E.; Wassermann, N. H.; Erlanger, B. F., Photochromic activators of the acetylcholine receptor. *Proceedings of the National Academy of Sciences of the United States of America* **1971,** *68* (8), 1820-3.

76. Izquierdo-Serra, M.; Gascon-Moya, M.; Hirtz, J. J.; Pittolo, S.; Poskanzer, K. E.; Ferrer, E.; Alibes, R.; Busque, F.; Yuste, R.; Hernando, J.; Gorostiza, P., Two-photon neuronal and astrocytic stimulation with azobenzene-based photoswitches. *Journal of the American Chemical Society* **2014,** *136* (24), 8693-701.

77. Banghart, M. R.; Mourot, A.; Fortin, D. L.; Yao, J. Z.; Kramer, R. H.; Trauner, D., Photochromic blockers of voltage-gated potassium channels. *Angewandte Chemie (International ed. in English)* **2009,** *48* (48), 9097-101.

78. Fortin, D. L.; Banghart, M. R.; Dunn, T. W.; Borges, K.; Wagenaar, D. A.; Gaudry, Q.; Karakossian, M. H.; Otis, T. S.; Kristan, W. B.; Trauner, D.; Kramer, R. H., Photochemical control of endogenous ion channels and cellular excitability. *Nature methods* **2008,** *5* (4), 331-8.

79. Sandoz, G.; Levitz, J.; Kramer, R. H.; Isacoff, E. Y., Optical control of endogenous proteins with a photoswitchable conditional subunit reveals a role for TREK1 in GABA(B) signaling. *Neuron* **2012,** *74* (6), 1005-14.

80. Broichhagen, J.; Frank, J. A.; Trauner, D., A roadmap to success in photopharmacology. *Accounts of chemical research* **2015,** *48* (7), 1947-60.

81. Klan, P.; Solomek, T.; Bochet, C. G.; Blanc, A.; Givens, R.; Rubina, M.; Popik, V.; Kostikov, A.; Wirz, J., Photoremovable protecting groups in chemistry and biology: reaction mechanisms and efficacy. *Chemical reviews* **2013,** *113* (1), 119-91.

82. Donato, L.; Mourot, A.; Davenport, C. M.; Herbivo, C.; Warther, D.; Leonard, J.; Bolze, F.; Nicoud, J. F.; Kramer, R. H.; Goeldner, M.; Specht, A., Water-soluble, donor-acceptor biphenyl derivatives in the 2-(o-nitrophenyl)propyl series: highly efficient two-photon uncaging of the neurotransmitter gamma-aminobutyric acid at lambda = 800 nm. *Angewandte Chemie (International ed. in English)* **2012,** *51* (8), 1840-3.

83. Fino, E.; Araya, R.; Peterka, D. S.; Salierno, M.; Etchenique, R.; Yuste, R., RuBi-Glutamate: Two-Photon and Visible-Light Photoactivation of Neurons and Dendritic spines. *Frontiers in neural circuits* **2009,** *3*, 2.

84. Rial Verde, E. M.; Zayat, L.; Etchenique, R.; Yuste, R., Photorelease of GABA with Visible Light Using an Inorganic Caging Group. *Frontiers in neural circuits* **2008,** *2*, 2.

85. Schonberger, M.; Trauner, D., A photochromic agonist for mu-opioid receptors. *Angewandte Chemie (International ed. in English)* **2014,** *53* (12), 3264-7.

Objectives

Objectives

In classical pharmacology, the use of current analgesic drugs is limited, in a significant proportion of patients, by lack of efficacy, development of tolerance, and sometimes life-threatening, adverse effects that originate from systemic actions of analgesic drugs. It's with this backdrop that, several groups have tried to avoid this side effects by targeting agents to precise locations in that area, and this strategy has proved challenging, sometimes resulting in serious side effects.

With this background in mind, we think that the use of light in optopharmacology applied, for example, in allosteric modulators for mGlu receptors could display a higher selectivity and offers a potential gain to spatiotemporal control in the corresponding receptors.

As I have previously commented metabotropic glutamate receptors are widely distributed along the pain neuraxis and modulate pain transmission. Hence, subtype-selective mGlu receptor ligands are considered as promising candidate drugs for the treatment of pain. Accordingly, selective negative allosteric modulators (NAMs) of $mGlu_1$ or $mGlu_5$ receptors, and agonists or positive allosteric modulators (PAMs) of $mGlu_4$ receptors have consistently been shown to display analgesic activity in experimental animal models of chronic pain.

Taking into account all what we have stated above I initiated my thesis-work with the following goals and ***objectives***:

1) **Design** and **synthesis** of new series of photoisomerisable metabotropic glutamate receptors subtype 4 PAMs, and metabotropic glutamate receptors subtype 5 NAMs (since they are indicated for treatment of pain), based in a "*cis-on*" approach, which means that the *cis*-isomer produce the bioactive effect into the receptor while the *trans*-isomer is inactive. In parallel with this, we will develop an evaluation of **photochemical properties** and a **pharmacological characterisation** of all compounds to further evaluation for those compounds showing interesting activities.

2) **Design** and **synthesis** of new irreversibly photoactivatable ligands (cage compounds), based in the structural modification of previous described drugs of $mGlu_1$ NAMs, $mGlu_4$ PAMs and $mGlu_5$ NAMs receptors that are involved in the pain transmission, to establish

the advantages and disadvantages respect to photoswitchable ligands. With these compounds in our hands, a full **photochemical characterisation** and uncaging will beperformed, as well as a cell **pharmacological evaluation** to bring the compounds to ***in-vivo*** assays assisted by light. We will finally extrapolate this method to drugs already in clinical use, targeting μ-opiod receptors one of the most relevant receptors in pain treatment.

Chapter 1

Chapter 1: Photoswitchable compounds with a *Cis-on* approach

As I mentioned before, the first objective in this thesis was to design and synthesize a new series of photoisomerisable metabotropic glutamate receptors subtype 4 PAMs and metabotropic glutamate receptors subtype 5 NAMs (since they are indicated for treatment of pain), based in a "*cis-on*" approach, which means the *cis*-isomer is producing the bioactive effect into the receptor while the *trans*-isomer is inactive; this objective include, as well, its photoisomerisation and pharmacological characterisation following, previous work carried out in Xavier Gomez Santacana's thesis at MCS group.

In this chapter we expose the results related to these objectives and their corresponding discussion.

Introduction

Azobenzenes

Azobenzene consists in a diazene (HN=NH) derivative where both hydrogens are replaced by phenyl, pyridine or other aromatic rings that are commonly known as azobenzenes, phenylazopyridines and azopyridines respectively. They are the most common photoswitchable molecules used in biological and material applications. Their synthesis is relatively easy and can offer a large functional variety with diverse chemical, photophysical and physiological properties[1].

Azobenzene and its derivatives can exist in either the *cis* or *trans* configurations. The *trans* to *cis* isomerization occurs following irradiation with UV-visible light, mechanical stress[2] or electrostatic stimulation[3]. Thermal *cis* to *trans* isomerization occurs spontaneously in the dark owing to the thermodynamic stability of the *trans*-isomer.

Azobenzene *trans*-isomers have usually a planar geometry with a dihedral angle of 180º and an extended delocalization of the π-electrons over the aromatic rings and the azo-bond also has a negligible dipolar moment. On the other hand, the *cis*-isomer has a bent geometry, is about 3 Å shorter than the *trans* one, with its phenyl rings twisted 55º out of the plane and a dihedral angle of the azo-bond of 11º and a dipolar moment of 3.7 Debye. The consequence of this geometry is the rupture of the π delocalization on the azo-bond[4].

This rupture of delocalization in *cis* isomer is producing a clearly distinct but overlapping absorption spectra (*Figure 22*) respect the *trans* isomer.

Whereas *trans*-azobenzene displays a weak signal corresponding to n- π^* band within 430-440 nm and strong π - π^* transition near 320 nm, the *cis*-azobenzene shows a strong transition n- π^* also within 430-440 nm and a weak signal from π- π^* bands at 280 and 250 nm.

Taking in account that *trans*-isomer is 10-12 Kcal/mol more stable than *cis*-isomer; there is a high predominance of *trans*-isomer in equilibrium in dark conditions[4].

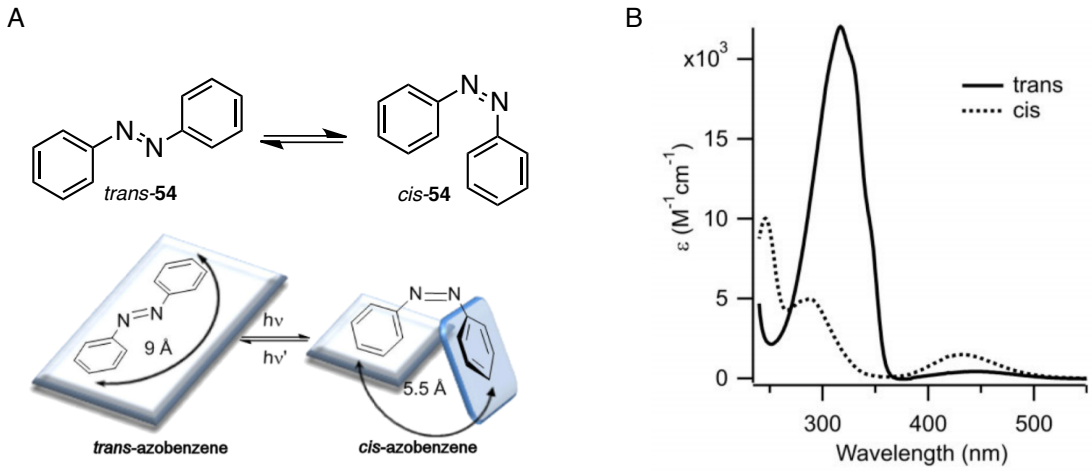

Figure 22: A) Structure of both isomers in 2D and 3D representation B) UV-Vis absorption spectrum of both isomers.

Ring substitution produce changes on the absorption, emission and photochemical properties of azobenzenes. Substituents also have the ability to make the *cis* isomer more thermodynamically stable than the *trans* isomer in some specific cases. From the perspective of the explotation of their photochemical properties, azobenzenes can be divided into three main families[1]: Azobenzenes (ABn), aminoazobenzenes (aAB) and push-pull azobenzenes (ppAZ).

Azobenzenes (ABn)

The azobenzene family consists in all the azobenzenes substituted with electron withdrawing groups (EWG) or mild electron donanting group (EDG), such as alkyl, aryl, halide, carbonyl carboxylic acid, amide, nitrile, nitro, or even amino and alkoxy in 2,4-substitution, including azopyridines and phenylazopyridines as aromatic rings.

The absorption spectra are similar to the unsubstituted azobenzene and are applied mainly in protein probes and molecular machines[1].

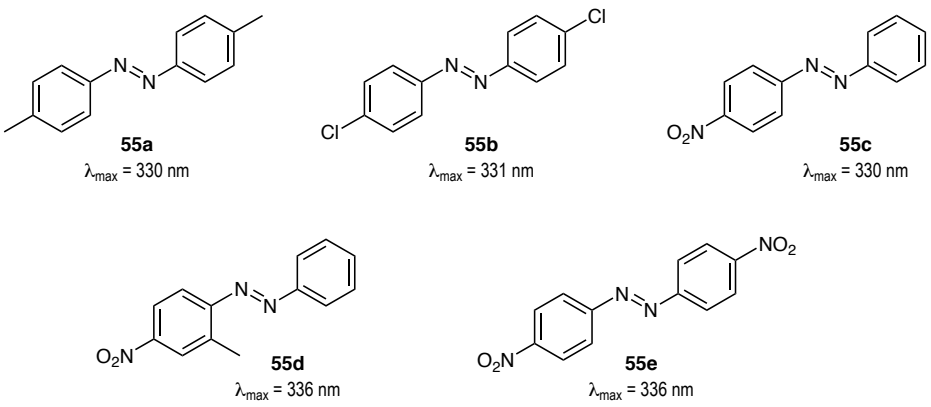

Figure 23: Some examples of Azobenzenes family (ABn)

Aminobenzenes (aAB)

The Aminoazobenzene family consists in those azobenzenes with one or more 2,4-substitution with amine, methoxy or hydroxyl groups. The electron donating group (EDG) shift the transition π-π* band to higher wavelengths and overlaps with the n-π* transition. This overlap between the two transitions depends on the number of amino substituents, degree of amine alkylation, and solvent polarity[1].

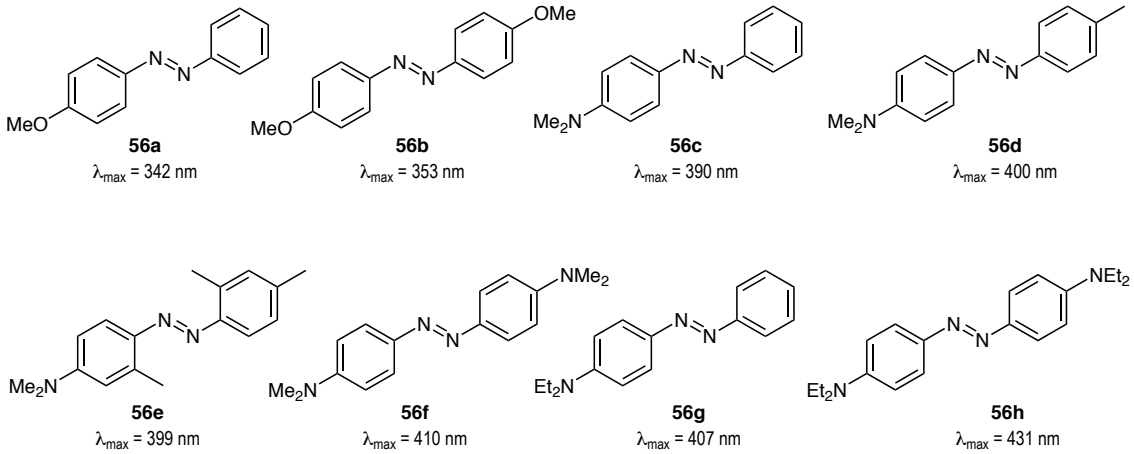

Figure 24: Some examples of Aminoazobenzenes family (aAB)

Many aminoazobenzenes are intensely coloured and are used in industry as dyes, pH indicators and metal ion indicators. Some compounds are potent carcinogens and are known to induce tumours in animal models[5]. They have also found applications in photoelectric and information devices or photoresponsive polymers.

Push-pull azobenzenes (ppAB)

They are composed of one strong electron donor and strong electron acceptor occupying usually the 4 and 4' position in the aromatic rings, but also position 2 and 2' can display this strong electronic effect. The donor-acceptor pairs can be also present in 2- or 4-pyridine or 2- or 4-methylpyridinium salts increasing the push-pull effect and reducing, at the same time, the relaxation half-life time.

Recent theoretical and experimental evidence in the push-pull azobenzenes (ppAZ), suggests that the n-π* state is clearly in lower energy than the π-π* state[6].

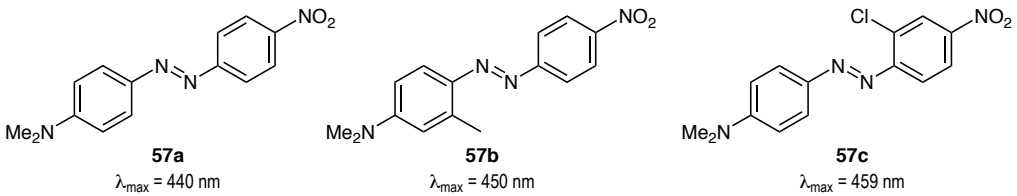

Figure 25: Some examples of push-pull azobenzenes family (ppAZ)

Other singular azobenzenes

Other azobenzenes to be considered in relation to their interesting photochemical properties and red-shifted isomerization wavelenghts are the tetra-*o*-substituted azobenzenes (toAB). The substitution in aromatic rings in this type of azobenzenes are 2, 6, 2', and 6', usually with methoxy or halogen groups. The toAB azobenzene isomerisation can be achieved from *trans* to *cis* isomer using green to red light illumination, and the back isomerisation with blue light.

Another remarkable group of azobenzenes are the bridged azobenzene (bAB). This class display an inverse photoisomerisation, since the *cis* isomer is thermally more stable than *trans* isomer, photoswitching *trans* to *cis* isomer at 500 nm and the back isomerisation from 370 to 400 nm[7].

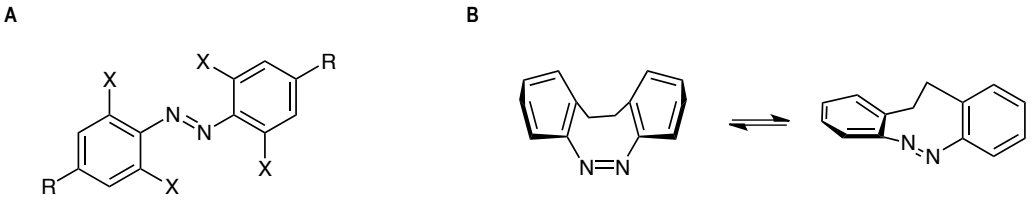

Figure 26: Structures of A) toAB and B) bAB

Alloswitch-1 and Optogluram: First trans-on allosteric modulators of mGluRs

With the objective of modulate metabotropic glutamate receptors focusing in $mGlu_4$ or $mGlu_5$ subtypes for potential treatment of pain, our group initiated this project five years ago. Initially, Dr. Xavier Gomez developed this task in his doctoral thesis.

In this work is described the first series of azobenzenes synthetized by our group, among of them, as I mentioned before, it is possible to found some photoisomerisable positive allosteric modulator (PAM) of $mGlu_5$, through azologisation[8]. Azologization is a term introduced by Trauner and collaborators[9] to describe the design of azobenzene biologically active compounds from other molecules no containing this group. In this way we can design an azobenzene candidate compound from the SAR studies on conventional ligands, expecting to preserve the molecular recognition in the receptor and adding the phoisomerization properties of azobenzene to the resulting molecule. The literature described several promising compounds, however, we opted for the well known $mGlu_4$ PAM VU0415374 (**33**)[10] because its potency (EC_{50} around 100 nM), its apparently easy synthesis, and especially for the presence of two amides between the aromatic rings, which were susceptible to be replaced by two azo groups to give relatively similar molecules[11].

Dr. Gomez´s thesis describe the replacement of the picolinic amide present in compound (**33**), replacement that allowed him to obtaining compound (**34**), this compound was named as alloswitch-1. In the same thesis is also described the same approach modifying the amide between the 2-chlorophenyl and the methoxyphenyl moiety, compound (**59**), and referred as optogluram.

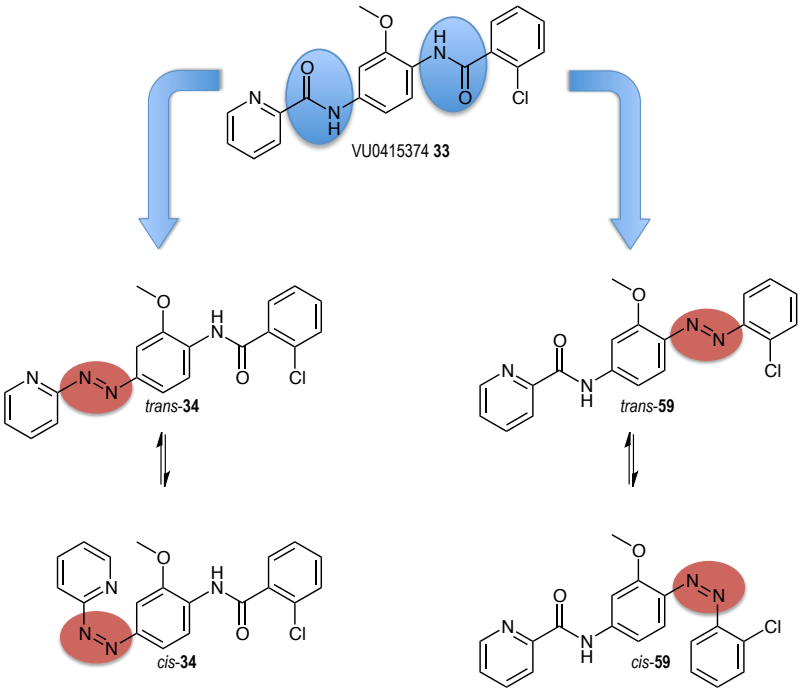

Figure 27: Azologisation approach of VU0415374 **33** to afford the azobenzene compounds **34** and **59**.

The next step was to pharmacologically characterise azobenzene compounds (**34** and **59**) and the reference molecule VU0415374 (**33**) by using inositol phosphate accumulation assay (IP-One) in $mGlu_4$ cell assays. Unfortunately, this first assay failed for compound **34**, which was completely inactive in mGlu4, in contrast, compound **59** was active as $mGlu_4$ PAM but with lower potency than the reference compound **33**.

Interestingly, compound **34** has a pyridine-azo-phenyl bond scaffold structurally related to compounds MPEP (**7**) or SIB-1757 (**13**), which are well known $mGlu_5$ NAMs[12]. For this reason, compounds **34** and **59** were also evaluated in $mGlu_5$ *in-vitro* using the IP-One cell assay in dark conditions and using quisqualate (**2**) as selective orthosteric ligand. Strikingly, it was found that alloswitch-1 (**34**) was an excellent $mGlu_5$ NAM with potency in the nanomolar range.

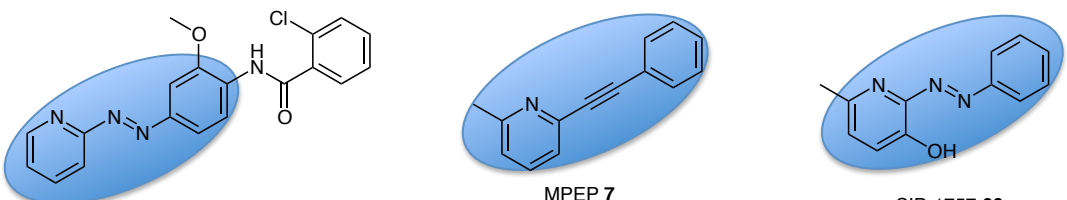

Figure 28: Comparison of alloswitch-1 (**34**) structure with MPEP (**7**) and SIB-1757 (**60**)

A more complete pharmacological characterisation was then performed evaluating the potency of alloswitch-1 (**34**) in $mGlu_5$ transfected cells by IP-One assay in dark conditions and under irradiation, showing a similar potency for the non-illuminated assay (IC_{50}=25 nM) in comparison with fenobam (**19**) a light inactive $mGlu_5$ NAM, and the potency for the illuminated ones was around 100-fold shifted, obtaining the first photoswitchable $mGlu_5$ NAM with a potency and selectivity not described for a GPCR before.

Afterwards, it was investigated compound **59** (optogluram) as PAM of $mGlu_4$. Despite its lower activity in comparison with VU0364770 (**58**), it could be also a good candidate for a suitable photoswitchable PAM of $mGlu_4$.

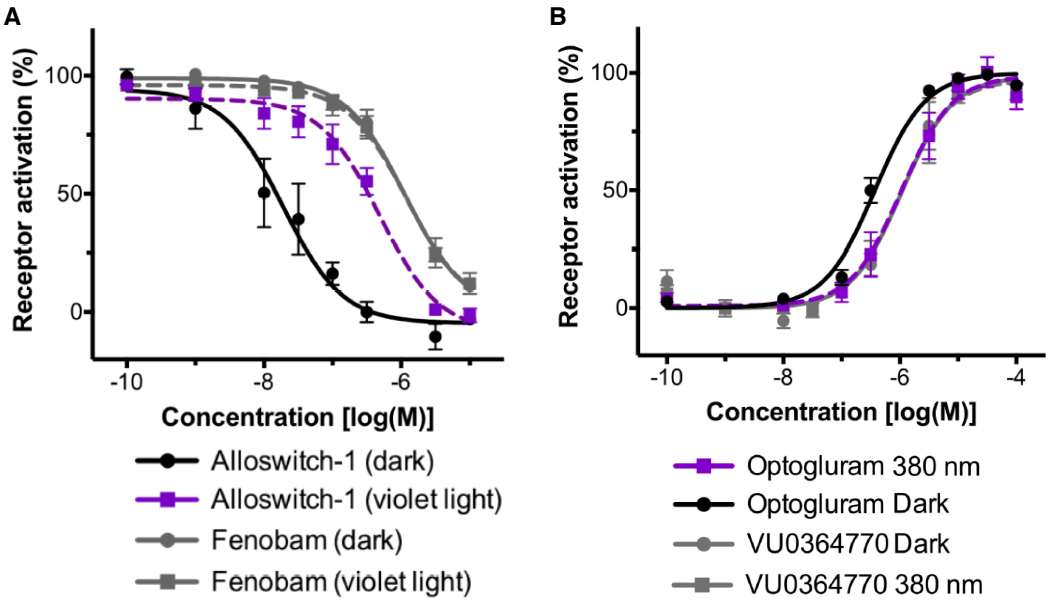

Figure 29: Dose-response curves evaluation by IP accumulation assay. A) Dose-response of Alloswitch-1. B) Dose-response of Optogluram.

Both compounds were also tested in mice and zebrafish to evaluate light-dependent behavioural responses, having unprecedented light-dependent effects *in vivo*[13].

Other series of *trans-on* azocompounds for mGluRs modulation

Several azocompounds were synthesized in Xavier Gomez's thesis for the modulation of metabotropic glutamate receptors. He presented a new series of phenylazopyridines related to alloswitch-1 (**34**), useful to obtain a fine control of $mGlu_5$ function with light[13].

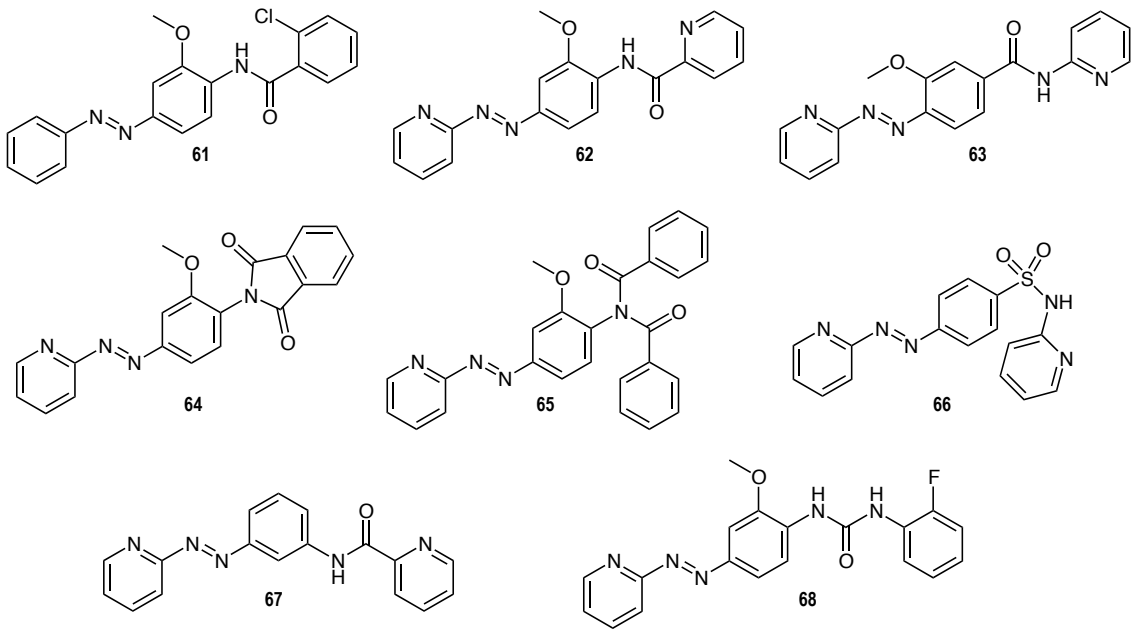

Figure 30: Some examples of phenylazopyridines series designed related to alloswitch-1 (**34**)[13].

Similarly, he describes a new series of compounds (*Figure 31*) based in the structure of alloswicth-1 **34** and optogluram **59** (*Figure 30*), which differ only in the position of methoxy group, but displays different pharmacological profiles. The main objective with this new series was to explore new chemical patterns to obtain dual $mGlu_4$ PAM and $mGlu_5$ NAM compounds that would be attractive to explore its potential synergic effects in native brain cells and that could have potential for the treatment of neurodegenerative diseases such as Parkinson disease, neuropathic pain or inflammatory pain[13].

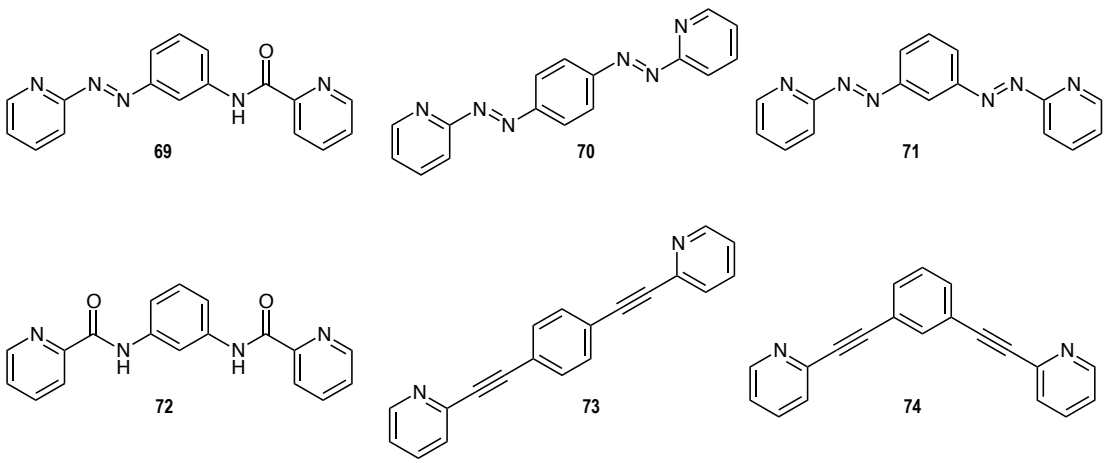

Figure 31: Some examples of the new series of compounds[13].

The *Cis-On* compounds, a new type of photoswitch with potential for therapeutic use.

All photoswitchable compounds previously described in X.Gomez's thesis were active in their *trans* configuration, which is thermodynamically the more stable isomer. The irradiation with violet light allows us to achieve the *cis* configuration with a loss of their biological activity.
This approach lead to understanding how metabotropic glutamate receptors work in their allosteric activation or inhibition and to investigate physiological processes with the possibilities of on/off switching signalling cascades with light. However, from the therapeutic point of view, it was not useful since their activity at receptor was obtained in the dark, and it only could be switched-off by applying light.

In any case, the possible applications of *trans-on* photoswitchable compounds do not seem suitable for possible therapeutic uses. The development of compounds biologically inactive in their thermodynamically stable disposition (*trans* configuration) and can be switched-on to a bioactive *cis* configuration is better for a possible therapeutic use. In this way, we could induce a pharmacological effect only in a specific region with high precision and spatiotemporal control using light, being inactive when are in non illuminated areas- This could result in a new generation of therapeutic drugs with potential for disease treatment by restricting the activity in its receptor to specific time and avoiding possible associated off-tissue side effects.

Again, an exhaustive bibliographic search of $mGlu_4$ PAMs and $mGlu_5$ NAMs was done focusing on molecules containing aromatic rings, which could fit in the binding allosteric site with a bent pose similar to that of cis azobenzene. However this was not found likely since most of the poses were more compatible with a trans azobenzene. Therefore a different approach was used starting with $mGlu_5$ receptor. The aim was to maintain a rigid structure necessary for a high affinity for the $mGlu_5$ allosteric site and to use the geometrical and size differences between *cis-trans* azobenzenes to add an extra azobenzene unit to disrupt the binding of the *trans* compound and to allow the *cis* one to fit in the transmembrane binding pocket (Figure 32B). In this approach, the bent position of *cis*-azo bond is expected to match the necessary structural, electronic and chemical properties to fit in the pocket, whereas the *trans* geometry having a higher length and planar geometry is designed to not fit into the allosteric pocket, disrupting binding and hence the pharmacological effect (*Figure 32B*). Upon illumination, a molecule with these features is expected to change from an inactive *trans* to an active *cis* configuration.

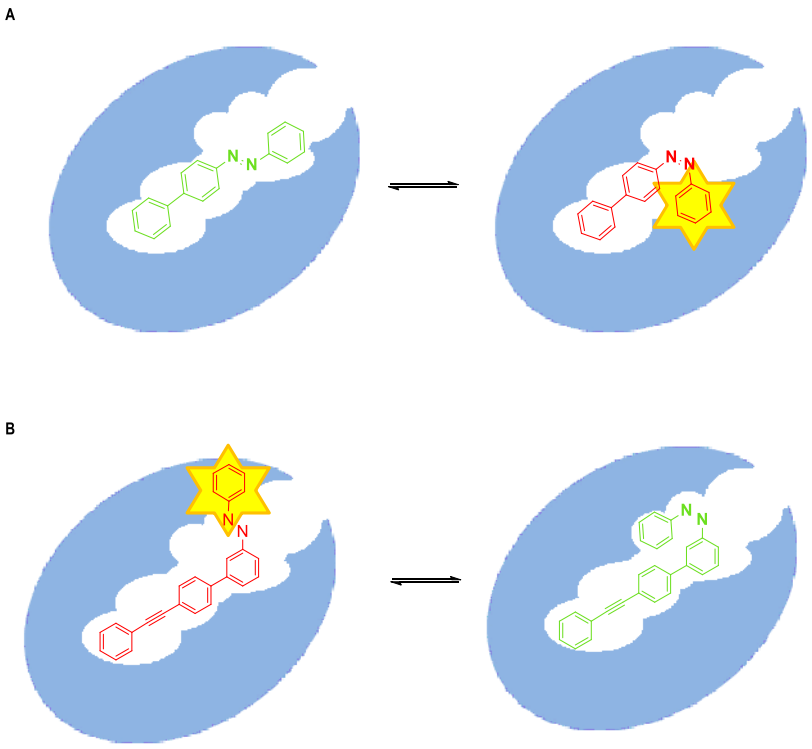

Figure 32: A) *Trans-on* approach for photoswitcable compound. B) *Cis-on* approach for photoswitcable compound.

When we reviewed the literature for $mGlu_4$ PAMs, we found that the *N*-phenylpicolinamide moiety was common in several positive allosteric modulators compounds, such as VU0364439 **75** or VU0415374 **33** (*Figure 33A*), or **64** and **65** (*Figure 30*), the combination of the substitutions in these compounds is found in compound **75** (*Figure 33*). They also reported other interesting molecules, such as compounds **77** and **78** where the *N*-phenylpicolinamide is linked to a large bent moiety susceptible for azo-replacement. Thus, a *cis*-azobenzene in that position could better reproduce the structure on binding of the bent diaryl moiety, whereas the corresponding *trans* isomer would probably clash to the pocket aminoacids avoiding its binding or reducing at least its affinity.

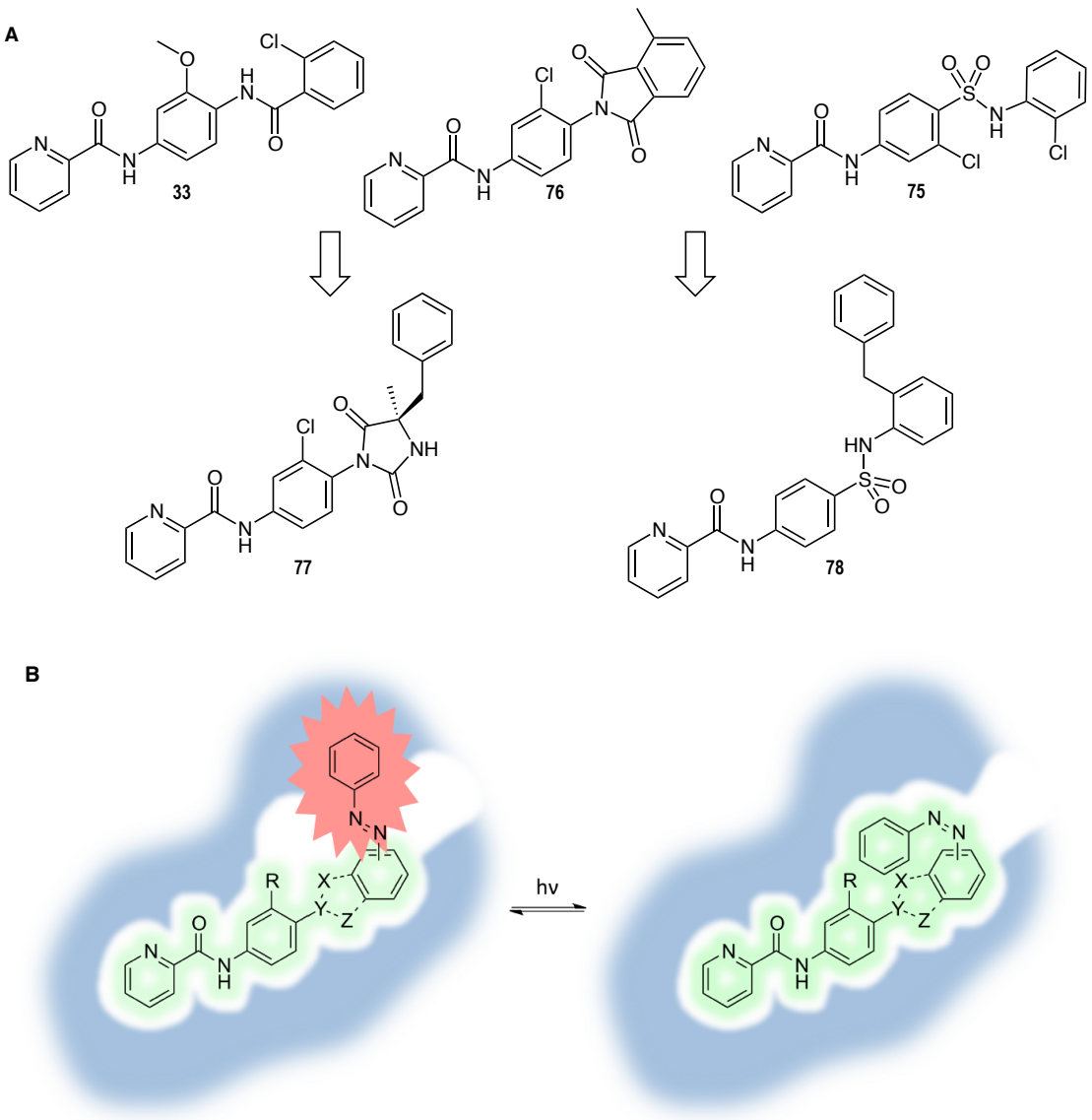

Figure 33: Design of *cis-on* photoswitchable $mGlu_4$ PAMs. A) Compounds found in the literature containing *N*-phenylpicolinamide moiety which some of them can be mimetised by an azobenzene. B) *Cis-on* approach for photoswitchable $mGlu_4$ compounds[13].

Concerning the $mGlu_5$ NAMs, a very common moiety in their allosteric modulators is an ethynyl group bridging two aromatic rings, that is found crossing a narrow channel inside the transmembrane $mGlu_5$ pocket[14]. A typical and clear example is MPEP **7**. In some cases, this ethynyl group is substituted for an amide, as in compound **83** (*Figure 34A*) conserving his potency. Additionally, the binding modes of $mGlu_5$ NAMs in the upper side of the pocket seem to be in angular geometry, as shown in mavoglurant bound to $mGlu_5$ crystal structure[14]. In fact, the

structure-activity correlation of **73**, **74**, **81** and **82** confirm this hypothesis, observing a decreasing between 10 to 30 fold in potency.

Thus, we designed a new photoswitcable compounds with 2-phenylethylpyridine scaffold by introducing an azobenzene group at the phenyl moiety with a linear geometry in *trans* disposition (*Figure 34B*).

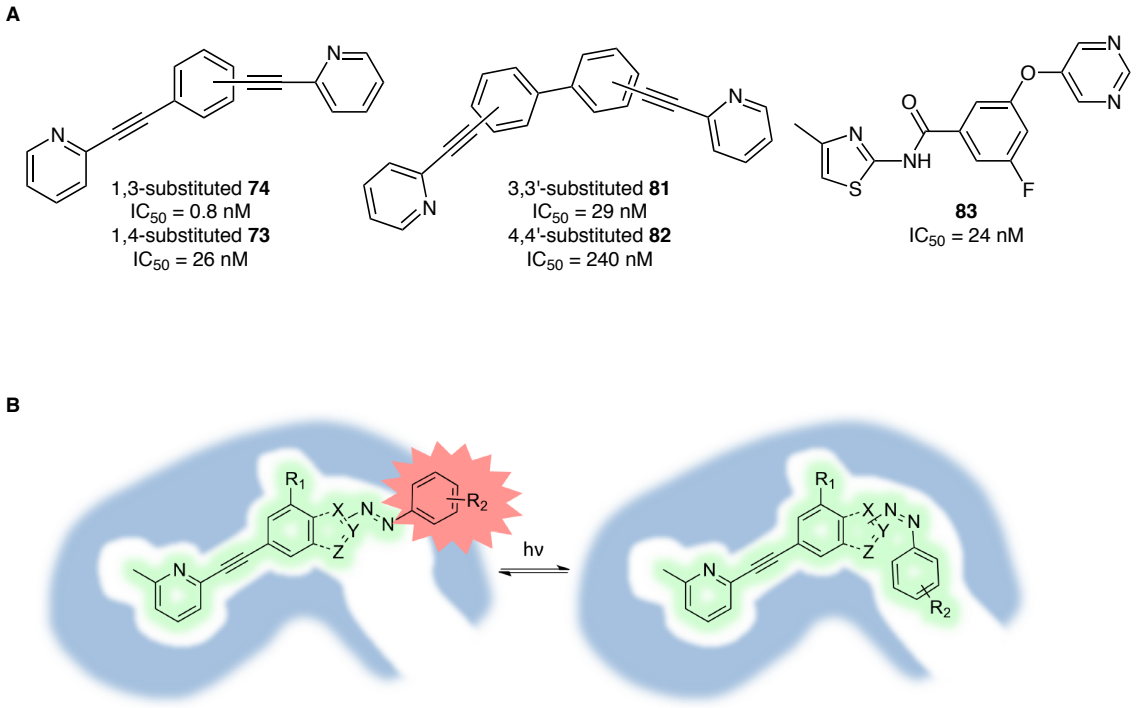

Figure 34: Design of *cis-on* photoswitchable $mGlu_5$ NAMs. A) Compounds found in the literature containing 2-pyridine-ethynyl moieties or other biososters such as methyl pyridine or methyl thiazoles. B) *Cis-on* approach for photoswitcbale $mGlu_5$ compounds[13].

The wavelength illumination is an important aspect to take into account when we design the photoswitch molecule. UV light is well known that is harmful for biological systems and has reduced tissue penetration, whereas visible light in moderated intensities is almost innocuous and displays a higher penetration in living tissues. For this reason it was decided to increase the maximum absorbance wavelengths of the azobenzenes using electron-donating substituents in *ortho* or *para* position on the aromatic rings, like dimethylamine or *N*-morpholine. Also interesting are the , push-pull azobenzenes, which contain electron donating substituents in *ortho* or *para*

position of one of the rings and and electron withdrawing (EWG) in in *ortho* or *para* position of the other azobenzene aromatic ring.

Considering all of those parameters previously described, the first series of photoswitchable *cis-on* compounds were synthesized.

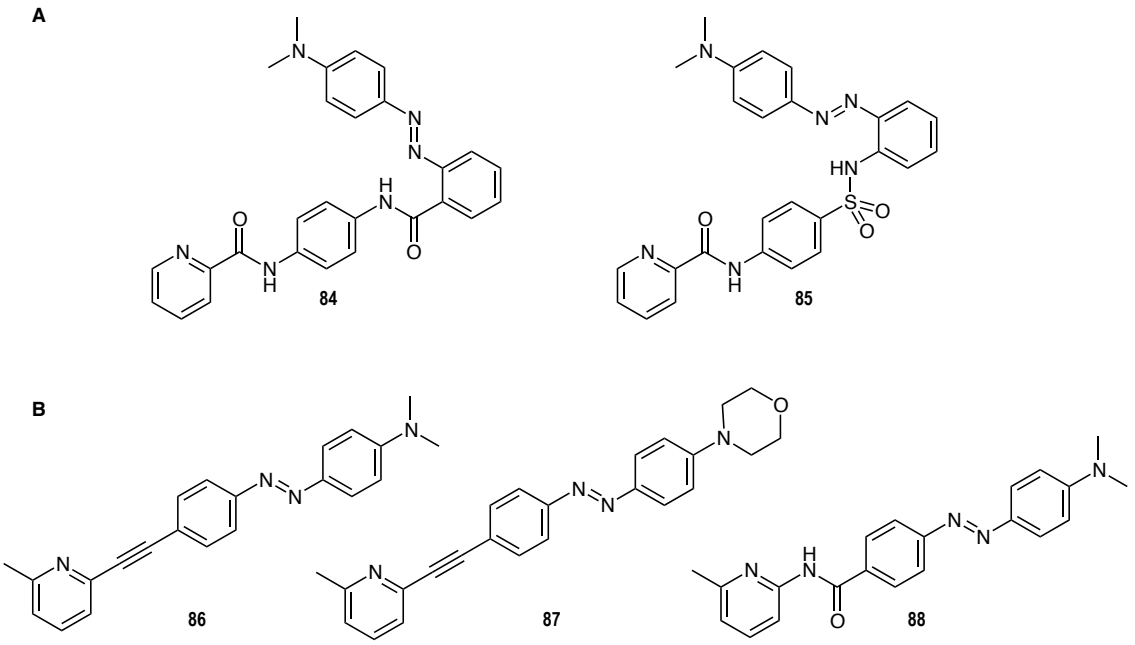

Figure 35: Compounds designed and synthesized by Xavier Gomez Santacana. A) Compounds designed to display a $mGlu_4$ PAM activity. B) Compounds designed to display a $mGlu_5$ NAM activity.

Compound **84** was based on VU0415374 (**33**) structure, but with a simplified scaffold by removing the chlorine or methoxy moiety from the central ring (*Figure 35*), the azo group was incorporated at the third ring to obtain a similar scaffold of compound **77**. Compound **85** (*Figure 35*) was based on the same idea but replacing the amide group by a sulphonamide similar to the described compound **78** (*Figure 33A*).

On the other hand, compounds **86**, **87**, and **88** were designed as $mGlu_5$ NAMs. Compounds **86** and **87** were based on rigid and linear geometry containing an ethynyl pyridine moiety like MPEP (**7**). In both compounds the rigidity and length the *trans* isomer should not allow to bind in the transmembrane $mGlu_5$ allosteric pocket, whereas the *cis* isomer may adopt a kinked geometry to fit into the pocket. Compound **88** was a derivative of **86** changing an ethynyl bond for *N*-amide[13].

Photochemical characterization

For all this new series, X.Gomez measured the UV-Vis absorption spectra for each one and their respective photoisomerisation. In contrast to other compounds presented until now, these new compounds present push-pull azobenzenes properties comprising an aromatic ring with electron donating groups, and the other one with electron withdrawing groups which confer a red-shifted wavelength of illumination and fast relaxation properties.

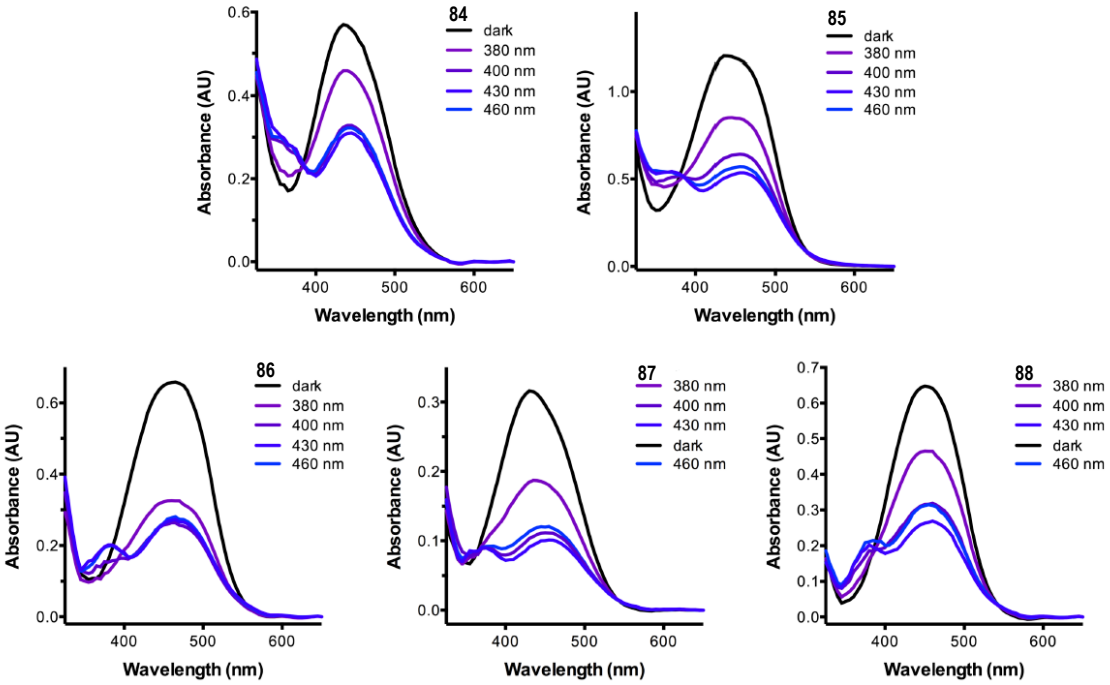

Figure 36: UV-Vis absorption spectra of compounds **84**, **85**, **86**, **87**, and **88** in dark conditions and after irradiation at different wavelengths[13].

The decrease of the height of π- π^* transition of the *trans* isomer, reach them to a qualitative photoisomerisation rate and either a good properties under irradiation at 460 and 430 nm, while back isomerisation at 380 nm recovered a major fraction of *trans* isomer in the photostationary state. This type of irradiation allows us to apply a different illumination wavelength in cell-based assays, illuminating at blue instead of the usual violet light.

Single dose response screening

The pharmacological activity evaluation was done of all compounds previously designed and described as NAMs of $mGlu_5$ and PAMs of $mGlu_4$.

We first performed a single dose response screening in HEK293 transfected cells with either rat $mGlu_4$ or $mGlu_5$ proteins using inositol phosphate accumulation assay (IP-One) based in homogenuous-time resolved fluorescence (see *Experimental part*). All compounds were evaluated as NAMs and PAMs of both mGluR 5 and 4 subtypes, due the expected activity for both receptors of the ligands.

The activity was measured simultaneously at the same plate in dark conditions and under blue light irradiation at 460 nm (see *Experimental part*). For the $mGlu_4$ assay, L-AP_4 orthosteric selective ligand was used, applying 3 nM concentrations to measure PAM effect and 300 nM to measure NAM effect. Concerning the $mGlu_5$ assay, a quisqualate orthosteric selective ligand was used, applying low concentrations (1 nM) and high concentrations (100 nM) to evaluate PAM and NAM effect respectively.

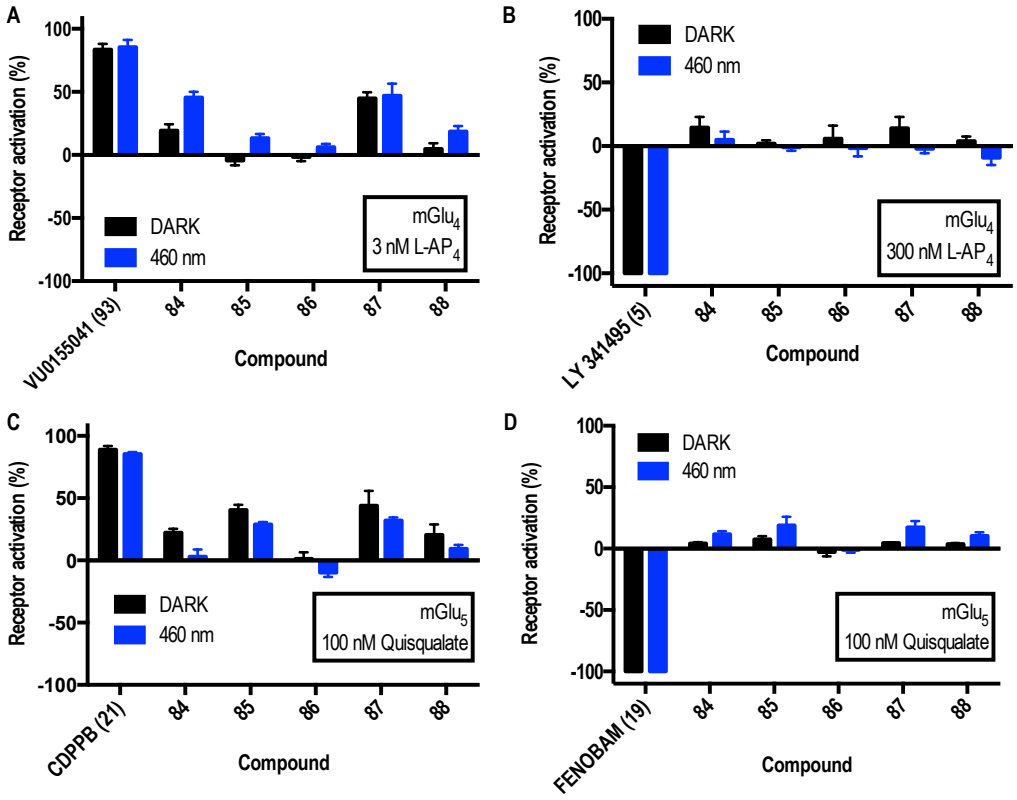

Figure 37: Single-dose screening of compounds **84**, **85**, **86**, **87** and **88**. A) $mGlu_4$ PAMs, B) $mGlu_4$ NAMs, C) $mGlu_5$ PAMs and D) $mGlu_5$ NAMs. FRET response was normalised to 0%-100% between the effect of the low concentration of agonist (EC_{20}) and the effect of the saturation of agonist for the PAM evaluation. For the NAM evaluation, FRET

response was normalised to -100%-0% between the effect of the saturation of an antagonist and the high concentration of agonist (EC_{80}). Each bar corresponds to the mean of minimum of two independent replicates with the corresponding SEM as error bars.

Unfortunately, as we observe in *figure 37*, we did not find a high effect under irradiation with blue light and neither a big difference between the activity in dark conditions and the illuminated of any tested compound. However, a weak difference which can let us think as a possibility of a *cis-on* behaviour were observed for compounds **84**, **85**, and **88**. Compound **84** was the most promising compound showing the best *cis-on* effect (*figure 37A*), but still without enough potency and the rest of compounds show some partial PAM effect in both dark and blue light conditions.

Dose-response curves

Further evaluation of the *cis*-on $mGlu_4$ PAM activity was done for the compounds described previously with potential activity, generating dose-response curves applying the IP accumulation assay in HEK293 cells transfected with rat $mGlu_4$ receptor and illuminating at 460 nm.

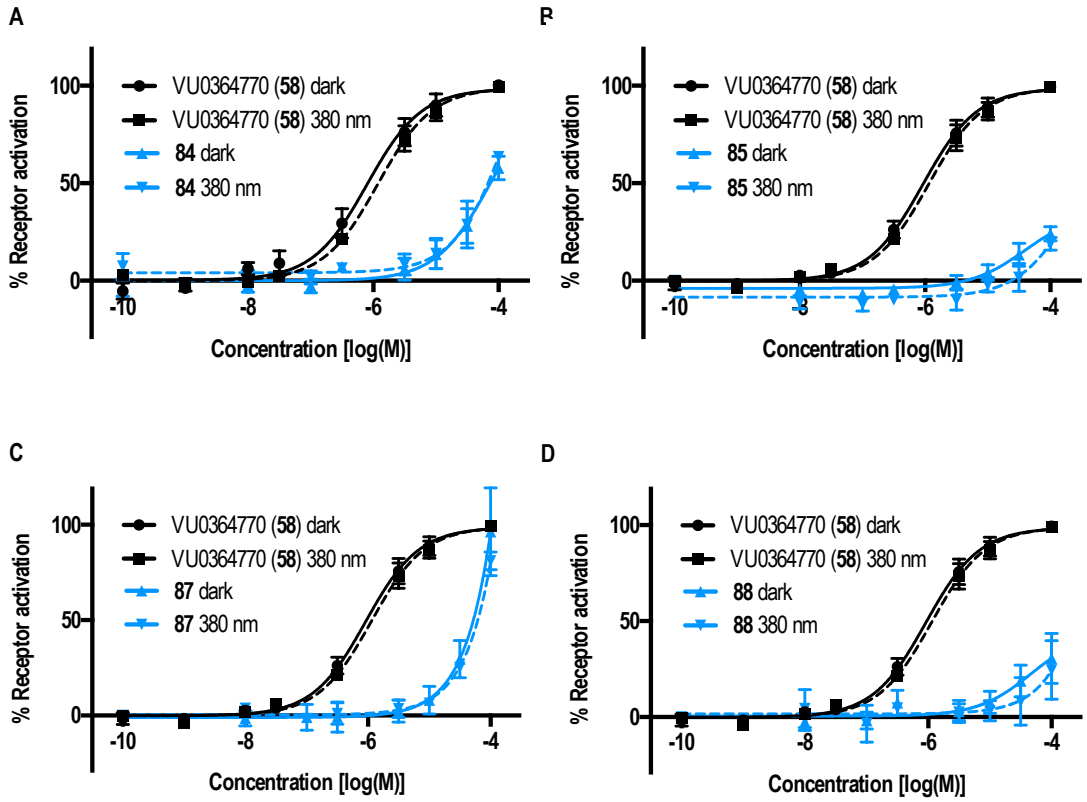

Figure 38: Dose-response curves with IP-One assay on HEK293 cells overexpressing $mGlu_4$ with a constant concentration of L-AP_4 (**4**) 3 nM. Flat lines correspond to incubated samples in dark conditions and dotted lines to

illuminated conditions at 460 nm. Each point corresponds to the mean of a minimum of three independent replicates with the corresponding SEM as error bars.

Unfortunately, we could not observe any apparent *cis*-on effect in the dose-response curves. In fact, the dose response results were not in agreement with the single-dose screenings and we did not appreciate any difference concerning the potency between the dark conditions versus the illuminated one, except for compound **87,** that did not display differences between the dark/light conditions in the single-dose experiment, whereas we obtained a sharp vertical curve in the dose response, which is probably due to a non-specific effect of the compound at high concentrations.

At this point, we thought to change some experimental conditions in last attempt to achieve some differentiation between the non-irradiated and the illuminated activity.

We generated two additional dose-response assays for compounds **84** and **85** due their better *cis*-on effect observed in single-dose screening. The protocol used until now for the dilution of compounds in the 96-well plate was changing the tips due the hydrophobicity of azocompounds, which stick in the tip of micropipette, and it could change the dilution concentration of each well following previous protocols designed by Xavier Gomez-Santacana. The new protocol, in this case, was without changing the tip (WCT) and an additional protocol was also evaluated incubating the plate 60 minutes instead of 30 minutes (LIT).
The aim on these changes in the assays was to avoid the loss of compound while changing the tips and accumulate a larger amount of IP inside the cells to amplify the FRET response of the assay.

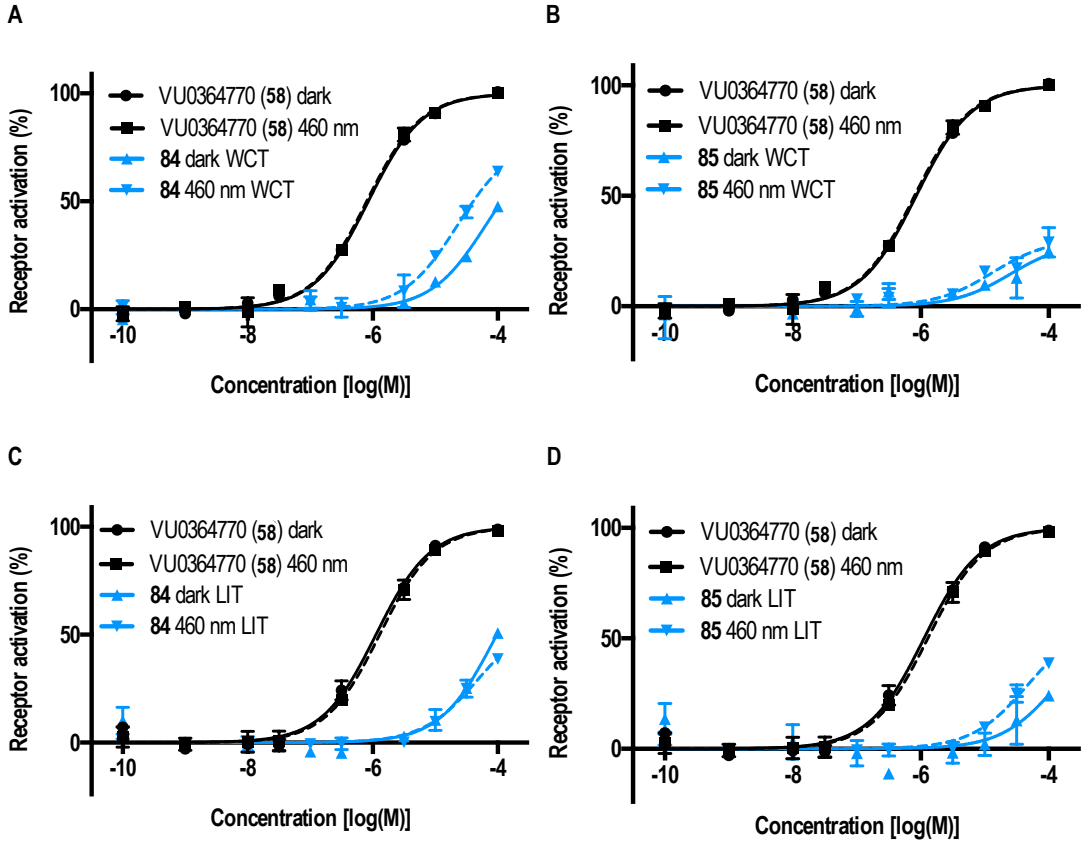

Figure 39: Dose-response curves of compounds **84** and **85** using "without changing tips" protocol (WCT) (A, B) and "long incubation time" (LIT) (C, D) with IP-One assay on HEK293 cells overexpressing $mGlu_4$ with a constant concentration of L-AP_4 (**4**) 3 nM. Flat lines correspond to incubated samples in dark conditions and dotted lines to illuminated conditions at 460 nm. Each point corresponds to the mean of a minimum of three independent replicates with the corresponding SEM as error bars.

The results obtained are more consistent, and we can appreciate a shift to the left of the dose-response curve under 460 nm illumination of compound **84** (*Figure 39A*) and compound **85** (*Figure 39D*).

Despite the results, the potency of the compounds is low and this probably is impeding to observe a clear difference under the different light conditions. However, we thought that this could be a good starting point for finding out new chemical approaches to obtain better *cis*-on compounds based in compounds **84** and **85**.

*Design and synthesis of new compounds based in **84** and **85***

The $mGlu_4$ PAM design approach used for **84** and **85** azobenzenes was the basis to define new derivatives. The rational addition of substituents on the chemical scaffold, could lead us to the desired *cis*-on compounds. In the literature we found $mGlu_4$ PAM compounds with the *N*-phenylpicolinamide scaffold such as VU0364770 (**58**), VU0361737 (**89**), VU0415374 (**33**) or VU0366037 (**90**) (*figure 40*)[15,16].

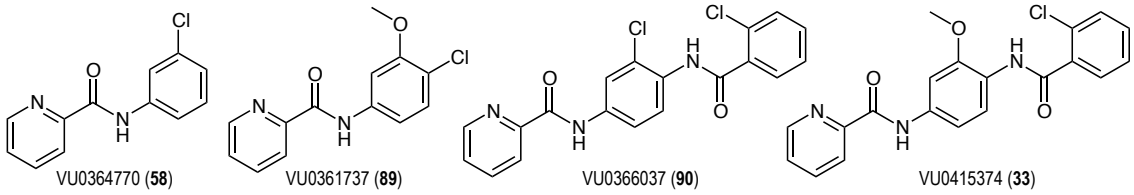

Figure 40: Structures of known $mGlu_4$ PAMs.

Common to all of these compounds is a methoxy or chlorine substituent in position 3 of the aromatic central ring was occupied by a group, being the chlorine-substitutions whose provided better potencies[15,16]. Therefore we decided to introduce this substitution in compound **84**, adding a methoxy or chlorine to give compound **91** and **92** respectively (*Figure 41*).

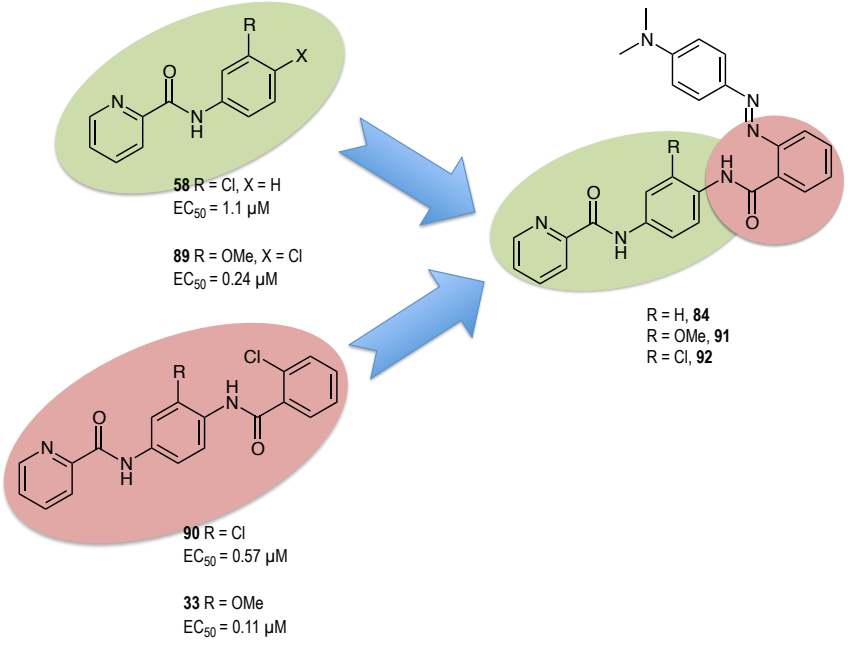

Figure 41: Design of new *cis*-on compounds $mGlu_4$ PAMs based on previously described **84** compound.

After the synthesis, carried out by Dr. Juan Lorenzo Catena, of both compounds, the UV-Vis absorption spectra was measured and the photoisomerization was tested under different wavelength (500, 460, 430, 400 or 380 nm) and a decrease of the height of the π-π* transition of *trans* isomer was obtained, compatible with a mixture of *cis-trans* isomers in the photostationary state for each wavelength. The maximum absorption was obtained at 460 and 500 nm illumination for compounds **91** and at 430 and 460 nm for compound **92**. To test the back isomerisation, the *trans* isomer was illuminated at 380 nm and only a fraction of the absorption of the dark compound was recovered, indicative of the photoisomerisation in these new compounds was not reflecting a clear and defined isomer predominance in any of the tested wavelengths.

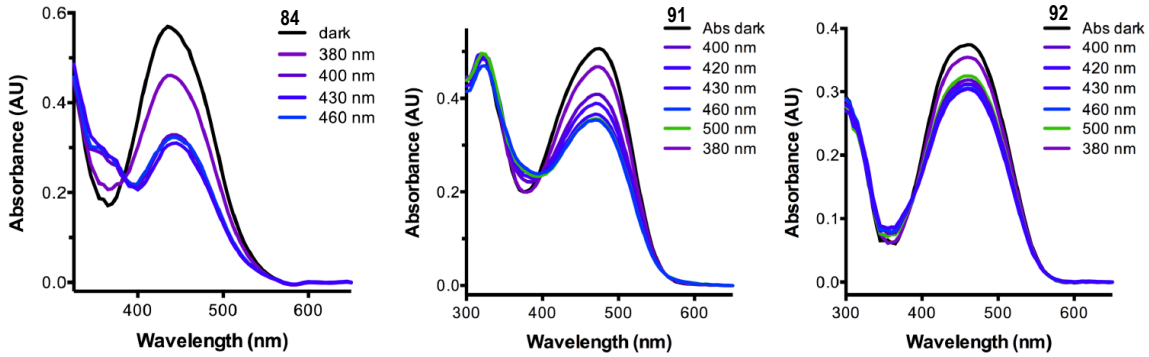

Figure 42: UV-Vis absorption spectra of compounds **84**, **91** and **92** in dark conditions and with several wavelength irradiations.

Dose-response curves

The assays were carried out by Dr Xavier Rovira, by using the same method applied in the first dose-response showed previously, evaluating the *cis*-on $mGlu_4$ PAM activity generating dose-response curves extracted from IP-One accumulation assay with HEK293 transfected with rat $mGlu_4$ and irradiating at 460 nm.

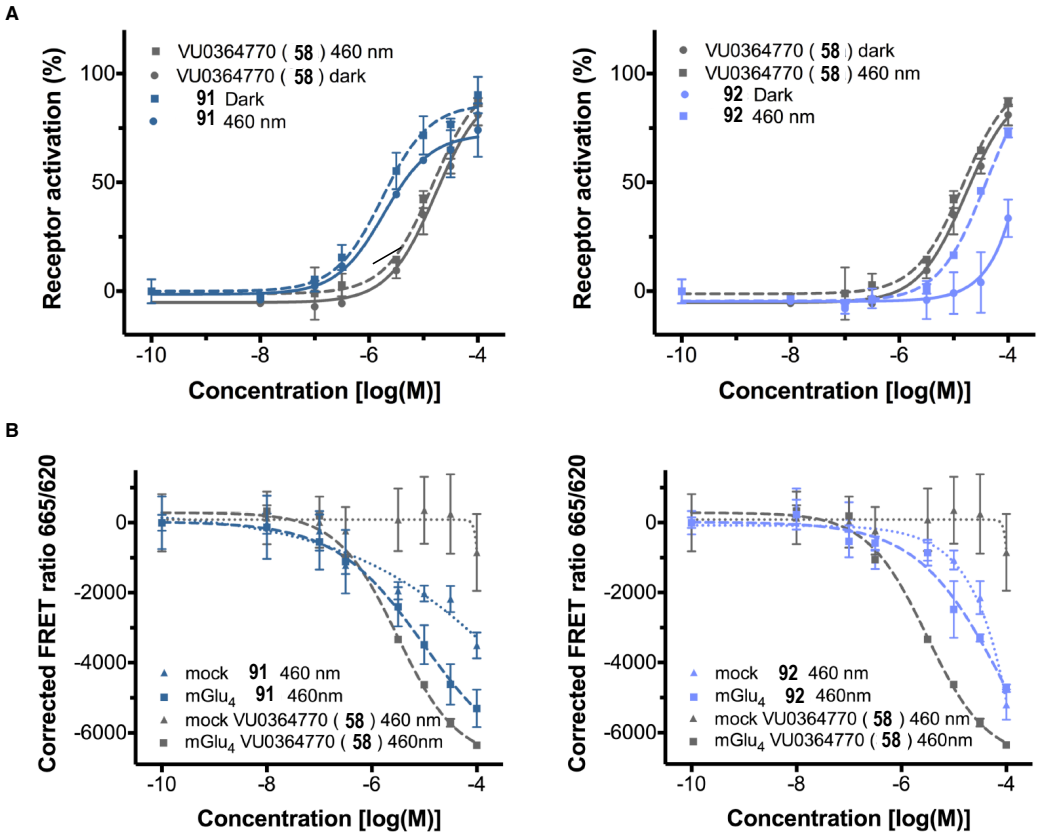

Figure 43: Dose-response curves with IP-One assay in HEK293 cells with compounds **91** and **92** using VU0364770 (**60**) as reference of $mGlu_4$ PAM. A) Dose-response curves using HEK293 cells overexpressing $mGlu_4$ with constant concentration of selective orthosteric ligand L-AP_4 (**4**) 3 nM. Flat lines correspond to he samples incubated in dark conditions and dotted lines corresponds the samples under irradiation at 460 nm. Each point corresponds to the mean of a minimum three independent replicates with the corresponding SEM as error bars. B) Large-dotted lines correspond to HEK293 cells overexpressing $mGlu_4$ and small-dotted lines correspond to HEK293 cells with no expression of $mGlu_4$. Both conditions were tested with constant concentration of L-AP_4 (**4**) 3 nM and under irradiation at 460 nm. Each point corresponds to the mean of minimum three independent replicates with the corresponding SEM as error bars.

We could observe from the graphs showed previously that we create a tendency concerning the potency to achieve a *cis*-on effect for both compounds. On the one hand, for **91** compound, an increase of potency was obtained in comparison with **84** compound with micromolar potency, and the irradiated one denotes an interesting *cis*-on positive tendency in the IC_{50} values but not sufficient to have a suitable *cis*-on compound (*Figure 43A)* for cell uses as a $mGlu_4$ receptor photoswitchable PAM ligand. On the other hand, compound **92** showed a weak modulation as $mGlu_4$ PAM in the dark whereas the irradiated curve at 460 nm turned out a noticeable effect with a micromolar potency (*Figure 43A*).

To confirm this result and complete the pharmacological characterisation, a negative control assay was performed to exclude non-specific effects. The experiments for both compounds were performed with continuous illumination with HEK293 cells transfected with $mGlu_4$ receptors and HEK293 cells after transfection of an empty DNA plasmid, which did not encode the $mGlu_4$ receptor (mock plasmid). Unfortunately, a relatively potent effect was observed for both compounds almost similar to the effect showed in $mGlu_4$-transfected cells. Moreover this effect was not observed in mock cells for $mGlu_4$ PAM reference VU0364770 (*Figure 43B*) as expected. In addition, this non-specific effect is stronger for compound **92**, which showed the higher *cis*-on activity, indicating that this effect is probably an artifact, which could be produced from the interaction of the azobenzenes with unknown endogenous receptors or proteins present in HEK293 cells and involved in intracellular IP production, but not due to a $mGlu_4$ activity.

***Cis-On* first approach, new photoswitchable compounds**

Design and Synthesis

At this point, with the objective of synthesize a *cis*-on photoswitchable compound, we started a new design strategy.

This time, we changed the "azo-extension" for the *cis*-on design, for an "azologisation" approach, based in the replacement of a bridge functional group between two aromatic rings by an azo group. First, we still focus in the design of $mGlu_4$ PAMs and $mGlu_5$ NAMs involved in treatment of pain based in known compounds described in the literature focusing in ones whose could mimic the structure scaffold by the replacement for an azo group in *cis* isomer disposition. A possible problem was that these compounds were not among the most potent in the families, and therefore the conversion to azobenzenes could result in low potency compounds.

We found several compounds in the literature that could be used as models in the design, but we were attracted for a described $mGlu_4$ PAM based in the standard VU0155041 (**93**), named as CD2267-0368 (**94**)[17], with an extension of the aromatic ring using an phenylether group, which could be suitable for the replacement of an azo group.

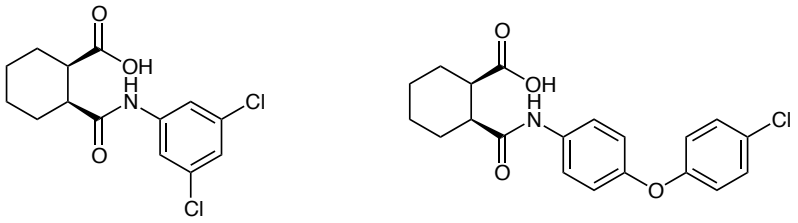

Figure 44: Structure of selective $mGlu_4$ PAMs[17].

The structural properties between a diphenyl ether group and an azobenzene in *cis* configuration are quite similar concerning the bond length and the angle bent joining the two aromatic rings. Whereas the *cis* azobenzene group describes a bond length around 2.8 to 3 Å of N=N, with an angles of 130º and 134º (*Figure 45A*), the diphenyl ether group has a bond length of C-O-C around 2.4 to 2.6 Å, and an angle around 124º (*Figure 45B*). Due this resemblance in the geometry, we tought that this could be a good approach to obtain the desired *cis*-on compound.

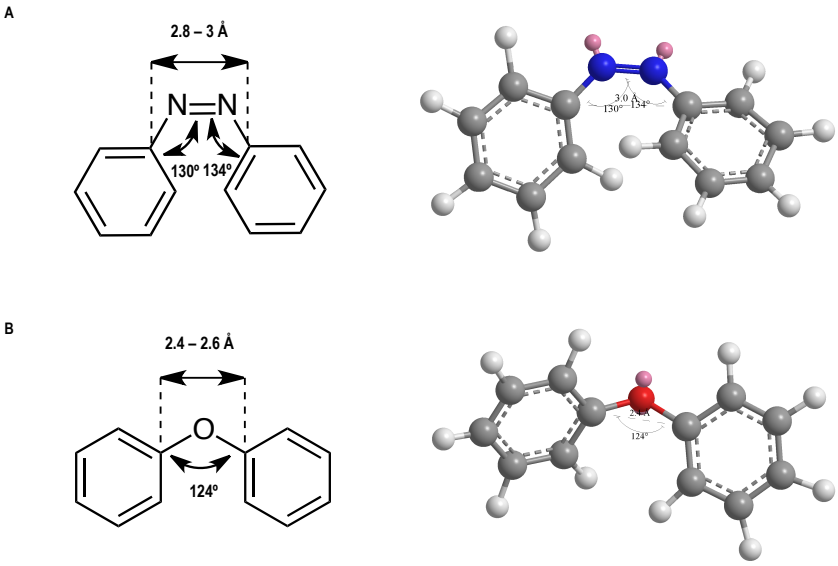

Figure 45: Structure of cis-azobenzene and diphenylether. A) Bond length and angle calculation of *cis*-azobenzene with minimize energy MM2. B) Bond length and angle calculation of diphenylether with minimize energy MM2.

Therefore several derivatives having the 2-(phenylcarbamoyl)cyclohexanecarboxylic acid as a common element anddifferently substituted aminoazobenzenes (*Figure 46*) were obtained.

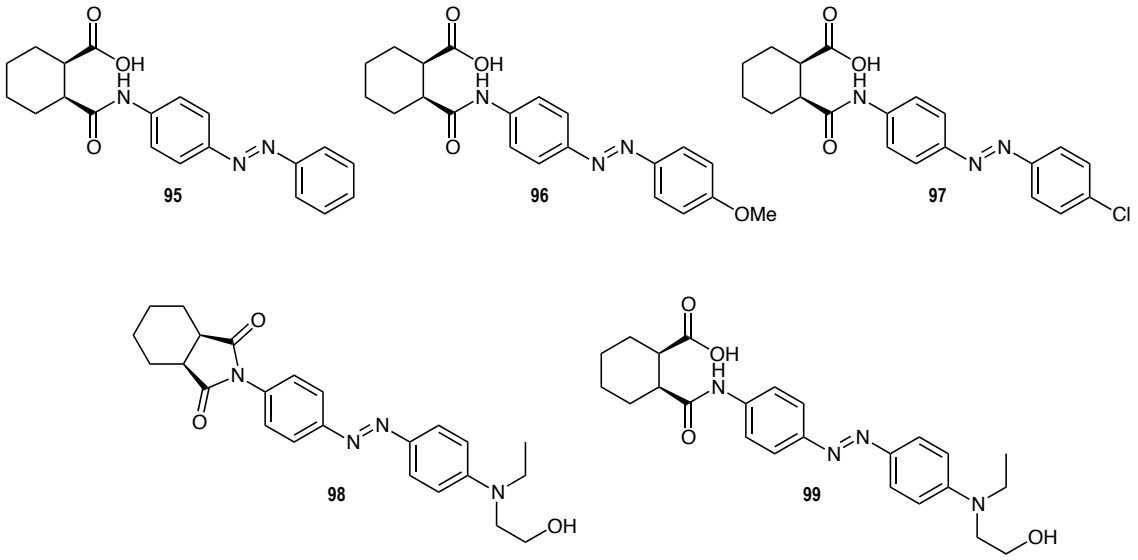

Figure 46: Compounds designed as putative *cis*-on to display $mGlu_4$ positive allosteric modulators.

Synthesis of compounds 95-99

Compound **95** was prepared following the synthetic strategy shown in *scheme 1*. The first step consisted in the reduction of the nitrophenyl moiety, present in the commercial compound **100b,** in order to obtain aniline **100c**. Then, condensation of **100c** with anhydride **100a** yielded the azobenzene **95**.

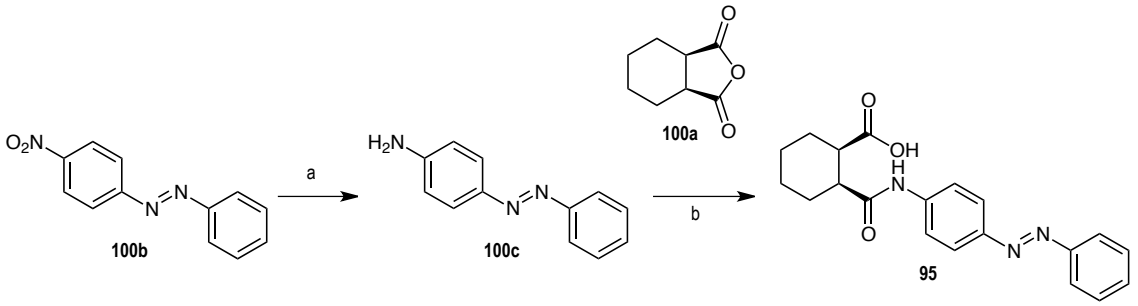

Scheme 1: Synthesis of compound **95**. Reagent and conditions: a) $Na_2S \cdot 9H_2O$, EtOH, reflux, 1h, 40%; b) **100a**, NEt_3, THF, reflux, overnight, 41%.

Compound **96** was synthesized following the procedure described in *scheme 2*. The commercial azobenzene **101a** was alkylated via Williamson reaction with iodomethane (step a), followed by the nitro reduction to the aniline **101c** (step b). Finally, compound **96** was afforded by the acylation of the amine by using anhydride **100a**.

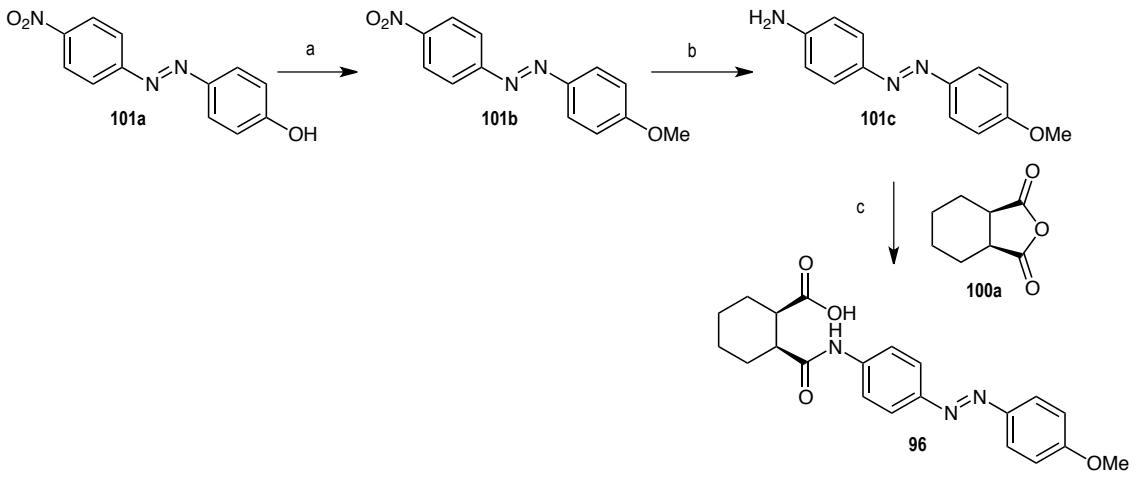

Scheme 2: Synthesis of compound **96**. Reagent and conditions: a) K_2CO_3, MeI, AcN, r.t., overnight, 47%; b) $Na_2S \cdot 9H_2O$, EtOH, reflux, 1h, 37%; c) **100a**, NEt_3, THF, reflux, overnight, 62%.

Generation of azocompound **97** was effective by formation of nitroso derivative from aniline **102b** and the subsequent azo formation by reacting it with diamine **102a** (step a). Finally, azocompound **102c** was coupled toanhydride **100a** yielding the expected compound **97**.

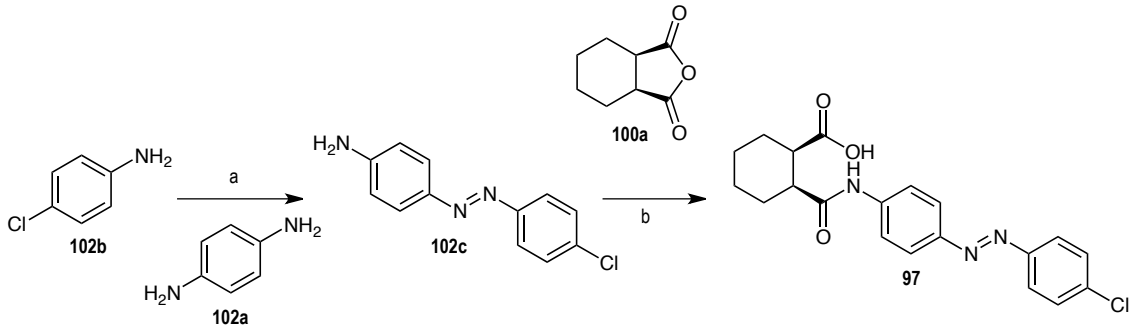

Scheme 3: Synthesis of compound **97**. Reagents and conditions: a) Oxone, DCM, AcOH, 24h, r.t., 45%; b) **100a**, NEt_3, THF, reflux, overnight, 42%.

In a repeated effort, compounds **98** and **99** were prepared (*scheme 4*) by a similar method; in this case from commercial azo compound **103a** by nitro to the group reduction to the corresponding aniline, to give compound **103b**, which was finally coupled to the anhydride **100a** to give a mixture of both compounds in the same reaction, which were isolated after chromatography.

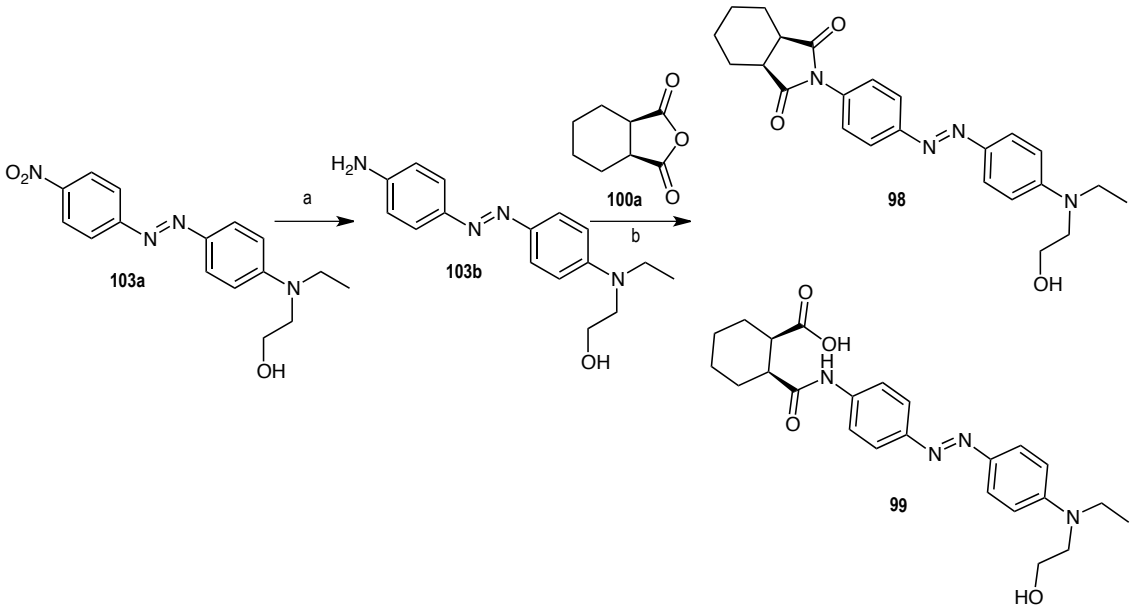

Scheme 4: Synthesis of compound **95**. Reagent and conditions: a) $Na_2S \cdot 9H_2O$, EtOH, reflux, 1h, 25%; b) **100a**, NEt_3, THF, reflux, overnight, (**98**) - 7%, (**99**) - 45%.

Photochemical Characterisation

The UV-Vis absorption spectra in dark conditions of every compound synthesized before was done in DMSO at 100 μM for each one.

After that, we tested the photoisomerisation in the same conditions (DMSO, 100 μM), under different light conditions (2 minutes continuous irradiation with wavelengths 460 and 380 nm) for **98** and **99** and we obtained a decrease of height of the π- π^* transition of the *trans* isomer achieving different UV-Vis spectra, corresponding to a photostationary mixture of *cis-trans* isomers for each illumination. In addition, as we could observe, compound **98** and **99** have push-pull substituents, which induce the maximum of absorption of the π- π^* transition around 460 nm and the recovery of the *trans* configuration upon 380 nm illumination (*Figure 47*).

On the other hand, the spectra for compounds **95**, **96** and **97**, as it was expected, showed the typical azobenzene π- π^* transition band at 370-390 nm and we could obtain the back isomerisation illuminating at 500 nm (*Figure 47*).

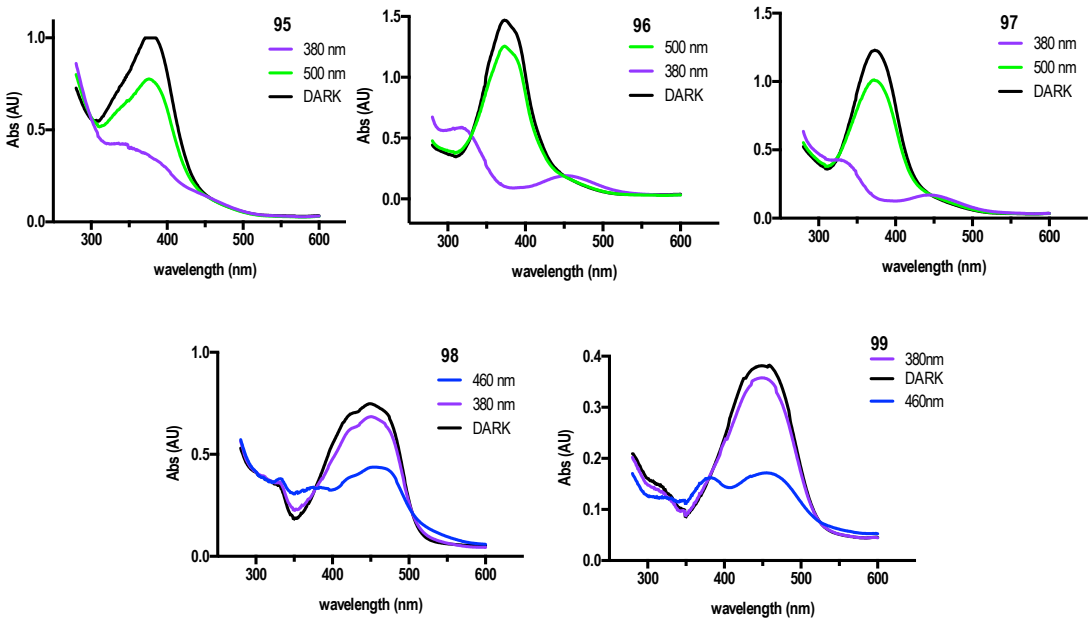

Figure 47: Photochemical characterisation of compounds **95**, **96**, **97**, **98** and **99**. UV-Vis absorption spectra in dark conditions (black line), under 380 nm (violet line), under 500 nm (green line) for compounds **95**, **96** and **97.** UV-Vis absorption spectra in dark conditions (black line), under 380 nm (violet line) and between 460 nm (blue line) for compounds **98** and **99**.

Pharmacological characterisation

Single dose screenings

To evaluate the pharmacological activity of all the new putative *cis*-on $mGlu_4$ PAMs or $mGlu_5$ NAMs a new single dose screening was done. As described before, we first screened at single dose the compounds in HEK293 cells transfected with rat $mGlu_4$ or $mGlu_5$ using inositol phosphate accumulation assay based on homogenous time resolved fluorescence (HTRF) assay (*experimental part*). Because of the related activity between $mGlu_4$ PAMs and $mGlu_5$ NAMs, both PAM and NAM effect on $mGlu_4$ and $mGlu_5$ were studied. Additionally, every measurement was performed simultaneously in dark conditions and under irradiation at the optimal wavelength for each compound (λ = 460 nm for **98** and **99**, λ = 380 nm for **95**, **96** and **97**). For $mGlu_4$, we used the orthosteric agonist L-AP_4 (**4**) at low concentration (3 nM) to evaluate a PAM activity and high concentration (300 nM) to evaluate NAM effect. For the assays on $mGlu_5$ receptor, the orthosteric

ligand quisqualate (**2**) was used at low concentrations (1 nM) for PAM effect, and high concentrations (100 nM) for NAM evaluation.

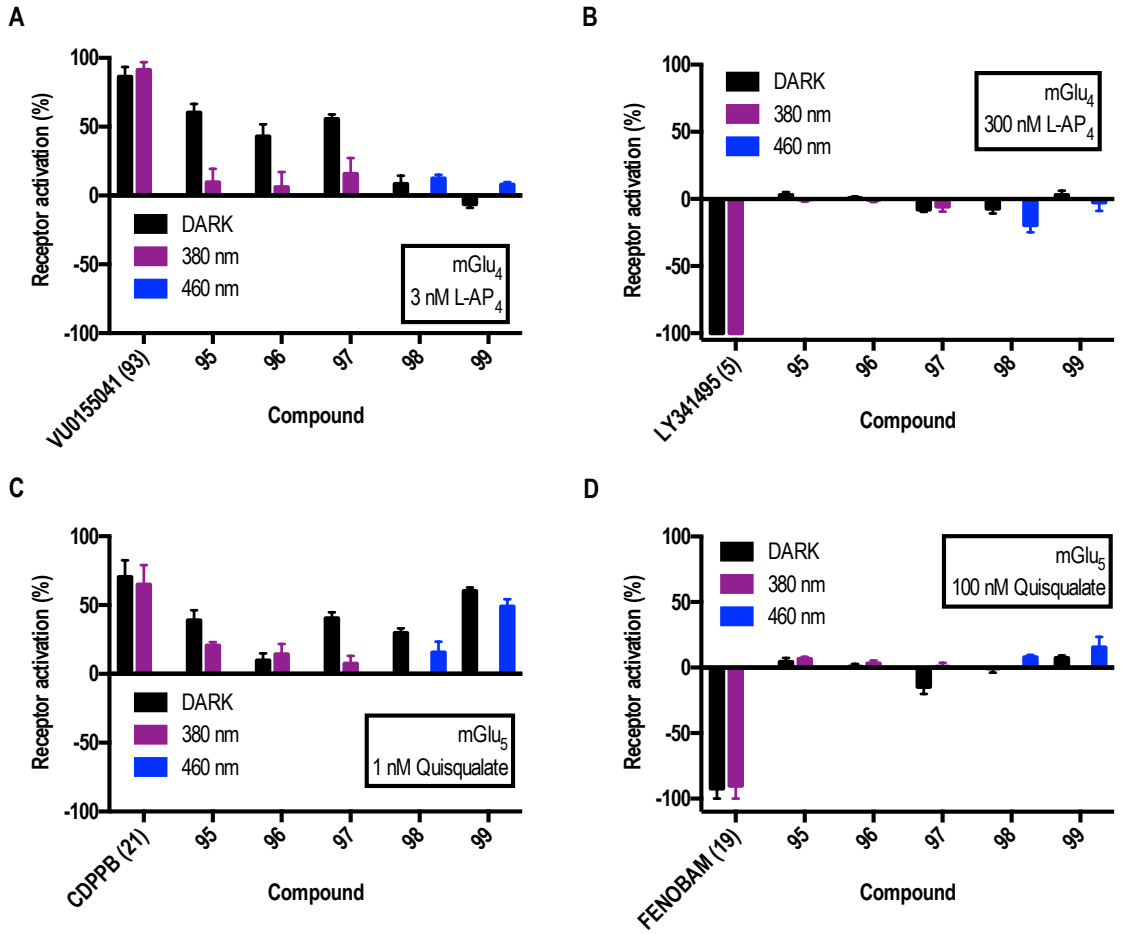

Figure 48: Single-dose screening of compounds **95**, **96**, **97**, **98** and **99**. A) $mGlu_4$ PAMs, B) $mGlu_4$ NAMs, C) $mGlu_5$ PAMs and D) $mGlu_5$ NAMs. FRET response was normalised to 0%-100% between the effect of the low concentration of agonist (EC_{20}) and the effect of the saturation of agonist for the PAM evaluation. For the NAM evaluation, FRET response was normalised to -100%-0% between the effect of the saturation of an antagonist and the high concentration of agonist (EC_{80}). Each bar corresponds to the mean of minimum of two independent replicates with the corresponding SEM as error bars.

Unfortunately, we could not achieve a clear and strong effect under illumination either in blue or violet light in $mGlu_4$ or $mGlu_5$ NAM assays. However, a significant difference in dark conditions respect the illuminated one was observed for compounds **95**, **96** and **97** as $mGlu_4$ PAM (*Figure 48A*), even though this effect was not defining *cis*-on active compounds as initially expected, but *trans*-on effect were obtained. Therefore, further pharmacological characterisation was performed for these compounds to compare the potency activity (EC_{50}) between them and the diphenylether reference compound CD2267-0368 (**94**).

Dose-response curves

The evaluation of the new *trans*-on compounds was carried out by generating dose-response curves using HEK293 cells transfected with rat $mGlu_4$ receptors, the data were obtained from an inositol phosphate accumulation assay using the "changing tips" protocol used previously and the experiments were done simultaneously in dark conditions and under irradiation at 380 nm.

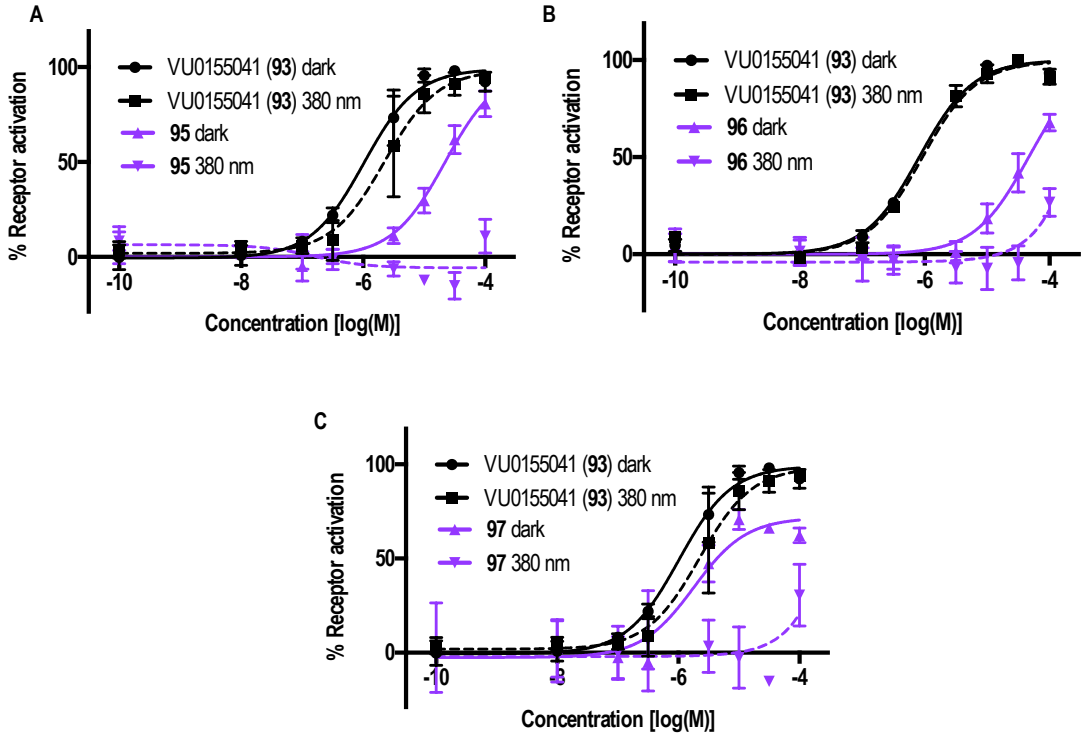

Figure 49: Dose-response curves with IP-One assay on HEK293 cells overexpressing $mGlu_4$ with a constant concentration of L-AP_4 (**4**) 3 nM. Flat lines correspond to incubated samples in dark conditions and dotted lines to illuminated conditions at 380 nm. Each point corresponds to the mean of a minimum of three independent replicates with the corresponding SEM as error bars.

Whereas, azocompounds **95** (EC_{50}= 22 μM) and **96** (EC_{50}= 46 μM) lost potency respect the reference compound **94** (EC_{50}= 0.5 μM), the derived azocompound **97** (EC_{50}= 2.7 μM) display a similar potency compared to diphenylether compound **94**, but in this case we could observe just a partial PAM effect (*figure 49C*).

Despite we could not achieve a *cis*-on compound, these results gives us a sense about how the compounds to interact with the protein. The substitution at *para* position of the azobenzene is

important, because H, OMe or disubstituted amine result in less active compounds than the reference compound **94.** In contrast, maintaining the *p*-chloro substituent in the azobenzene, keeps the potency on the order of that of compound **94,** as it could be expected.
Additionally, the azobenzene seems to be a good approach for the substitution of ether groups but disappointingly the *trans* isomer still is more active than *cis* in the cell functional activity assays.

Cis-On **second approach, a new series of photoswitchable compounds**

Design and Synthesis

Previously reported in the first series of *cis*-on, we were not able to define an azocompound to lead us a new *cis*-on compounds to modulate mGlu receptors in cells.

As was mentioned above, we were involved in verifying if ether groups could be a good starting structure to define azobenzenes in *cis* disposition due to the structural resemblance of diphenylethers and azobenzenes. Despite we found out new series of *trans*-on compounds, we finally failed in the fact that maybe the ether group is not adjusting into the receptor in the same geometry as *cis* disposition of azobenzene, due the free mobility of the diphenylether bond allowing a rotation on the link axis of the ether group, contrary to azobenzene bond which is more rigid (*Figure 50A*). Actually, certain conformations of the aromatic ring of the ether group could be difficult to be attained by azobenzenes.
In this section, we thought in the redesign of the same molecules exploring the three possible positions in the first aromatic ring (*ortho*, *meta, para*) to mimic the possible disposition of ether group into the receptor and see difference between *trans* and *cis* disposition in each possibility (*Figure 50B*) and to connect this to the 2-(phenylcarbamoyl)cyclohexanecarboxylic acid scaffold to define a new library of azocompounds with expected activity as $mGlu_4$ PAMs.

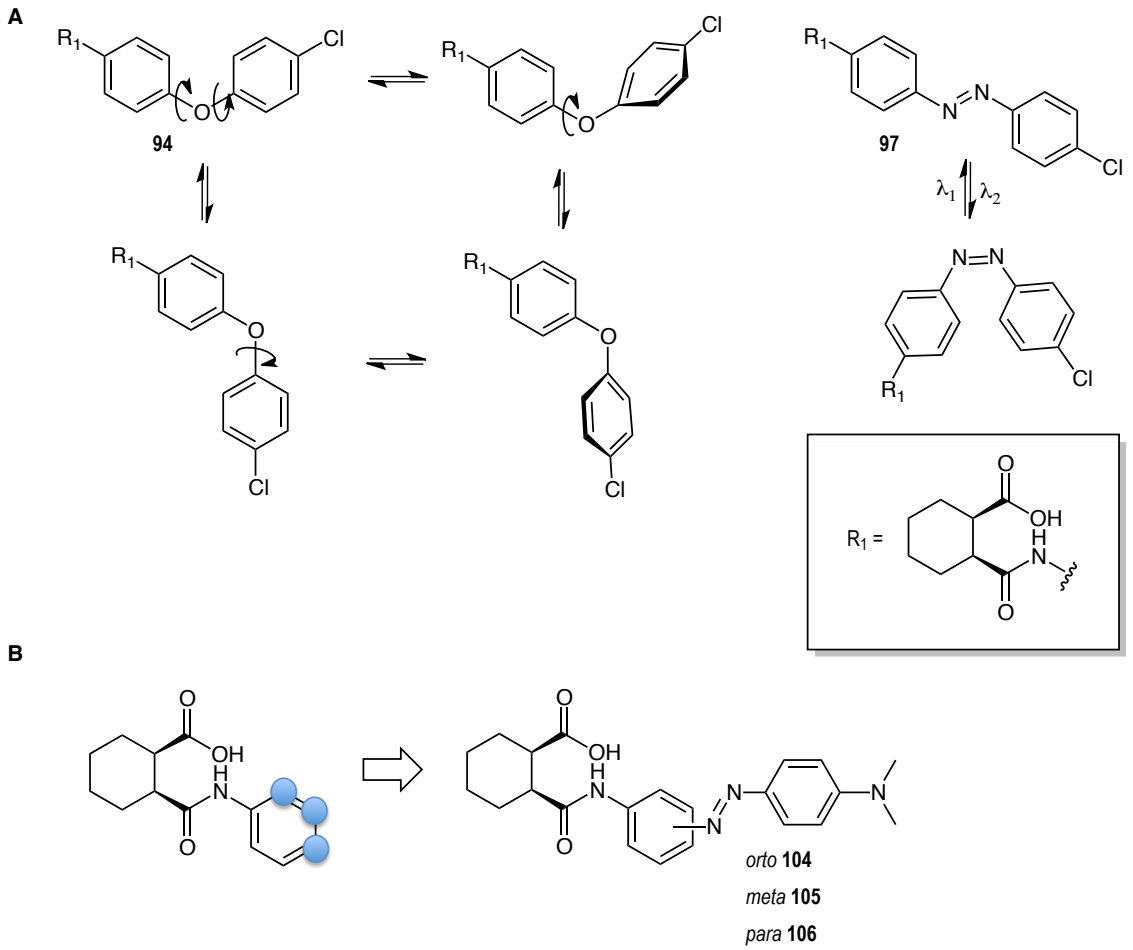

Figure 50: A) Possible mobility of **94** into the receptor around the ether bond axis in comparison with its rigid azocompound derivative **97**. B) Structure of new azocompounds with putative *cis*-on effect to study differences between the aromatic substitutions.

We decided to design a new small series of azocompounds with a dimethyl amine substitution instead of halide to maintain the push pull substituent properties and compounds **104**, **105** and **106** were obtained. We expected to achieve an effective photoisomerisation irradiating at visible wavelength (430-460 nm) for the experimental *in-vitro* assays, since illumination at 380 nm is less penetrant than blue light.

All azocompounds intermediates synthesized and described previously, were joined to a well-known moiety belonging to CD2267-0368 (**94**) trying to develop a functional activity as $mGlu_4$ PAM, but other several chemical scaffolds can be studied. One of these, which is well known in the literature and especially in our group, is the picolinic amide (*Figure 51*) that could be

combined with the azobenzenes to mimic a previous described compound optogluram (**59**) a $mGlu_4$ PAM obtained in X.Gomez thesis.

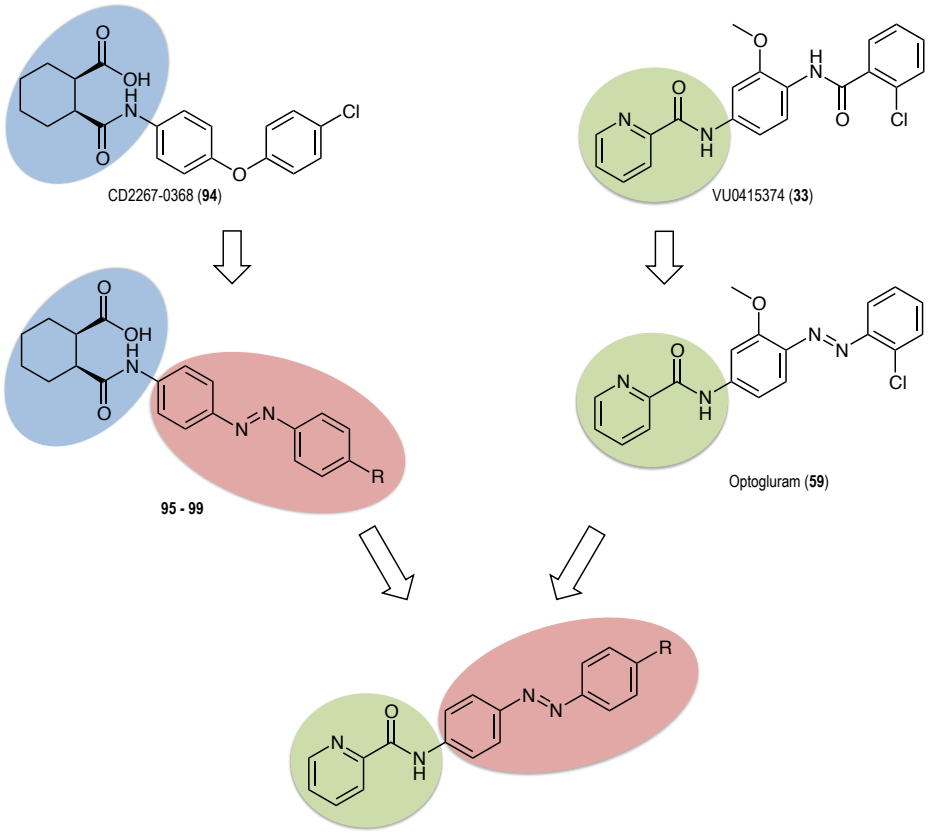

Figure 51: New structural design for library of new azocompounds as $mGlu_4$ PAMs.

Therefore, all the intermediates azocompounds were desgined as previously described above, generating the following $mGlu_4$ PAM candidates (*Figure 52*).

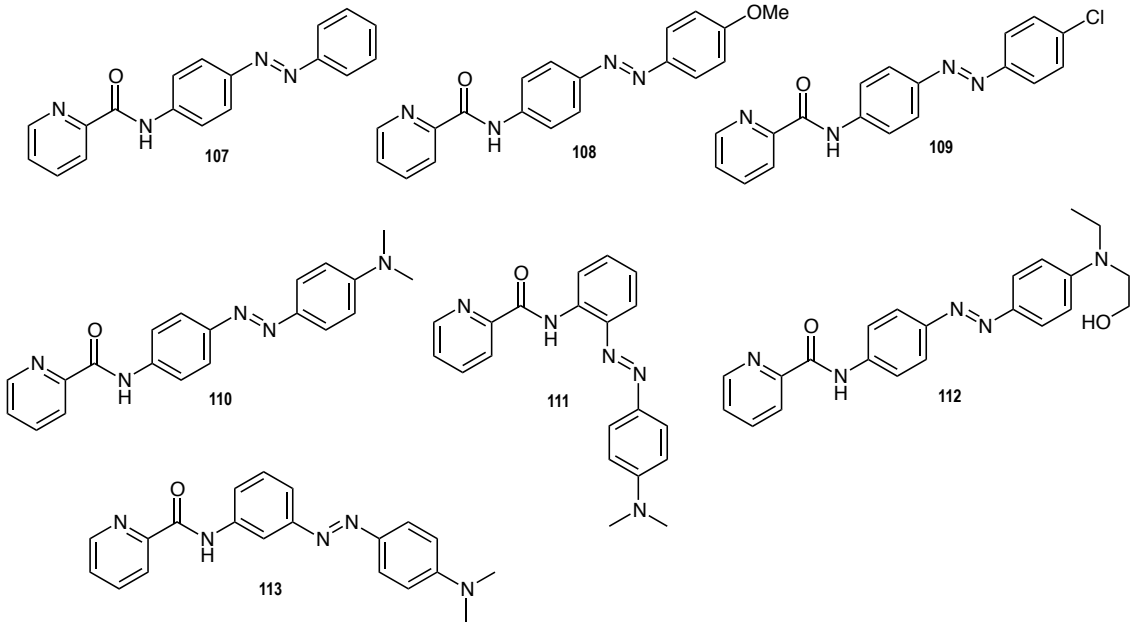

Figure 52: Structures of new library of azocompounds for $mGlu_4$ PAMs

Finally, two additional molecules were added to this library to preliminary explore $mGlu_5$ activity. The first one is based in the well-described $mGlu_5$ PAM **114** (*Figure 53A*), since no azocompound for potentiators of functional activity in $mGlu_5$ were obtained previously in the group. We used the "azologisation" approach for the exchange of an amide to an azo group (*Figure 53A*). On the other hand, a second molecule was based in alloswitch-1 (**34**), but in this case we just change the first pyridine ring by a fluorophenyl because the related allosteric activity in $mGlu_5$ when a molecular switch between this two different aromatic rings happens, shifting the activity from a negative allosteric modulator to a positive allosteric modulator[18] (*Figure 53B*).

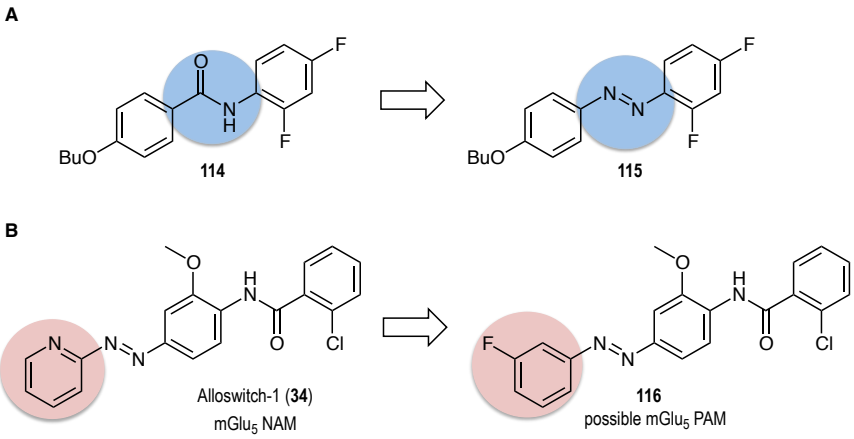

Figure 53: Structures of new library of azocompounds for $mGlu_5$ PAMs

*Synthesis compounds **104-116***

Compounds **104** and **106** were synthesized following the procedure describe in *Scheme 5*. Azobenzene **106** were prepared from reaction of *p*-phenylenediamine with nitrosoaniline **117a** catalysed by acetic acid obtaining **117c** in 20% yield, followed by acylation with anhydride **100a**, Compound **106,** was obtained with 41% of yield.

On the other hand, nitrosoaniline **117a** reacted with *o*-phenylenediamine at melting point with powdered potassium hydroxide to give the azoaniline **117e** in 57% yield following a described procedure (POSAR REF). Then acylation with anhydride **100a** gave compound **104** in 28% yield.

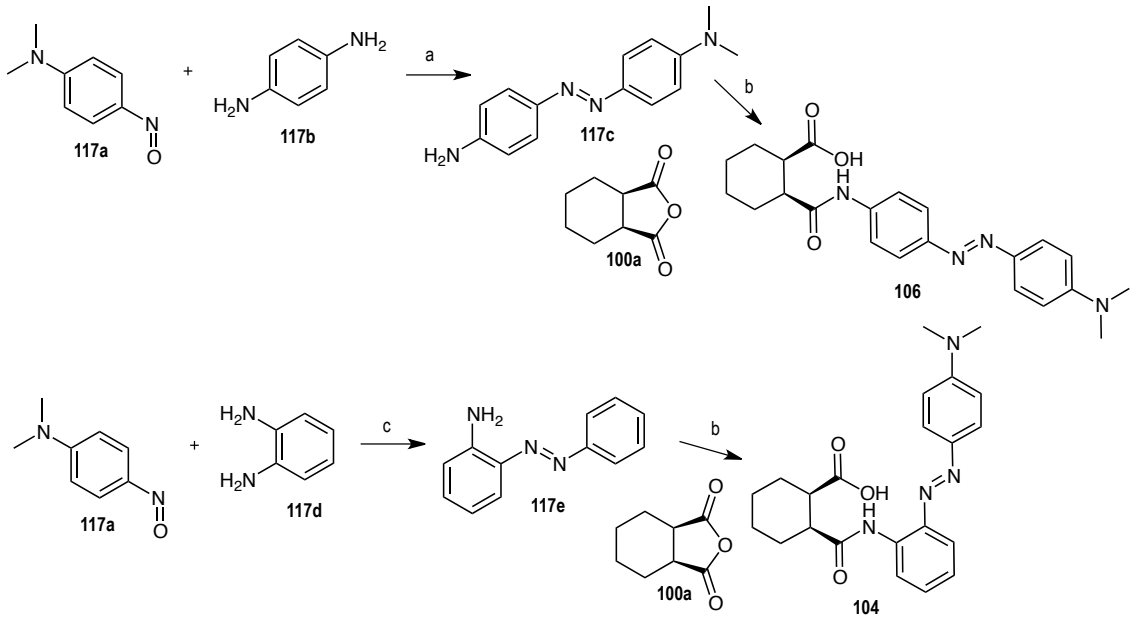

Scheme 5: Synthesis of **104** and **106**. Reagents and conditions: a) AcOH, DCM r.t., 24h, 20%; b) **100a**, NEt_3,THF, reflux, overnight, (**104**)- 28%, (**106**)- 41%; c) (i) KOH (solvent-free); (ii) toluene 90ºC, 1h, 57%.

Compound **105** was synthesized following the procedure shown in *scheme 6.* Azobenzene **118c** was prepared by reaction of aniline **118a** and nitroaniline **118b** in 45% of yield (*step a*) by the nitroso-aniline condensation. Next azobenzene **118c** reduction lead to compound **118d** in 69% yield. The final compound **105** was obtained by acylation with anhydride **100a** in 35% yield.

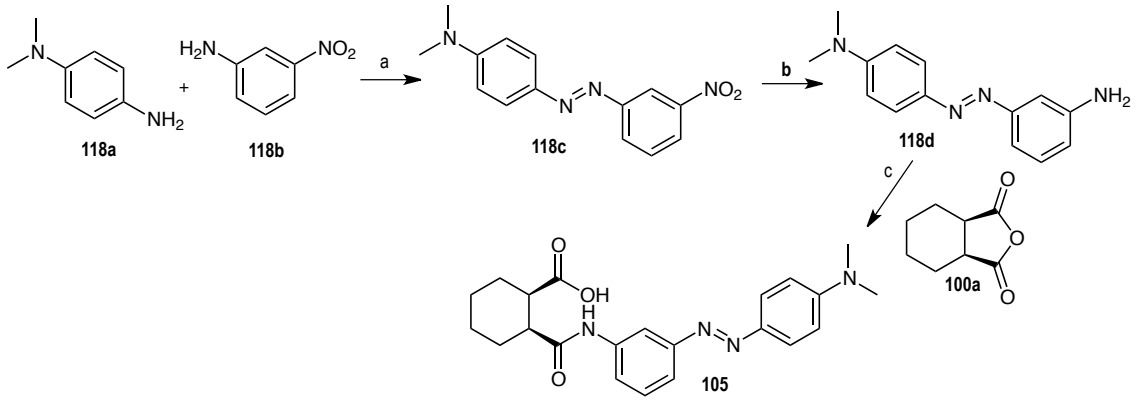

Scheme 6: Synthesis of **105**. Reagents and conditions: a) Oxone, DCM, AcOH, 24h, r.t. 45%; b) $Na_2S \cdot 9H_2O$, EtOH, reflux, 1h, 69%; c) **100a**, NEt_3, THF, reflux, overnight, 35%.

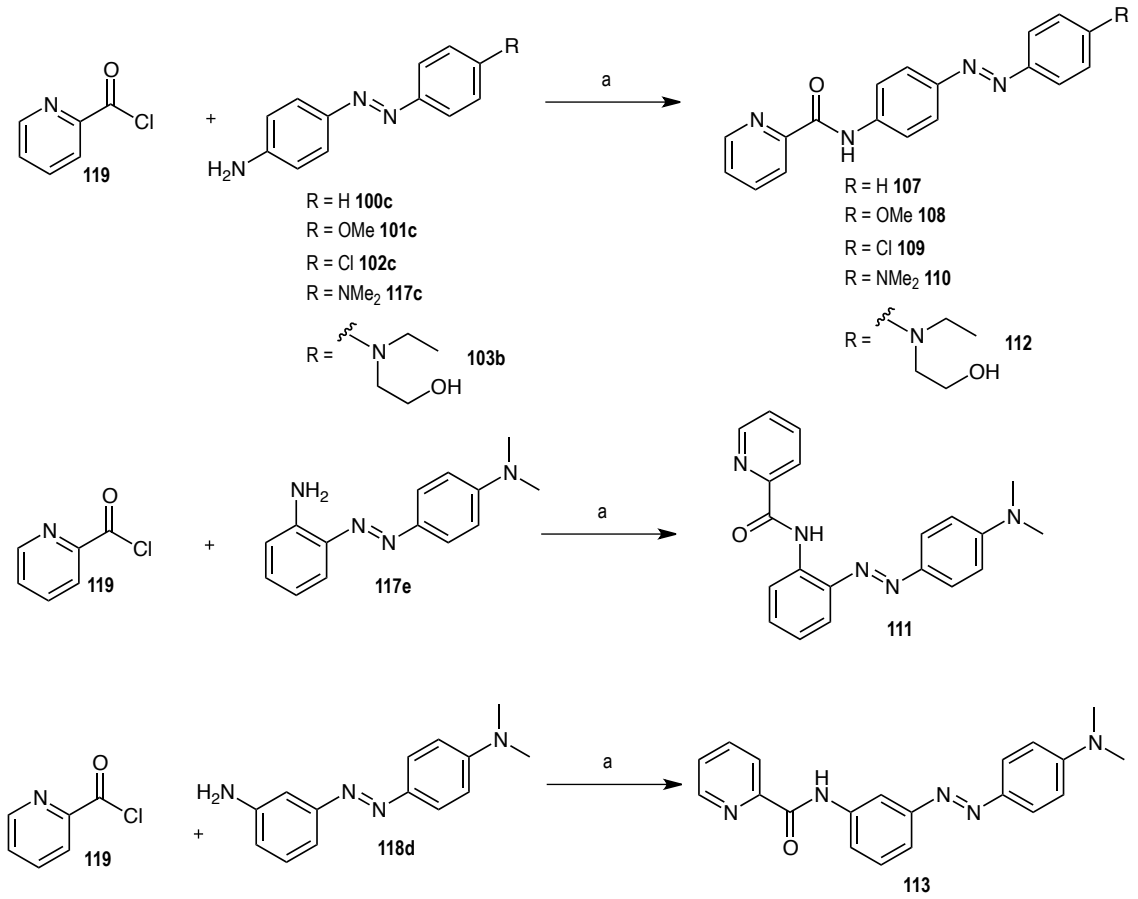

Scheme 7: Synthesis of **107**, **108**, **109**, **110**, **111**, **112** and **113**. Reagents and conditions: a) NEt_3, DCM 40ºC, 24h, (**107**)- 10%, (**108**)- 15%, (**109**)- 11%, (**110**)- 22%, (**111**)- 22%, (**112**)- 13%, (**113**)- 26%.

Compounds from **107** to **113** were synthesized following the procedure depicted in *scheme 7*. Taking advantage of all aminoazobenzene intermediates synthesized, they were reacted with the commercial 2-picolinylchloride to give the final compounds in 10-26% unoptimized yields.

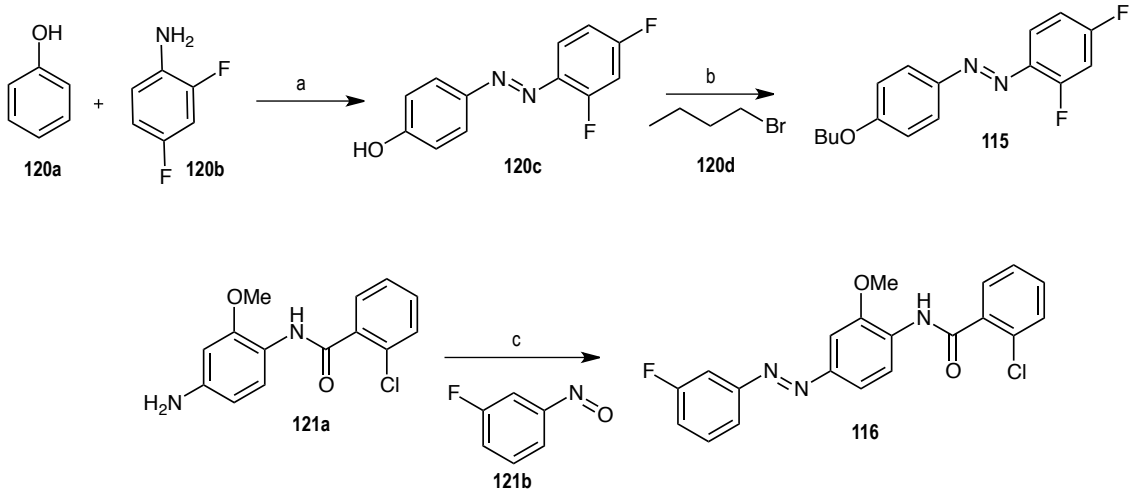

Scheme 8: Synthesis of compounds **115** and **116**. Reagents and conditions: a) $NaNO_2$, NaOH, HCl, H_2O 0ºC, 2h, 41%; b) K_2CO_3, DMF r.t., 24h, 68%, c) Oxone, DCM, AcOH, 24h, r.t. 42%.

Compounds **115** and **116** were prepared as described above in *scheme 8*. Azocompound **120c** was synthesized through azo coupling. Aniline **120a** gave the diazonium salt intermediate that reacted with phenol in basic media to give **120c** in 41% of yield. Compound **115** was obtained by Williamson synthesis with bromobutane in 68% of yield. The azocompound **116** was obtained by reaction of aniline **121a** (previously described in X.Gomez thesis) and the nitrosoaniline **121b** prepared in situ from Oxone oxidation of 3-fluoroaniline to give **116** in 42% of yield.

Photochemical characterisation

The UV-Vis absorption spectra of azobenzene compounds synthesized were measured in DMSO at 100 µM. After that, we tested the photoisomerisation properties (DMSO, 100 µM) under different light conditions (2 minutes continuous irradiation with wavelengths 460 and 380 nm) for **104**, **105**, **106**, **110**, **111**, **112** and **113** compounds and we obtained a decrease of height of the π-π* transition of the *trans* isomer achieving different UV-Vis spectra, corresponding to a photosationary mixture of *cis-trans* isomers for each illumination. In addition, as we could observe, compounds **104**, **105**, **106**, **110**, **111**, **112** and **113** have push-pull substituent properties having the corresponding π- π* transition absorption maximum around 460 nm and the recover *trans* back isomerization wavelengths near 380 nm (*Figure 54*).

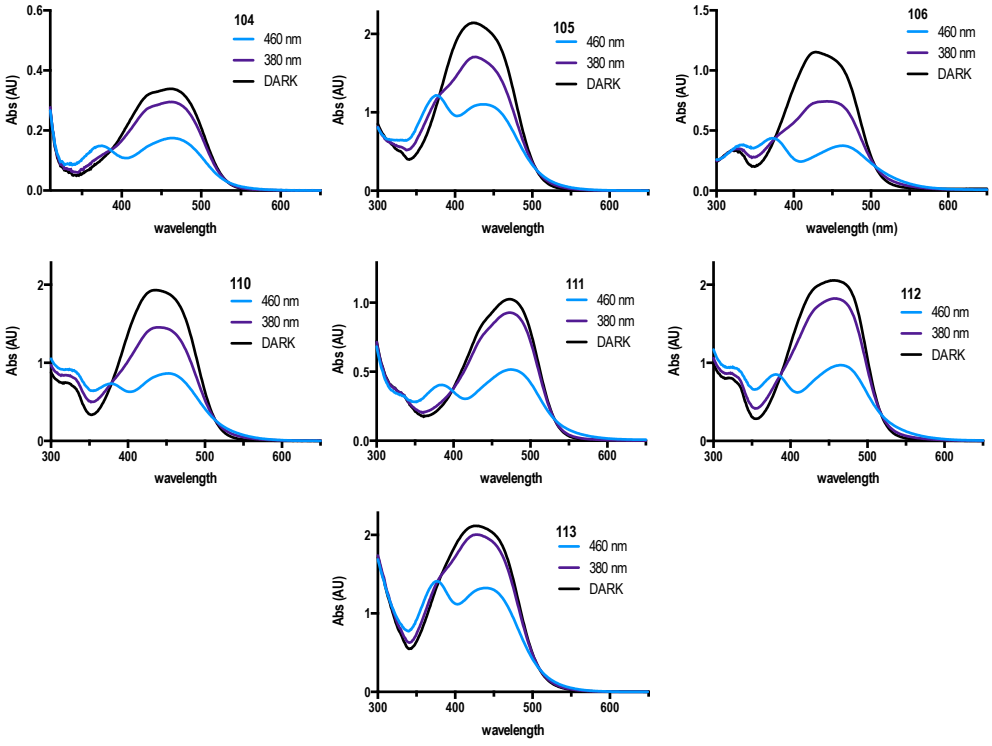

Figure 54: Photochemical characterisation of compounds **104**, **105**, **106**, **110**, **111**, **112** and **113**. UV-Vis absorption spectra in dark conditions (black line), under 460 nm (blue line) and under 380 nm (violet line).

On the other hand, compounds **107**, **108**, **109**, **115** and **116**, as it was expected, showed spectra with the typical azobenzene π-π^* transition band at 370-390 nm and we could back isomerisation at 500 nm wavelength (*figure 55*).

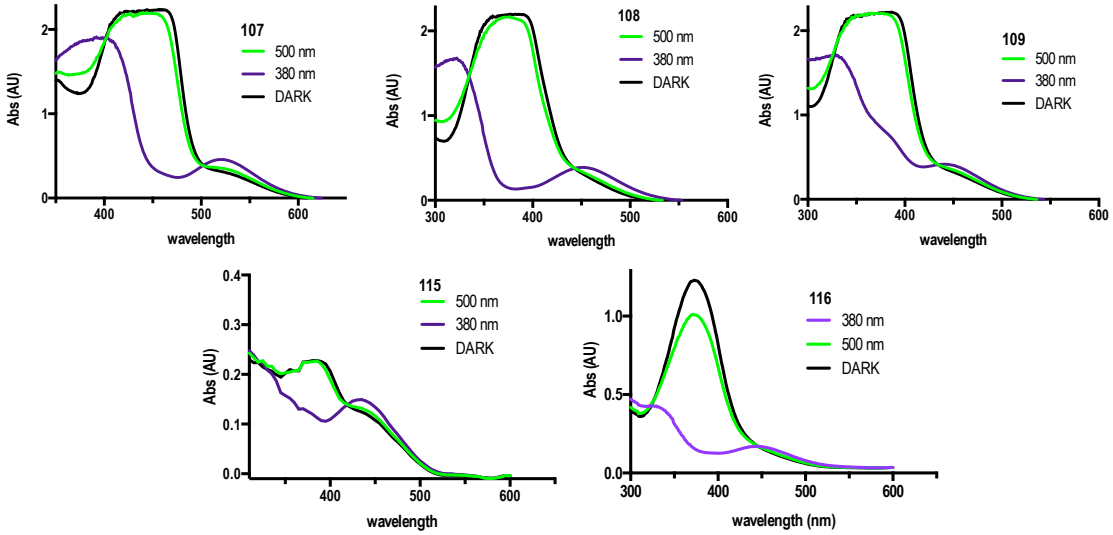

Figure 55: Photochemical characterisation of compounds **107**, **108**, **109**, **115** and **116**. UV-Vis absorption spectra in dark conditions (black line), under 380 nm (violet line) and under 500 nm (green line).

Pharmacological characterisation

Single dose screenings

To evaluate the pharmacological activity of all the new putative *cis*-on $mGlu_4$ PAMs or $mGlu_5$ NAMs of compounds **104**, **105** and **106,** a new single dose screening was done. At the same time the library of compounds was tested as well, to study their effect in both receptors and to examine if these compounds could have the expected *cis*-on behaviour.

As it was reported in first approach, we first screened the compounds in HEK293 cells transfected with rat $mGlu_4$ or $mGlu_5$ using inositol phosphate accumulation assay based on homogenous time resolved fluorescence (HTRF) assay (*experimental part*). Because of the related activity between $mGlu_4$ PAMs and $mGlu_5$ NAMs, the PAM and NAM effect of $mGlu_4$ and $mGlu_5$ were measured. Additionally, every measurement was performed simultaneously in dark conditions and under illumination at the selected wavelength for each compound (λ = 460 nm for

104, **105**, **106**, **110**, **111**, **112** and **113**, λ = 380 nm for **107**, **108**, **109**, **115** and **116**). For $mGlu_4$, we used the orthosteric agonist L-AP_4 (**4**) at low concentration (3 nM) to evaluate a PAM activity and high concentration (300 nM) to evaluate NAM effect. For the evaluation of $mGlu_5$ receptor, the orthosteric ligand quisqualate (**2**) was used at low concentrations (1 nM) for PAM effect, and high concentrations (100 nM) for NAM evaluation.

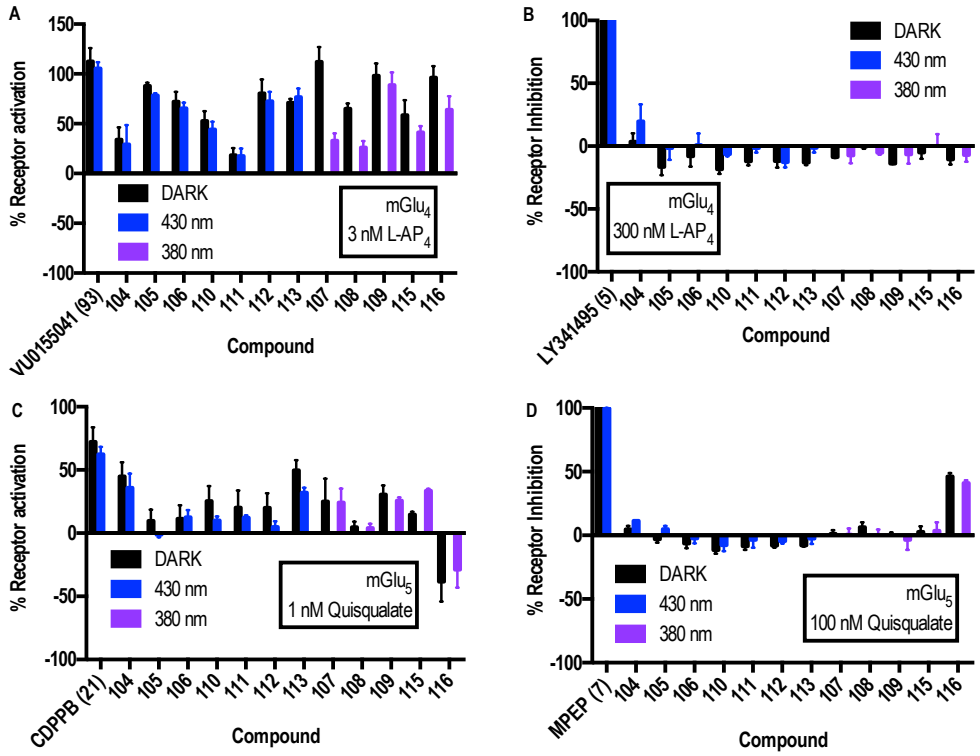

Figure 56: Single-dose screening of compounds **104-116** A) $mGlu_4$ PAMs, B) $mGlu_4$ NAMs, C) $mGlu_5$ PAMs and D) $mGlu_5$ NAMs. FRET response was normalised to 0%-100% between the effect of the low concentration of agonist (EC_{20}) and the effect of the saturation of agonist for the PAM evaluation. For the NAM evaluation, FRET response was normalised to 0%-100% between the effect of the saturation of an antagonist and the high concentration of agonist (EC_{80}). Each bar corresponds to the mean of minimum of two independent replicates with the corresponding SEM as error bars.

Disappointingly, as we observed in the single-dose screening results, we could not achieve a *cis*-on activity, except perhaps for compounds **104** as $mGlu_4$ NAM and **115** as $mGlu_5$ PAM, which show a slight tendency for activity increase in the *cis* isomer respect to the *trans* one despite the low potency of both compounds.

On the other hand, the new small library of compounds designed as $mGlu_4$ PAMs showed high potency in some of them, such as **107**, **109** and **116**, and mild activity for **105**, **112** and **113**, but

without a significant photocontrol in any of them. Additionally, we found out an interesting compound (**116**), which could display high affinity as $mGlu_4$ PAM and $mGlu_5$ NAM. This compound due its dual activity could be a good compound to study this concept with pharmacology potential as a neuroprotective molecule.

In spite of this good results concerning the library, we focus in evaluate further the biological activity of compounds **104** and **115** that showed a minimal *cis*-on activity.

Dose-response curves

This further evaluation of new *cis*-on compounds was carried out by generating dose-response curves using HEK293 cells transfected with rat $mGlu_4$ receptors for compound **104** and with rat $mGlu_5$ receptors for compound **115**, the data were obtained from an inositol phosphate accumulation assay using the "changing tips" protocol used previously and the experiments were done simultaneously in dark conditions and under irradiation at 460 nm for compound **104** and 380 nm for compound **115**.

At the same time, because of the off-targets effects showed previously in the first series of X.Gomez, we additionally performed experiments for both compounds with continuous illumination with HEK293 cells transfected with empty DNA plasmid, which did not encode the $mGlu_4$ or $mGlu_5$ receptor (mock plasmid).

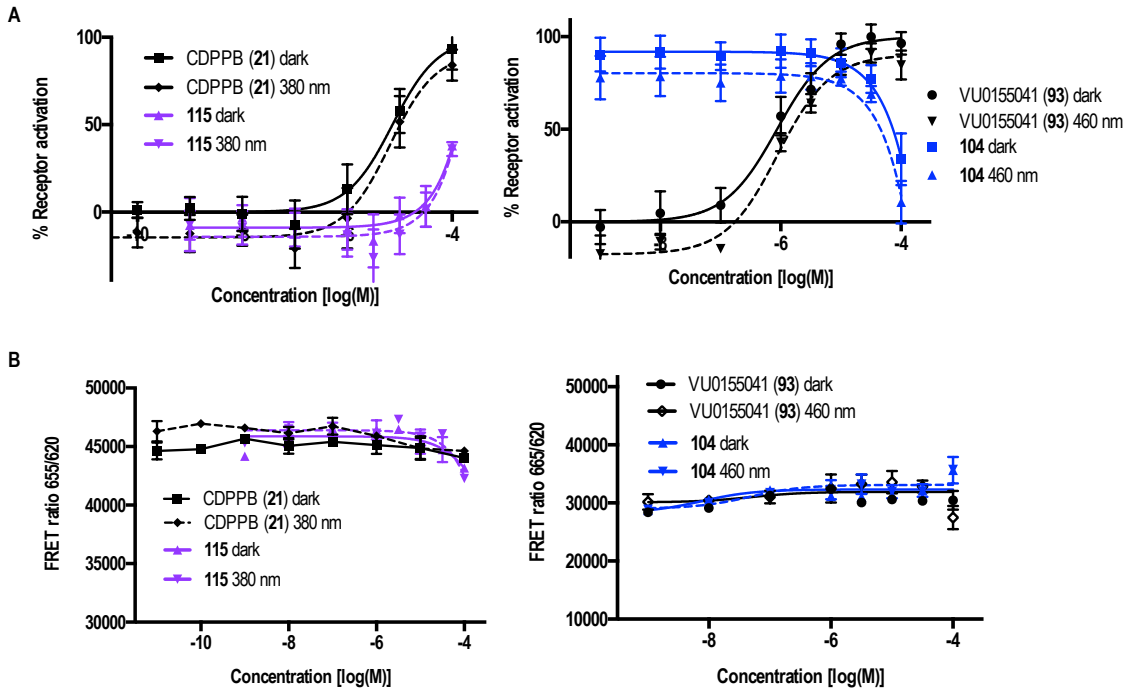

Figure 57: Dose-response curves with IP-One assay in HEK293 cells with compounds **104** and **115** using VU015541 (**93**) as reference of $mGlu_4$ and CDPPB as reference of $mGlu_5$. A) Dose-response curves using HEK293 cells overexpressing $mGlu_5$ for **115** with constant concentration of selective orthosteric ligand Quisqualate (**2**) 100 nM and HEK293 cells overexpressing $mGlu_4$ for **104** with constant concentration of selective orthosteric ligand L-AP_4 (**4**) 300 nM and 3 nM for its reference compound VU0155041 (**93**). Flat lines correspond to he samples incubated in dark conditions and dotted lines corresponds the samples under irradiation at 460 nm for **104** and 380 nm for **115**. Each point corresponds to the mean of a minimum three independent replicates with the corresponding SEM as error bars. B) Dose-response curves using HEK293 cells with no expression of $mGlu_4$ for **104** and HEK293 cells with no expression of $mGlu_5$ for **115**. Both experiments were tested with constant concentration of its selective orthosteric compound (L-AP_4 (**4**) 300 nM for **104** and 3 nM for its reference VU0155041 (**93**) in dark (flat lines) and under irradiation at 460 nm (dotted lines) or Quisqualate (**2**) 100 nM for **115** in dark (flat lines) and under irradiation at 460 nm (dotted lines)). Each point corresponds to the mean of minimum three independent replicates with the corresponding SEM as error bars.

In both cases, a clear difference between the assays in dark conditions and under irradiation ones was not achieved in line with the photoisomerization experiments obtained for these compounds. The evaluation of non-specific effects with HEK293 cells transfected with an empty DNA plasmid was also not clear, but at higher concentrations both compounds show unspecific effect which seems to indicate that, again, we obtained some off-target effects possibly involved in IP production or an interference of the azobenzene with the fluorescence readout.

Summary of results

In X.Gomez thesis, compounds **84** and **85** were designed as a new class of phostoswitchable compounds to potentially display a *cis*-on activity as $mGlu_4$ PAM and compounds **86**, **87** and **88** to display a *cis*-on activity as $mGlu_5$ NAM based on a literature search with a bent disposition to mimic *cis* azobenzene geometry. Therefore the *trans* disposition would expected to be long to fit in the receptor, just adapting to the allosteric pocket when the irradiation takes place.
In addition these compounds were designed to display a *trans* to *cis* isomerisation in the visible range, with the addition of electron donating substituents in the aromatic rings of azobenzenes. The final optimal wavelength obtained was between 430 and 460 nm.

After the first pharmacological evaluation, the compounds that showed a small *cis*-on effect in screening assays were subjected to further evaluation obtaining dose-response assays. A very weak $mGlu_4$ PAM *cis*-on light dependent effect was observed for 2-picolinamide **84.**

The new designed picolinamides **91** and **92** were synthesized an evaluated pharmacologically in the dark and under irradiation conditions obtaining a more increased *cis*-on effect especially for compound **92**. However, when both compounds were tested in the same assays in cells without expressing $mGlu_4$ receptors very similar results were obtained, indicating that this interesting *cis*-on effect was probably due to an off-target activity.

We designed compounds **95**, **96**, **97**, **98** and **99** as potential candidates to display a PAM $mGlu_4$ activity based on a literature described diphenylether compound **94**. The replacement of the diphenylether by an azobenzene due its geometrical resemblance was attempted trying to mimic **94** $mGlu_4$ PAM activity. The optimal photoisomerisation conditions were studied and biological evaluation was done. The first screening evaluation on the new design in dark and under irradiation did not show the desired effect, but a new series of trans-on was discovered for compounds **95**, **96** and **97** performing a biological dose-response assays for a further evaluation.

After we failed in this first series, new compounds were designed obtaining **104**, **105** and **106** exploring other substitutions of the azo group in the first aromatic ring due the several free mobility of diphenylether group.

In addition, several compounds were designed to start a new library of photoswitchable compounds to display $mGlu_4$ PAMs and $mGlu_5$ PAMs synthesizing compounds **107**-**116**. All compounds had been designed to display a *trans* to *cis* isomerisation in the visible range, with the addition of electron donating substituents in the aromatic rings of azobenzenes. The final optimal wavelength obtained was between 430 and 460 nm.

Compounds **104** to **116** were tested in a single dose screening assay in the dark and under irradiation, and in this case we detected two compounds that showed a weak effect in *cis* disposition, one as $mGlu_4$ NAM (**104**) and another as $mGlu_5$ PAM (**115**).

Further evaluation of compounds **104** and **115** was done in their respective target receptor, performing dose-response assays, but a very weak *cis*-on effect was measured in low potency compounds. However, when both compounds were tested in HEK293 cells transfected with empty DNA plasmid (mock control), showed a small effect at higher concentrations. These results are interpreted as the cis-on activity observed was originated from an unknown activity in HEK293 cells.
Moreover, a new photoswitchable $mGlu_4$ PAM and $mGlu_5$ NAM (**116**) was identified with a good potency but without having light differentiation between *cis* and *trans* configurations.

Conclusions

We evaluated at single dose activity assays for $mGlu_4$ and $mGlu_5$ allosteric responses compounds **84**, **85**, **86**, **87** and **88** in the dark and under illumination, with putative *cis*-on behaviour at this receptor obtaining two promising compounds (**84** and **85**) having an increase of activity when illuminated. Further evaluation for both compounds was performed with dose response curves, which did not result in a clear-cut *cis*-on activity.

Two new compounds (**91** and **92**) were designed, synthesized and evaluated in dose response curves as PAMs of $mGlu_4$ obtaining positive results concerning *cis*-on activity when measured in a IP-One assay in HEK293 cells. These results were not confirmed in a negative control assay using cells not having expressed $mGlu_4$ receptor, which showed a similar result to that obtained in cells expressing $mGlu_4$. Therefore, the observed *cis*-on activity is attributed to unspecific effects inducing a response in the IP-one assay.

We designed and synthesized compounds **95**, **96**, **97**, **98** and **99** with putative *cis*-on behaviour as PAMs of $mGlu_4$. We characterized their photochemical properties and the pharmacological assays performing single dose screening first, and dose response curves after, to evaluate the active compounds but, unfortunately, all showed a weak *trans*-on activity.

We designed and synthesized new compounds **104**, **105** and **106** to obtain $mGlu_4$ PAM compounds with *cis*-on effect. Moreover, compounds from **107**-**116** were designed and synthesized for small library as photoswitchable $mGlu_4$ and $mGlu_5$ PAMs. All compounds were characterized their photochemical and pharmacological properties on this receptor. Compounds **104** and **115** were further evaluated due a slight tendency to *cis*-on effect. These results could not be confirmed in control experiments in the absence of the target receptor, therefore the observed *cis*-on effect can be attributed to unspecific activities on the IPone cell assay.

Bibliography

1. Bandara, H. M.; Burdette, S. C., Photoisomerization in different classes of azobenzene. *Chemical Society reviews* **2012,** *41* (5), 1809-25.
2. Turansky, R.; Konopka, M.; Doltsinis, N. L.; Stich, I.; Marx, D., Switching of functionalized azobenzene suspended between gold tips by mechanochemical, photochemical, and opto-mechanical means. *Physical Chemistry Chemical Physics* **2010,** *12* (42), 13922-13932.
3. Tong, X.; Pelletier, M.; Lasia, A.; Zhao, Y., Fast Cis–Trans Isomerization of an Azobenzene Derivative in Liquids and Liquid Crystals under a Low Electric Field. *Angewandte Chemie International Edition* **2008,** *47* (19), 3596-3599.
4. Szymanski, W.; Beierle, J. M.; Kistemaker, H. A.; Velema, W. A.; Feringa, B. L., Reversible photocontrol of biological systems by the incorporation of molecular photoswitches. *Chemical reviews* **2013,** *113* (8), 6114-78.
5. Miller, J. A.; Miller, E. C., The Carcinogenicity of 3-Methoxy-4-aminoazobenzene and Its N-Methyl Derivatives for Extrahepatic Tissues of the Rat. *Cancer Research* **1961,** *21* (8), 1068.
6. Toro, C.; Thibert, A.; De Boni, L.; Masunov, A. E.; Hernández, F. E., Fluorescence Emission of Disperse Red 1 in Solution at Room Temperature. *The Journal of Physical Chemistry B* **2008,** *112* (3), 929-937.
7. Siewertsen, R.; Neumann, H.; Buchheim-Stehn, B.; Herges, R.; Näther, C.; Renth, F.; Temps, F., Highly Efficient Reversible Z−E Photoisomerization of a Bridged Azobenzene with Visible Light through Resolved S1(nπ*) Absorption Bands. *Journal of the American Chemical Society* **2009,** *131* (43), 15594-15595.
8. Broichhagen, J.; Frank, J. A.; Trauner, D., A roadmap to success in photopharmacology. *Accounts of chemical research* **2015,** *48* (7), 1947-60.
9. Schoenberger, M., Development of a New Photochromic Ion Channel Blocker. **2014,** *5* (7), 514-8.
10. East, S. P.; Bamford, S.; Dietz, M. G.; Eickmeier, C.; Flegg, A.; Ferger, B.; Gemkow, M. J.; Heilker, R.; Hengerer, B.; Kotey, A.; Loke, P.; Schanzle, G.; Schubert, H. D.; Scott, J.; Whittaker, M.; Williams, M.; Zawadzki, P.; Gerlach, K., An orally bioavailable positive allosteric modulator of the mGlu4 receptor with efficacy in an animal model of motor dysfunction. *Bioorganic & medicinal chemistry letters* **2010,** *20* (16), 4901-5.

11. Pittolo, S.; Gomez-Santacana, X.; Eckelt, K.; Rovira, X.; Dalton, J.; Goudet, C.; Pin, J. P.; Llobet, A.; Giraldo, J.; Llebaria, A.; Gorostiza, P., An allosteric modulator to control endogenous G protein-coupled receptors with light. *Nat. Chem. Biol* **2014,** *10* (10), 813-5.

12. (a) Gasparini, F.; Lingenhohl, K.; Stoehr, N.; Flor, P. J.; Heinrich, M.; Vranesic, I.; Biollaz, M.; Allgeier, H.; Heckendorn, R.; Urwyler, S.; Varney, M. A.; Johnson, E. C.; Hess, S. D.; Rao, S. P.; Sacaan, A. I.; Santori, E. M.; Velicelebi, G.; Kuhn, R., 2-Methyl-6-(phenylethynyl)-pyridine (MPEP), a potent, selective and systemically active mGlu5 receptor antagonist. *Neuropharmacology* **1999,** *38* (10), 1493-503; (b) Varney, M. A.; Cosford, N. D.; Jachec, C.; Rao, S. P.; Sacaan, A.; Lin, F. F.; Bleicher, L.; Santori, E. M.; Flor, P. J.; Allgeier, H.; Gasparini, F.; Kuhn, R.; Hess, S. D.; Velicelebi, G.; Johnson, E. C., SIB-1757 and SIB-1893: selective, noncompetitive antagonists of metabotropic glutamate receptor type 5. *The Journal of pharmacology and experimental therapeutics* **1999,** *290* (1), 170-81.

13. Santacana, X. G. Design, synthesis and characterisation of photoswitchable allosteric modullators of metabotropic glutamate receptors. Universitat de Barcelona, 2016.

14. Dore, A. S.; Okrasa, K.; Patel, J. C.; Serrano-Vega, M.; Bennett, K.; Cooke, R. M.; Errey, J. C.; Jazayeri, A.; Khan, S.; Tehan, B.; Weir, M.; Wiggin, G. R.; Marshall, F. H., Structure of class C GPCR metabotropic glutamate receptor 5 transmembrane domain. *Nature* **2014,** *511* (7511), 557-62.

15. Engers, D. W.; Niswender, C. M.; Weaver, C. D.; Jadhav, S.; Menon, U. N.; Zamorano, R.; Conn, P. J.; Lindsley, C. W.; Hopkins, C. R., Synthesis and evaluation of a series of heterobiarylamides that are centrally penetrant metabotropic glutamate receptor 4 (mGluR4) positive allosteric modulators (PAMs). *Journal of medicinal chemistry* **2009,** *52* (14), 4115-8.

16. Engers, D. W.; Field, J. R.; Le, U.; Zhou, Y.; Bolinger, J. D.; Zamorano, R.; Blobaum, A. L.; Jones, C. K.; Jadhav, S.; Weaver, C. D.; Conn, P. J.; Lindsley, C. W.; Niswender, C. M.; Hopkins, C. R., Discovery, synthesis, and structure-activity relationship development of a series of N-(4-acetamido)phenylpicolinamides as positive allosteric modulators of metabotropic glutamate receptor 4 (mGlu(4)) with CNS exposure in rats. *Journal of medicinal chemistry* **2011,** *54* (4), 1106-10.

17. Niswender, C. M.; Johnson, K. A.; Weaver, C. D.; Jones, C. K.; Xiang, Z.; Luo, Q.; Rodriguez, A. L.; Marlo, J. E.; de Paulis, T.; Thompson, A. D.; Days, E. L.; Nalywajko, T.; Austin, C. A.; Williams, M. B.; Ayala, J. E.; Williams, R.; Lindsley, C. W.; Conn, P. J., Discovery, characterization, and antiparkinsonian effect of novel positive allosteric modulators of metabotropic glutamate receptor 4. *Molecular pharmacology* **2008,** *74* (5), 1345-58.

18. Wood, M. R.; Hopkins, C. R.; Brogan, J. T.; Conn, P. J.; Lindsley, C. W., "Molecular switches" on mGluR allosteric ligands that modulate modes of pharmacology. *Biochemistry* **2011,** *50* (13), 2403-10.

Chapter 2

Chapter 2: Cage compounds for allosteric modulators of metabotropic Glutamate receptors

The objectives developed in this chapter were the design and synthesis of new cage allosteric compounds for metabotropic glutamate receptors (mGluRs) amenable for *in vivo* activation with light. These comprise NAMs for metabotropic glutamate receptor subtype 5 ($mGlu_5$), NAMs for metabotropic glutamate receptors subtype 1 ($mGlu_1$) and PAMs for metabotropic glutamate receptors subtype 4 ($mGlu_4$), which modulate pain transmission and have consistently been shown to display analgesic activity in experimental animal models of chronic pain[1]. In addition, photochemical and pharmacological *in-vitro* and *in-vivo* characterisations of such compounds will also be evaluated.

In this chapter we show the results obtained from these objectives and their corresponding discussion.

Introduction

Cage compounds

Cage compounds are molecules whose biological activity is controlled by light, usually by photolytic conversion from an inactive to an active form. These compounds are based on two approaches: (i) small biologically active species that are trapped inside a large framework (*Figure 59A*) can be liberated upon illumination or (ii) in nearly all successful caged molecules so far, simple covalent bond formation masks some feature important for biological recognition and photochemical cleavage of that single bond releases the active species. In this chapter we will focus on this second cage compounds approach (*Figure 59B*)[2].

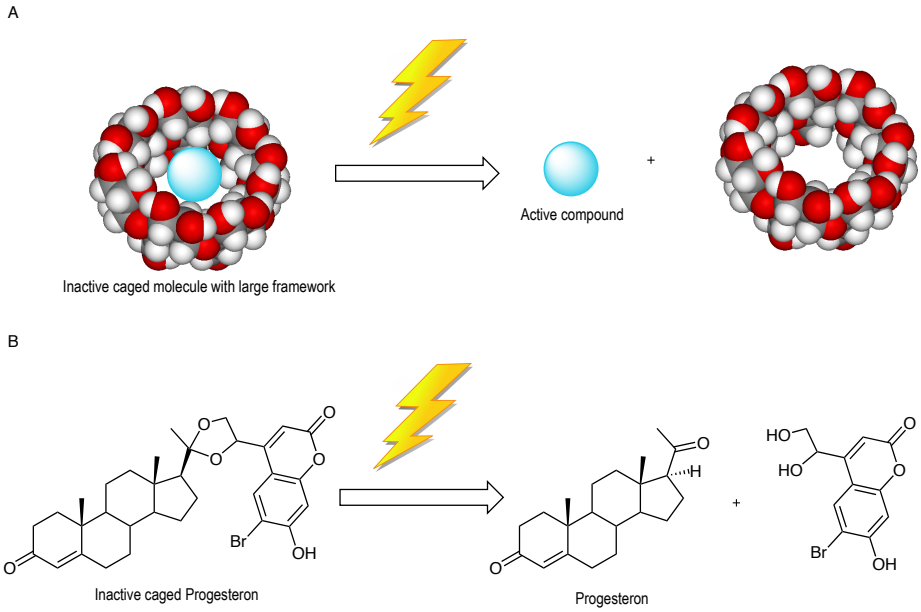

Figure 59: Examples of two types of caged compounds. A) Active species trapped inside a large framework. B) Caged compound trapped by a simple bond.

Caged compounds are biologically useful because illumination can be easily controlled in timing, location, and amplitude. Therefore, abrupt or localized changes in concentration of active species can be generated with controlled wavelengths. Photolysis of caged compounds is one of the best techniques to examine the fast kinetics or spatial heterogeneity of biochemical responses in such systems[2].

Modifying the desired biomolecule with a suitable photoremovable protecting group or caging group leads to the best design for cage compounds. To be useful in biological experiments this group must satisfy (at least partially) several criteria: It should render the biomolecule inert to the biological system used, release the biomolecule in high yield at sufficient speed by photolysis at wavelengths of light that are non-hazardous to the biological process and any photoproduct other than the desired biomolecule should not interact or interfere with the biological system.

In addition, some of these caging groups could have especial characteristics concerning their behaviour in dependence of the light source, which could be of two types, the single or one photon excitation (1PE) and the two-photon excitation (2PE).

Whereas classical one-photon excitation consists in the absorption of one photon of a single chromophore to reach an excited state (less stable); in the two-photon excitation, the single

chromophore absorbs two non-resonant photons of the same wavelength nearly simultaneously to produce the electronically excited effect, exploiting the virtual excited state is delivering the same energy (*Figure 60*).

In two-photon excitation, after photolysis excitation, the mechanistic steps are not different of those resulting of the process assuming it was initiated through conventional one-photon excitation. However, the process of excitation is different. High light intensities are required to generate an appreciable amount of two-photon excitation, because the probability of simultaneous two-photon absorption depends on the square of the intensity of light. The result is that the excitation occurs only on the focus of the laser beam, which can be as small as 1 μm^3 for a tightly focused laser. Outside of this space, no excitation occurs, in contrast with 1PE process, which lacks 3D selectivity of excitation because all of the photons, not just those ones in the focus of laser, have enough energy to excite the chromophore[3] (*Figure 60*).

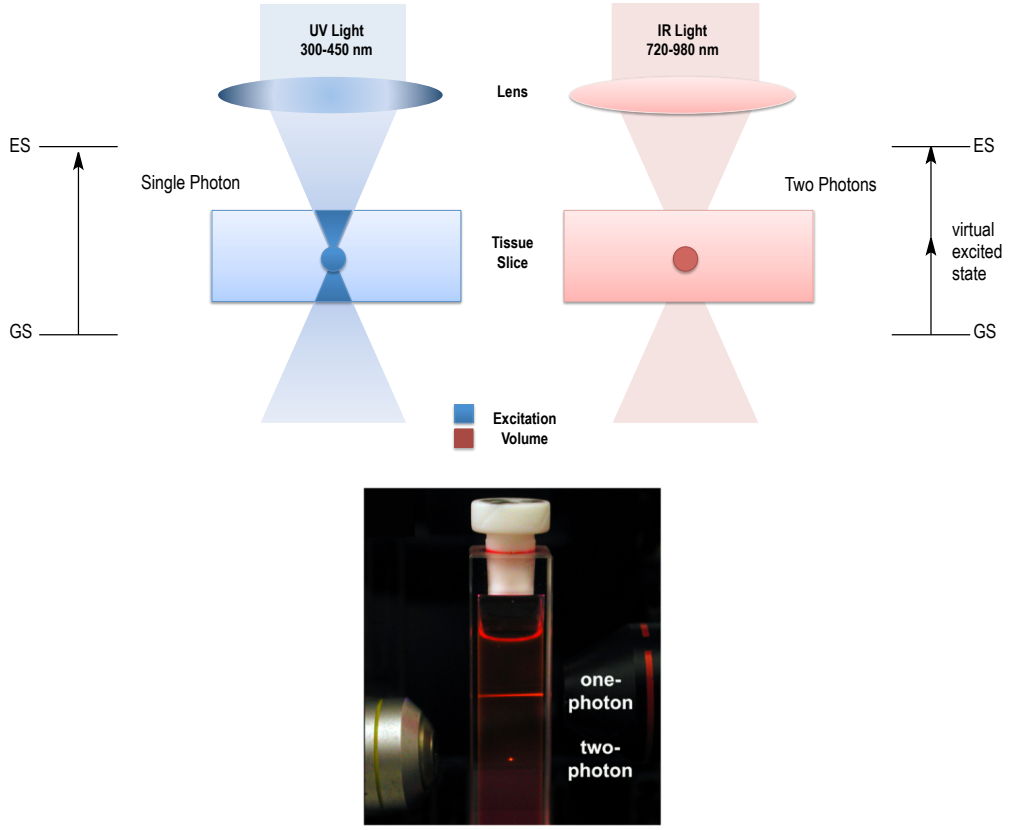

Figure 60: Depicted one-photon excitation versus two-photon excitation of a single chromophore (Adapted from Givens[3]).

These excitations do not follow the squared dependence on incident light power. Different quantum mechanical selection rules apply to 2PE, and large differences between 1PE and 2PE

spectra can exist[4]. The wavelength for which a chromophore is most sensitive to 2PE is not always twice the single-photon absorbance maximum, but this is a good qualitative prediction of where 2PE of a chromophore will occur[5].

Types of cage molecules

Working in biological and physiological processes, in order to achieve the maximum absorption of the caged-drug (which will be determined in dependence of the cage molecule) is critical to irradiate in an adequate wavelength because there are some factors which will affect the successful un-caging.

The wavelength applied for irradiation should be in a safe range for the living systems, notwithstanding whether they are cells, rats or humans. It is well known that deep UV light (250-350 nm) will be dangerous, although is the most energetic in this range, and other biomolecules could be affected. Therefore, the importance to move in the visible safe range is crucial and, in addition, the shift from the UV light (380 nm) to red light (650 nm) could allow penetrate deeper in any tissue (*Figure 61*).

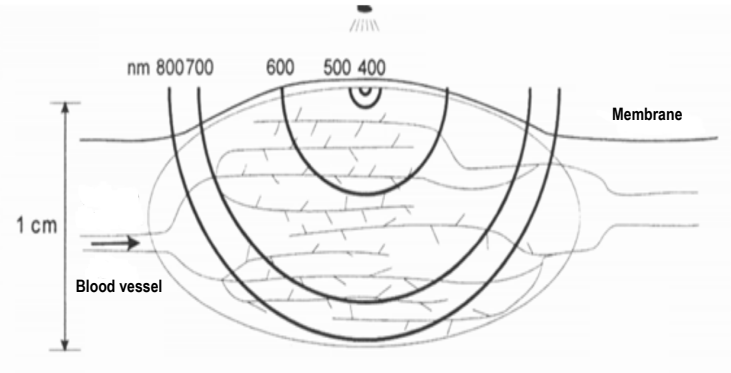

Figure 61: Schematic penetration in living tissues depending on the wavelength.

Nowadays, several cage molecules have been developed to be applied considering all the facts exposed before. In this chapter, we will focus in photopharmacology, modifying structurally potential drugs previously described in the literature with different types of caged molecules. Despite there exists lot of caged molecules, we will focus mainly in two families: The nitrobenzyl derivatives and the coumarin family[3].

Nitrobenzyl derivatives family

Nitrobenzyl-derived cages (NB) were first developed for release of biologically active ligands with near-UV photolysis (300 to 400 nm) wavelength range. Some of the currently used NB-derived protecting groups are depicted in *Figure 62*. They have been applied to the liberation of phosphates, carboxylic acids, amides, alcohols and carbonyl functions, as well as of metal ions. However, concerning NB neuroactive amino acids, generally show poor hydrolytic stability. Due to this reason, a carbamate linker between the alcohol and amino group generates stable and efficient cages of amino acids, but their slow fragmentation kinetics restricts their use to slow signalling processes[6].

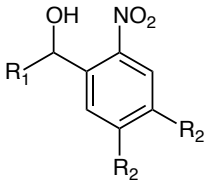

122a R_1 = H; R_2 = H (NB-OH)
122b R_1 = COOH; R_2 = H (CNB-OH)
122c R_1 = Me; R_2 = H (NPE-OH)
122d R_1 = H; R_2 = OMe (DMNB-OH)
122e R_1 = Me; R_2 = OMe (DMNPE-OH)

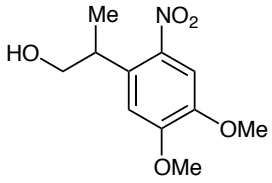

122f

Figure 62: Some of the currently used nitrobenzyl-derived protecting groups.

The mechanistic aspects of photocleavage of such compounds was previously reported by Walker and collaborators[7] for caged ATP. An important aspect of the mechanism was the decay of the intermediate *aci*-nitro anion **123c** (*Scheme 9*), which was the rate-determining step for ATP release. It was noted that the *aci*-nitro decay rate was proportional to proton concentration below pH 9: The lower pH limit of this proportionality was not determined[7]. The pH dependence was attributed, without specific evidence, to protonation of non-bridging oxygen in the triphosphate chain. However, computational and experimental studies[8] suggest as an alternative explanation that the *aci*-nitro anion must reprotonate to allow the closure to the benzisoxazoline **123e** and subsequent reaction, shown in a general case in *Scheme 9*, where X is the caged species and R is any substituent depicted in *Figure 62*.

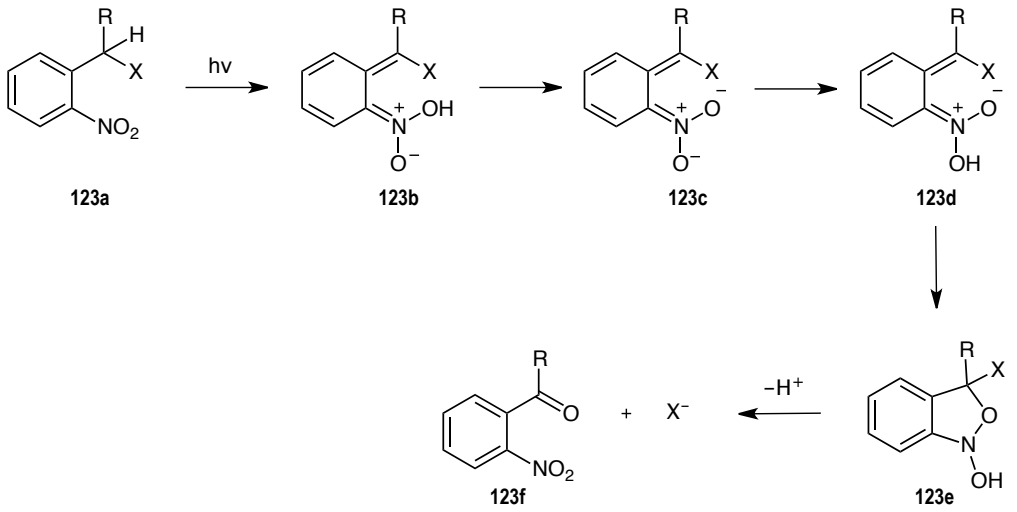

Scheme 9: Detailed reaction scheme for photolysis of generalized nitrobenzyl-caged compounds.

Other groups introduced by Amit[9] in the mid 1970s were the 7-Nitroindoline (NI) derivatives as carboxylic acid protecting groups for photolysis in aqueous solution and specifically adapted to the photorelease of neuroactive amino acids.

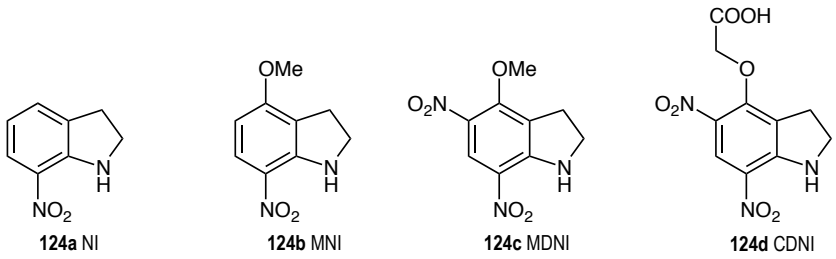

Figure 63: Some 7-Nitroindoline-derived cage molecules.

The effect of substitutions on the indole core was examined, and maximum photolysis efficiency was found with 4-methoxy-7-nitroindolinyl (MNI) derivatives[10]. Mechanistic investigations have shown that the product of the photolysis of 7-nitroindolines depends on the medium and is different when the irradiation is performed in an aprotic solvent or in water. In an aprotic solvent with about 1% water, 7-nitroindoline is formed through a solvent-assisted mechanism, whereas in water the photoproduct is the substituted 7-nitrosoindole, formed without intervention of the solvent[10].

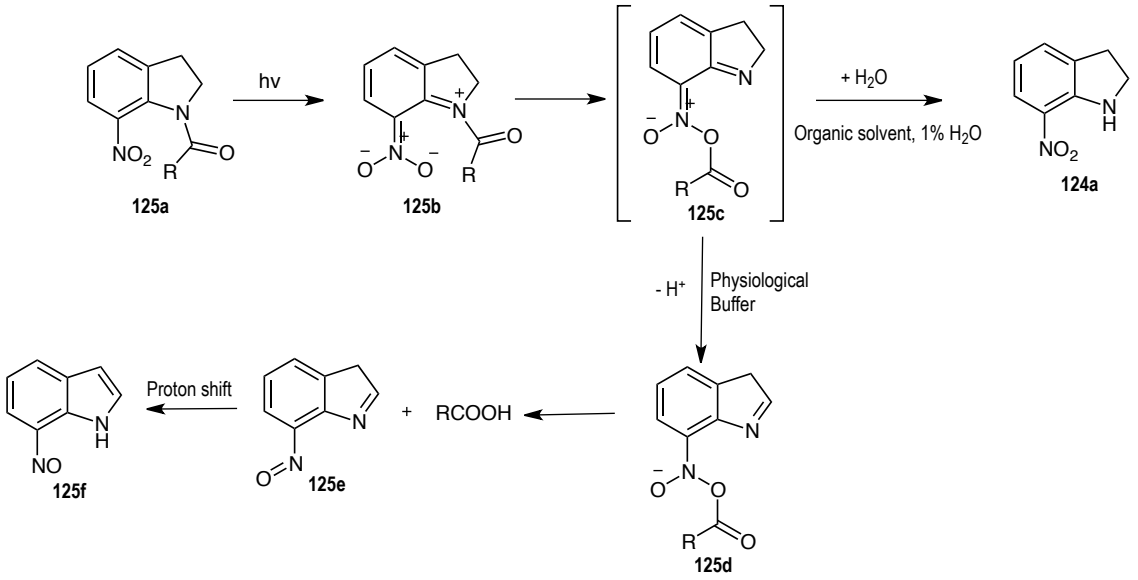

Scheme 10: Photolysis mechanism of 1-Acyl-7-nitroindoline alternate pathways in dependence of the solvent.

Coumarin family

Coumarin-4-ylmethyl groups are developed phototriggers that have been used to make caged molecules of several compounds, such as phosphates, carboxylates, amines, alcohols, phenols and carbonyl functional groups. We can distinguish four coumarin-4-ylmethyl families with different photochemical and physiological properties, MCM (7-Alkoxy-Substituted Coumarins), DMCM (6,7- Dialkoxy-Substituted Coumarins), DEACM (7-Dialkylamino-Substituted Coumarins) and Bhc (6-Bromo-7-alkoxy-Substituted Coumarins).

MCM family

The MCM family comprises the MCM (methoxy coumarin), ACM (acetyl coumarin), PCM (propyl coumarin), HCM (hydroxyl coumarin) and CMCM (carboxylic methylene coumarin) groups (*Figure 64*). Each group has a membrane-permeable and a water-soluble structural variant. They are designed to facilitate methods to incorporate the compounds into biological systems. These groups can cage carboxylates, sulfates and alcohols but they are mostly reported for caging phosphate esters. The ACM and the PCM groups are designed to improve the membrane permeability, which after incorporation into live systems will be hydrolysed by intrinsic estereases to produce a more polar HCM group. CMCM is almost fully ionized at physiological pH and, consequently, the CMCM-caged compounds should be highly water-soluble[11].

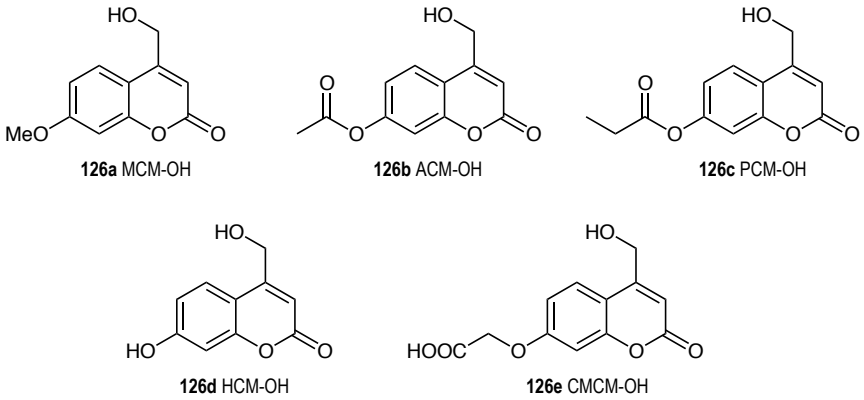

Figure 64: Corresponding structures of MCM family coumarins

DMCM Family

This family is quite similar to MCM group, but with different substitution. The DMCM group is divided in three main subgrups: BCMCM (Biscarboxylic methylene coumarin), BECMCM (Bisethylcarobxy methylene coumarin) and DMCM (Dimethoxy coumarin) (*figure 65*), and they are mostly utilized to make caged compounds of phosphates and alcohols.

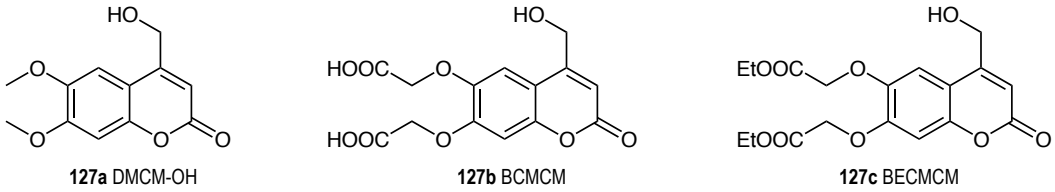

Figure 65: Corresponding structures of DMCM family coumarins

The BMCM has two carboxylic acids and renders the corresponding caged compounds highly water-soluble. The BECMCM is the membrane-permeable version of BCMCM due to the conversion in ethyl esters instead of carboxylic acid, and the negative charges are thereby masked. In addition, the hydrolysis of these ethyl esters by intrinsic estereases is postulated after the compound is incorporated into live cells[12].

DEACM family

This group is composed of two general compounds described in the literature until now, DEACM and DMACM (*Figure 66*). Dialkylamino substitution on C7 improved more new spectroscopic and photochemical properties than permeability. The absorption maxima of these compounds are

around 390-400 nm and with quantum yields of photolysis as high as 0.3, which is the highest value among the reported coumarin cages. No remarkable differences between DEACM (Diethylamino coumarin) and DMACM (Dimethylamino coumarin) variants are apparent, except for their fluorescence intensity. The DEACM group can be used to protect carboxylates, amines, diols and carbonyl compounds[13].

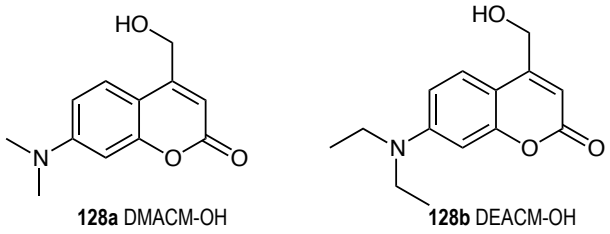

Figure 66: Corresponding structures of DEACM family coumarins

Concerning the photolytic-cleavage of the groups shown above, Hagen and Bending proposed a mechanism for the photolytic cleavage of MCM, DCMC and DCEAM groups[14], involving the heterolysis of the CH_2-OX bond from the lowest excited state, an escape of the resulting ion pairs from the solvent cage, and trapping of the coumarin-4-ylmethyl cation by the solvent (*Scheme 11*).

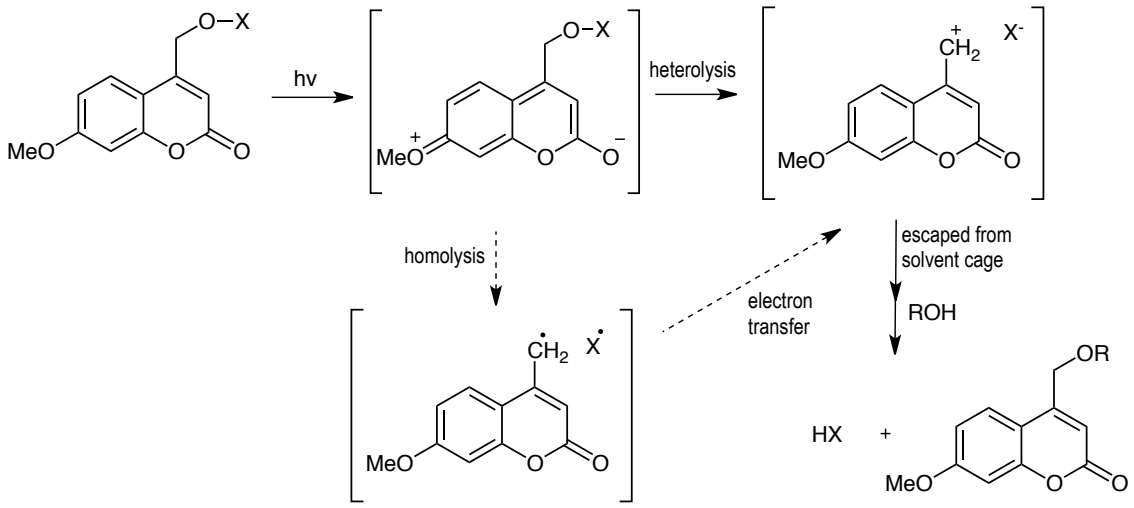

Scheme 11: Proposed mechanism of the photolysis of MCM, DCMC, DEACM-caged compounds.

Bhc Family

The Bhc group (Bromo hydroxyl coumarin) has been applied to cage carboxylates, amines, phosphates, alcohols and carbonyl compounds. It has been proved to be a replacement for

conventional 2-nitrobenzyl-type phototriggers. The Bhc group can add a substantial amount of water solubility to corresponding caged compounds because most C7 phenolic hydroxyl moiety in the Bhc is ionized at physiological pH. On the other hand, Bhc group has some advantages over other phototriggers, including other coumarins, because satisfies the following criteria[15]:

·It has a strong absorption band at more than 350 nm

· It has a substantially high photolysis quantum yield

· It has a practically usable stability

· It renders a water soluble target molecule

· It adds membrane permeability by simple modification (**131b**)

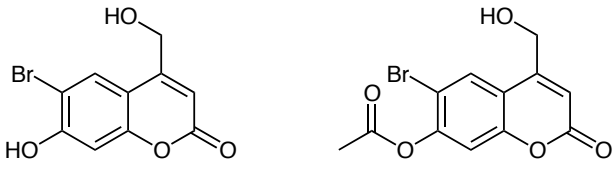

131a Bhc-OH **131b** Bhc/Ac-OH

Figure 67: Corresponding structures of Bhc family coumarins.

This family was mostly used for alcohol and amines protection by modification of this functional group obtaining carbonates or carbamates, respectively. The photolysis of these compounds in physiological conditions led to a decarboxylation, releasing the corresponding alcohol and amine[15] (*Scheme 12*).

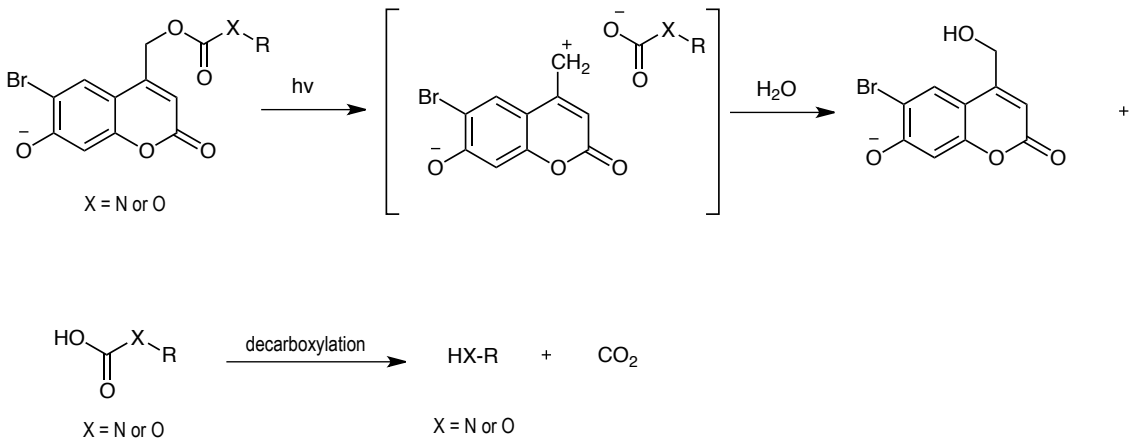

Scheme 12: Photolysis of Bchmoc-caged alcohols and amines.

Considering all the caging groups exposed before, the importance of choosing a good cage molecule to join to the desired drug is critical to obtain an optimum drug delivery assisted by light. One factor to be considered in order to choose one cage molecule instead of another is the

wavelength. As we exposed above, several wavelengths could be reached depending on the family applied, which, in addition, will provide other characteristics in the caged compound such as solubility, permeability, penetration and toxicity.

The wavelength applied to a caged compound needs to be non-dangerous in biological systems. Whereas energetic wavelengths as UV light (250-380 nm) are hazardous to promote a cellular death, shifting to less energetic visible light from blue-green (400-530 nm) to red or infrared (600-900 nm) ensures a biocompatibility with live systems. In addition, due to their less energetic wavelength, more penetration in tissues can be achieved, which is interesting for drug delivery in animals with non-invasive techniques (*Figure 68*).

Other important characteristics, which are associated one each other, are the solubility and the permeability. Targeting receptors that are widely distributed in the CNS means that the designed caged compounds should be permeable to cross the blood brain barrier, but at the same time, depending on the drug administration, a hydrophilic component needs to be incorporated to solubilise them as much as possible.

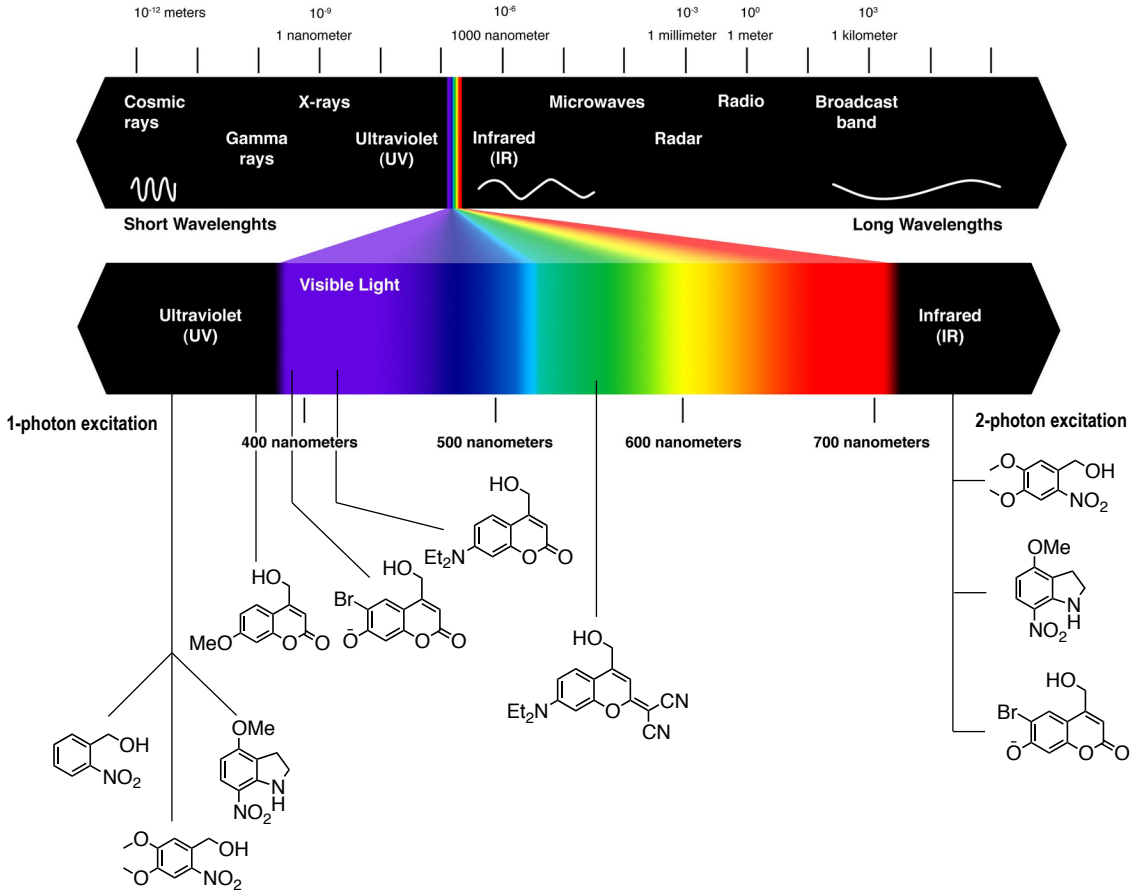

Figure 68: Schematic UV-Vis spectra with corresponding maximum absorption of cage molecules.

Caged compounds for allosteric modulator of metabotropic glutamate receptor subtype 5

Design and synthesis

First of all, an exhaustive bibliographic search was done looking for negative allosteric modulators of metabotropic glutamate receptor subtype 5 ($mGlu_5$) because their analgesic functionality for pain targeting was previously reported. The chosen compound will be modified with a simple bond to mask the biological activity. Due to this reason, the new compound needs to fulfill some requirements:

a) To present an associated high inhibition (IC_{50}) of the functional activity;

b) It needs to be inert in presence of light or under irradiation; and

c) To include the presence of a functional group to be chemically modified.

Under these requirements, we finally opted for compound ADX10059 or Raseglurant (**18**), which seems to accomplish all the requirements mentioned before. That is, the original drug is a potent NAM of the $mGlu_5$ receptor (IC_{50} = 10 nM) with non-described degradation under light and, the most important point, it includes the presence of aminopyridine functionality which can be easily modified to be caged with a photolabile compound.

Once the active specie was selected, we focused in the strategic design for molecular caging.

Because of the different photochemical possibilities in dependence of the cage molecule, we designed four caged compounds along the UV-Visible spectra generating a carbamate (*Figure 69*) in all of them due to its good uncaging performance and stability at physiological conditions. Other strategies like simple N-C bond in the bridge between active specie and caging molecule were discarded because of the highest energy necessary for uncaging it.

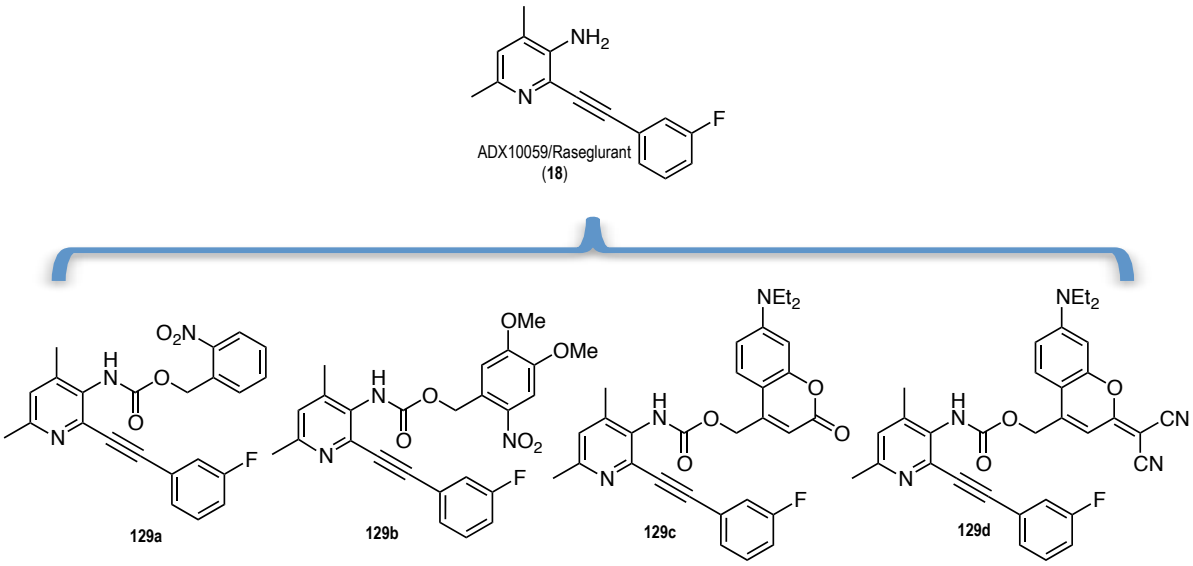

Figure 69: Caged compound structures design from $mGlu_5$ NAM Raseglurant/ADX10059.

Synthesis

Raseglurant (**18**) was synthesized by using Sonogashira coupling conditions (*Step a, Scheme 13*), copper/palladium catalysis and several vacuum cycles to avoid oxidative species which could reach to dimerization of the acetylene.

Compounds **129a** and **129b** were afforded using triphosgene to produce the isocyanate of raseglurant *in-situ*. The excess of phosgene produced was removed and the corresponding hydroxylated caging molecule **122a** and **122d** were added, respectively (*Step b, Scheme 13*). The same pathway was used in case of *Step c*, generating the isocyanate of raseglurant by removing the extra phosgene produced and adding the mixture of the corresponding coumarin with sodium hydride in THF, due to the lower nucleophilicity of the coumarin alcohol functionality.

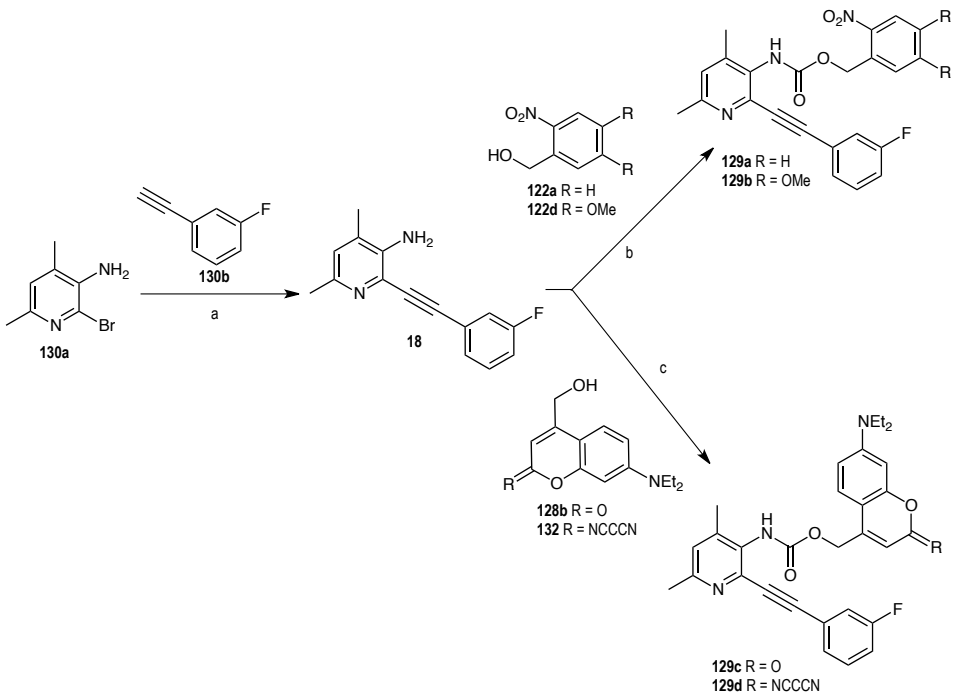

Scheme 13: Synthesis of compounds **18**, **129a**, **129b**, **129c** and **129d**. a) $Pd(PPh_3)_2Cl_2$, CuI, NEt_3, DMF, 40ºC, 8h, 83%; b) **122a** or **122d**, triphosgene, NEt_3, toluene, 100ºC, overnight, 70% for **129a** and 65% for **129b**; c) **128b** or **132**, triphosgene, NEt_3, NaH, toluene, THF, 90ºC, overnight, 55% for **129c** and 20% for **129b**.

Photochemical characterization

The synthesized caged compounds of raseglurant were characterized by measuring their UV-Vis spectra to evaluate the optimal wavelength to irradiate each compound in comparison with the active compound (*Figure 70A*). The uncaging at different times was followed by UV-Vis (*Figure 70B*) to calculate the photochemical parameters (*Table 9*).

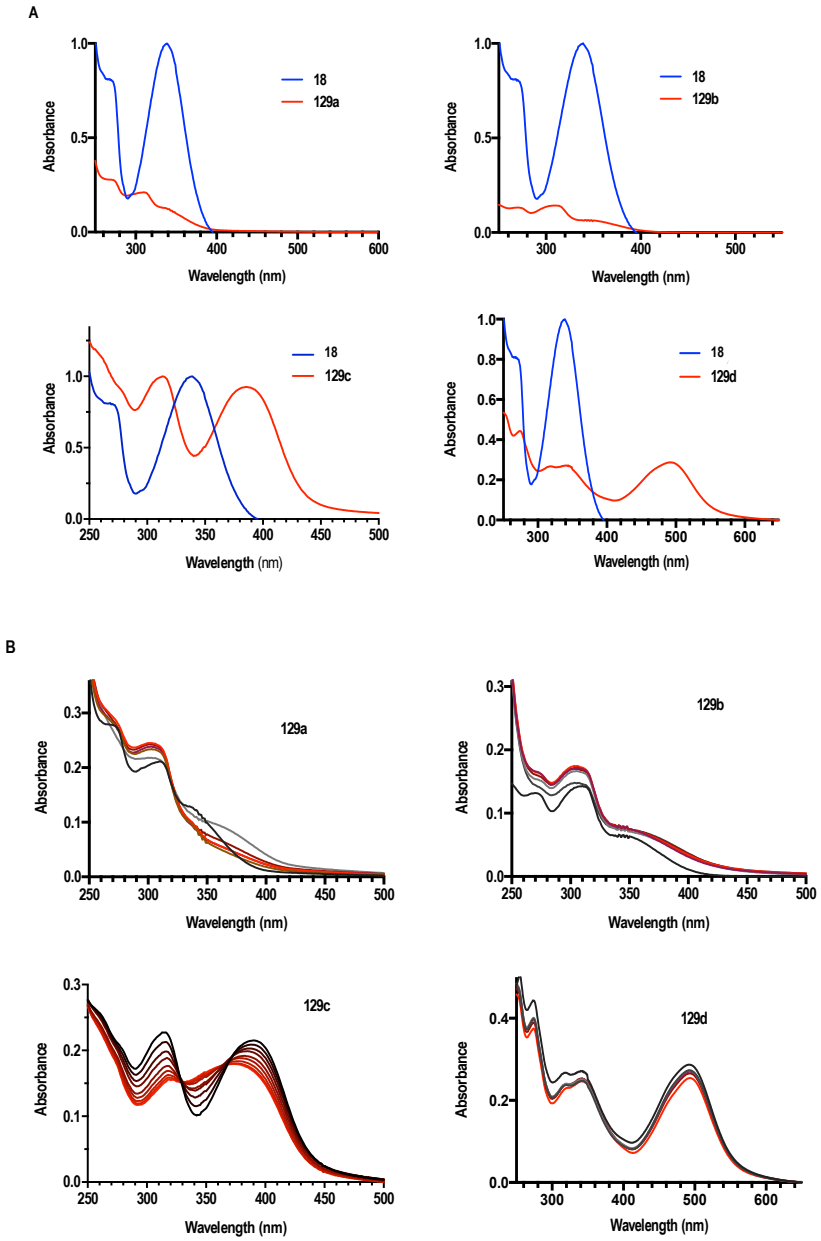

Figure 70: UV-Vis spectra for raseglurant cages from **129a-d**. A) UV-Vis spectra without irradiation of every caged compound in comparison with Raseglurant. B) Uncaging at corresponding wavelengths for every caged compound at different time, the black line corresponds to the sample without irradiation (0 sec) and the red lines to the samples irradiated at different times (*see experimental part*).

	129a	129b	129c	129d
ε (M^{-1} cm^{-1})	10.000	6.800	21.200	11.440
λ_{abs} (nm)	305	310	385	490
ϕ	0.032	0.005	0.180	0.063

Table 9: Photochemical parameters of different caged compounds of raseglurant (ε molar attenuation coefficient, λ_{abs} maximum absorption, ϕ quantum yield).

Compounds **129a** and **129b** had a low absorption at UVA light (300-350 nm); therefore, they should not be suitable for application in biological systems. In contrast, compounds **129c** and **129d** absorb in the visible range at 390-405 nm (violet-blue light) and 480-490 nm (blue- green light), respectively.

Excellent quantum yield was obtained for cage **129c** and poor for **129a**, **129b** and **129d**, where the last ones were at least 10 times less labile than the first one, at corresponding wavelengths for each of them (*experimental part*). We could identify from best compound **129c** in the photochemistry point of view, the different bands of the UV-Vis spectra. At 400 nm we could see the band of coumarin **128b** chromophore, which after irradiation is decreasing its absorption whereas the raseglurant chromophore (at 350 nm) increases it. Other compounds uncaging the kinetics were difficult to analyse due to their low quantum yields or by absorption spectroscopy.

Preliminary experiments for the study of uncaging were performed for all raseglurant cage compounds assisted by HPLC to analyse the photolysis kinetics.

In this way, all caged compounds were illuminated at the corresponding wavelength except for **129a** and **129b**, which were irradiated at 405 nm due to the lack of lasers to irradiate at these wavelengths and the impossibility of applying UV light in living systems. Samples of 1 mM concentration in DMSO of caged compounds were tested and the concentration of raseglurant released was measured. A straight calibration of this active specie was obtained before to extrapolate the concentration after illumination.

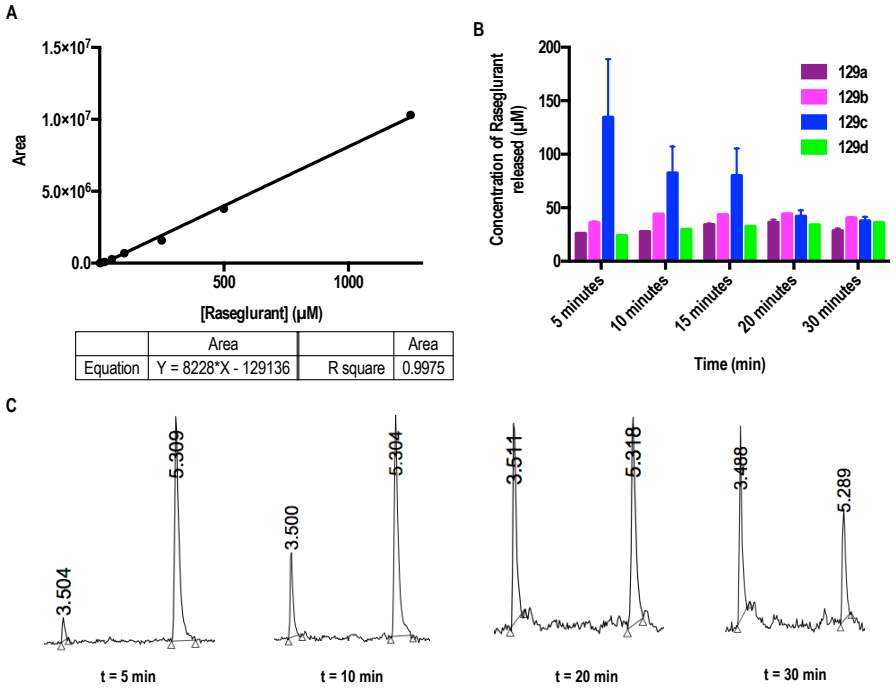

Figure 71: Preliminary experiments of uncaging assisted by HPLC. A) Straight calibration for quantification of raseglurant using cross dilutions. B) Concentration of raseglurant released for each caged compound versus time of irradiation. Each bar corresponds to the mean of two independent replicates with the corresponding SEM as error bars. C) Example of obtained HPLC chromatogram of uncaging of **129b** at 405 nm, filtered by PDA at 380 nm (maximum absorption of raseglurant), showing a retention time of 3.50 for raseglurant and 5.30 for caged compound **129b**.

The results for these experiments showed good uncaging for **129c** due to the irradiation at 405 nm (its maximum absorption), moderate for compound **129d** irradiated at 530 nm (maximum absorption at 483 nm) and low uncaging for compounds **129a** and **129b**, because their maximum absorption are in deepest UV but they are irradiated at 405 nm, the wavelength to be used in the pharmacology in vivo experiments.

Concerning the uncaging of compound **129c** after 5 minutes, a degradation of raseglurant was observed due to the decrease of concentration. Unfortunately, as it was not expected, the irradiation affected our active specie degrading almost all raseglurant after 10 minutes (*Figure 72*).

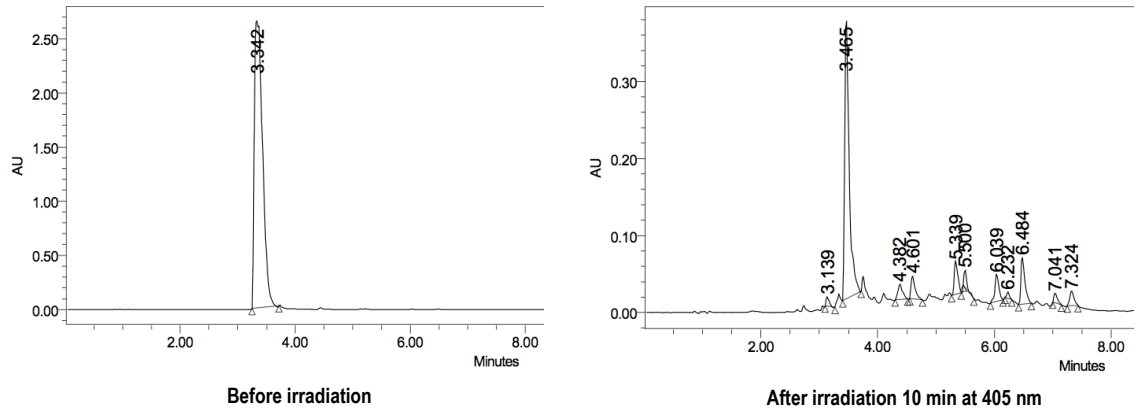

Figure 72: HPLC chromatogram before and after irradiation of a raseglurant sample of 1 mM concentration at 405 nm

The unexpected degradation of raseglurant was a drawback to test it *in-vitro* and eventually for future *in-vivo* assays. We thought that the fact of using DMSO as a solvent in these preliminary uncaging experiments should have different effects due to the different stability depending on the solvation environment of the compounds. Theoretically, once the irradiation takes place, we transfer energy to electrons from the ground energy state to an excitation state and, after the relaxation time, the electrons go back to the ground state emitting energy (fluorescense) or they could stay in an intermediate state called the triplet state. At this state, while we are illuminating, the organic solvent could stabilize the electrons and promote the degradation of the compound. However, after the change of the organic solvent to physiological conditions, photons would interact more with the aqueous solvent disturbing the triplet state decreasing the maximum absorption wavelength to the deeper UV and avoiding this degradation when irradiation was done at 405 nm. For this reason we performed this assay by using PBS solution instead of DMSO with 1 mM concentration of raseglurant (*Figure 73*).

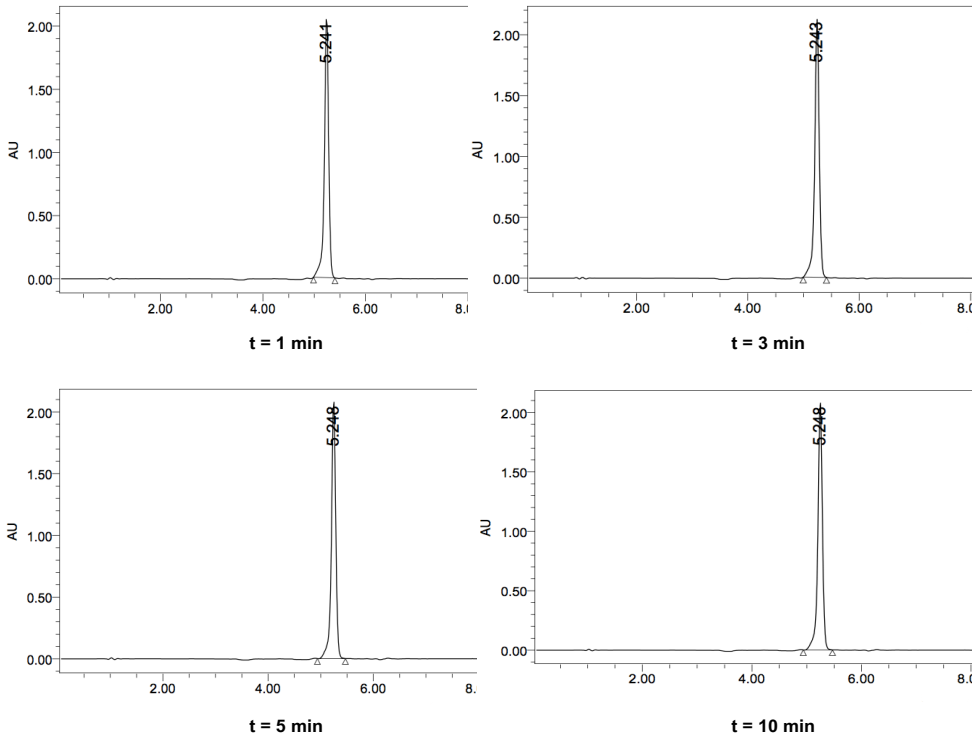

Figure 73: HPLC chromatogram after irradiation of a raseglurant sample of 1 mM concentration at 405 nm in physiological conditions.

We could observe that buffer photolysis completely abolished raseglurant degradation, opening the possibility of using this compound in animal experiments. Afterwards, the uncaging of the most interesting compound (**129c**) was examined again in the same HPLC conditions (*Experimental part*) as shown previously, obtaining first, a new straight calibration of raseglurant in physiological conditions.

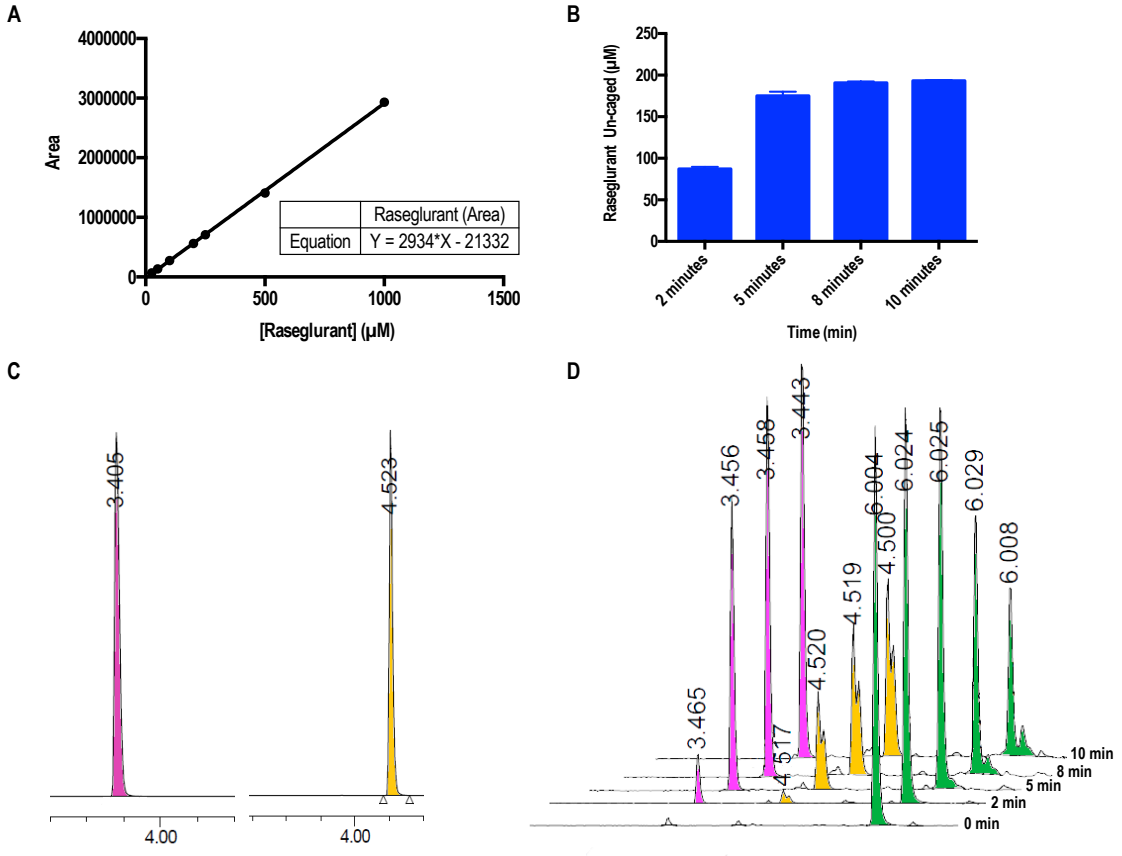

Figure 74: Uncaging experiments assisted by HPLC for compound **129c**. A) Straight calibration for quantification of raseglurant using cross dilutions in physiological conditions. B) Concentration of raseglurant released for **129c** caged compound versus time of irradiation. Each bar corresponds to the mean of two independent replicates with the corresponding SEM as error bars. C) HPLC chromatogram of pure Raseglurant (Rt = 3.40) and DEACM (Rt = 4.52) D) HPLC uncaging chromatogram of **129c** at 405 nm at different times, filtered by PDA at 380 nm (maximum absorption of raseglurant), showing a retention time of 3.45 for Raseglurant (violet pics), 4.52 for DEACM (yellow pics) and 6.00 for caged compound **129c** (green pics).

At physiological conditions, we finally achieved a good uncaging for compound **129c** without degradation of the active species raseglurant, reaching at the same time, a similar quantity of uncaged raseglurant to that released in DMSO solvent.

With the results obtained from the photochemical characterisation, we decided to evaluate *in-vitro* all the compounds through dose-response curves by using IP accumulation assays.

Pharmacological characterisation

First of all, due to the raseglurant degradation shown before, a first evaluation was done irradiating the compound at 405 nm in DMSO conditions first and at physiological conditions after, to check biologically what we could do to avoid this degradation.

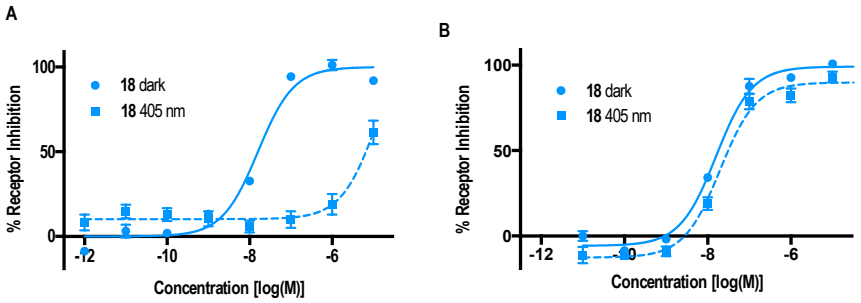

Figure 75: Comparative biological effect upon irradiation of raseglurant at 405 nm during 5 minutes. A) Illuminating with DMSO conditions. B) Illuminating at physiological conditions. Each point corresponds to the mean of three independent replicates with the corresponding SEM as error bars.

Once we demonstrated that irradiation during five minutes under physiological conditions did not affect our *in-vitro* experiments, we performed dose-response curves in HEK203 cells transfected with $mGlu_5$, for all cage compounds.

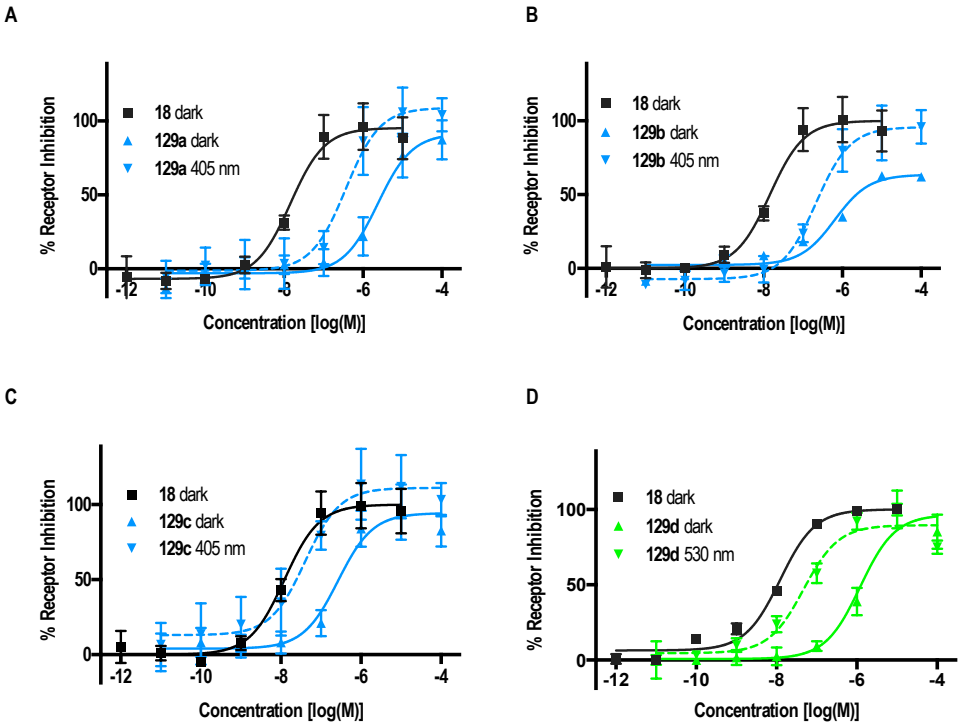

Figure 76: Dose-response curves of uncaging caged-raseglurant compounds with IP-one assays on HEK cells overexpressing $mGlu_5$ with a constant concentration of quisqualate (**2**) 100 nM. Flat lines correspond to the samples incubated in dark conditions and dotted lines to the samples under 405 nm (blue) and 530 nm (green) illumination. Each point corresponds to the mean of a minimum of three independent replicates with the corresponding SEM as error bars.

Despite we could not reach the same activity upon irradiation of compounds **129a** and **129b** as that obtained with pure raseglurant (**18**), probably because of the unoptimal 405 nm wavelength used for NB cages, we obtained about 10 fold-shifted curves between the caged compounds in dark conditions and the illumination ones. In contrast, the compounds that have strong absorption at 405 nm such as **129c** and **129d** could reproduce almost the total effect of raseglurant after five minutes irradiation.

The most interesting compound, due to its strong photokinetic lability (**129c**), appeared as a good candidate to be further evaluated biologically and to progress to in *in-vivo* experiments. However, the main issue observed in dose-response experiments were the activity of the non-irradiated caged compounds by themselves.

This unexpected hurdle represented a serious problem because we need a completely inactive compound before illumination that, after it is administered, can be released upon illumination in a specific region of the body with fully temporal control.

Even though there was a possibility that these caged compounds could have an associated activity, we thought that it was difficult to explain that such big molecules were able to bind into the narrow $mGlu_5$ receptor allosteric site, especially for compounds **129c** and **129d**. Considering that this binding of the cage raseglurant was not likely, another reason should be responsible for this activity. Attending to the high activity of raseglurant in $mGlu_5$, we hypothesized that the presence of small amounts of the active compound in the cage samples coming from adventitious photolysis during manipulation could account for this activity. Alternatively, an unspecific effect (off-target activity) or a coumarin effect could also be contemplated.

We first focused in the evaluation of the biological aspects described before, taking **129c** as the reference compound because of its labile behaviour. Two IP-one accumulation assays were performed with HEK293 cells overexpressing $mGlu_5$, checking the activity of the coumarin **128b** in dark and upon irradiation conditions (*Figure 77A*) and with HEK293 cells with an empty

plasmid (pRk6), testing **128b** coumarin, **129c** caged compound and raseglurant (**18**) to discriminate the unspecific effects (*Figure 77B*).

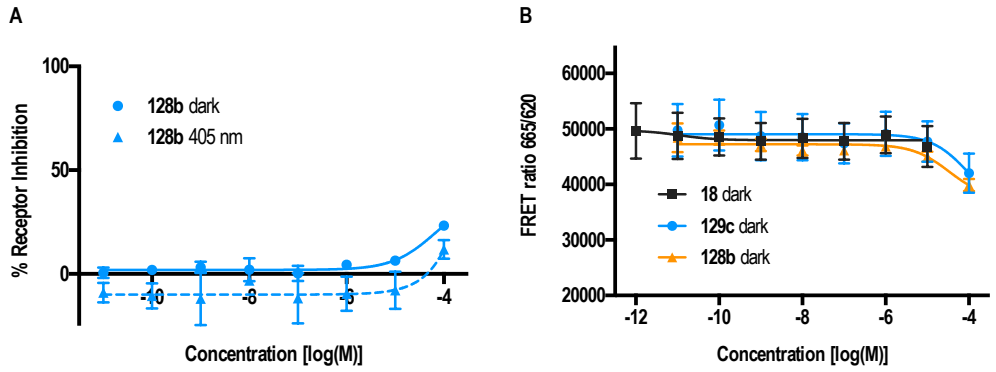

Figure 77: Dose-response curves in IP-one accumulation. A) HEK293 cells overexpressing $mGlu_5$ evaluating coumarin **128b**. B) HEK293 cells with empty plasmid (pRk6). Each point corresponds to the mean of a minimum of three independent replicates with the corresponding SEM as error bars.

As it is depicted in *Figure 77A*, dose-response curves of the coumarin **128b** did not show any effect in HEK293 cells with transfected $mGlu_5$ receptor nor in the negative control with HEK293 cells transfected with empty plasmid. Analysis of unspecific effects for all components before and after uncaging did not show an off-target activity. Considering the last results, we discarded any effect concerning the biological activity of all compounds involved in the uncaging reaction.

Therefore, we decided to deeply analyse the samples to check the purity of the caged compound **129c** for the presence of residual raseglurant. The samples were analysed by HPLC-MS, performing first a calibration to quantify raseglurant (*Figure 78A*), and a 1 mM sample of **129c** was analyzed, which showed the presence of 1% of raseglurant (*Figure 78B*). This would mean that **129c** would have an apparent IC_{50} 100-fold shifted from the IC_{50} of raseglurant (20 nM), which indeed, was similar to the measured activity in the first dose-response curve (*Figure 76C*) of the impure sample. For this reason, we repurified several times **129c** compound to remove as much as possible the residual raseglurant present (*experimental part*) and taking extreme precautions for keeping the samples protected from light.

Afterwards, the new sample was analysed again by HPLC-MS using the same methodology described, to determine the quantity of residual raseglurant (*Figure 78B*) in the purified batch.

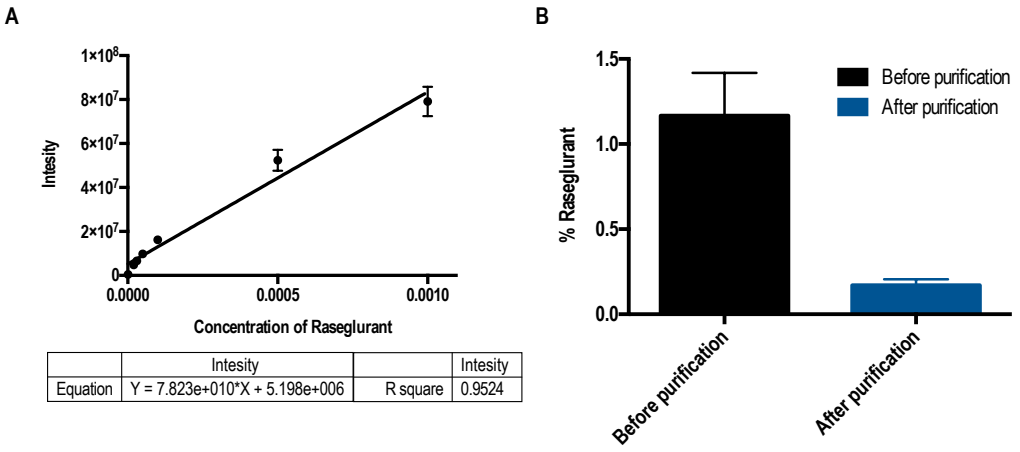

	Intesity		Intesity
Equation	Y = 7.823e+010*X + 5.198e+006	R square	0.9524

Figure 78: A) Straight calibration in HPLC-MS conditions. B) Percentage of active specie (raseglurant) in 1 mM sample of **129c** before and after purification.

After purification we could obtain at least 10 times less concentration of undesired compound reaching a 0.15% of raseglurant in the sample. That means we will be able to shift the dose-response curve of the non-irradiated caged compound at least one log concentration less potent in case this impurity was disturbing the potency of the caged compound. Therefore, a new dose-response curve was performed by IP-one accumulation assay using the same methodology previously described.

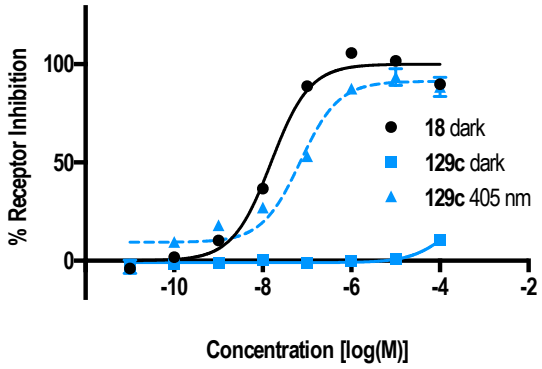

Figure 79: Dose-response uncaging of purified **129c**. Flat lines correspond to the samples incubated in dark conditions and dotted lines to the samples after 405 nm (blue) illumination. Each point corresponds to the mean of a minimum of three independent replicates with the corresponding SEM as error bars.

Remarkably, after the purification we could abolish almost all the activity of non-illuminated **129c** showing that this compound is not active in $mGlu_5$ (*Figure 76C*) and, in addition, after five minutes

illumination we reached mostly the same $mGlu_5$ inhibition obtained with the raseglurant active molecule.

These positive results encouraged us to carry out further studies with caged compound **129c**, evaluating some important points such us the selectivity of all compounds involved in the uncaging, to be sure, at least, that any of them is affecting other metabotropic glutamate receptors.

The selectivity assays were performed over the eight mGlu subtypes at a single dose of 1μM of the raseglurant cage compound **129c**. We used the IP-one assay in HEK293 cell overexpressing the corresponding receptors with different concentrations of orthosteric agonists (*experimental part*), which were selected depending on the mGlu subtype and the desired effect to measure; either potentiation (PAM) or inhibition (NAM) of its activity (*Figure 80A and 80B respectively*). The corresponding results showed that the caged compound **129c** and coumarin (**128b**) were not affecting any subtype (neither $mGlu_5$) acting as a NAM, but we saw a little effect as a PAM of $mGlu_4$ and $mGlu_2$. In contrast, raseglurant did not show any effect as PAM or NAM for any subtype except (obviously), as a NAM of $mGlu_5$.

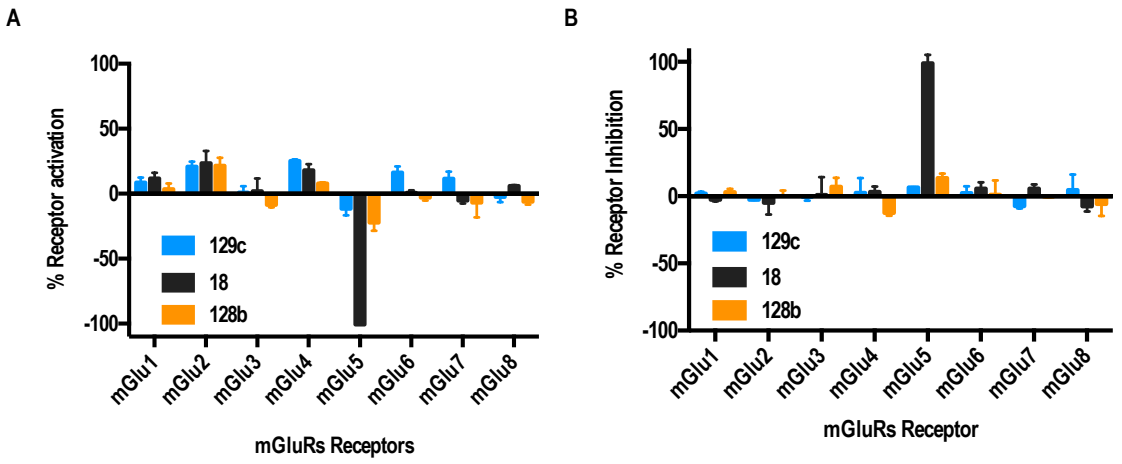

Figure 80: Selectivity profile of compounds **18**, **129c** and **128b** among all the mGlu subtypes as PAM (A) and NAM (B) all in dark conditions. Data represent normalized receptor activation for PAM and normalized inhibition for NAM for at least three independent replicates, done in duplicate, and are represented as mean ± SEM.

To give some evidence of the spatial and temporal delivery of the cage **129c**, we monitored intracellular calcium in real-time individual cell calcium imaging (*in collaboration with Thor Moller,*

IGF, Montpellier) in HEK293 cells overexpressing the $mGlu_5$ receptor (*Figure 81*).

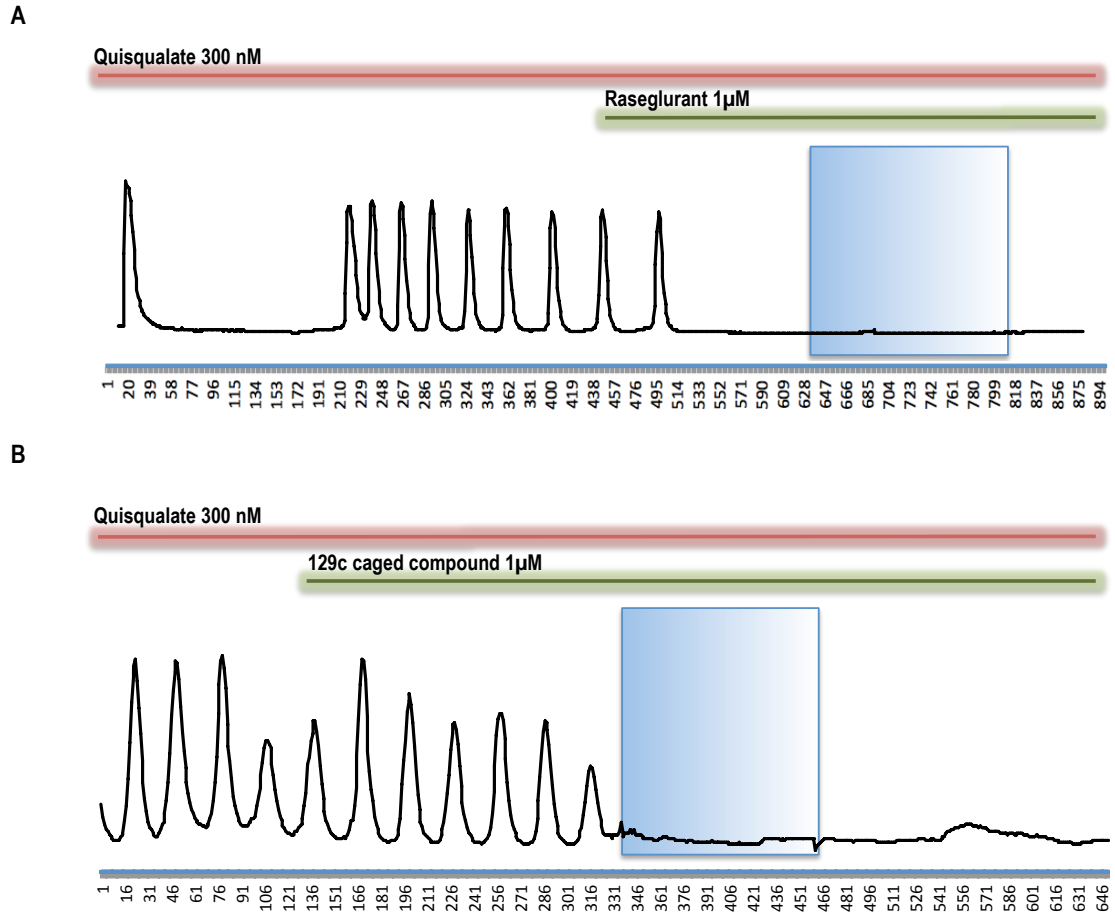

Figure 81: Real-time calcium imaging with HEK293 cells overexpressing $mGlu_5$. A) Time course of calcium indicator fluorescence (F_{340}/F_{380}) in individual cells treated with agonist (300 nM quisqualate) and raseglurant (**18**). Blue box indicates a blue illumination (405 nm). B) Time course of calcium indicator fluorescence (F_{340}/F_{380}) in individual cells treated with agonist (300 nM quisqualate) and **129c**. Blue box indicates a blue illumination (405 nm).

In this experiment, the application of quisqualate (**2**), in the reading chamber, produced intracellular calcium oscillations with a frequency proportional to the amount of activated $mGlu_5$ receptor on the cellular membrane[16]. After the subsequent application of **129c**, these oscillations keep constant as well as with the addition of quisqualate and, after irradiation at 405 nm, these oscillations were completely and irreversibly inhibited. The reference NAM (raseglurant) was also applied as a reference, to see the oscillations inhibited after addition in presence of the orthosteric ligand quisqualate.

This full pharmacological characterisation allowed us to move to *in-vivo* assays applying this method to peripheral and central nervous system in animals.

In-vivo pharmacological characterisation of compound ***129c***

In collaboration with Marc López, Francisco Ciruela and Ferdinando Nicoletti, we assessed the *in-vivo* analgesic activity of **129c** activated by light in two established models of pain in mice: the chronic constriction injury (CCI) model of neuropathic pain and the formalin test (*Figure 82A*)[17].

First, the validity of our approach was proved in mice subjected to unilateral CCI of the sciatic nerve, in which we explored the contribution of central $mGlu_5$ receptors by photomodulating these receptors in the ventrobasal thalamus, a pivotal relay and processing point for somatosensory information ascending from the spinal cord to the cerebral cortex[18]. Optical fibers were implanted in the brain to allow precise light delivery into the ventrobasal thalamus (*figure 82A*) by using LED lamp illumination system and assessed mechanical pain threshold by means of von Frey filaments.

Interestingly, systemic injection of raseglurant (10 mg/kg) significantly increased pain thresholds in CCI mice regardless of light irradiation (*Figure 82B*). In contrast, systemic injection of **129c** (10 mg/kg) significantly increased pain thresholds in CCI mice only after thalamic irradiation (*Figure 82B*).

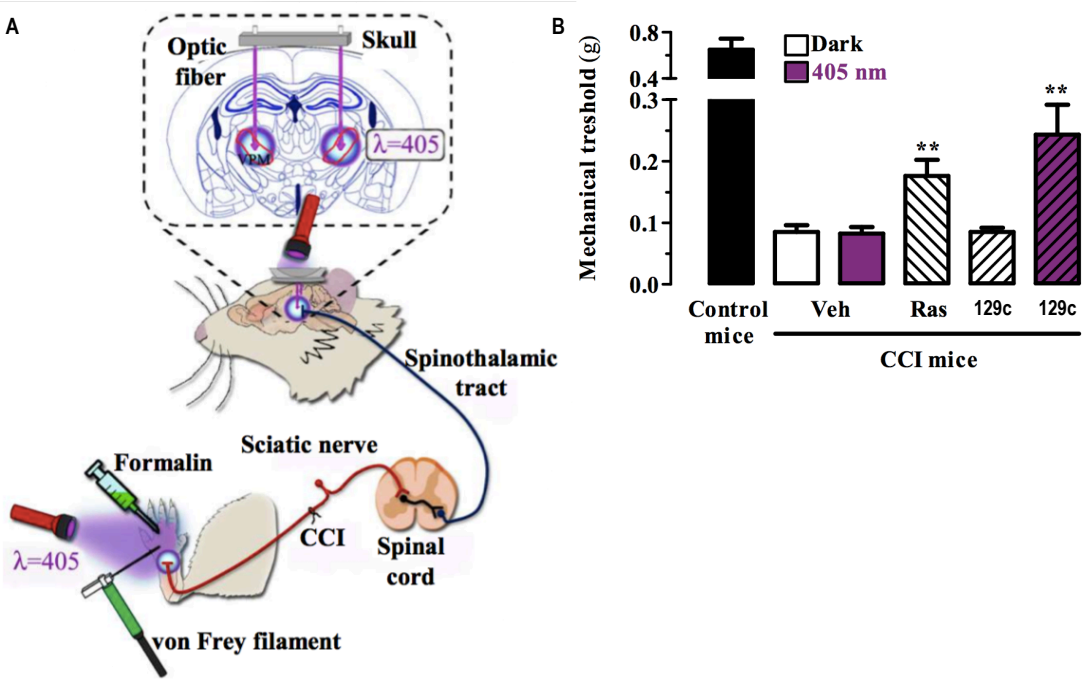

Figure 82: A) Schematic induction of chronic constriction injury (CCI) and *in-vivo* un-caging. B) Mechanical pain threshold by means of von Frey filaments (** *P*< 0.01 of significance).

On the basis of this proof of principle success, we took advantage of a different mice model of pain to further investigate the analgesic activity of light-delivered **129c** either in the periphery or in ventrobasal thalamus.

The formalin test, which allows an objective analysis of pain based on nocifensive behaviour, displays a first phase of pain (5 minutes after formalin injection in the hind paw), which models the acute inflammatory pain, and a second phase (20-30 minutes after formalin injection), which models chronic inflammatory pain and reflects the development of central sensitization[17].

Formalin injection into the mouse hind paw induced an innate licking behaviour that was significantly reduced both at phase I and phase II by the systemic administration of raseglurant (10 mg/kg), thus demonstrating an antinociceptive efficacy mediated by the inhibition of pheripheral (70±3%) and central (97±1%) $mGlu_5$ receptors, respectively. Therefore, the hind paw was directly irradiated with external 405 nm light (*Figure 82A*) following the experimental scheme shown in *Figure 83A*.

Noteworthy, while **129c** (10 mg/kg) was unable to promote antinociception in dark conditions, it elicited antinociception following direct hind paw irradiation both at phase I (54±5%) and phase II (34±5%) (*Figure 83B*), demonstrating that **129c** was able to be peripherally photoactivated by a non-invasive procedure. On the other hand, we also evaluated the effects of **129c** by delivering light into the ventrobasal thalamus. As shown in *Figure 83B*, implantation of the illumination system by itself did not affect nocifensive responses in the formalin test and did not alter the analgesic activity of raseglurant, as it was expected. Whereas **129c** (10 mg/kg) was inactive under basal conditions, it was able to cause analgesia both in phase I (45±9%) and phase II (90±4%) of the formalin test in response to the thalamic irradiation (*Figure 83B*).

Uncaging of **129c** in the thalamus produced a stronger analgesic effect in phase II, which reflects a mechanism of central sensitization. Significantly, the thalamic irradiation effects of **129c** were obtained after intraperitoneal administration, demonstrating its effective brain penetration in mice.

The demonstrated analgesic effects in two different models of pain upon local and thalamic irradiation raise the interesting possibility that localized targeting of the peripheral and thalamic $mGlu_5$ receptors represents a valuable strategy for the treatment of pain diseases.

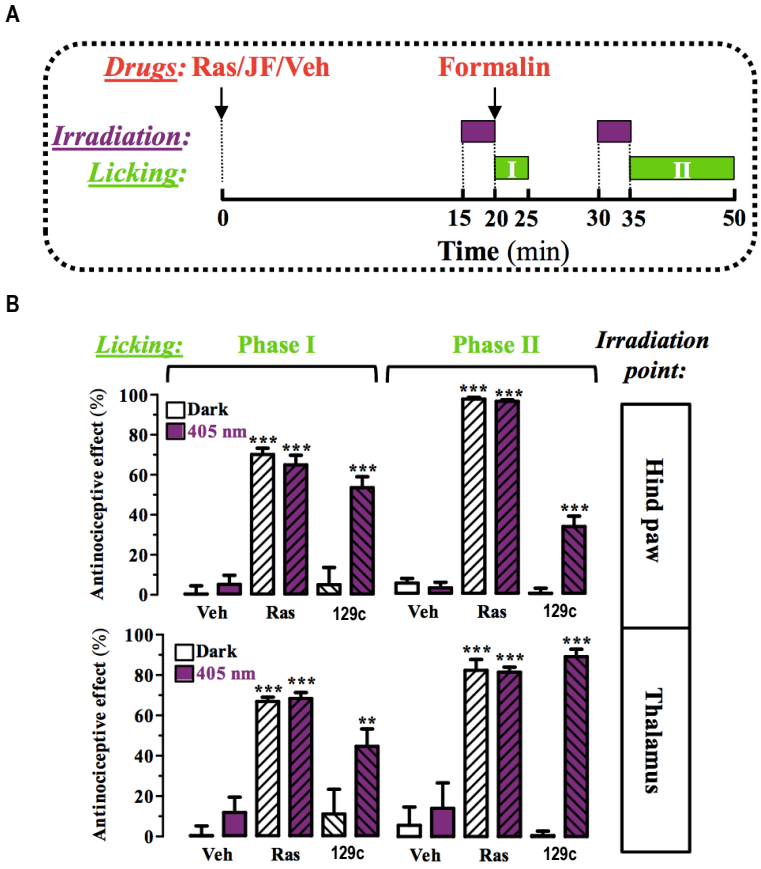

Figure 83: A) Schematic formalin test either in periphery and central nervous system. B) Normalized of antinociceptive effect calculated from licking time of mice (*** *P*< 0.001 of significance).

These good results open new possibilities in neuroscience to work further in photopharmacology with caged drugs in *in-vivo* experiments, for which until now there are not any referenced experiments with living systems neither in mice nor in mGluRs, in general.

Caged compounds for allosteric modulators of subtypes 1 & 4 mGlu receptors

Design and synthesis

In order to validate the method exposed above, we thought to design new allosteric modulators involving other subtypes of metabotropic glutamate receptors for the treatment of pain.

The first idea was to synthesize two selective allosteric modulators of mGlu subtypes localized one in post synapses and another in pre synapses. As it was explained previously, a negative allosteric modulator for post synapses ($mGlu_1$ and $mGlu_5$) or a positive allosteric modulator for pre synapses (group II and III) was needed due to their contribution in pain transmission.

Despite we already have a good example of negative allosteric modulator for post synapses ($mGlu_5$ NAM raseglurant), we decided to obtain an $mGlu_1$ NAM but with different biological and structural characteristics.

The chemical scaffold of this new compound should be completely inert to the irradiation either in aqueous or organic solvent. In addition, the compound should have the functional group joined to a cage molecule. Regarding biological aspects, apart from being a selective compound of $mGlu_1$ receptor, it should have mild potency in order to maintain the caged compound inactive despite the low impurities.

The bibliographic data provided us several compounds, but we finally opted for the selective compound YM-298198 (**15**)[19], because it does not contain acetylene groups that could be degraded by light, bears a functional aniline group to be chemically connected with the DEACM coumarin and especially for its potency using quisqualate as a selective orthosteric agonist (IC_{50} = 100 nM).

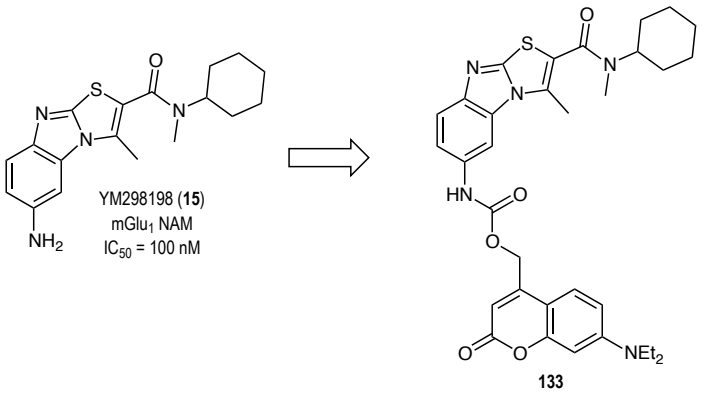

Figure 84: Chemical structure of YM298198 and design of its caged compound **133**.

Regarding new presynaptic compounds to be caged, we selected the mGlu subtype 4 because its modulation by photopharmacology had been well developed by our group and collaborators.

We assumed the same conditions described for the $mGlu_1$ NAM designed before, and we opted finally for compound TCN-22A (**134**)[20] (*Figure 85*). However, this time we decided to use a simpler cage molecule, which could have two-photon excitation properties to be easy to synthesize and handle it.

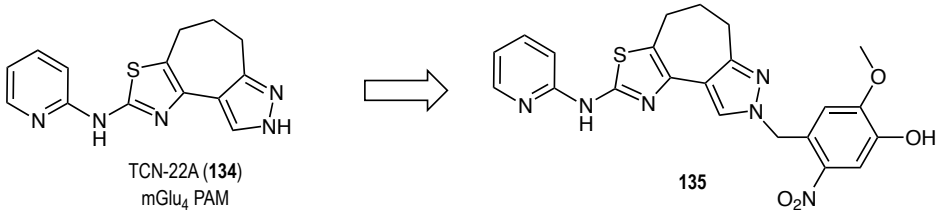

Figure 85: Chemical structure of TCN-22A and design of its cage compound **135**.

Synthesis

The DEACM caged compound **133** for YM-298198 was synthesized following the synthetic strategy shown in *Scheme 14*[19]. Starting from the mercaptobenzoimidazole **136a,** it was alkylated with compound **136b** affording compound **136c**, which after a simple treatment was cycled with pyridine and acetic anhydride to give the isomeric compounds **136d**. Afterwards, both isomeric esters were hydrolysed in basic medium to obtain the carboxylic acids **136e** followed by an acylation to obtain the amides **136g**. YM-298198 (**15**) was afforded by the reduction of compound **136g** and isolation of the corresponding isomer compound.

Once the active compound was synthesized and isolated, its cage derivative was synthesized following the same methodology used for raseglurant in *Scheme 13*, forming a carbamate with the DEACM coumarin (**128b**).

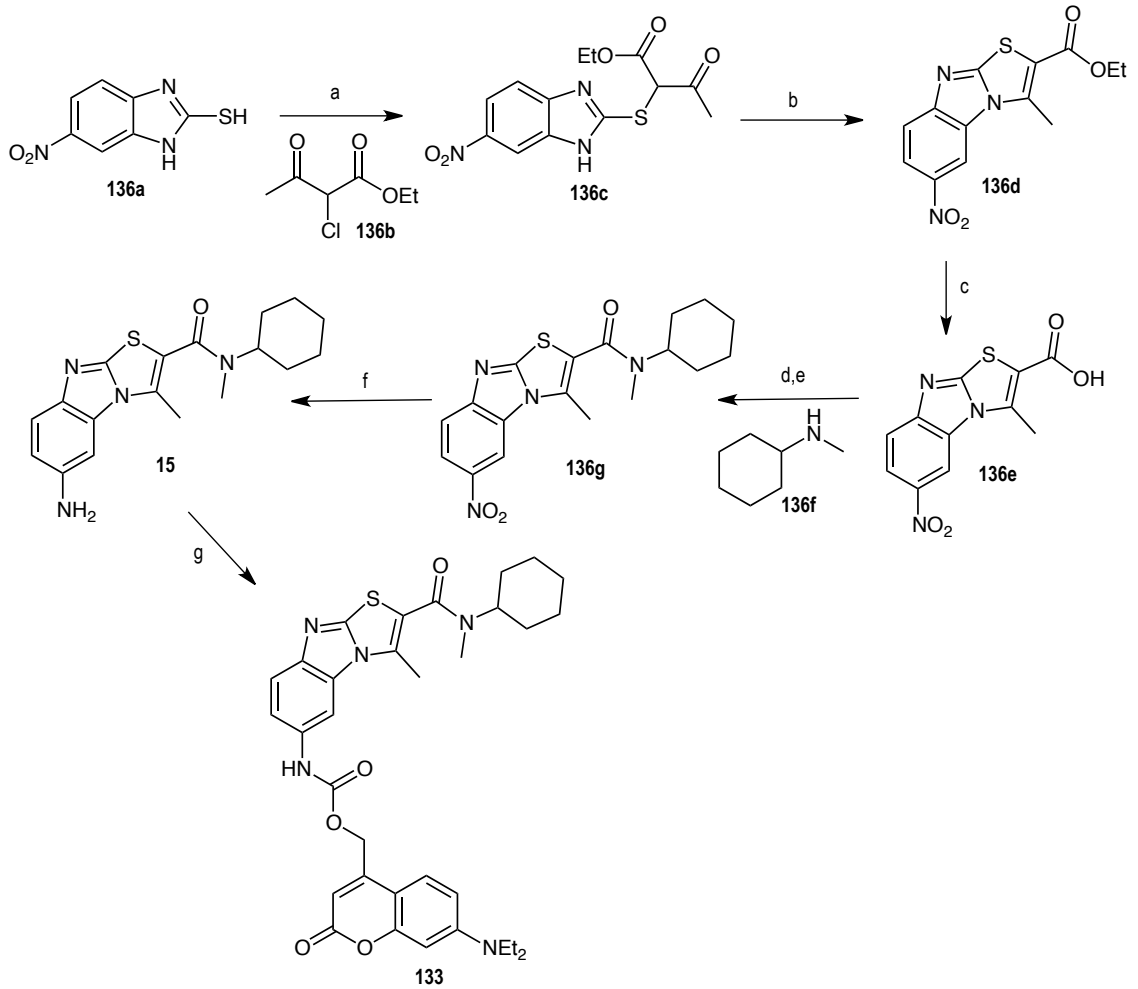

Scheme 14: Synthesis of compound **133** and **15**. Reagents and conditions: a) KOH, EtOH, 80ºC, 18h; b) Pyridine/Acetic anhydride 3:1, 100ºC, 3 h, 40% (over two steps a and b); c) NaOH, EtOH/Dioxane 1:1, r.t., 6 h, 94%; d) Tionyl chloride, reflux, 2 h, e) NEt_3, DCM, r.t., overnight, 21% over two steps; f) $Na_2S_2O_3$, HCl, THF/MeOH 1:1, r.t., 39%; g) **128b**, triphosgene, NaH, toluene, THF, 100ºC, overnight, 10%.

The mGlu4 PAM caged compound **135** was synthesized following the synthetic strategy[20] shown in *Scheme 15.* Starting from cyclopentanone (**137a**), it was reacted with compound **137b** obtaining the enolsilane **137c**, which was followed by a cycloaddition with **137d** to afford compound **137e**.

Afterwards, **137e** was reacted with zinc and acetic acid to afford compound **137f** (*Step c*), followed by a cyclation in commercial DMF-DMA and hydrazine to obtain pyrazole **137g**. An alkylation of pyrazole was done with cage molecule **137l** (synthesized from compound **122d** in *Step i*), affording compound **137h**, and a bromination in α–position of the carbonyl was produced (*Step f*), followed by a thiazole synthesis using the thiourea **137k** to finally obtain the caged compounds **135**.

The active compound TCN-22A (**134**) was obtained at microwave irradiation in acidic conditions to remove the protecting group.

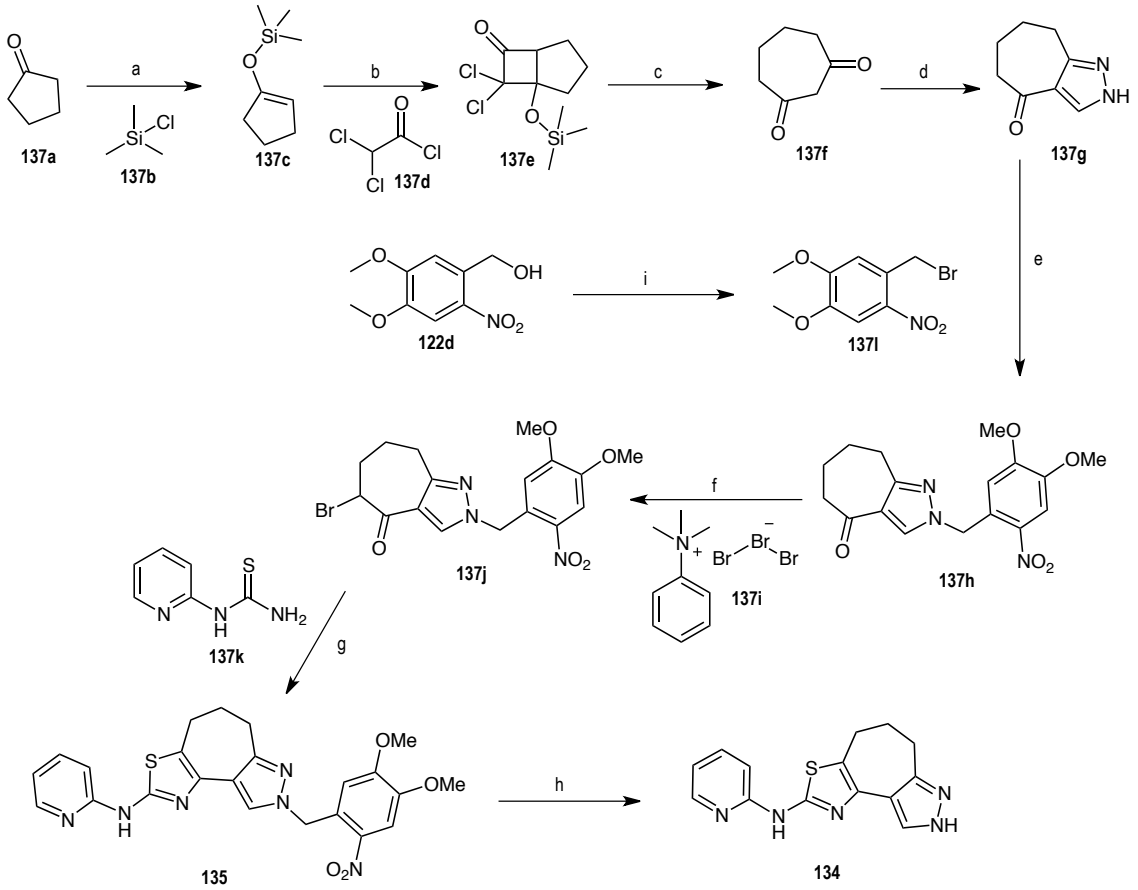

Scheme 15: Synthesis of compounds **134** and **135**. Reagents and conditions: a) NaI, NEt_3, can, r.t., overnight, 56%; b) NEt_3, Hexane, r.t., 18 h, 80%; c) 2-propanol, water, Zn, AcOH, -10ºC, 30 min, 96%; d) DMF-DMA, Hydrazine, 0ºC, 1 hour, 46%; e) K_2CO_3, can, 60ºC, 3 days, 30%; f) DCM, reflux, 1.5 h, 98%; g) EtOH, reflux, overnight, 70%; h) TFA, MW, 30 min, 100ºC, 84%; i) PBr_3, DCM, reflux, 3 h, 62%.

Photochemical characterisation

As we depicted previously for other compounds, the maximum absorption of both mGlu1 and mGlu4 caged compounds were measured, obtaining the UV-Vis spectra of each compound in comparison with the active compound (*Figure 86A*). The uncaging at different time was followed by UV-Vis (*Figure 86B*) to determine the photochemical parameters (*Table 10*).

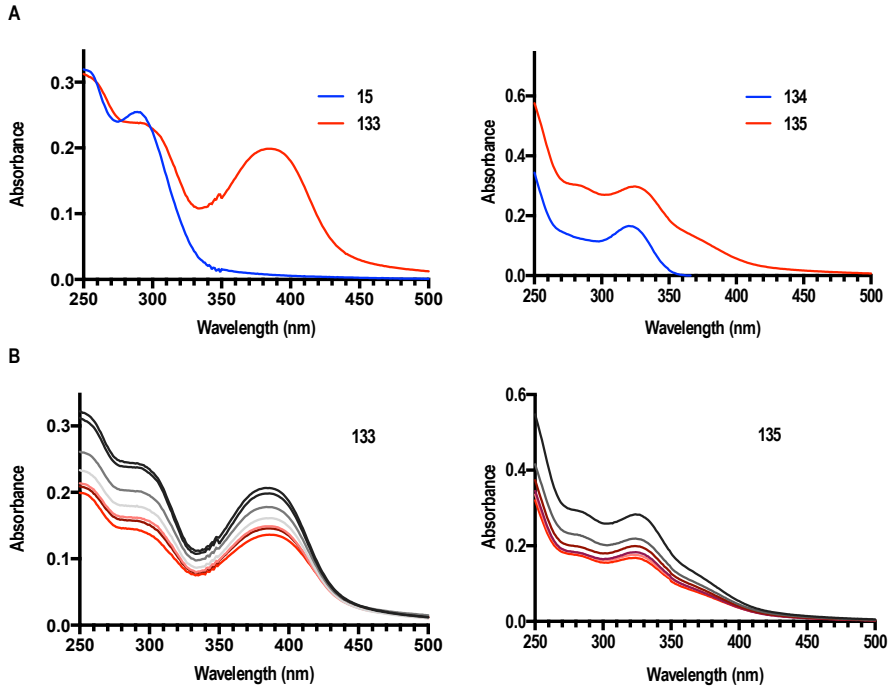

Figure 86: UV-Vis spectra for caged compounds **133** and **135**. A) UV-Vis spectra without irradiation of every caged compound in comparison with its corresponding active compound. B) Uncaging at corresponding wavelengths for every caged compound at different time, the black line corresponds to the sample without irradiation (0 sec) and the red lines to the samples irradiated at diferent times (*see experimental part*).

	133	**135**
ε **(M^{-1} cm^{-1})**	8.256	11.280
λ_{abs} **(nm)**	385	325-350
ϕ	0.03	0.034

Table 10: Photochemical parameters of caged compounds **133** and **135** (ε molar attenuation coefficient, λ_{abs} maximum absorption, ϕ quantum yield).

As it was expected, compound **133** reached a maximum absorption similar to caged raseglurant **129c** due to its same cage coumarin DEACM **128b** that promotes this maximum absorption near to the blue light range. But, its quantum yield was lower than the calculated for cage compound **129c**. In contrast, we acquired a maximum absorption in the UV for compound **135**, which at some point could be interesting to be uncaged by 2-photon excitation. In addition, in both cases we could observe that their respective bands corresponding to the chromophore of the cage molecule were decreasing its absorption when the irradiation time was increased.

Because of the photodegradation problems observed in raseglurant **18**, we attempted to irradiate during five minutes at 405 nm in DMSO conditions to make sure that, in this case, the corresponding active compounds **15** and **134** are not being affected under light.

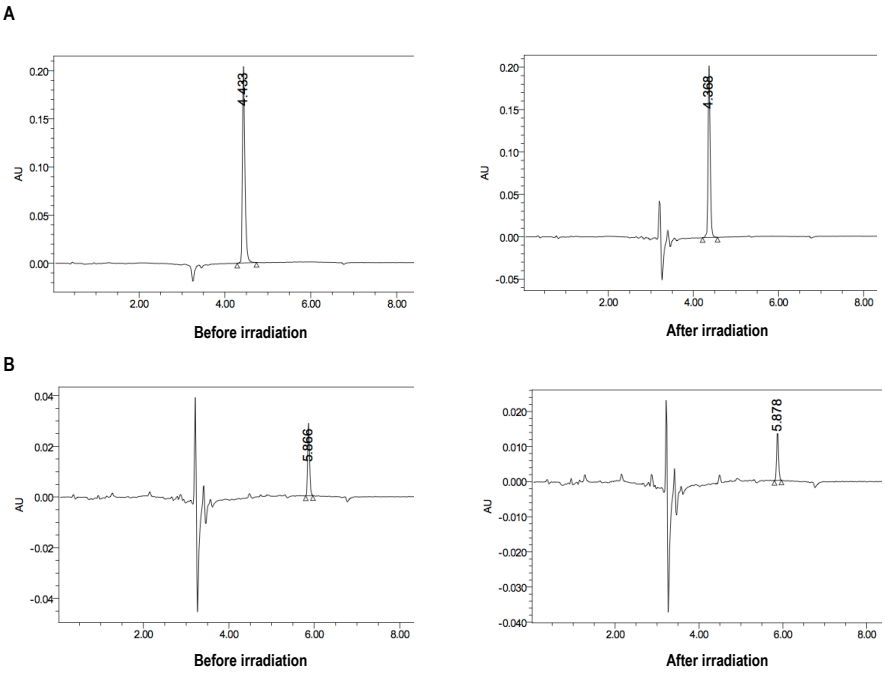

Figure 87: HPLC chromatogram before and after irradiation of the active species. A) Compound **15**. B) Compound **134**.

The degradation of the active compounds was not observed, as we expected due to the removing of functional groups that could be reactive in front of a source of light. Avoided this possible problem, full pharmacological characterisation of uncaging experiments was performed.

Pharmacological characterisation

Pharmacological characterisation of caged compounds **133** and **135** was performed using the IP-one accumulation assay on HEK293 cells overexpressing the corresponding receptor ($mGlu_1$ for **133** and $mGlu_4$ for **135**) illuminating both at 405 nm light (*Figure 88*).

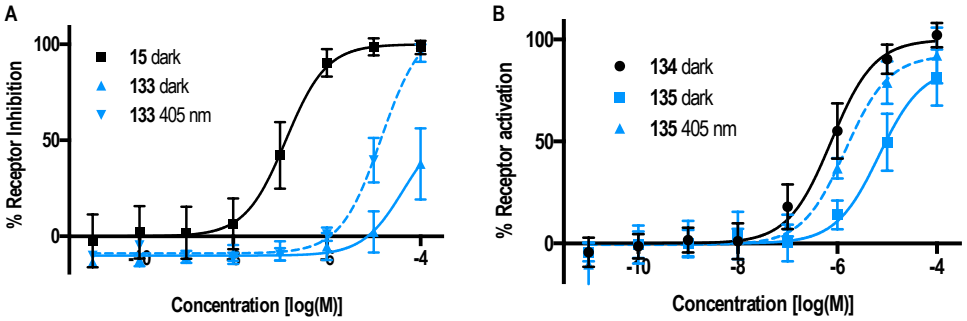

Figure 88: Dose-response assay with IP-one accumulation assays of uncaging at 5 minutes irradiation. A) Dose-response for compound **133** in HEK293 cells overexpressing $mGlu_1$. B) Dose-response for compound **135** in HEK293 cells overexpressing $mGlu_4$. Flat lines correspond to the samples incubated in dark conditions and dotted lines to the samples under 405 nm (blue) illumination. Each point corresponds to the mean of a minimum of three independent replicates with the corresponding SEM as error bars.

Concerning compound **133**, we afforded a good caged compound regarding its inactive behaviour before being activated upon light irradiation. In addition, this compound seems not to be as labile as caged-raseglurant **129c**, for which we could obtain a 100% of inhibition (*Figure 78*) after 5 minutes exposed to light. In this case, we should apply a more potent light source or an extended illumination time to get the same effect as for the reference NAM **15**. However, this $mGlu_1$ receptor will be a study object for *in-vivo* assays to release the compound selectively in brain regions where $mGlu_1$ is overexpressed such as cerebellum to study locomotion apart from pain.

In contrast, caged compound **135** seems to have an induced effect by itself without irradiation, and after the corresponding illumination at 405 nm, we could not achieve the 100% of receptor activation. We thought that the approach exposed in the design of the **135** compound was not optimal, probably because of its binding to the receptor. The pyrazole group, which had been modified joining the cage molecule, maybe it is not as important as we thought, and what is really interacting into the pocket is the pyridine group. Considering this issue, the next step to cage this compound would be modifying the amino group between the pyridine and the thiazole, obstructing the binding to obtain a completely inactive cage compound.

Caged compounds for the μ-Opioid receptor

Design and synthesis

In addition to metabotropic glutamate receptors, other G-protein coupled receptors are involved in pain transmission.

As we mentioned in *general introduction*, several families of GPCRs are present along the central and peripheral nervous system. One of the most common receptors from the rhodopsin family (class A), is the μ-opioid receptor, for which its crystal structure is well-defined in the protein data bank[21] and, in addition, one of the most used drugs targeting this receptor for the treatment of either acute or chronic pain, which is already in the market, is morphine and its derivatives.

The main problem presented by morphine is the potential side effects such as a decreased respiratory effort and low blood pressure. Moreover, it has a high potential for addiction, abuse and other common side effects include drowsiness, vomiting, and constipation.

For these common and dangerous side effects, morphine could be a good option to be caged preventing all these drawbacks just controlling its dose regulated by light.

The design strategy was quite simple because of the structure of morphine, which satisfy all requirements to be caged for the two main characteristics previously explained.

One requirement was the scaffold, which will not promote any degradation upon irradiation, and the second, and most important, is the presence of a functional group as phenol or allyl alcohol that could be easily modified.

Concerning the two functional groups present in morphine, we could achieve at least three new structures as caged compounds, functionalizing one of the two positions or both at the same time (*Figure 89A*).

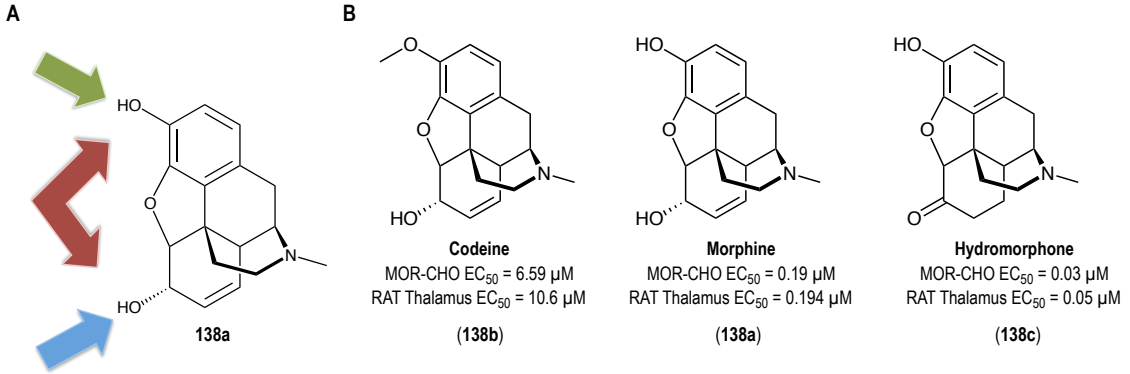

Figure 89: Structure of morphine and derivatives. A) Functional groups to be modified. B) Morphine and some of its derivatives with their corresponding biological activity.

As it is shown in *Figure 89B*, Thompson and collaborators[22] studied the biological activity of morphine and some of its derivatives. Interestingly, we could see a decrease of almost 100 times of its potency only when phenol was modified (codeine). In contrast, if the allyl alcohol was changed by ketone (hydromorphone), the activity still maintains its potency.

With this evidence, we decided to modify the phenol, which seems important because of its functionality, and inactivate it.

Another important point was the cage molecule to be joined. We chose again DEACM (**128b**), used before to reach higher wavelengths, but we changed the functional group used to join the coumarin.

Until now, we used carbamates as a bridge between the active compound and the cage molecules because of its lability when uncaging and its stability in biological processes. But this time, we needed to generate a carbonate for which is well-known its lower metabolic stability and also from the chemical point of view. This could be a problem due to the liberation of our active compound without illumination losing the selectivity and the control of released dose. For this reason, a direct O-C bond between morphine and coumarin **128b** was designed to avoid these issues despite the expected extra energy cost to break this bond upon irradiation.

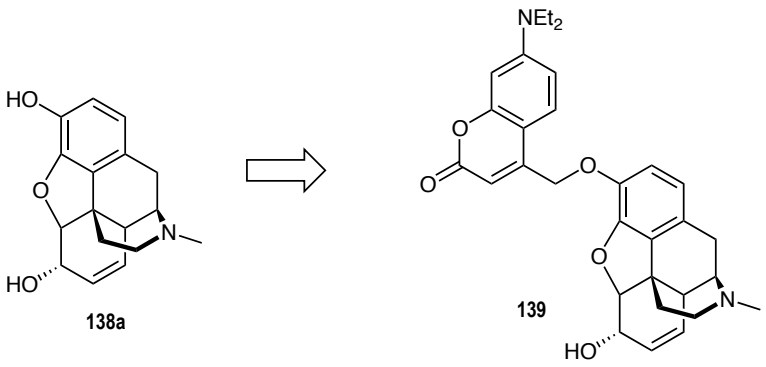

Figure 90: Design of caged-morphine **139**.

Synthesis

Compound **139** was easily afforded by one step reaction as is shown in *Scheme 16*. Commercial morphine was alkylated with coumarin **140** previously synthesized from coumarin **128b** (*Step b*), to obtain caged compound **139** in hydrochloride salt formulation.

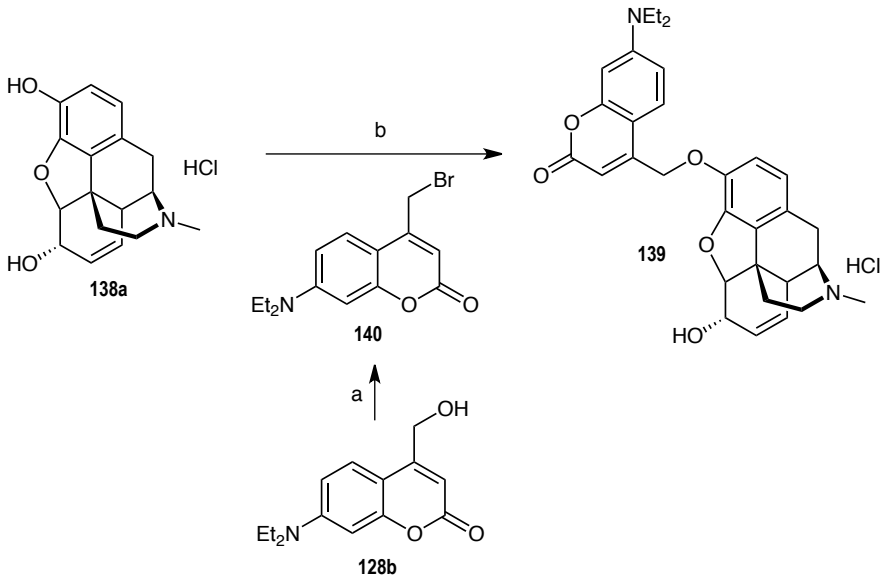

Scheme 16: Synthesis of caged compound **139**. Reagents and conditions: a) NEt_3, MsCl, LiBr, DCM, THF, r.t., 3 h, 44%. b) K_2CO_3, DMF, r.t., 4 days, 47%.

Photochemical characterisation

Again, UV-Vis spectra were measured in comparison with morphine, and the uncaging was followed afterwards (*Figure 91*), to calculate the photochemical parameters exposed in *Table 11.*

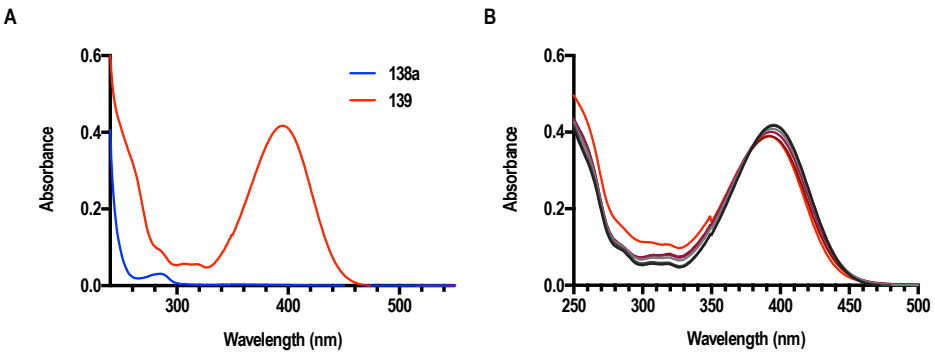

Figure 91: UV-Vis spectras. A) UV-Vis spectra without irradiation of **139** in comparison with Morphine (**138a**). B) Uncaging at corresponding wavelengths for **139** at different time, the black line corresponds the sample without irradiation (0 sec) and the red lines the samples irradiated at different times (*see experimental part*).

	139
ε (M^{-1} cm^{-1})	16.800
λ_{abs} (nm)	395
ϕ	0.035

Table 11: Photochemical parameters of caged compound **139** (ε molar attenuation coefficient, λ_{abs} maximum absorption, ϕ quantum yield).

Despite the uncaging, this time it was not as labile as showed for compounds with the same coumarin (**128b**) as a cage molecule. Probably due to the fact of how it was bound with morphine (direct C-O bond), confirming the obtained low quantum yield (0.03), we could see a shifting of the UV spectra, meaning that uncaging was taking place but without a relevant quantity of released morphine.

Considering this poor un-caging, we performed again an assay assisted by HPLC to verify the quantity released during time (*Figure 92*).

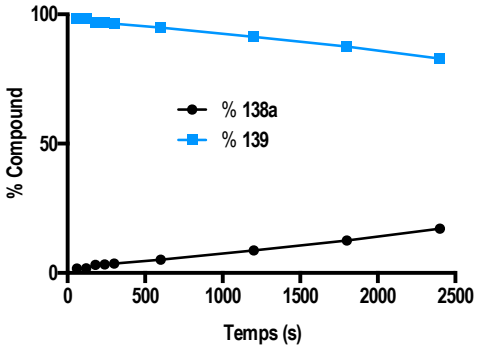

Figure 92: % of compounds **138a** and **139** in uncaging versus time of irradiation at 405 nm.

As we expected, in the first 60 seconds (*experimental part*), we could just see 1.7% of released morphine from an irradiated 0.7-mM concentration of **139**.

This low percentage of uncaging could be interesting at some point to apply this concept *in-vivo*,

to obtain a precise control of the released local concentration and, in addition, to reduce the side effects associated to this compound without impairment of the biological activity. If the morphine photochemical release from **139** is efficient enough for its use when a localized effect is therapeutically warranted remains to be determined.
The caged morphine compound **139** will be tested *in-vivo* at Francisco Ciruela's group and the results of the corresponding assays will be subjected to future validation.

Summary of results

We designed caged compounds **129a**, **129b**, **129c** and **129d** from the previously described active compound raseglurant (**18**) to display NAM activity of $mGlu_5$ receptor for the treatment of pain, which were delivered by photo control. In addition, we solved a number of problems such as their degradation in organic solvents or their necessary extra purity because of their very high potencies.

All raseglurant caged compounds were photochemically characterised obtaining a good quantum yield for compounds **129a**, **129b** and **129c**, but taking as the most photochemically interesting **129c** because of its labile behaviour irradiating at safe violet-blue light range.

Cage compound **129c** showed the same activity after irradiation as its active compound raseglurant and was completely inactive before irradiation requiring a high purity. This compound did not interact with other mGluRs subtypes and, in addition, was tested in *in-vivo* assays with mice models of neuropathic, chronic and acute pain via peripheral and central nervous system photoreleases obtaining significant effects before and after irradiation in comparison with raseglurant.

We designed also caged compounds **133** and **135** from the described active molecules YM298198 (**15**) and TCN-22A (**134**) as $mGlu_1$ NAM and $mGlu_4$ PAM, respectively, which are potential targets for pain transmission.

Coumarine compound **139** was also designed and synthesized as a cage compound of morphine, which is a validated agonist of μ-opioid receptors and is extensively employed in

clinical applications.

All these cage compounds were photochemically characterised and their UV-Vis spectra were performed. The uncaging by UV-Vis and HPLC to quantify the quantum yields and photochemical parameters was carried out.

After photochemical evaluation, a pharmacological characterisation was done for compounds **133** and **135** with IP-One assays, showing an inactive cage compound before irradiation with a mild potency after irradiation for compound **133**. In contrast, caged compound **135** had an associated activity before illuminating shifting just 10 times the concentration respect its active compound, meaning that mGlu4 PAM cage compounds will need a new design.

Conclusions

We synthesized caged compounds as NAMs directed to $mGlu_1$ (**133**) using **15** and **DEACM** as caging functionality, and $mGlu_5$ using the NAM raseglurant and **122a** (**129a)**, **122d** (**129b)**, **DEACM** (**129c)** and **132** (**129d**). We also synthesized an $mGlu_4$ PAM (**135**) using **134** and **137I**. Moreover, a morphine derivative using **DEACM** (**128b**) was also synthesized as a caged agonist for μ-opioid receptors.

Caged compounds were fully characterized and their photochemical properties and parameters determined. The quantum yields were 0.03 for **133,** 0.032 for **129a**, 0.005 for **129b**, 0.063 for **129d**, 0.034 for **135** and 0.035 for **139**. The DEACM caged raseglurant compound **129c** results the most effective compound concerning its quantum yield (0.18).

All compounds were pharmacologically characterized using commercial IP-One assays for each target receptor, being almost inactive in its caged form, except compound **135**, which had $mGlu_4$ PAM activity. After irradiation at suitable wavelength for each caging group, the IP-One assays show an effect compatible with the photolysis of the caging functionality and the release of the active ligand. Compound **129c** presents the most effective photorelease, and we could obtain the same activity with the uncaged compound and the parent compound raseglurant.

Compound **129c** was tested *in-vivo* in acute, chronic and neuropathic pain models in mice. The results obtained in these experiments show an effective peripheral analgesic effect dependent on treatment with **129c** localized at tissues containing $mGlu_5$ receptor relevant for pain transmission, whereas no effect was obtained with raseglurant photorelease at tissues containing $mGlu_5$ receptor which are not relevant for pain transmission.

Bibliography

1. Santina Chiechio, Z. M., Robert W Gereau, Ferdinando Nicoletti, Targeting Chronic Pain with Epigenetic Drugs: Focus on mGlu2 Receptors. *Molecular and Cellular Pharmacology* **2009,** *1* (4), 194-199.
2. Adams, S. R.; Tsien, R. Y., Controlling cell chemistry with caged compounds. *Annual review of physiology* **1993,** *55*, 755-84.
3. Maurice Goeldner, R. G., *Dynamic Studies in Biology*. WILEY-VCH: 2005.
4. (a) Xu, C.; Webb, W. W., Multiphoton Excitation of Molecular Fluorophores and Nonlinear Laser Microscopy. In *Topics in Fluorescence Spectroscopy: Volume 5: Nonlinear and Two-Photon-Induced Fluorescence*, Lakowicz, J. R., Ed. Springer US: Boston, MA, 2002; pp 471-540; (b) Xu, C.; Zipfel, W.; Shear, J. B.; Williams, R. M.; Webb, W. W., Multiphoton fluorescence excitation: new spectral windows for biological nonlinear microscopy. *Proceedings of the National Academy of Sciences* **1996,** *93* (20), 10763-10768.
5. Denk, W.; Piston, D. W.; Webb, W. W., Two-Photon Molecular Excitation in Laser-Scanning Microscopy. In *Handbook of Biological Confocal Microscopy*, Pawley, J. B., Ed. Springer US: Boston, MA, 1995; pp 445-458.
6. Bort, G.; Gallavardin, T.; Ogden, D.; Dalko, P. I., From one-photon to two-photon probes: "caged" compounds, actuators, and photoswitches. *Angewandte Chemie (International ed. in English)* **2013,** *52* (17), 4526-37.
7. Walker, J. W.; Reid, G. P.; McCray, J. A.; Trentham, D. R., Photolabile 1-(2-nitrophenyl)ethyl phosphate esters of adenine nucleotide analogs. Synthesis and mechanism of photolysis. *Journal of the American Chemical Society* **1988,** *110* (21), 7170-7177.
8. Il'ichev, Y. V.; Wirz, J., Rearrangements of 2-Nitrobenzyl Compounds. 1. Potential Energy Surface of 2-Nitrotoluene and Its Isomers Explored with ab Initio and Density Functional Theory Methods. *The Journal of Physical Chemistry A* **2000,** *104* (33), 7856-7870.
9. Amit, B.; Ben-Efraim, D. A.; Patchornik, A., Light-sensitive amides. The photosolvolysis of substituted 1-acyl-7-nitroindolines. *Journal of the American Chemical Society* **1976,** *98* (3), 843-844.
10. Papageorgiou, G.; Ogden, D. C.; Barth, A.; Corrie, J. E. T., Photorelease of Carboxylic Acids from 1-Acyl-7-nitroindolines in Aqueous Solution: Rapid and Efficient Photorelease of l-Glutamate1. *Journal of the American Chemical Society* **1999,** *121* (27), 6503-6504.

11. Furuta, T.; Momotake, A.; Sugimoto, M.; Hatayama, M.; Torigai, H.; Iwamura, M., Acyloxycoumarinylmethyl-Caged cAMP, the Photolabile and Membrane-Permeable Derivative of cAMP That Effectively Stimulates Pigment-Dispersion Response of Melanophores. *Biochemical and Biophysical Research Communications* **1996,** *228* (1), 193-198.

12. Hagen, V.; Bendig, J.; Frings, S.; Wiesner, B.; Schade, B.; Helm, S.; Lorenz, D.; Benjamin Kaupp, U., Synthesis, photochemistry and application of (7-methoxycoumarin-4-yl)methyl-caged 8-bromoadenosine cyclic 3′,5′-monophosphate and 8-bromoguanosine cyclic 3′,5′-monophosphate photolyzed in the nanosecond time region. *Journal of Photochemistry and Photobiology B: Biology* **1999,** *53* (1–3), 91-102.

13. Eckardt, T.; Hagen, V.; Schade, B.; Schmidt, R.; Schweitzer, C.; Bendig, J., Deactivation Behavior and Excited-State Properties of (Coumarin-4-yl)methyl Derivatives. 2. Photocleavage of Selected (Coumarin-4-yl)methyl-Caged Adenosine Cyclic 3‘,5‘-Monophosphates with Fluorescence Enhancement. *The Journal of Organic Chemistry* **2002,** *67* (3), 703-710.

14. Schade, B.; Hagen, V.; Schmidt, R.; Herbrich, R.; Krause, E.; Eckardt, T.; Bendig, J., Deactivation Behavior and Excited-State Properties of (Coumarin-4-yl)methyl Derivatives. 1. Photocleavage of (7-Methoxycoumarin-4-yl)methyl-Caged Acids with Fluorescence Enhancement. *The Journal of Organic Chemistry* **1999,** *64* (25), 9109-9117.

15. Nishigaki, T.; Wood, C. D.; Tatsu, Y.; Yumoto, N.; Furuta, T.; Elias, D.; Shiba, K.; Baba, S. A.; Darszon, A., A sea urchin egg jelly peptide induces a cGMP-mediated decrease in sperm intracellular Ca2+ before its increase. *Developmental Biology* **2004,** *272* (2), 376-388.

16. Nash, M. S.; Schell, M. J.; Atkinson, P. J.; Johnston, N. R.; Nahorski, S. R.; Challiss, R. A., Determinants of metabotropic glutamate receptor-5-mediated Ca2+ and inositol 1,4,5-trisphosphate oscillation frequency. Receptor density versus agonist concentration. *The Journal of biological chemistry* **2002,** *277* (39), 35947-60.

17. Mogil, J. S., Animal models of pain: progress and challenges. *Nature reviews. Neuroscience* **2009,** *10* (4), 283-94.

18. Kolber, B. J., mGluRs head to toe in pain. *Progress in molecular biology and translational science* **2015,** *131*, 281-324.

19. Hayashibe, S.; Itahana, H.; Okada, M.; Kohara, A.; Maeno, K.; Yahiro, K.; Shimada, I.; Tanabe, K.; Negoro, K.; Kamikubo, T., Nouveaux derives de thiazolobenzimidazole. Google Patents: 2000.

20. Hong, S. P.; Liu, K. G.; Ma, G.; Sabio, M.; Uberti, M. A.; Bacolod, M. D.; Peterson, J.; Zou, Z. Z.; Robichaud, A. J.; Doller, D., Tricyclic thiazolopyrazole derivatives as metabotropic

glutamate receptor 4 positive allosteric modulators. *Journal of medicinal chemistry* **2011,** *54* (14), 5070-81.

21. Manglik, A.; Kruse, A. C.; Kobilka, T. S.; Thian, F. S.; Mathiesen, J. M.; Sunahara, R. K.; Pardo, L.; Weis, W. I.; Kobilka, B. K.; Granier, S., Crystal structure of the micro-opioid receptor bound to a morphinan antagonist. *Nature* **2012,** *485* (7398), 321-6.

22. Thompson, C. M.; Wojno, H.; Greiner, E.; May, E. L.; Rice, K. C.; Selley, D. E., Activation of G-proteins by morphine and codeine congeners: insights to the relevance of O- and N-demethylated metabolites at mu- and delta-opioid receptors. *The Journal of pharmacology and experimental therapeutics* **2004,** *308* (2), 547-54.

Summary and Conclusions

The results obtained in *Chapter 1* indicate that the first attempt in the design of *cis-on* of positive allosteric modulators of $mGlu_4$ and negative allosteric modulators of $mGlu_5$ using an approach based on extending the length of compounds with azobenzene units failed due to the unspecific effect observed in cellular assays not involving metabotropic glutamate receptors.

In the design of first series of *cis-on* for positive allosteric modulators of $mGlu_4$, we based on the azo-replacement of the ether group of the known compound CD2267-0368 (**94**), to mimic the spatial conformation of azobenzene in *cis* configuration, obtaining new *trans-on* as PAMs of $mGlu_4$ with similar potency to the reference one.

A second series designed for positive allosteric modulators of $mGlu_4$ was based on the reference compound CD2267-0368 (**94**), but exchanging the aromatic substitution of the azo group to study all the possible conformations of the azobenzene due to the free mobility of the ether group. Moreover, with the generated intermediates it was synthesized a library of azocompounds directed to $mGlu_4$ with a picolinic amide moiety and $mGlu_5$ PAMs based on the azo-replacement testing all of them in a screening assay.

In *Chapter 2* we designed caged compounds acting as negative allosteric modulators of $mGlu_5$ based in the well-known and potent compound Raseglurant (**18**), which possesses an aromatic amine functional group that was used to insert several caging groups with active wavelengths in the UV-Vis range. The most interesting compound (**129c**) has a DEACM caging group having a photo labile behaviour for biological applications and a good quantum yield.

Caged compounds of raseglurant were tested in *in-vitro* assays under dark and illumination conditions. Caged compound **129c** was also tested in *in-vivo* assays against neuropathic, chronic and acute pain mice models with and without illumination, obtaining an analgesic response upon irradiation at blue range wavelenghts and being inactive in dark conditions.

We also designed two caged compounds for negative allosteric modulator of $mGlu_1$ and positive allosteric modulator of $mGlu_4$, modifying an aniline and a pyrazole with a coumarin and a nitrobenzyl group respectively, obtaining poor quantum yields.

Those compounds were tested in *in-vitro* assays reaching a good caged compound for $mGlu_1$ NAM, being inactive in dark conditions and partially active upon irradiation at visible blue light due to its quantum yield. Disappointingly, the caged compound of $mGlu_4$ PAM results in an active compound in dark conditions 10 times less potent than its corresponding active molecule needing to be redesigned.

To establish this method, we aimed to apply it to drugs already in the market which produce several side effects and in addition target other GPCRs such as morphine (which targets the μ-opioid receptor, class A GPCRs). We designed a caged morphine by its phenol group with a coumarin due to its probable importance in the receptor since the biological activity decrease almost 100 times substituting this position. Photochemical characterisation was done obtaining poor un-caging probably because of the formed N-C bond between the phenol and the coumarin.

The morphine-cage will be probably tested in *in–vitro* assays for analgesia, especially for the treatment of acute and chronic pain in peripheral nervous system.

Experimental Part

Synthetic Chemistry

Materials and methods

Chemicals and solvents

All the chemicals and solvents were obtained from commercial sources and used without purification, except anhydrous solvents, which were treated, previously through a system of solvent purification (*PureSolv*), degasified with inert gases and dried over alumina or molecular sieve (dimethylformamide). Dry triethylamine was obtained from commercial sources.

Reaction monitoring

Reactions were monitored by thin layer chromatography (60 F, 0.2 mm, *Macherey-Nagel*) by visualisation under 254 and/or 365 nm lamp.

Purification of compounds

Flash column chromatography was performed over *Panreac* Silica Gel 60, 40-63 microns RE. *Flash* column chromatography automated with *Isolera One* with UV-Vis detection (*Biotage*) was performed with reverse phase C18 SNAP KP-C18-HS 50 microns columns (*Biotage*) or normal phase silica SNAP KP-Sil 50 microns columns (*Biotage*).

Melting Points

Melting points were measured with *Melting Point B-545* (*Büchi*), ramp 2°C/min with a digital temperature measurement.

Nuclear Magnetic Resonance (NMR)

Characterisation of compounds with Nuclear Magnetic Resonance spectroscopy was performed with a *Variant-Mercury 400 MHz* instrument. Chemical shifts δ are reported in parts per million

(ppm) against the reference compound tetramethylsilane using the signal of the residual non-deuterated solvent (Chloroform δ = 7.26 ppm (^{1}H), δ = 77.16 ppm (^{13}C), DMSO δ =2.50 ppm (^{1}H) δ = 39.51 ppm (^{13}C), Methanol δ = 4.87 ppm δ = 3.31 ppm (^{1}H), δ =49.3 ppm (^{13}C)).

High-Performance Liquid Chromatography

Purity of compounds were determined with High-Performance Liquid Chromatography *Thermo Ultimate 3000SD* (*Thermo Scientific Dionex*) coupled to a photodiode array detector and mass spectrometer *LTQ XL ESI-ion trap* (*Thermo Scientific)* (HPLC-PDA-MS)); 5 µL of sample 2.5 mM in DMSO were injected, using a C18 column at 30 °C. Two different methods have been used (A and B). The mobile phase used in method A, was a mixture of A = formic acid 0.05% in water and B = formic acid 0.05% in acetonitrile (MeCN) with the method described as follows: flow 0.9 mL/min, 5%B-90%B 5 min, 90%B 2 min, 90%B-100%B 1 min, 100%B 2 min total runtime 15 min (column *ZORBAX Eclipse Plus C18* 4.6x150mm; 3.5µm (S.N. USUXC04483)). The mobile phase used in method B, was a mixture of A = NH_4HCO_3 aquous buffer 10 mM pH = 7.4 and B = Acetonitrile with the method described as follows: flow 0.4 mL/min, 5%B-100%B 5 min, 100%B 4 min, total runtime 15 min (column *Acquity UPLC BEH C18* (*Waters*) 1,7 µm 2,1x100 mm (SN 021532354157 76)). Purity is given as % of absorbance at 254 nm; UV-Vis spectra were collected every 0.2 s between 650 and 275 nm and bands are % of maximal absorbance; data from mass spectra were analysed by electrospray ionization in positive and negative mode every 0.3 s between 50 and 1000 Da and peaks are given m/z (% of basis peak).

High resolution mass spectra (HRMS) and elemental composition were analysed by FIA (flux injected analysis) with Ultrahigh-Performance Liquid Chromatography (UPLC) *Aquity* (*Waters*) coupled to *LCT Premier Orthogonal Accelerated Time of Flight* Mass Spectrometer (TOF) (*Waters*). Data from mass spectra were analysed by electrospray ionization in positive and negative mode. Spectra were scanned between 50 and 1500 Da with values every 0.2 seconds and peaks are given m/z (% of basis peak). Data was acquired with *MassLynx* software version 4.1 (*Waters*) and analyses were performed at the mass spectroscopy service of IQAC-CSIC.

All high-resolution mass spectra (HRMS) were analysed by FIA (flux injected analysis) with Ultrahigh-Performance Liquid Chromatography (UPLC) *Aquity* (*Waters*) coupled a *LCT Premier Orthogonal Accelerated Time of Flight* Mass Spectrometer (TOF) (*Waters*). Data were obtained in the same conditions as used for UPLC/MS and acquires with MassLynx software version 4.1 (*Waters*).

Synthetic procedures

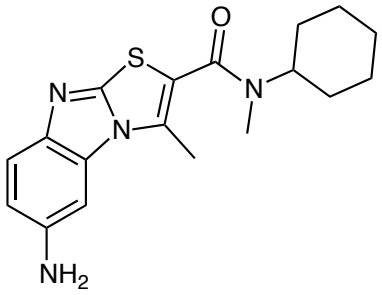

6-amino-*N*-cyclohexyl-*N*,3-dimethylbenzo[4,5]imidazo[2,1-*b*]thiazole-2-carboxamide (**15**) A solution of *N*-cyclohexyl-*N*,3-dimethyl-6-nitrobenzo[4,5]imidazo[2,1-*b*]thiazole-2-carboxamide and *N*-cyclohexyl-*N*,3-dimethyl-7-nitrobenzo[4,5]imidazo[2,1-*b*]thiazole-2-carboxamide (**136g**) (280 mg, 0.75 mmol) and sodium dithionite (654 mg, 3.76 mmol) in a mixture of THF/MeOH 8:3 (6 mL) was stirred 12 hours at room temperature. After this time, concentrated HCl (0.2 mL) was added and refluxed for 1 hour. The organic solvents were removed under reduced pressure, water was added (5 mL), the mixture was neutralized with ammonia and extracted with AcOEt (2x 15 mL), dried over Na_2SO_4 and concentrated under vacuum. The crude was purified through *flash* silica column chromatography using DCM/MeOH (97:3) isolating the active compound (**15**) (50 mg, 20%)[8]. ^{1}H-NMR (400 MHz, DMSO-d_6) δ 7.35 (d, J = 8.7 Hz, 1H), 7.11 (d, J = 2.0 Hz, 1H), 6.68 (dd, J = 8.7, 2.1 Hz, 1H), 2.91 (s, 3H), 2.63 (s, 3H), 1.80 – 1.50 (m, 9H), 1.37 – 1.24 (m, 2H). HRMS (m/z): $[M+H]^+$ calcd. for $C_{18}H_{22}N_4O_1S$, 343.1593; found, 343.1563.

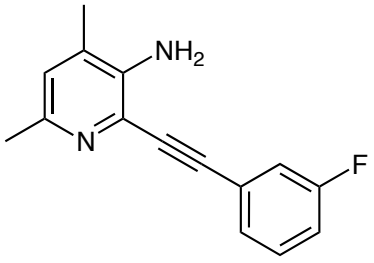

2-((3-fluorophenyl)ethynyl)-4,6-dimethylpyridin-3-amine (**18**): A solution of 2-bromo-4,6-dimethylpyridin-3-amine (200 mg, 0.99 mmol), bis(triphenylphosphine)palladium (II) dichloride (35 mg, 0.05 mmol) and copper iodide (10 mg, 0.05 mmol), previously purged with argon, in 1 mL of anhydrous DMF, 1-ethynyl-3-fluorobenzene (0,12 mL, 1.094 mmol) and dry triethylamine (0,42 mL, 2.98 mmol) were added and the reaction mixture was stirred at 40ºC over 8 hours.

After this time, 40 mL of ethyl acetate was added and the mixture was washed with 40 mL of saturated solution of $NaHCO_3$ and 40 mL of brine, the organic layer was dried over Na_2SO_4 filtered and evaporated under vacuum. The residue was purified trough flash column chromatography with AcOEt-hexane 1:4.

A brown palid solid (**18**) was isolated (197 mg, 83%), which one portion was solved in ether and HCl 1N was added, the precipitate was collected by filtration, the hydrochloride salt was obtained as a yellow solid[5]. mp: 97-99 ºC. ^{1}H-NMR (400 MHz, DMSO-d_6) δ 7.75 – 7.71 (m, 1H), 7.63 (dd, J = 7.6, 1.2 Hz, 1H), 7.56 (td, J = 8.0, 5.9 Hz, 1H), 7.50 (s, 1H), 7.39 (td, J = 8.6, 2.5 Hz, 1H), 4.00 (s, 4H), 2.54 (s, 3H), 2.34 (s, 3H). ^{13}C-NMR (101 MHz, DMSO-d_6) δ 162.92, 160.49, 145.61, 141.44, 140.80, 131.08, 131.00, 128.21, 128.18, 127.78, 122.66, 122.56, 118.59, 118.36, 117.57, 117.36, 113.15, 101.11, 79.92, 18.37, 17.88. HPLC-PDA-MS (using method A) RT: 5.13 min, λmax = 239, 280, 369, 385 nm; purity > 99.9% (254 nm). HRMS (m/z): [M+H]+ calcd. for $C_{15}H_{13}FN_2$, 241.1141; found, 241.1112.

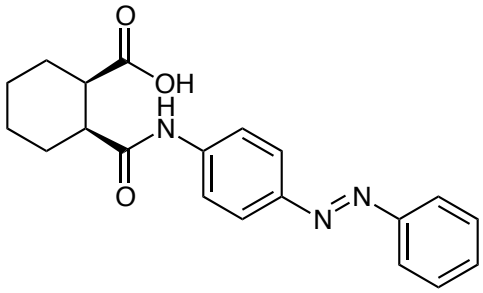

(1*S*,2*R*)+(1*R*,2*S*)-2-((4-((*E*)-phenyldiazenyl)phenyl)carbamoyl)cyclohexanecarboxylic acid (**95**): A mixture of (*E*)-4-(phenyldiazenyl)aniline (**100c**) (200 mg, 1.01 mmol) and (3a*S*,7a*R*)+(3a*R*,7a*S*)-hexahydroisobenzofuran-1,3-dione (156.2 mg, 1.01 mmol) in THF (10 mL), 3 drops of anhydrous TEA was added and the reaction mixture was stirred and refluxed overnight. Afterwards, the organic solvent was removed under reduced pressure, AcOEt (30 mL) was added and washed three times with brine (30 mL), dried over $MgSO_4$, filtered off, and the solvent was removed under vacuum. The dark crude was purified through *flash* silica column chromatography using gradient solvents from DCM/MeOH (99:1) to DCM/MeOH (93:7), to give the desired title compound (**95**) as orange solid (146 mg, 41%). Mp: 189-191°C. ^{1}H-NMR (400 MHz, DMSO-d_6) δ 12.00 (s, 1H), 10.11 (s, 1H), 7.98 – 7.74 (m, 6H), 7.56 (dt, *J* = 13.7, 6.9 Hz, 3H), 3.00 (q, *J* = 5.0 Hz, 1H), 2.63 (dt, *J* = 9.3, 4.5 Hz, 1H), 2.23 – 1.94 (m, 2H), 1.86 – 1.59 (m, 3H), 1.53 – 1.27 (m, 3H). ^{13}C-NMR (101 MHz, DMSO-d_6) δ 175.05, 173.20, 152.02, 147.21, 142.77, 130.95, 129.40, 123.60, 122.28, 119.18, 65.09, 42.65, 41.99, 27.63, 25.16, 24.01, 22.30. HPLC-PDA-MS (using

method B) RT: 3.55 min, λ_{max} = 239, 307, 352, 382 nm; purity > 99% (254 nm). HRMS (m/z): $[M+H]^+$ calcd. for $C_{20}H_{21}N_3O_3$, 352.1661; found, 352.1655.

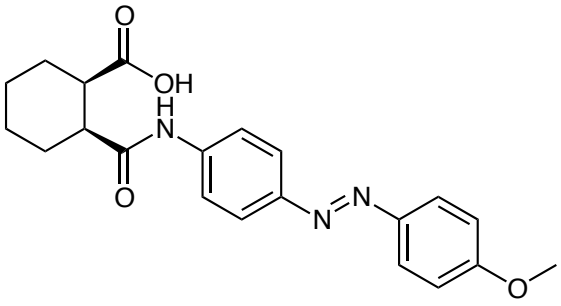

(1*S*,2*R*)+(1*R*,2*S*)-2-((4-((*E*)-(4-methoxyphenyl)diazenyl)phenyl)carbamoyl)-cyclohexanecarboxylic acid (**96**): A mixture of (*E*)-4-((4-methoxyphenyl)diazenyl)aniline (**101c**) (44 mg, 0.176 mmol) and (3a*S*,7a*R*)+(3a*R*,7a*S*)-hexahydroisobenzofuran-1,3-dione (27.6 mg, 0.176 mmol) in THF (3 mL), 3 drops of TEA anhydrous was added and the reaction mixture was stirred and refluxed overnight. Afterwards, the organic solvent was removed under reduced pressure, AcOEt (20 mL) was added and washed three times with brine (20 mL), dried over $MgSO_4$, filtered off, and the solvent was removed under vacuum. The dark crude was purified through *flash* silica column chromatography using gradient solvents from DCM/MeOH (99:1) to DCM/MeOH (97:3), to give the desired title compound (**96**) as orange solid (42 mg, 62%). Mp: 191-193°C. ^{1}H-NMR (400 MHz, DMSO-d_6) δ 11.99 (s, 1H), 10.07 (s, 1H), 7.82 (d, *J* = 9.0 Hz, 2H), 7.76 (d, *J* = 3.3 Hz, 4H), 7.08 (d, *J* = 9.0 Hz, 2H),3.86 (s, 3H), 2.99 (q, *J* = 4.9 Hz, 1H), 2.62 (dd, *J* = 9.5, 4.7 Hz, 1H), 2.16 – 1.97 (m, 2H), 1.71 (dtt, *J* = 27.3, 8.8, 4.5 Hz, 3H), 1.46 – 1.27 (m, 3H). ^{13}C-NMR (101 MHz, dmso) δ 175.05, 173.09, 161.56, 147.28, 146.22, 142.09, 124.20, 123.14, 119.19, 114.55, 55.60, 42.62, 41.99, 24.01. HPLC-PDA-MS (using method B) RT: 3.52 min, λ_{max} = 241, 363, 382 nm; purity > 99% (254 nm). HRMS (m/z): $[M+H]^+$ calcd. for $C_{21}H_{23}N_3O_4$, 382.1767; found, 382.1773.

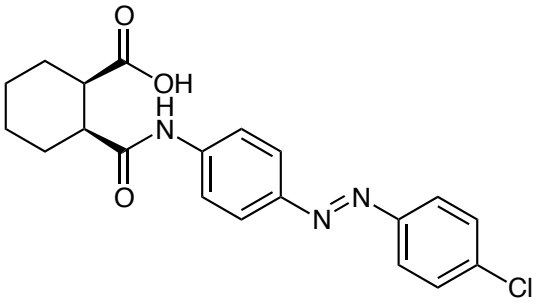

(1*S*,2*R*)+(1*R*,2*S*)-2-((4-((*E*)-(4-chlorophenyl) diazenyl)phenyl)carbamoyl) cyclo hexane-carboxylic acid (**97**): A mixture of (*E*)-4-((4-chlorophenyl)diazenyl)aniline (**102c**) (130 mg, 0.56 mmol) and (3a*S*,7a*R*)+(3a*R*,7a*S*)-hexahydroisobenzofuran-1,3-dione (86 mg, 0.56 mmol) in THF (10 mL), 3 drops of TEA anhydrous was added and the reaction mixture was stirred and refluxed overnight. Afterwards, the organic solvent was removed under reduced pressure, AcOEt (30 mL) was added and washed three times with brine (30 mL), dried over $MgSO_4$, filtered off, and the solvent was removed under vacuum. The dark crude was purified through *flash* silica column chromatography using DCM/MeOH (98:2) as a mobile phase, to give the desired title compound (**97**) as orange solid (90 mg, 42%). Mp: 180-182°C. ^{1}H-NMR (400 MHz, DMSO-d_6) δ 12.01 (s, 1H), 10.15 (s, 1H), 7.98 – 7.76 (m, 6H), 7.64 (d, *J* = 8.7 Hz, 2H), 3.00 (q, *J* = 4.9 Hz, 1H), 2.63 (dt, *J* = 9.6, 4.6 Hz, 1H), 2.17 – 2.11 (m, 1H), 2.05 – 1.97 (m, 1H), 1.83 – 1.57 (m, 3H), 1.47 – 1.27 (m, 3H). ^{13}C-NMR (101 MHz, DMSO-d_6) δ 206.47, 175.05, 173.25, 150.62, 147.08, 143.07, 135.34, 129.52, 123.95, 123.79, 119.19, 42.67, 42.02, 30.69, 27.61, 25.18, 24.01, 22.30. HPLC-PDA-MS (using method B) RT: 3.83 min, λ_{max} = 238, 354, 368 nm; purity 97% (254 nm). HRMS (m/z): $[M+H]^+$ calcd. for $C_{20}H_{20}N_3O_3Cl$, 386.1271; found, 386.1263.

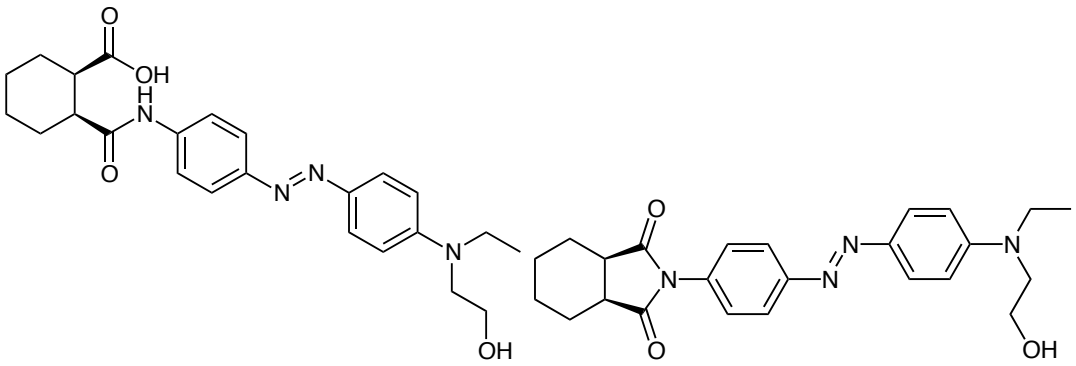

(1*S*,2*R*)+(1*R*,2*S*)-2-((4-((*E*)-(4-(ethyl(2-hydroxyethyl)amino)phenyl)diazenyl)phenyl)-carbamoyl)cyclohexanecarboxylic acid (**98**) and **(3a*R*,7a*S*)+(3a*R*,7a*S*)-2-(4-((*E*)-(4-(ethyl(2-hydroxyethyl)amino)phenyl)diazenyl)phenyl)hexahydro-1*H*-isoindole-1,3(2*H*)-dione** (**99**): A mixture of (*E*)-2-(ethyl(4-((4-nitrophenyl)diazenyl)phenyl)amino)ethanol (**103b**) (100 mg, 1.01 mmol) and (3a*S*,7a*R*)+(3a*R*,7a*S*)-hexahydroisobenzofuran-1,3-dione (54.2 mg, 1.01 mmol) in THF (6 mL), 3 drops of anhydrous TEA was added and the reaction mixture was stirred and refluxed overnight. Afterwards, the organic solvent was removed under reduced pressure, AcOEt (30 mL) was added and washed three times with brine (30 mL), dried over $MgSO_4$, filtered off, and the solvent was removed under vacuum. The dark crude was purified through *flash* silica column chromatography using a gradient solvents from DCM/MeOH (99:1) to DCM/MeOH (93:7),

isolating the desired title compound (**98**) as red solid (10 mg, 7%), Mp: 175-177°C. ^{1}H-NMR (400 MHz, Chloroform-d) δ 7.92 (d, *J* = 8.7 Hz, 2H), 7.86 (d, *J* = 9.1 Hz, 2H), 7.42 (d, *J* = 8.7 Hz, 2H), 6.80 (d, *J* = 9.2 Hz, 2H), 3.87 (t, *J* = 5.6 Hz, 2H), 3.66 – 3.48 (m, 4H), 3.11 – 2.99 (m, 2H), 1.98 – 1.88 (m, 4H), 1.57 – 1.50 (m, 4H), 1.24 (t, *J* = 7.0 Hz, 4H). ^{13}C-NMR (101 MHz, Chloroform-d) δ 178.44, 126.61, 125.36, 122.75, 111.55, 60.29, 40.17, 24.01, 21.88, 12.05. HPLC-PDA-MS (using method B) RT: 3.50 min, λ_{max} = 236, 262, 436, 458, 474 nm; purity 89% (254 nm). HRMS (m/z): $[M+H]^+$ calcd. for $C_{24}H_{28}N_4O_3$, 421.2240; found,421.2239. And compound (**99**) as a red-dark oil (70 mg, 45%). ^{1}H-NMR (400 MHz, Chloroform-d) δ 7.78 (d, *J* = 9.1 Hz, 2H), 7.72 (d, *J* = 8.7 Hz, 2H), 6.74 (t, *J* = 8.8 Hz, 4H), 4.27 (t, *J* = 6.4 Hz, 2H), 3.60 (t, *J* = 6.4 Hz, 2H), 3.46 (q, *J* = 7.1 Hz, 2H), 2.92 – 2.75 (m, 2H), 2.10 – 1.88 (m, 2H), 1.77 (m, 2H), 1.57 – 1.35 (m, 4H), 1.20 (t, *J* = 7.0 Hz, 3H). ^{13}C-NMR (101 MHz, DMSO-d_6) δ 174.68, 173.30, 151.14, 148.74, 143.14, 142.81, 123.91, 123.66, 113.42, 111.34, 79.16, 61.40, 48.12, 44.63, 26.08, 23.40, 23.15, 12.01. HPLC-PDA-MS (using method B) RT: 3.46 min, λ_{max} = 254, 321, 447 nm; purity > 99% (254 nm). HRMS (m/z): $[M+H]^+$ calcd. for $C_{24}H_{30}N_4O_4$, 439.2345; found, 439.2364.

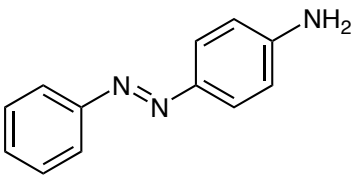

(*E*)-4-(phenyldiazenyl)aniline (**100c**): A solution of (*E*)-1-(4-nitrophenyl)-2-phenyldiazene (**100b**) (691 mg, 3.04 mmol) and sodium sulfide nonahydrate (729 mg, 3.04 mmol) in EtOH (9 mL), was stirred 1 hour at reflux. Water (50 mL) and AcOEt (50 mL) were added and the precipitate was removed by filtration, the organic layer was separate from the aqueous layer and washed three times with brine, dried over $MgSO_4$, filtered off, and the solvent was removed under vacuum. The resulting brown crude was purified through a *flash* silica column chromatography using DCM 100% as mobile phase, to give the title compound (**100c**) as an orange solid (230 mg, 40%), which was previously described[1]. ^{1}H-NMR (400 MHz, Chloroform-d) δ 7.84 (m, 4H), 7.48 (t, *J* = 7.5 Hz, 2H), 7.41 (m, 1H), 6.75 (d, *J* = 8.7 Hz, 2H), 4.05 (s, 2H). ^{13}C-NMR (101 MHz, Chloroform-d) δ 153.10, 149.69, 145.70, 129.93, 129.10, 125.24, 122.47, 114.76, 77.16, 60.54, 21.20, 14.34.

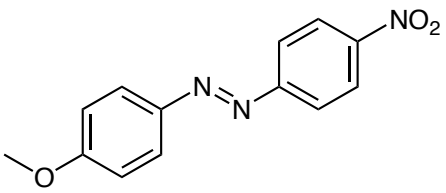

(*E*)-1-(4-methoxyphenyl)-2-(4-nitrophenyl)diazene (**101b**): A solution of commercial (*E*)-4-((4-nitrophenyl)diazenyl)phenol (**101a**) (300 mg, 1.23 mmol) and K_2CO_3 (177 mg, 2.95 mmol) in MeCN (7 mL), was stirred at room temperature 10 minutes, after this time, MeI (0.1 mL, 1.47 mmol) was added, and the reaction mixture was stirred overnight at room temperature. The day after, the solvent was removed under reduced pressure, AcOEt (20 mL) was added and washed three times with ammonia 1N (20 mL), brine (20 mL), dried over $MgSO_4$, filtered off, and the organic solvent was removed under vacuum. The resulting brown crude was purified through a *flash* silica column chromatography using DCM 100% as mobile phase, to give the title compound (**101b**) as orange-red solid. (147 mg, 47%) which was previously reported[3]. ^{1}H-NMR (400 MHz, Chloroform-d) δ 8.37 (d, *J* = 9.0 Hz, 2H), 7.98 (dd, *J* = 9.0, 3.1 Hz, 4H), 7.05 (d, *J* = 9.0 Hz, 2H), 3.92 (s, 3H). ^{13}C NMR (101 MHz, Chloroform-d) δ 163.41, 156.18, 147.10, 125.76, 124.86, 123.26, 114.62, 55.86.

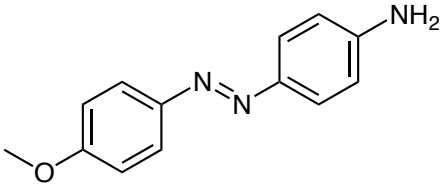

(*E*)-4-((4-methoxyphenyl)diazenyl)aniline (**101c**): A solution of (*E*)-1-(4-methoxyphenyl)-2-(4-nitrophenyl)diazene (**101b**) (136 mg, 0.52 mmol) and sodium sulfide nonahydrate (124 mg, 0.52 mmol) in EtOH (3 mL), was stirred 1 hour at reflux. Water (50 mL) and AcOEt (50 mL) were added and the precipitate was removed by filtration, the organic layer was separate from the aqueous layer and washed three times with brine, dried over $MgSO_4$, filtered off, and the solvent was removed under vacuum. The resulting brown crude was purified through a *flash* silica column chromatography using DCM 100% as mobile phase, to give the title compound (**101c**) as a orange solid (44 mg, 37%) which was previously reported[3]. ^{1}H-NMR (400 MHz, Chloroform-d) δ 7.84 (d, *J* = 9.0 Hz, 2H), 7.77 (d, *J* = 8.7 Hz, 2H), 6.99 (d, *J* = 9.0 Hz, 2H), 6.74 (d, *J* = 8.7 Hz, 2H), 3.99 (s, 2H), 3.88 (s, 3H). ^{13}C-NMR (101 MHz, Chloroform-d) δ 161.29, 149.11, 147.39, 145.79, 124.81, 124.18, 114.86, 114.26, 55.68.

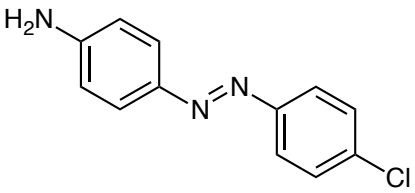

(*E*)-4-((4-chlorophenyl)diazenyl)aniline (**102c**): A solution of Oxone (1.9 g, 3.13 mmol) in water (7 mL) was added to a solution of 4-chloroaniline (**102b**) (200 mg, 1.56 mmol) in DCM (5 mL) at room temperature and the resulting mixtures was stirred 2 hours at room temperature with vigorous agitation. The layers were separated and the organic one was washed with brine (5 mL), dried over Na_2SO_4 and filtered, the resulting solution was disposed in a round bottom flask and a solution of benzene-1,4-diamine (**102a**) (168 mg, 1.56 mmol) in DCM (2 mL) was added, 3 drops AcOH was added to the resulting mixture which was stirred 24 hours at room temperature. The solvent was removed under vacuum and remaining AcOH was removed by co-evaporation under vacuum with toluene (2x5 mL). The resulting dark crude was purified trough a *flash* silica column chromatography using DCM 100% as mobile phase to give the title compound (**102c**) (160 mg, 45%) as a red-orange solid which was reported previously[4]. ^{1}H-NMR (400 MHz, Chloroform-d) δ 7.80 (dd, *J* = 8.5, 4.0 Hz, 4H), 7.44 (d, *J* = 8.3 Hz, 2H), 6.74 (d, *J* = 8.3 Hz, 2H), 4.09 (s, 2H).

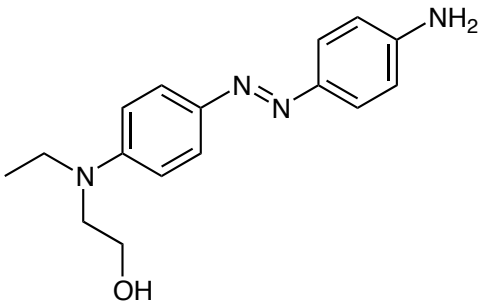

(*E*)-2-((4-((4-aminophenyl)diazenyl)phenyl)(ethyl)amino)ethanol (**103b**): A solution of commercial (*E*)-2-(ethyl(4-((4-nitrophenyl)diazenyl)phenyl)amino)ethanol (**103a**) (1.4 g, 4.45 mmol) and sodium sulfide nonahydrate (1.07 g, 4.45 mmol) in EtOH (14 mL), was stirred 1 hour at reflux. Water (50 mL) and AcOEt (50 mL) were added and the precipitate was removed by filtration, the organic layer was separate from the aqueous layer and washed three times with brine, dried over $MgSO_4$, filtered off, and the solvent was removed under vacuum. The resulting brown crude was purified through a *flash* silica column chromatography using DCM/MeOH 99:1 as mobile phase, to give the title compound (**103b**) as a red-black solid, which was previously described[2]. (304 mg, 25%). ^{1}H-NMR (400 MHz, DMSO-d_6) δ 7.62 (d, 8.9 Hz, 2H), 7.53 (d, 8.9 Hz, 2H), 6.76 (d, *J* = 9.0 Hz, 2H), 6.63 (d, *J* = 9.0 Hz, 2H), 5.74 (s, 2H), 4.78 (s, 1H) 3.57 (q, *J* = 5.8

Hz, 2H), 3.51 – 3.38 (m, 4H), 1.12 (t, *J* = 7.0 Hz, 3H). ^{13}C-NMR (101 MHz, DMSO-d$_6$) δ 151.01, 149.11, 143.23, 142.45, 123.84, 123.75, 113.48, 111.06, 58.38, 52.15, 44.95, 12.07.

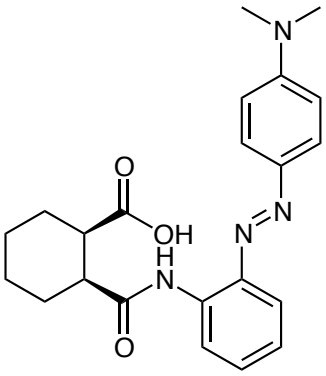

(1*S*,2*R*)+(1*R*,2*S*)-2-((2-((*E*)-(4-(dimethylamino)phenyl)diazenyl)phenyl)carbamoyl)-cyclohexanecarboxylic acid (**104**): A mixture of (*E*)-4-((2-aminophenyl)diazenyl)-*N*,*N*-dimethylaniline (**117d**) (60 mg, 0.25 mmol) and (3a*S*,7a*R*)+(3a*R*,7a*S*)-hexahydroisobenzofuran-1,3-dione (36.7 mg, 0.238 mmol) in THF (3 mL), 3 drops of TEA anhydrous was added and the reaction mixture was stirred and refluxed overnight. Afterwards, the organic solvent was removed under reduced pressure, AcOEt (10 mL) was added and washed three times with brine (10 mL), dried over $MgSO_4$, filtered off, and the solvent was removed under vacuum. The dark crude was purified through *flash* silica column chromatography using DCM/MeOH (95:5) as a mobile phase, to give the desired title compound (**104**) as orange solid (27 mg, 28%). Mp: 160-162°C. ^{1}H-NMR (400 MHz, Chloroform-d) δ 10.54 (s, 1H), 8.59 (dd, *J* = 8.4, 1.3 Hz, 1H), 7.85 – 7.75 (m, 3H), 7.34 (ddd, *J* = 8.6, 7.4, 1.6 Hz, 1H), 7.14 (ddd, *J* = 8.4, 7.4, 1.3 Hz, 1H), 6.76 (d, *J* = 9.1 Hz, 2H), 3.11 (s, 6H), 3.03 – 2.91 (m, 2H), 2.30 – 2.11 (m, 2H), 2.02 – 1.93 (m, 1H), 1.81 – 1.64 (m, 3H), 1.56 – 1.47 (m, 2H). ^{13}C-NMR (101 MHz, Chloroform-d) δ 176.38, 173.12, 152.78, 143.45, 139.76, 134.68, 130.91, 124.94, 124.25, 123.77, 120.87, 120.33, 116.89, 111.79, 46.04, 42.75, 40.63, 40.53, 40.46, 23.86, 23.54, 22.09. HPLC-PDA-MS (using method B) RT: 3.83 min, λ_{max} = 235, 268, 459 nm; purity > 99% (254 nm). HRMS (m/z): $[M+H]^+$ calcd. for $C_{22}H_{26}N_4O_3$, 395.2083; found, 395.2078.

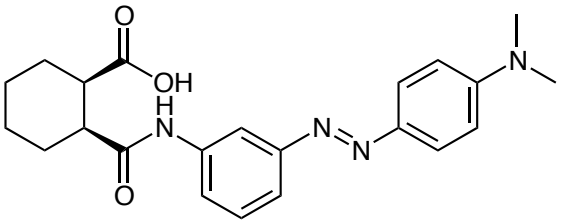

(1*S*,2*R*)+(1*R*,2*S*)-2-((3-((*E*)-(4-(dimethylamino)phenyl)diazenyl)phenyl)carbamoyl)-cyclohexanecarboxylic acid (**105**): A mixture of (*E*)-*4*-((3-aminophenyl)diazenyl)-N,N-dimethylaniline (**118d**) (40 mg, 0.16 mmol) and (3a*S*,7a*R*)+(3a*R*,7a*S*)-hexahydroisobenzofuran-1,3-dione (30 mg, 0.18 mmol) in THF (2 mL), 3 drops of TEA anhydrous was added and the reaction mixture was stirred and refluxed overnight. Afterwards, the organic solvent was removed under reduced pressure, AcOEt (10 mL) was added and washed three times with brine (10 mL), dried over $MgSO_4$, filtered off, and the solvent was removed under vacuum. The dark crude was purified through *flash* silica column chromatography using DCM/MeOH (98:2) as a mobile phase, to give the desired title compound (**105**) as red-orange oil (23 mg, 35%). ^{1}H-NMR (400 MHz, DMSO-d_6) δ 12.12 (s, 1H), 9.91 (s, 1H), 8.08 (t, *J* = 1.9 Hz, 1H), 7.79 (d, *J* = 9.1 Hz, 2H), 7.59 (dt, *J* = 7.6, 1.8 Hz, 1H), 7.53 – 7.36 (m, 2H), 6.83 (d, *J* = 9.2 Hz, 2H), 3.06 (s, 6H), 2.86 – 2.71 (m, 2H), 1.96 – 1.86 (m, 2H), 1.86 – 1.76 (m, 3H), 1.76 – 1.63 (m, 3H). ^{13}C-NMR (101 MHz, DMSO-d_6) δ 175.08, 174.63, 173.64, 172.88, 152.74, 152.49, 142.52, 140.38, 129.63, 129.20, 124.66, 120.13, 117.66, 111.56, 111.16, 51.20, 42.01, 41.65, 41.54, 25.99, 25.63, 23.37, 23.20. HPLC-PDA-MS (using method B) RT: 3.55 min, λ_{max} = 237, 419 nm; purity > 99% (254 nm). HRMS (m/z): $[M+H]^+$ calcd. for $C_{22}H_{26}N_4O_3$, 395.2083; found, 395.2079.

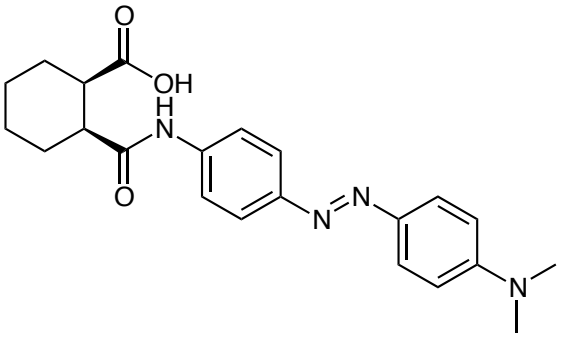

(1*S*,2*R*)+(1*R*,2*S*)-2-((4-((*E*)-(4-(dimethylamino)phenyl)diazenyl)phenyl)carbamoyl)-cyclohexanecarboxylic acid (**106**): A mixture of (*E*)-4-((4-aminophenyl)diazenyl)-*N*,*N*-dimethylaniline (**117b**) (60 mg, 0.25 mmol) and (3a*S*,7a*R*)+(3a*R*,7a*S*)-hexahydroisobenzofuran-1,3-dione (36.7 mg, 0.238 mmol) in THF (3 mL), 3 drops of TEA anhydrous was added and the reaction mixture was stirred and refluxed overnight. Afterwards, the organic solvent was removed

under reduced pressure, AcOEt (10 mL) was added and washed three times with brine (10 mL), dried over $MgSO_4$, filtered off, and the solvent was removed under vacuum. The dark crude was purified through *flash* silica column chromatography using DCM/MeOH (97:3) as a mobile phase, to give the desired title compound (**106**) as orange solid (36 mg, 38%). Mp: 201-203°C. ^{1}H NMR (400 MHz, DMSO-d_6) δ 11.96 (s, 1H), 9.96 (s, 1H), 7.88 – 7.61 (m, 6H), 6.81 (d, *J* = 9.2 Hz, 2H), 3.05 (s, 6H), 2.98 (q, *J* = 4.9 Hz, 1H), 2.60 (dt, *J* = 9.3, 4.5 Hz, 1H), 2.18 – 1.99 (m, 2H), 1.81 – 1.61 (m, 3H), 1.52 – 1.27 (m, 3H).^{13}C NMR (101 MHz, DMSO-d_6) δ 175.04, 172.86, 152.06, 147.71, 142.63, 140.99, 124.25, 122.45, 119.17, 111.49, 56.02, 42.61, 42.05, 27.68, 25.15, 24.01, 22.32, 18.50. HPLC-PDA-MS (using method B) RT: 3.55 min, λ_{max} = 237, 257, 312, 374, 425, 445, 457 nm; purity > 99% (254 nm). HRMS (m/z): $[M+H]^+$ calcd. for $C_{22}H_{26}N_4O_3$, 395.2083; found, 395.2109.

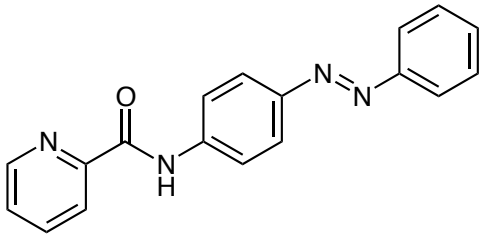

(*E*)-*N*-(4-(phenyldiazenyl)phenyl)picolinamide (**107**): In a round bottom flask was displaced (*E*)-4-(phenyldiazenyl)aniline(**100c**) (24 mg, 0.12 mmol), picolinic acid (**119**) (19 mg, 0.13 mmol) and DIPEA (42µL, 0.24 mmol) in DCM (2 mL), and the resulting mixture was stirred 24 hours at 40 °C. Afterwards, 10 mL of DCM was added and the mixture was washed with saturated $NaHCO_3$ (15 mL), water (15 mL) and brine (15 mL), dried over Na_2SO_4, filtered and evaporated to dryness. The obtained crude was purified through *flash* silica column chromatography using DCM 100% as mobile phase, to obtain (**107**) as orange solid (4 mg, 10%). Mp: 171-173°C. ^{1}H-NMR (400 MHz, Chloroform-d) δ 10.24 (s, 1H), 8.64 (d, *J* = 4.9, 1.2 Hz, 1H), 8.32 (d, 1H), 8.02 – 7.85 (m, 7H), 7.55 – 7.42 (m, 4H). ^{13}C-NMR (101 MHz, Chloroform-d) δ 162.23, 152.87, 149.65, 149.21, 148.17, 140.43, 137.93, 130.85, 129.19, 126.83, 124.26, 122.87, 122.66, 122.53, 119.90, 65.98, 53.55, 15.41. HPLC-PDA-MS (using method A) RT: 4.01 min, λ_{max} = 233, 267, 354, 367 nm; purity > 99% (254 nm). HRMS (m/z): $[M+H]^+$ calcd. for $C_{18}H_{14}N_4O$, 303.1246; found, 303.1261.

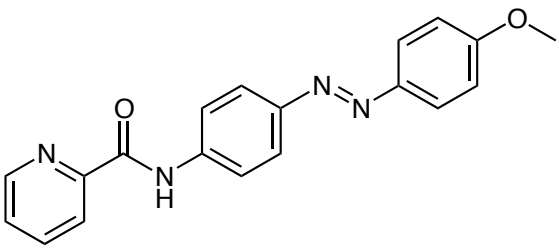

(*E*)-*N*-(4-((4-methoxyphenyl)diazenyl)phenyl)picolinamide (**108**): In a round bottom flask was displaced (*E*)-4-((4-methoxyphenyl)diazenyl)aniline (**101c**) (40 mg, 0.17 mmol), picolinic acid (**119**) (27 mg, 0.19 mmol) and DIPEA (60µL, 0.35 mmol) in DCM (2 mL), and the resulting mixture was stirred 24 hours at 40 °C. Afterwards, 10 mL of DCM was added and the mixture was washed with saturated $NaHCO_3$ (15 mL), water (15 mL) and brine (15 mL), dried over Na_2SO_4, filtered and evaporated to dryness. The obtained crude was purified through *flash* silica column chromatography using DCM 100% as mobile phase, to obtain (**108**) as orange solid (9 mg, 15%). Mp: 165-167°C. ^{1}H-NMR (400 MHz, Chloroform-d) δ 10.21 (s, 1H), 8.66 – 8.59 (m, 1H), 8.31 (d, *J* = 7.8 Hz, 1H), 7.97 – 7.86 (m, 7H), 7.50 (ddd, *J* = 7.6, 4.8, 1.2 Hz, 1H), 7.00 (d, *J* = 9.0 Hz, 2H), 3.88 (s, 3H). ^{13}C-NMR (101 MHz, DMSO-d_6) δ 162.20, 162.02, 149.73, 149.36, 148.17, 147.25, 139.86, 137.94, 126.80, 124.75, 123.91, 123.41, 122.66, 122.59, 121.65, 119.95, 119.88, 114.36, 113.97, 55.74. HPLC-PDA-MS (using method A) RT: 3.95 min, λ_{max} = 237, 369, 385 nm; purity 98% (254 nm). HRMS (m/z): $[M+H]^+$ calcd. for $C_{19}H_{16}N_4O_2$, 333.1352; found, 333.1358.

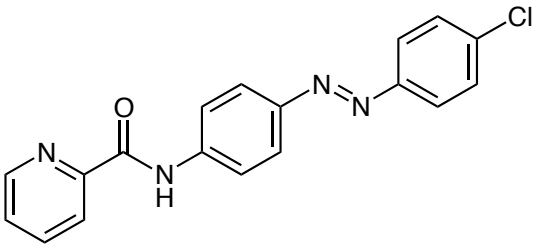

(*E*)-*N*-(4-((4-chlorophenyl)diazenyl)phenyl)picolinamide (**109**): In a round bottom flask was displaced (*E*)-4-((4-chlorophenyl)diazenyl)aniline (**102c**) (50 mg, 0.21 mmol), picolinic acid (**119**) (33 mg, 0.23 mmol) and DIPEA (75µL, 0.43 mmol) in DCM (2 mL), and the resulting mixture was stirred 24 hours at 40 °C. Afterwards, 10 mL of DCM was added and the mixture was washed with saturated $NaHCO_3$ (15 mL), water (15 mL) and brine (15 mL), dried over Na_2SO_4, filtered and evaporated to dryness. The obtained crude was purified through *flash* silica column chromatography using DCM 100% as mobile phase, to obtain (**109**) as orange solid (8 mg, 11%). Mp: 210-212°C. ^{1}H-NMR (400 MHz, Chloroform-d) δ 10.26 (s, 1H), 8.65 (ddd, *J* = 4.8, 1.7, 0.9

Hz, 1H), 8.33 (d, *J* = 7.8 Hz, 1H), 8.04 – 7.92 (m, 5H), 7.87 (d, *J* = 8.7 Hz, 2H), 7.56 – 7.51 (m, 1H), 7.48 (d, *J* = 8.7 Hz, 2H). ^{13}C-NMR (101 MHz, Chloroform-d) δ 162.29, 149.04, 148.20, 140.70, 137.98, 136.72, 129.47, 129.30, 126.89, 124.40, 124.16, 122.71, 122.45, 121.91, 119.95, 119.69. HPLC-PDA-MS (using method A) RT: 4.33 min, λ_{max} = 233, 358 nm; purity 91% (254 nm). HRMS (m/z): $[M+H]^+$ calcd. for $C_{18}H_{13}N_4O_1Cl$, 337.0856; found, 337.0865.

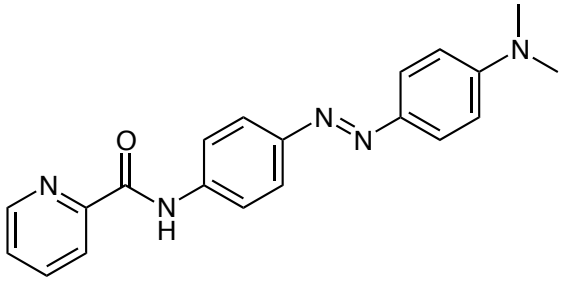

(*E*)-*N*-(4-((4-(dimethylamino)phenyl)diazenyl)phenyl)picolinamide (**110**): In a round bottom flask was displaced (*E*)-4-((4-aminophenyl)diazenyl)-*N*,*N*-dimethylaniline (**117b**) (15 mg, 0.06 mmol), picolinic acid (**119**) (10 mg, 0.07 mmol) and DIPEA (22µL, 0.12 mmol) in DCM (2 mL), and the resulting mixture was stirred 24 hours at 40 °C. Afterwards, 10 mL of DCM was added and the mixture was washed with saturated $NaHCO_3$ (15 mL), water (15 mL) and brine (15 mL), dried over Na_2SO_4, filtered and evaporated to dryness. The obtained crude was purified through *flash* silica column chromatography using DCM 100% as mobile phase, to obtain (**110**) as orange solid (5 mg, 22%). Mp: 196-198°C. ^{1}H-NMR (400 MHz, Chloroform-d) δ 10.19 (s, 1H), 8.64 (ddd, *J* = 4.8, 1.7, 0.9 Hz, 1H), 8.32 (d, *J* = 7.8 Hz, 1H), 7.96 – 7.91 (m, 5H), 7.88 (d, *J* = 9.0 Hz, 2H), 7.50 (ddd, *J* = 7.6, 4.8, 1.2 Hz, 1H), 6.77 (d, *J* = 9.1 Hz, 2H), 3.09 (s, 6H). ^{13}C-NMR (101 MHz, DMSO-d_6) δ 149.85, 148.15, 138.97, 137.90, 126.70, 124.99, 123.43, 122.62, 119.96, 111.76, 40.52. HPLC-PDA-MS (using method A) RT: 3.99 min, λ_{max} = 236, 259, 311, 435, 446, 458 nm; purity > 99% (254 nm). HRMS (m/z): $[M+H]^+$ calcd. for $C_{20}H_{19}N_5O_1$, 346.1668; found, 346.1654.

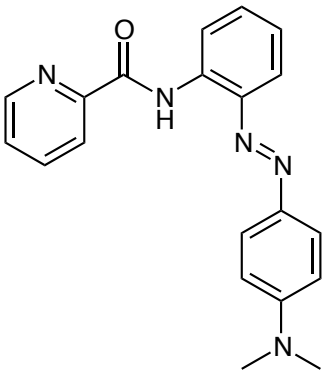

(*E*)-*N*-(2-((4-(dimethylamino)phenyl)diazenyl)phenyl)picolinamide (**111**): In a round bottom flask was displaced (*E*)-2-((4-aminophenyl)diazenyl)-*N*,*N*-dimethylaniline (**117d**) (50 mg, 0.21 mmol), picolinic acid (**119**) (32 mg, 0.23 mmol) and DIPEA (70µL, 0.33 mmol) in DCM (2 mL), and the resulting mixture was stirred 24 hours at 40 °C. Afterwards, 10 mL of DCM was added and the mixture was washed with saturated $NaHCO_3$ (15 mL), water (15 mL) and brine (15 mL), dried over Na_2SO_4, filtered and evaporated to dryness. The obtained crude was purified through *flash* silica column chromatography using DCM 100% as mobile phase, to obtain (**111**) as red solid (16 mg, 22%). Mp: 128-130°C. ^{1}H-NMR (400 MHz, Chloroform-d) δ 12.48 (s, 1H), 8.85 (d, *J* = 8.2, 1.3 Hz, 1H), 8.74 (d, *J* = 4.0 Hz, 1H), 8.33 (d, *J* = 7.9 Hz, 1H), 8.07 (d, *J* = 9.1 Hz, 2H), 7.91 (td, *J* = 7.7, 1.7 Hz, 1H), 7.86 (dd, *J* = 8.1, 1.5 Hz, 1H), 7.49 (ddd, *J* = 7.6, 4.7, 1.2 Hz, 1H), 7.46 – 7.40 (m, 1H), 7.18 (ddd, *J* = 8.2, 7.3, 1.4 Hz, 1H), 6.80 (d, *J* = 9.1 Hz, 2H), 3.12 (s, 6H). ^{13}C-NMR (101 MHz, cdcl$_3$) δ 162.46, 152.72, 150.78, 148.36, 144.01, 140.72, 137.63, 135.50, 130.90, 126.36, 125.36, 123.80, 122.58, 120.09, 118.50, 111.70, 68.11, 51.01, 40.47, 25.75. HPLC-PDA-MS (using method A) RT: 4.32 min, λ_{max} = 231, 263, 456, 466 nm; purity > 99% (254 nm). HRMS (m/z): $[M+H]^+$ calcd. for $C_{20}H_{19}N_5O$, 346.1668; found, 346.1677.

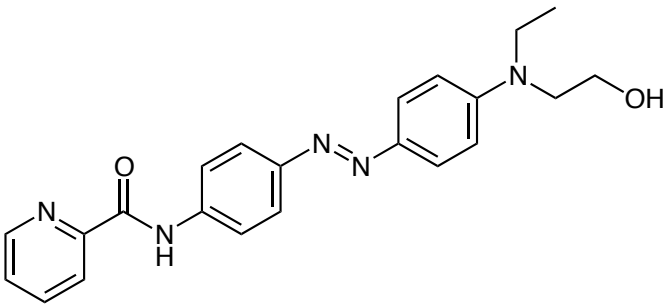

(*E*)-*N*-(4-((4-(ethyl(2-hydroxyethyl)amino)phenyl)diazenyl)phenyl)picolinamide (**112**): In a round bottom flask was displaced (*E*)-2-(ethyl(4-((4-nitrophenyl)diazenyl)phenyl)amino)ethanol (**103b**) (60 mg, 0.21 mmol), picolinic acid (**119**) (33 mg, 0.23 mmol) and DIPEA (70µL, 0.42 mmol) in DCM (2 mL), and the resulting mixture was stirred 24 hours at 40 °C. Afterwards, 10 mL

of DCM was added and the mixture was washed with saturated $NaHCO_3$ (15 mL), water (15 mL) and brine (15 mL), dried over Na_2SO_4, filtered and evaporated to dryness. The obtained crude was purified through *flash* silica column chromatography using DCM/MeOH (98:2) as mobile phase, to obtain (**112**) as dark solid (11 mg, 13%). Mp: 180-183°C. ^{1}H-NMR (400 MHz, Chloroform-d) δ 10.19 (s, 1H), 8.64 (d, *J* = 4.8 Hz, 1H), 8.32 (d, *J* = 7.8 Hz, 1H), 7.97 – 7.90 (m, 5H), 7.85 (d, *J* = 9.1 Hz, 2H), 7.50 (ddd, *J* = 7.6, 4.8, 1.2 Hz, 1H), 6.81 (d, *J* = 9.1 Hz, 2H), 3.88 (q, *J* = 5.8 Hz, 2H), 3.59 (t, *J* = 5.9 Hz, 2H), 3.54 (q, *J* = 7.1 Hz, 2H), 1.67 (s, 1H), 1.24 (t, *J* = 7.1 Hz, 3H). ^{13}C-NMR (101 MHz, Chloroform-d) δ 162.11, 150.48, 149.83, 148.15, 143.94, 139.01, 137.90, 126.71, 125.16, 123.45, 122.61, 119.96, 111.81, 60.49, 52.59, 46.02, 12.24. HPLC-PDA-MS (using method A) RT: 3.51 min, λ_{max} = 236, 259, 304, 329, 443, 462 nm; purity 93% (254 nm). HRMS (m/z): $[M+H]^+$ calcd. for $C_{22}H_{23}N_5O_2$, 390.1930; found, 390.1933.

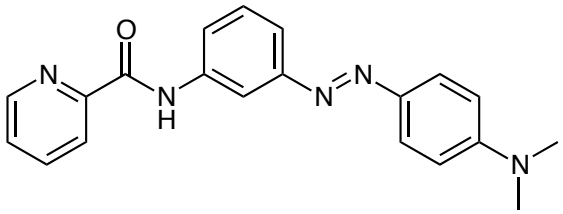

(*E*)-*N*-(3-((4-(dimethylamino)phenyl)diazenyl)phenyl)picolinamide (**113**): In a round bottom flask was displaced (*E*)-3-((4-aminophenyl)diazenyl)-*N*,*N*-dimethylaniline (**118d**) (15 mg, 0.16 mmol), picolinic acid (**119**) (26 mg, 0.18 mmol) and DIPEA (50µL, 0.33 mmol) in DCM (2 mL), and the resulting mixture was stirred 24 hours at 40 °C. Afterwards, 10 mL of DCM was added and the mixture was washed with saturated $NaHCO_3$ (15 mL), water (15 mL) and brine (15 mL), dried over Na_2SO_4, filtered and evaporated to dryness. The obtained crude was purified through *flash* silica column chromatography using DCM 100% as mobile phase, to obtain (**113**) as red solid (15 mg, 26%). Mp: 144-146°C. ^{1}H-NMR (400 MHz, Chloroform-d) δ 10.16 (s, 1H), 8.63 (dd, *J* = 4.8, 0.8 Hz, 1H), 8.32 (d, *J* = 7.8 Hz, 1H), 8.12 (t, *J* = 2.0 Hz, 1H), 7.98 (ddd, *J* = 8.1, 2.2, 1.0 Hz, 1H), 7.95 – 7.88 (m, 3H), 7.68 – 7.63 (m, 1H), 7.54 – 7.46 (m, 2H), 6.76 (d, *J* = 9.1 Hz, 2H), 3.09 (s, 6H). ^{13}C-NMR (101 MHz, Chloroform-d) δ 162.21, 153.99, 152.64, 149.90, 148.13, 143.72, 138.58, 137.81, 129.71, 126.62, 125.24, 122.57, 120.64, 119.45, 112.43, 111.62, 65.99, 40.44, 29.84, 15.41. HPLC-PDA-MS (using method A) RT: 3.98 min, λ_{max} = 237, 261, 295, 377, 424, 443, 454, 464 nm; purity > 99% (254 nm). HRMS (m/z): $[M+H]^+$ calcd. for $C_{20}H_{19}N_5O$, 346.1668; found, 346.1664.

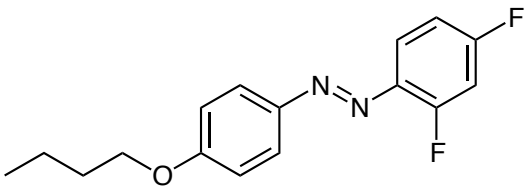

(*E*)-1-(4-butoxyphenyl)-2-(2,4-difluorophenyl)diazene (**115**): A solution of (*E*)-4-((2,4-difluorophenyl)diazenyl)phenol (**120c**) (150 mg, 0.64 mmol) and K_2CO_3 (212 mg, 1.53 mmol) in DMF (3 mL) was stirred 15 minutes and after this time, a solution of 1-bromobutane (**120d**) (0.08 mL, 0.77 mmol) in DMF (0.5 mL), was added to the first solution and the reaction mixture was stirred 24 hours at room temperature. Afterwards, AcOEt (10 mL) was added and was washed with a saturated solution of $NaHCO_3$ (3x10 mL), brine (3x10 mL), dried over Na_2SO_4, filtered off and the solvent was removed under vacuum. The brown crude was purified through *flash* silica column chromatography using DCM 100% as mobile phase, to give the desired title compound (**115**) (126 mg, 68%) as an orange solid. Mp: 50-52°C. ^{1}H-NMR (400 MHz, Chloroform-d) δ 7.92 (d, *J* = 9.0 Hz, 2H), 7.79 (td, *J* = 8.8, 6.3 Hz, 1H), 7.10 – 6.85 (m, 4H), 4.05 (t, *J* = 6.5 Hz, 2H), 1.87 – 1.72 (m, 2H), 1.60 – 1.46 (m, 2H), 1.00 (t, *J* = 7.4 Hz, 3H). ^{13}C-NMR (101 MHz, Chloroform-d) δ 162.28, 147.10, 125.23, 119.13, 114.90, 114.39, 111.72, 111.68, 105.35, 105.11, 105.09, 104.85, 68.24, 31.37, 19.37, 13.99. HPLC-PDA-MS (using method A) RT: 4.60 min, λ_{max} = 239, 352, 363, 373 nm; purity 97% (254 nm). HRMS (m/z): $[M+H]^+$ calcd. for $C_{16}H_{16}N_2OF_2$,291.1309; found, 291.1319.

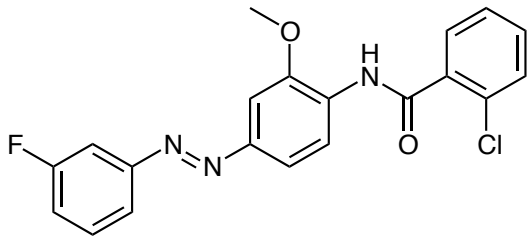

(*E*)-2-chloro-*N*-(4-((3-fluorophenyl)diazenyl)-2-methoxyphenyl)benzamide (**116**): A solution of Oxone (1.1 g, 1.8 mmol) in water (5 mL) was added to a solution of 3-fluoroaniline (100 mg, 0.9 mmol) in DCM (3 mL) at room temperature and the resulting mixtures was stirred 2 hours at room temperature with vigorous agitation. The layers were separated and the organic one was washed with brine (5 mL), dried over Na_2SO_4 and filtered, the resulting solution was disposed in a round bottom flask and a solution of *N*-(4-amino-2-methoxyphenyl)-2-chlorobenzamide (**121a**) (60 mg, 0.21 mmol) in DCM (1 mL) was added, 3 drops AcOH was added to the resulting mixture which was stirred 24 hours at room temperature. The solvent was removed under vacuum and

remaining AcOH was removed by co-evaporation under vacuum with toluene (2x5 mL). The resulting dark crude was purified trough a *flash* silica column chromatography using DCM:Hexanes 90:10 as mobile phase to give the title compound (**116**) (35 mg, 42%) as a red-orange solid. Mp: 107-109°C. ^{1}H-NMR (400 MHz, Chloroform-d) δ 8.80 (s, 1H), 8.77 (d, *J* = 8.6 Hz, 1H), 7.82 (dd, *J* = 7.4, 1.9 Hz, 1H), 7.77 – 7.70 (m, 2H), 7.63 – 7.58 (m, 1H), 7.53 – 7.35 (m, 5H), 7.17 (tdd, *J* = 8.2, 2.6, 1.0 Hz, 1H), 4.00 (s, 3H). ^{13}C-NMR (101 MHz, Chloroform-d) δ 164.68, 162.22, 154.32, 148.86, 148.77, 135.19, 132.01, 130.98, 130.96, 130.69, 130.40, 130.32, 127.45, 121.18, 120.41, 120.38, 119.60, 117.69, 117.47, 108.32, 108.09, 101.31, 56.25. HPLC-PDA-MS (using method A) RT: 4.24 min, λ_{max} = 236, 310, 354, 369, 391 nm; purity > 99% (254 nm). HRMS (m/z): $[M+H]^+$ calcd. for $C_{20}H_{15}N_3O_2FCl$, 384.0915; found, 384.0927.

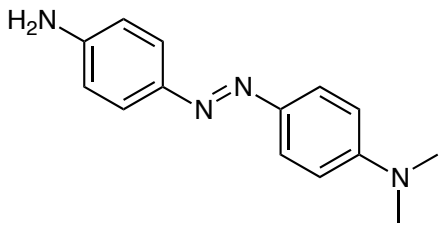

(*E*)-4-((4-aminophenyl)diazenyl)-*N*,*N*-dimethylaniline (**117b**): A solution of benzene-1,4-diamine (**102a**) (200 mg, 1.85 mmol) and *N*,*N*-dimethyl-4-nitrosoaniline (**117a**) (306 mg, 2.03 mmol) in DCM (7 mL) with 3 drops of AcOH, purged previously with Nitrogen, was stirred 24 hours at room temperature. The solvent was removed under vacuum and remaining AcOH was removed by co-evaporation under vacuum with toluene (2x5 mL). The resulting dark crude was purified trough a *flash* silica column chromatography using DCM/MeOH (99:1) as mobile phase, to give the desired title compound (**117b**) as red solid (83 mg, 20%). ^{1}H-NMR (400 MHz, Chloroform-d) δ 7.81 (d, *J* = 9.1 Hz, 2H), 7.73 (d, *J* = 8.7 Hz, 2H), 6.74 (t, *J* = 9.1 Hz, 4H), 3.92 (s, 2H), 3.05 (s, 6H).

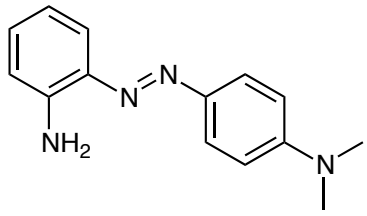

(*E*)-4-((2-aminophenyl)diazenyl)-*N*,*N*-dimethylaniline (**117d**): A solid mixture of 1,2-diaminobenzene (**117c**) (0.80 g, 7.4 mmol), *N*,*N*-dimethyl-4-nitrosoaniline (**117a**) (0.57 g, 3.8 mmol), and potassium hydroxide (0.62 g, 9.4 mmol) in powder was mixed thoroughly using a

spatula while heating at 90 °C for 10 min. Toluene (10 mL) was added and the reactions was stirred at 90 °C for 1 hour and the resulting mixture was diluted with EtOAc (50 mL) and washed with water (30 mL), brine (2x30 mL). The organic phase was dried over anhydrous $MgSO_4$, filtered and evaporated to dryness. The obtained solid was purified through silica *flash* column using *Biotage Isolera* equipment (SNAP KP-Sil 50g, A=hexanes B=EtOAc; 0%B 3CV, 0%B-12%B 1CV, 12%B-20%B 8CV, 20%B-40%B 3.5CV, 40%B-100%B 1CV, 100%B 8.5 CV) to afford (**117d**) (0.52 g, 57%) as a red solid. ^{1}H-NMR (400 MHz, Chloroform-d) δ 7.82 (d, *J* = 9.0 Hz, 2H), 7.74 (dd, *J* = 8.0, 1.5 Hz, 1H), 7.15 (t, *J* = 7.6 Hz, 1H), 6.80 (t, *J* = 7.1 Hz, 1H), 6.77 – 6.72 (m, 3H), 5.55 (br, 2H), 3.07 (s, 6H).

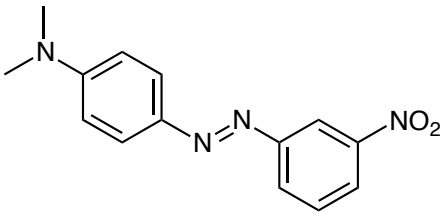

(*E*)-*N*,*N*-dimethyl-4-((3-nitrophenyl)diazenyl)aniline (**118c**): A solution of Oxone (1.8 g, 3 mmol) in water (7 mL) was added to a solution of 3-nitroaniline (**118b**) (207 mg, 1.5 mmol) in DCM (5 mL) at room temperature and the resulting mixtures was stirred 2 hours at room temperature with vigorous agitation. 5 mL of DCM was added and the layers were separated and the organic one was washed with brine (10 mL), dried over Na_2SO_4 and filtered, the resulting solution was disposed in a round bottom flask and a solution of *N*,*N*-dimethylbenzene-1,4-diamine (**118a**) (249 mg, 1.8 mmol) in DCM (2 mL) was added, 3 drops AcOH was added to the resulting mixture which was stirred 24 hours at room temperature. The solvent was removed under vacuum and remaining AcOH was removed by co-evaporation under vacuum with toluene (2x5 mL). The resulting dark crude was purified trough a *flash* silica column chromatography using DCM/MeOH (95:5) as mobile phase to give the title compound (**118c**) (185 mg, 45%) as a red-orange solid. ^{1}H-NMR (400 MHz, Chloroform-d) δ 8.63 (t, *J* = 2.0 Hz, 1H), 8.16 (dd, *J* = 20.0, 8.3 Hz, 2H), 7.89 (d, *J* = 9.1 Hz, 2H), 7.60 (t, *J* = 8.0 Hz, 1H), 6.74 (d, *J* = 9.1 Hz, 2H), 3.10 (s, 6H).

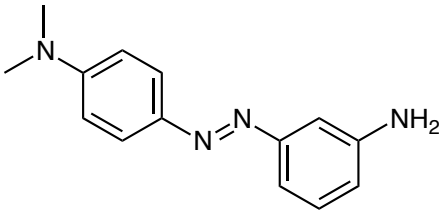

(*E*)-4-((3-aminophenyl)diazenyl)-N,N-dimethylaniline (**118d**): A solution of (*E*)-*N*,*N*-dimethyl-4-((3-nitrophenyl)diazenyl)aniline (**118c**) (185 mg, 0.68 mmol) and sodium sulfide nonahydrate (329 mg, 1.37 mmol) in EtOH (8 mL), was stirred 1 hour at reflux. Water (20 mL) and AcOEt (20 mL) were added and the precipitate was removed by filtration, the organic layer was separate from the aqueous layer and washed three times with brine, dried over $MgSO_4$, filtered off, and the solvent was removed under vacuum. The resulting brown crude was purified through a *flash* silica column chromatography using DCM 100% as mobile phase, to give the title compound (**118d**) as a red solid. (113 mg, 69%). ^{1}H-NMR (400 MHz, Chloroform-d) δ 7.86 (d, *J* = 9.1 Hz, 2H), 7.29 – 7.25 (m, 2H), 7.16 (dd, *J* = 2.0, 1.3 Hz, 1H), 6.76 (d, *J* = 9.1 Hz, 2H), 6.74 – 6.68 (m, 1H), 3.77 (s, 2H), 3.08 (s, 6H).

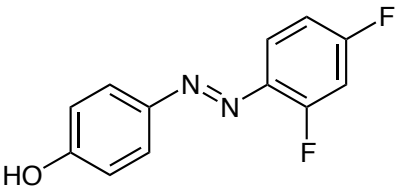

(*E*)-4-((2,4-difluorophenyl)diazenyl)phenol (**120c**): To a solution of 2,4-difluoroaniline (**120b**) (0.53 mL, 5.31 mmol) in a mixture of water/acetone 1:1 (24 mL), concentrated HCl was added (0.88 mL) and the mixture was cooled at 0°C. After 15 minutes, a solution of sodium nitrite (696 mg, 10.1 mmol) in water (12 mL) was added dropwise. The mixture was stirred 15 minutes at room temperature and a solution of phenol (500 mg, 5.31 mmol), sodium hydroxide (319 mg, 8 mmol) and sodium carbonate (788 mg, 7.4 mmol) in water (12 mL) was added dropwise and the reaction mixture was stirred 2 hours at 0°C. The generated suspension was filtered off and the filtrate was concentrated. The red crude was purified by *flash* silica column chromatography using DCM 100% as mobile phase, to afford the title compound (**120c**) (514 mg, 41%) as an orange solid. ^{1}H-NMR (400 MHz, Chloroform-d) δ 7.89 (d, *J* = 8.8 Hz, 2H), 7.78 (td, *J* = 8.8, 6.3 Hz, 1H), 7.04 – 6.89 (m, 4H), 5.54 (s, 1H). ^{13}C-NMR (101 MHz, Chloroform-d) δ 161.48, 147.21, 129.63, 125.28, 118.98, 115.84, 115.71, 111.80, 111.77, 105.20, 104.97, 104.94.

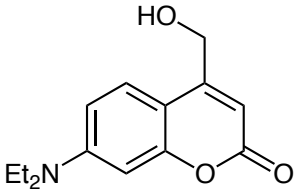

7-(diethylamino)-4-(hydroxymethyl)-2*H*-chromen-2-one (**128b**): A solution of 7-(diethylamino)-2-oxo-2*H*-chromene-4-carbaldehyde (**142**) (2 g, 8.15 mmol) in EtOH (40 mL), $NaBH_4$ (308 mg, 8.15 mmol) was added portion wise, the reaction mixture was stirred 12 hours t room temperature. The mixture was quenched with HCl (1N) and extracted with DCM (2x80 mL), washed with brine (2x80 mL), dried over Na_2SO_4, filtered off and concentrate under reduced pressure. The dark crude oil was purified by *flash* column chromatography using DCM/Acetone 80:20, to give the title compound (**128b**) (608 mg, 30%) as orange solid[9]. ^{1}H-NMR (400 MHz, Chloroform-d) δ 7.33 (d, *J* = 8.9 Hz, 1H), 6.60 (d, *J* = 8.8 Hz, 1H), 6.53 (d, *J* = 2.3 Hz, 1H), 6.27 (s, 1H), 4.83 (s, 2H), 3.41 (q, *J* = 7.1 Hz, 4H), 1.20 (t, *J* = 7.1 Hz, 6H).

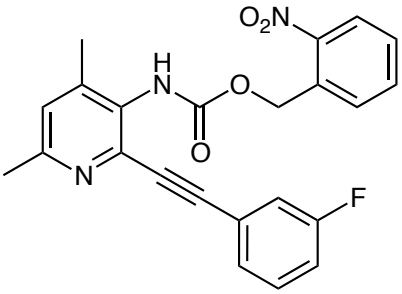

2-nitrobenzyl-(2-((3-fluorophenyl)ethynyl)-4,6-dimethylpyridin-3-yl)carbamate (**129a**): A solution of triphosgene (50 mg, 0.16 mmol) in 1 mL of toluene, was added a mixture of 2-((3-fluorophenyl)ethynyl)-4,6-dimethylpyridin-3-amine (**18**) (109 mg, 0.45 mmol) and dry triethylamine (0,11 mL, 0.84 mmol) in 1 mL of toluene, and the reaction mixture was stirred over 3 hours (the reaction was monitored by TLC).

Afterwards, the reaction mixture was purged under nitrogen over 20 minutes to remove the phosgene produced during the reaction, the crude was solved with 2 mL of toluene and 2-nitrobenzyl alcohol (**122a**) (26 mg, 0.17 mmol) was added and heated at 100ºC overnight.

The mixture was evaporated at vacuum and 20 mL of ethyl acetate was added, washed with 20 mL of brine, dried over Na_2SO_4, filtered and evaporated at vacuum. The residue was purified by flash column chromatography in ethyl acetate/hexane 3:7.

A white solid was obtained and it was purified again at isolera biotage in reverse phase conditions: 4VC (H2O:Acetonitrile 95:5), 3VC (H2O:Acetonitrile 40:60), 10 VC (H2O:Acetonitrile 0:100), the crude was liophilized overnight. A white solid (**129a**) was obtained (50 mg, 70%). mp:

170-172 ºC. ^{1}H-NMR (400 MHz, Chloroform-d) δ 8.09 (d, J = 8.1 Hz, 1H), 7.65 (s, 1H), 7.52 – 7.42 (m, 2H), 7.40 – 7.28 (m, 2H), 7.25 – 7.21 (m, 1H), 7.09 (tdd, J = 8.4, 2.6, 1.2 Hz, 1H), 7.03 (s, 1H), 5.64 (s, 2H), 2.56 (s, 3H), 2.33 (s, 3H). ^{13}C-NMR (101 MHz, Chloroform-d) δ 167.48, 163.61, 161.15, 133.91, 132.64, 130.32, 130.23, 128.90, 128.80, 128.31, 128.28, 125.93, 125.21, 119.07, 118.84, 117.11, 116.90, 64.31, 29.84, 18.41. HPLC-PDA-MS (using method A) RT: 6.43 min, λmax = 214, 268, 303 nm; purity > 99% (254 nm). HRMS (m/z): [M+H]+ calcd. for $C_{23}H_{18}FN_3O_4$, 420.1360; found, 420.1359

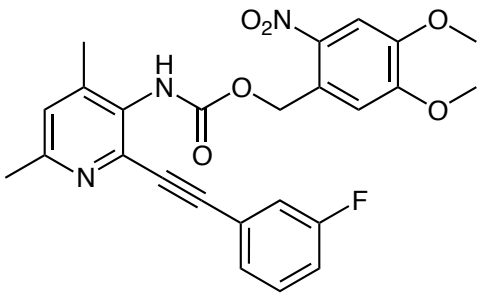

4,5-dimethoxy-2-nitrobenzyl-(2-((3-fluorophenyl)ethynyl)-4,6-dimethylpyridin-3-yl)carbamate (**129b**): A solution of triphosgene (50 mg, 0.16 mmol) in 1 mL of toluene, was added a mixture of 2-((3-fluorophenyl)ethynyl)-4,6-dimethylpyridin-3-amine (**18**) (109 mg, 0.45 mmol) and dry triethylamine (0,11 mL, 0.84 mmol) in 1 mL of toluene was added, and the reaction mixture was stirred over 3 hours (the reaction was monitored by TLC).

Afterwards, the reaction mixture was purged under nitrogen over 20 minutes to remove the phosgene produced during the reaction, the crude was solved with 2 mL of toluene and (4,5-dimethoxy-2-nitrophenyl)methanol (**122d**) (36 mg, 0.17 mmol) was added and heated at 100ºC overnight.

The mixture was evaporated at vacuum and 20 mL of ethyl acetate was added, washed with 20 mL of brine, dried over Na_2SO_4, filtered and evaporated at vacuum. The residue was purified by flash column chromatography in ethyl acetate/hexane 3:7.

A white solid was obtained and it was purified again at isolera biotage in reverse phase conditions: 4VC (H_2O:Acetonitrile 95:5), 3VC (H_2O:Acetonitrile 40:60), 10 VC (H_2O:Acetonitrile 0:100), the crude was liophilized overnight. A white solid (**129b**) was obtained (53 mg, 65%). Mp: 178-180°C. ^{1}H-NMR (400 MHz, Chloroform-d) δ 7.67 (s, 1H), 7.31 – 7.26 (m, 2H), 7.17 (dd, *J* = 9.0, 2.3 Hz, 1H), 7.11 – 7.02 (m, 2H), 6.65 (s, 1H), 5.61 (s, 2H), 3.91 (s, 3H), 3.79 (s, 3H), 2.52 (s, 3H), 2.32 (s, 3H). ^{13}C-NMR (101 MHz, Chloroform-d) δ 163.65, 161.19, 153.64, 130.35, 130.27, 128.08, 118.94, 118.71, 116.98, 108.31, 86.44, 64.63, 56.52, 56.40, 24.16. HPLC-PDA-

MS (using method A) RT: 5.91 min, λ_{max} = 221, 273, 303 nm; purity 96% (254 nm). HRMS (m/z): $[M+H]^+$ calcd. for $C_{25}H_{22}N_3O_6F$, 480.1571; found, 480.1606.

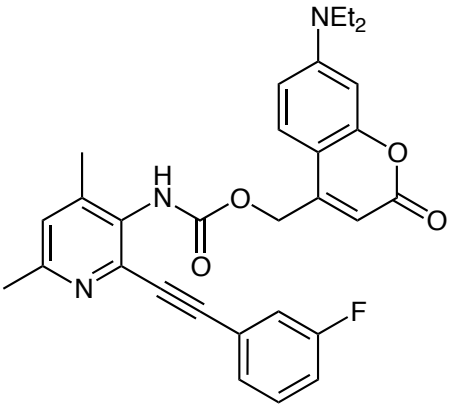

(7-(diethylamino)-2-oxo-2*H*-chromen-4-yl)methyl-(2-((3-fluorophenyl)ethynyl)-4,6-dimethylpyridin-3-yl)carbamate (**129c**): A solution of triphosgene (100 mg, 0.33 mmol) in 2 mL of toluene, a mixture of 2-((3-fluorophenyl)ethynyl)-4,6-dimethylpyridin-3-amine (**18**) (218 mg, 0.91 mmol) and dry triethylamine (0,22 mL, 1.68 mmol) in 2 mL of toluene was added, and the reaction mixture was stirred over 3 hours (the reaction was monitored by TLC).

Afterwards, the reaction mixture was purged under nitrogen over 20 minutes to remove the phosgene produced during the reaction, the crude was solved with 2 mL of toluene and a solution of 7-(diethylamino)-4-(hydroxymethyl)-2*H*-chromen-2-one (**128b**) (83 mg, 0.33 mmol) and sodium hydride (14 mg, 0.33 mmol) in 1 mL of THF previously stirred at room temperature during 10 minutes, was added and heated at 100ºC overnight.

The mixture was evaporated at vacuum and 40 mL of ethyl acetate was added, washed with 40 mL of brine, dried over Na_2SO_4, filtered and evaporated at vacuum. The residue was purified by flash column chromatography in ethyl acetate/hexanes 3:2.

A yellow-orange solid was obtained and it was purified again at isolera biotage in reverse phase conditions: 4VC (H2O:Acetonitrile 95:5), 3VC (H2O:Acetonitrile 40:60), 10 VC (H2O:Acetonitrile 0:100), the crude was liophilized overnight. A yellow solid (**129c**) was obtained (95 mg, 55%). mp: 77-79 ºC. ^{1}H-NMR (400 MHz, Methanol-d_4) δ 7.50 (s, 1H), 7.41 – 7.29 (m, 3H), 7.28 – 7.21 (m, 2H), 7.19 – 7.12 (m, 1H), 6.67 (d, J = 9.1 Hz, 1H), 6.53 (s, 1H), 6.19 (s, 1H), 5.42 (s, 2H), 3.46 (q, J = 7.1 Hz, 6H), 1.20 (t,J=7.1Hz,9H). ^{13}C-NMR (101 MHz, Methanol-d_4) δ 163.55, 156.93, 156.10, 151.01, 147.16, 130.23, 130.14, 127.60, 127.57, 125.33, 124.78, 118.02, 117.78, 116.28, 116.07, 108.94, 105.74, 96.83, 44.15, 21.87, 16.38, 11.28. HPLC-PDA-MS (using method A) RT: 3.69 min, λ_{max} = 221, 273, 303, 320, 385 nm; purity 99% (254 nm). HRMS (m/z): [M+H]+ calcd. for

$C_{30}H_{28}FN_3O_4$, 514.2142; found, 514.2125.

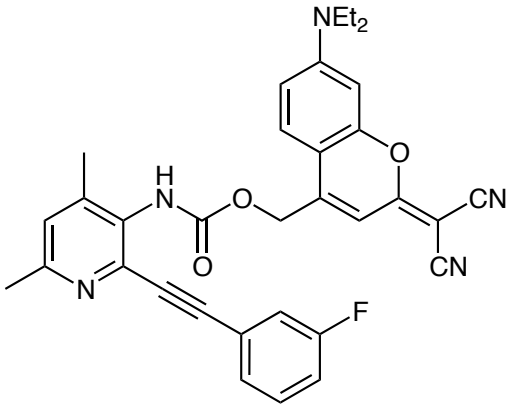

(2-(dicyanomethylene)-7-(diethylamino)-2*H*-chromen-4-yl)methyl-(2-((3-fluorophenyl)ethynyl)-4,6-dimethylpyridin-3-yl)carbamate (**129d**): A solution of triphosgene (100 mg, 0.33 mmol) in 2 mL of toluene, a mixture of 2-((3-fluorophenyl)ethynyl)-4,6-dimethylpyridin-3-amine (**18**) (218 mg, 0.91 mmol) and dry triethylamine (0,22 mL, 1.68 mmol) in 2 mL of toluene was added, and the reaction mixture was stirred over 3 hours (the reaction was monitored by TLC).

Afterwards, the reaction mixture was purged under nitrogen over 20 minutes to remove the phosgene produced during the reaction, the crude was solved with 2 mL of toluene and a solution of 2-(7-(diethylamino)-4-(hydroxymethyl)-2*H*-chromen-2-ylidene)malononitrile (**132**) (99 mg, 0.33 mmol) and sodium hydride (14 mg, 0.33 mmol) in 1 mL of THF previously stirred at room temperature during 10 minutes, was added and heated at 100ºC overnight.

The mixture was evaporated at vacuum and 40 mL of ethyl acetate was added, washed with 40 mL of brine, dried over Na_2SO_4, filtered and evaporated at vacuum. The residue was purified by flash column chromatography in ethyl acetate/hexane 3:2.

A yellow-orange solid was obtained and it was purified again at isolera biotage in reverse phase conditions: 4VC (H_2O:Acetonitrile 95:5), 3VC (H_2O:Acetonitrile 40:60), 10 VC (H_2O:Acetonitrile 0:100), the crude was liophilized overnight. A red solid (**129d**) was obtained (35 mg, 20%). Mp: 190-192°C. ^{1}H-NMR (400 MHz, Chloroform-d) δ 7.70 (dd, *J* = 5.7, 3.4 Hz, 1H), 7.51 (dd, *J* = 5.7, 3.4 Hz, 1H), 7.28 (q, *J* = 4.1 Hz, 3H), 7.19 – 7.13 (m, 1H), 7.10 – 7.02 (m, 3H), 6.62 – 6.53 (m, 3H), 5.35 (s, 3H), 3.40 (q, *J* = 7.2 Hz, 7H), 2.53 (s, 4H), 2.34 (s, 4H), 1.20 (t, *J* = 7.1 Hz, 9H). ^{13}C-NMR (101 MHz, Chloroform-d) δ 160.97, 130.87, 130.11, 130.03, 128.79, 127.93, 125.66, 124.85, 118.77, 118.54, 116.70, 113.71, 110.61, 106.82, 105.71, 97.28, 44.89, 24.00, 12.38.

HPLC-PDA-MS (using method A) RT: 3.69 min, λ_{max} = 220, 307, 383 nm; purity > 99% (254 nm). HRMS (m/z): $[M+H]^+$ calcd. for $C_{33}H_{29}N_5O_3F$, 562.2254; found, 562.2278.

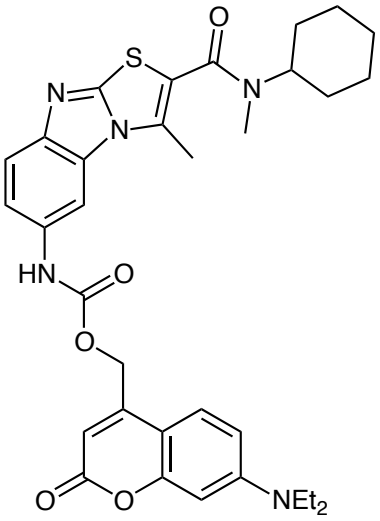

(7-(diethylamino)-2-oxo-2*H*-chromen-4-yl)methyl (2-(cyclohexyl(methyl)carbamoyl)-3-methylbenzo[4,5]imidazo[2,1-*b*]thiazol-6-yl)carbamate (**133**): A solution of triphosgene (48 mg, 0.16 mmol) in 2 mL of toluene, a mixture of 6-amino-*N*-cyclohexyl-*N*,3-dimethylbenzo[4,5]imidazo[2,1-*b*]thiazole-2-carboxamide (**15**) (27 mg, 0.08 mmol) and dry triethylamine (0,045 mL, 0.32 mmol) in 2 mL of toluene was added, and the reaction mixture was stirred over 3 hours (the reaction was monitored by TLC).

Afterwards, the reaction mixture was purged under nitrogen over 20 minutes to remove the phosgene produced during the reaction, the crude was solved with 2 mL of toluene and a solution of 7-(diethylamino)-4-(hydroxymethyl)-2*H*-chromen-2-one (**128b**) (20 mg, 0.08 mmol) and sodium hydride (4 mg, 0.08 mmol) in 1 mL of THF previously stirred at room temperature during 10 minutes, was added and heated at 100ºC overnight.

The mixture was evaporated at vacuum and 40 mL of ethyl acetate was added, washed with 40 mL of brine, dried over Na_2SO_4, filtered and evaporated at vacuum. The residue was purified by flash column chromatography in ethyl acetate/hexanes 3:2.

A yellow-orange solid was obtained and it was purified again at isolera biotage in reverse phase conditions: 4VC (H_2O:Acetonitrile 95:5), 3VC (H_2O:Acetonitrile 40:60), 10 VC (H_2O:Acetonitrile 0:100), the crude was liophilized overnight. A yellow solid (**133**) was obtained (5 mg, 10%). Mp: 220-222°C. ^{1}H-NMR (400 MHz, DMSO-d_6) δ 10.12 (s, 1H), 8.30 (s, 1H), 7.64 (d, *J* = 8.8 Hz, 1H), 7.52 (d, *J* = 9.0 Hz, 1H), 7.48 – 7.35 (m, 1H), 6.73 (dd, *J* = 9.1, 2.6 Hz, 1H), 6.57 (d, *J* = 2.5 Hz, 1H), 6.10 (s, 1H), 5.39 (s, 2H), 3.44 (q, *J* = 7.0 Hz, 5H), 2.93 (s, 4H), 2.67 (d, *J* = 2.1 Hz, 4H),

1.80 – 1.57 (m, 7H), 1.41 – 1.22 (m, 5H), 1.13 (t, *J* = 7.0 Hz, 8H). ^{13}C-NMR (101 MHz, Chloroform-d) δ 162.52, 162.21, 156.36, 150.83, 150.14, 130.49, 129.15, 128.34, 124.47, 119.43, 108.86, 106.24, 106.05, 101.92, 97.91, 68.10, 62.08, 44.89, 41.08, 29.82, 25.60, 25.36, 13.47, 12.57. HPLC-PDA-MS (using method A) RT: 3.79 min, λ_{max} = 215, 235, 288, 382 nm; purity > 99% (254 nm). HRMS (m/z): $[M+H]^+$ calcd. for $C_{33}H_{37}N_5O_5S$, 616.2594; found, 616.2633.

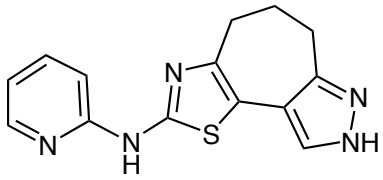

***N*-(pyridin-2-yl)-4,5,6,8-tetrahydropyrazolo[4',3':3,4]cyclohepta[1,2-*d*]thiazol-2-amine** (**134**): In a microwave tube was placed 8-(4,5-dimethoxy-2-nitrobenzyl)-*N*-(pyridin-2-yl)-4,5,6,8-tetrahydropyrazolo-[4',3':3,4]cyclohepta[1,2-*d*]thiazol-2-amine (**135**) (100 mg, 0.248 mmol) solved with trifluoroacetic acid (1.9 mL, 24.8 mmol), the tube was sealed and irradiated in the microwave 30 min at 100°C, 150 PSI, 100W and 2 min of hold ramp. The brown solution was transferred to a round-bottom flask and AcOEt (10 mL) was added, the precipitate was collected by filtration and washed with AcOEt (3x10 mL), to give the title compound (**134**) (59 mg, 84%)[7]. ^{1}H-NMR (400 MHz, DMSO-d_6) δ 11.14 (s, 1H), 8.24 (dd, *J* = 5.2, 1.7 Hz, 1H), 7.71 – 7.60 (m, 2H), 7.03 (d, *J* = 8.3 Hz, 1H), 6.87 (dd, *J* = 7.1, 5.1 Hz, 1H), 2.99 – 2.93 (m, 4H), 2.02 – 1.93 (m, 2H). HPLC-PDA-MS (using method A) RT: 2.50 min, λ_{max} = 233, 333 nm; purity > 99% (254 nm). HRMS (m/z): $[M+H]^+$ calcd. for $C_{14}H_{13}N_5S$, 284.0970; found, 284.0964.

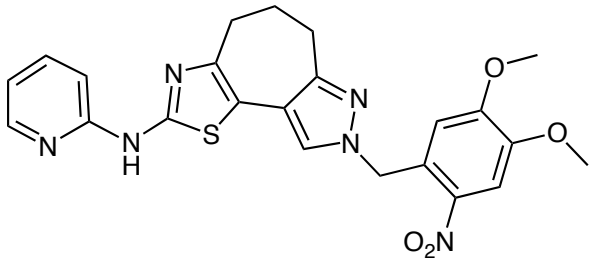

8-(4,5-dimethoxy-2-nitrobenzyl)-*N*-(pyridin-2-yl)-4,5,6,8-tetrahydropyrazolo-[4',3':3,4]cyclohepta[1,2-*d*]thiazol-2-amine (**135**): A solution of 5-bromo-2-(4,5-dimethoxy-2-nitrobenzyl)-5,6,7,8-tetrahydrocyclohepta[*c*]pyrazol-4(2*H*)-one (**137j**) (380 mg, 0.89 mmol) and 1-(pyridin-2-yl)thiourea (**137k**) in ethanol (17 mL) was refluxed overnight. The reaction was cooled to room temperature and the precipitate was collected by filtration and washed with cold ethanol (3x10 mL) to give the desired compound (**135**) as a pale yellow solid (300 mg, 70%)[7]. Mp: 207-

209°C. ^{1}H-NMR (400 MHz, Chloroform-d) δ 8.40 (d, *J* = 5.1 Hz, 1H), 8.32 (s, 1H), 7.79 (t, *J* = 7.6 Hz, 1H), 7.75 (s, 1H), 7.22 (s, 1H), 7.14 (dd, *J* = 7.3, 5.1 Hz, 1H), 6.28 (s, 1H), 5.73 (s, 2H), 3.96 (s, 3H), 3.82 (s, 3H), 3.12 – 3.06 (m, 2H), 3.05 – 2.99 (m, 2H), 2.16 (q, *J* = 5.5 Hz, 2H). ^{13}C-NMR (101 MHz, Chloroform-d) δ 160.13, 153.73, 151.09, 148.41, 139.80, 129.75, 127.03, 119.65, 110.56, 108.36, 56.44, 56.35, 53.44, 28.90, 27.50, 22.54. HPLC-PDA-MS (using method A) RT: 5.98 min, λ_{max} = 238, 322 nm; purity 98% (254 nm). HRMS (m/z): $[M+H]^+$ calcd. for $C_{23}H_{22}N_6O_4S$, 479.1502; found, 479.1366.

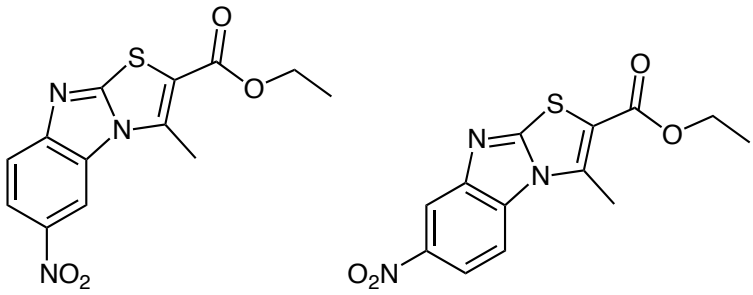

ethyl 3-methyl-6-nitrobenzo[4,5]imidazo[2,1-*b*]thiazole-2-carboxylate and ethyl 3-methyl-7-nitrobenzo[4,5]imidazo[2,1-*b*]thiazole-2-carboxylate (**136d**): A stirred mixture containing 6-nitro-1*H*-benzo[*d*]imidazole-2-thiol (**136a**) (5 g, 25.6 mmol) and potassium hydroxide (1.7 g, 25.6 mmol) in EtOH (50 mL), was heated at 80°C for 10 minutes. After cooling the resulting solution to 30°C, ethyl 2-chloro-3-oxobutanoate (**136b**) (3.54 mL, 25.6 mmol) was added in one portion, and the mixture was stirred 18 hours at room temperature. Afterwards, the reaction mixture was pulled in 70 mL ice-water, and the precipitate was collected by filtration. The solid was displaced in a mixture of pyridine (5 mL) and acetic anhydride (2.5 mL), which was heated at 100°C for 3 hours. After cooling to 0°C, 250 mL of ice-water was added and stirred for 30 minutes at 0°C. The precipitate was collected by filtration, washed with water and dried under vacuum overnight to give the title compound (**136d**) (2.2 g, 40%) as yellow solid[8]. ^{1}H-NMR (400 MHz, Chloroform-d) δ 8.75 (d, *J* = 2.2 Hz, 1H), 8.64 (d, *J* = 2.2 Hz, 1H), 8.34 (dd, *J* = 9.0, 2.2 Hz, 1H), 8.19 (dd, *J* = 9.0, 2.2 Hz, 1H), 7.92 (d, *J* = 8.9 Hz, 1H), 7.82 (d, *J* = 9.0 Hz, 1H), 4.48 – 4.36 (m, 4H), 3.19 (s, 3H), 3.15 (s, 3H), 1.47 – 1.32 (m, 6H).

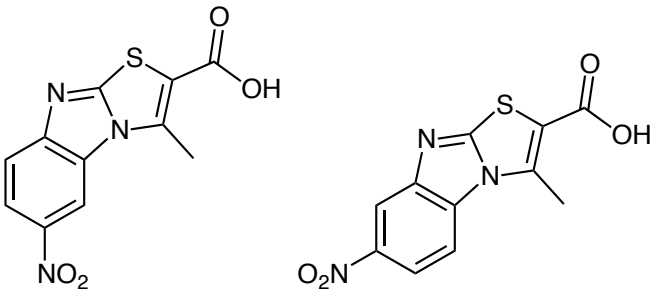

3-methyl-6-nitrobenzo[4,5]imidazo[2,1-*b*]thiazole-2-carboxylic acid and 3-methyl-7-nitrobenzo[4,5]imidazo[2,1-*b*]thiazole-2-carboxylic acid (**136e**): A solution containing the isomer mixture ethyl 3-methyl-6-nitrobenzo[4,5]imidazo[2,1-*b*]thiazole-2-carboxylate and ethyl 3-methyl-7-nitrobenzo[4,5]imidazo[2,1-*b*]thiazole-2-carboxylate (**136d**) (2.2 g, 6.55 mmol) in EtOH/Dioxane 1:1 (30 mL), NaOH (1N) was added and stirred 6 hours at room temperature. Water (60 mL) was added and the resulting mixture was acidified with concentrated HCl until pH 3-4. The precipitate was collected by filtration and washed with cold water, to give the title compounds and (**136e**) (1.7 g, 94%)[8]. ^{1}H-NMR (400 MHz, DMSO-d_6) δ 8.83 (d, *J* = 2.3 Hz, 1H), 8.58 (d, *J* = 2.2 Hz, 1H), 8.32 (dd, *J* = 9.1, 2.2 Hz, 1H), 8.28 (d, *J* = 9.0 Hz, 1H), 8.19 (dd, *J* = 9.0, 2.3 Hz, 1H), 7.90 (d, *J* = 9.1 Hz, 1H), 3.18 (s, 3H), 3.12 (s, 3H).

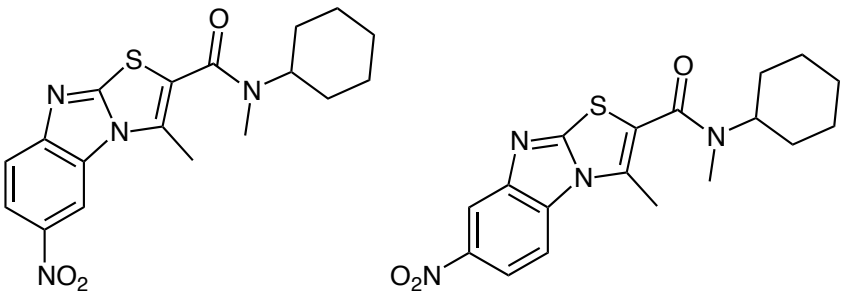

***N*-cyclohexyl-*N*,3-dimethyl-6-nitrobenzo[4,5]imidazo[2,1-*b*]thiazole-2-carboxamide and *N*-cyclohexyl-*N*,3-dimethyl-7-nitrobenzo[4,5]imidazo[2,1-*b*]thiazole-2-carboxamide** (**136g**): 3-methyl-6-nitrobenzo[4,5]imidazo[2,1-*b*]thiazole-2-carboxylic acid and 3-methyl-7-nitrobenzo[4,5]imidazo[2,1-*b*]thiazole-2-carboxylic acid (**136e**) (1.6 g, 5.88 mmol) were suspended in thionyl chloride (10 mL, 88 mmol) and the reaction mixture were stirred and heated to reflux 2 hours. Afterwards, thionyl chloride was removed purging under nitrogen and the solid crude was resolved in DCM (25 mL). A solution of *N*-methylcyclohexanamine (0.96 mL, 7.35 mmol) and triethylamine (1.64 mL, 11.7 mmol) in DCM (2 mL) was added to the first solution dropwise. The reaction mixture was stirred overnight at room temperature. Afterwards, DCM (100 mL) was added and the mixture was washed with HCl (1N) (2x60 mL), NaOH (1N) (2x 60 mL),

brine (2x 50 mL), dried over Na_sSO_4 and concentrated under vacuum. The crude was purified by *flash* silica column chromatography using DCM/Hexanes 95:5, to afford the title compounds (**136g**) (460 mg, 21%)[8]. ^{1}H-NMR (400 MHz, Chloroform-d) δ 8.74 (d, *J* = 2.2 Hz, 1H), 8.72 (d, *J* = 2.1 Hz, 1H), 8.36 (dd, *J* = 9.1, 2.2 Hz, 1H), 8.22 (dd, *J* = 9.0, 2.2 Hz, 1H), 7.89 (d, *J* = 9.0 Hz, 1H), 7.86 (d, *J* = 8.9 Hz, 1H), 3.01 (s, 3H), 3.01 (s, 3H), 2.86 (s, 3H), 2.81 (s, 3H), 1.90 – 1.74 (m, 11H), 1.71 – 1.53 (m, 11H).

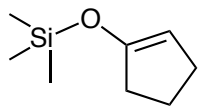

(cyclopent-1-en-1-yloxy)trimethylsilane (**137c**): In a 3-neck round-bottom flask, a solution of sodium iodide (11.1 g, 74.3 mmol) in AcN (99 mL) was placed and cyclopentanone (**137a**) (5.26 mL, 59.4 mmol) and triethylamine (10.36 mL, 74.3 mmol) were added. The flask was fitted with additional funnel charged with chloromethylsilane (**137b**) (8.60 mL, 67.8 mmol), which was added dropwise since it was finished and the resulting suspension was stirred overnight at room temperature. Afterwards, 70 mL of hexane were added and the biphasic system was stirred vigorously 10 min. The phases were separated and the can layer was extracted with hexane (3 x 40 mL). The combined phases were washed with water (2 x 35 mL) and brine (2 x 35 mL), dried over Na_2SO_4, filtered off and the solvent was removed under reduced pressure to afford a colourless oil (**137c**) (5.26 g, 56%)[6]. The product was used for next step without further purification. ^{1}H-NMR (400 MHz, Chloroform-d) δ 4.61 (s, 1H), 2.25 (ddt, *J* = 7.5, 4.3, 1.8 Hz, 4H), 1.84 (p, *J* = 7.7 Hz, 2H), 0.20 (s, 9H).

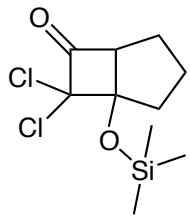

7,7-dichloro-1-((trimethylsilyl)oxy)bicyclo[3.2.0]heptan-6-one (**137e**): A solution of (cyclopent-1-en-1-yloxy)trimethylsilane (**137c**) (5.26 g, 33.7 mmol) and triethylamine (6.57 mL, 47.1 mmol) in Hexane (64 mL) was stirred at room temperature and a solution of 2,2-dichloroacetyl chloride (**137d**) (4.47 mL, 46.5 mmol) in Hexane (27 mL) was added to the first mixture, and the resulting solution was stirred 18 hours at room temperature. The brown suspension was filtered rinsing with AcOEt (3x32 mL) and the brown solution was concentrated under reduced pressure. The crude was filtered through Al_2O_3 (neutral) using AcOEt as eluent and remove it after under

vacuum, obtaining a brown oil (**137e**) (7.15 g, 80%)[6]. The product was used for next step without further purification.[1]H-NMR (400 MHz, Chloroform-d) δ 3.71 – 3.62 (m, 1H), 2.61 – 2.48 (m, 1H), 2.10 – 2.02 (m, 2H), 1.99 – 1.86 (m, 2H), 1.61 – 1.53 (m, 1H), 0.25 (s, 9H).

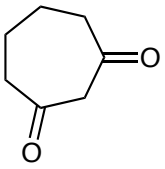

cycloheptane-1,3-dione (**137f**): 7,7-dichloro-1-((trimethylsilyl)oxy)bicyclo[3.2.0]heptan-6-one (**137e**) (7 g, 26.2 mmol) was solved in a round-bottom flask with a mixture of 2-propanol (26.7 mL) and milliQ water (26.7 mL) and the suspension was cooled to 10°C. Zinc dust (7.71 g, 118 mmol) was added in four portions, and acetic acid (8.65 g, 144 mmol) dissolved in water (21 mL) was added dropwise while keeping the temperature below 0°C. The reaction was stirred for an additional 30 min at -10°C and after this time the reaction mixture was allowed to warm to room temperature and stirring overnight. The reaction was filtered, rinsing with isopropyl alcohol (12.75 mL) and the mixture was cooled to 0°C and neutralized by portion wise addition of K_2CO_3 (20 g, 144 mmol). The viscous suspension was filtered, rinsing with water (12.75 mL) and AcOEt (38.25 mL). The biphasic system was concentrated under reduced pressure and extracted with DCM. The combined organics were dried over Na_2SO_4, filtered and concentrated under reduced pressure, affording a yellow pale solid (**137f**) (3.1 g, 96%) which was used to next step without further purification[6]. [1]H-NMR (400 MHz, Chloroform-d) δ 3.55 (d, *J* = 5.8 Hz, 2H), 2.57 – 2.51 (m, 4H), 1.97 – 1.91 (m, 4H).

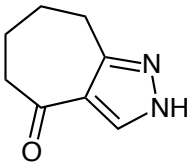

5,6,7,8-tetrahydrocyclohepta[*c*]pyrazol-4(2*H*)-one (**137g**): A mixture of cycloheptane-1,3-dione (**137f**) (2 g, 15.4 mmol) in DMF-DMA (6.33 mL, 47.7 mmol) was stirred at reflux for 1 hour. After that, the suspension was concentrated under reduced pressure. The residue was solved in MeOH (15 mL) and the solution was cooled to 0°C and hydrazine (0.75 mL, 15.4 mmol) was added dropwise, the reaction mixture was stirred over 1 hour and concentrated under reduced pressure obtaining an orange solid (**137g**) (1.05 g, 46%)[7]. [1]H-NMR (400 MHz, Chloroform-d) δ 8.03 (s, 1H), 3.03 (dd, *J* = 6.8, 5.6 Hz, 2H), 2.86 – 2.66 (m, 2H), 2.07 – 1.99 (m, 2H), 1.99 – 1.92

(m, 2H).

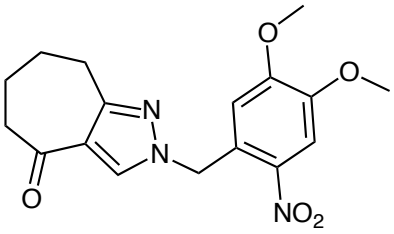

2-(4,5-dimethoxy-2-nitrobenzyl)-5,6,7,8-tetrahydrocyclohepta[*c*]pyrazol-4(2*H*)-one (**137h**): A solution of 5,6,7,8-tetrahydrocyclohepta[*c*]pyrazol-4(2*H*)-one (**137g**) (1 g, 3.62 mmol), K_2CO_3 (0.62 g, 4.53 mmol) and 1-(bromomethyl)-4,5-dimethoxy-2-nitrobenzene (0.45 g, 3.02 mmol) in MeCN (9 mL), was stirred at 60°C over 3 days. Afterwards, the solvent was removed under reduced pressure and AcOEt was added, washed with water (3x10 mL), brine (2x10 mL), dried over Na_2SO_4, filtered and concentrated under vacuum. The resulting crude was purified by *flash* column chromatography using AcOEt/Hexanes 2:3 as mobile phase, to afford the title compound (**137h**) (315 mg, 30%)[7]. ^{1}H-NMR (400 MHz, Chloroform-d) δ 7.98 (s, 1H), 7.71 (s, 1H), 6.44 (s, 1H), 5.63 (s, 2H), 3.95 (s, 3H), 3.83 (s, 3H), 3.01 – 2.92 (m, 2H), 2.73 – 2.64 (m, 2H), 2.01 – 1.84 (m, 4H).

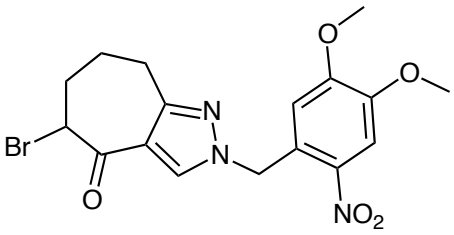

5-bromo-2-(4,5-dimethoxy-2-nitrobenzyl)-5,6,7,8-tetrahydrocyclohepta[*c*]pyrazol-4(2*H*)-one (**137j**): A mixture of 2-(4,5-dimethoxy-2-nitrobenzyl)-5,6,7,8-tetrahydrocyclohepta[*c*]pyrazol-4(2*H*)-one (**137h**) (315 mg, 0.91 mmol) and phenyltrimethylammonium tribromide (343 mg, 0.91 mmol) in chloroform (5.4 mL) was stirred and heated to reflux during 1.5 hours. Afterwards, the reaction mixture was cooled to room temperature, and DCM (10 mL) was added, washed with water (15 mL), brine (2x10 mL). The organic layer was dried over Na_2SO_4, filtered and concentrated under vacuum to afford the title compound (**137j**) as an orange solid (380 mg, 98%)[7]. ^{1}H NMR (400 MHz, Chloroform-*d*) δ 8.05 (s, 1H), 7.73 (s, 1H), 6.35 (s, 1H), 5.30 (s, 2H), 4.81 (dd, *J* = 5.7, 3.3 Hz, 1H), 3.96 (s, 3H), 3.84 (s, 3H), 3.20 – 3.12 (m, 1H), 3.09 – 3.04 (m, 1H), 3.01 – 2.96 (m, 1H), 2.91 – 2.82 (m, 1H), 2.41 – 2.35 (m, 2H).

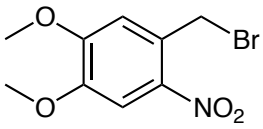

1-(bromomethyl)-4,5-dimethoxy-2-nitrobenzene (**137l**): A solution of (4,5-dimethoxy-2-nitrophenyl)methanol (**122d**) (1g, 4.7 mmol) in DCM (15 mL) was cooled to 0°C, tribromophosphine (0.49 mL, 113 mmol) was added dropwise and the reaction mixture was stirred 1 hour at room temperature. After this time the mixture was heated to reflux 2 hours and was poured into NaOH (1N), extracted with DCM (2x50 mL), washed with brine (2x50 mL), dried and concentrated under vacuum to give the title compound (**137l**) (800 mg, 62%) as a yellow solid[11]. ^{1}H-NMR (400 MHz, Chloroform-d) δ 7.67 (s, 1H), 6.94 (s, 1H), 4.86 (s, 2H), 3.99 (s, 3H), 3.96 (s, 3H).

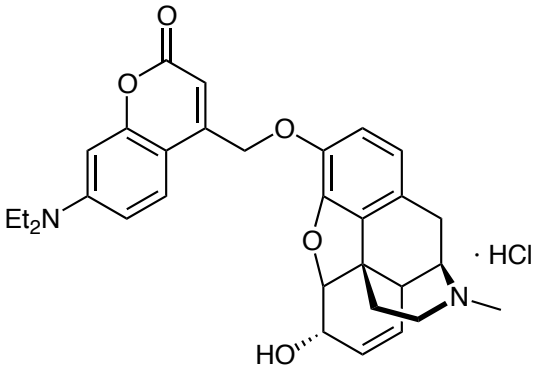

7-(diethylamino)-4-((((4*R*,7*S*,12b*S*)-7-hydroxy-3-methyl-2,3,4,4a,7,7a-hexahydro-1*H*-4,12-methanobenzofuro[3,2-*e*]isoquinolin-9-yl)oxy)methyl)-2*H*-chromen-2-one hydrochloride (**139**): A solution of (4*R*,7*S*,12b*S*)-3-methyl-2,3,4,4a,7,7a-hexahydro-1*H*-4,12-methanobenzofuro[3,2-*e*]isoquinoline-7,9-diol hydrochloride (**138a**) (250 mg, 0.87 mmol) and K_2CO_3 (266 mg, 1.93 mmol) in DMF (7 mL) was stirred 15 minutes and after this time a solution of 4-(bromomethyl)-7-(diethylamino)-2*H*-chromen-2-one (**140**) (299 mg, 0.96 mmol) in DMF (2 mL), was added to the first solution and the reaction mixture was stirred 4 days at room temperature. Afterwards, AcOEt (50 mL) was added and was washed with a saturated solution of $NaHCO_3$ (3x50 mL), brine (3x50 mL), dried over Na_2SO_4, filtered off and the solvent was removed under vacuum. The brown crude was purified through *flash* silica column chromatography using DCM/MeOH 94:6 as mobile phase, the fluorescent-yellow oil, was solved in 7 mL of ether and HCl in dioxane (4N) was added dropwise. The precipitate was collected by filtration and washed

several times with ether, to afford the title compound (**139**) (215 mg, 47%) as a yellow solid. Mp: 301-303°C. ^{1}H-NMR (400 MHz, DMSO-d_6) δ 7.57 (d, *J* = 9.0 Hz, 1H), 6.83 (d, *J* = 8.2 Hz, 1H), 6.71 (dd, *J* = 9.1, 2.5 Hz, 1H), 6.58 (d, *J* = 8.3 Hz, 1H), 6.55 (d, *J* = 2.5 Hz, 1H), 6.14 (s, 1H), 5.73 – 5.66 (m, 1H), 5.33 (s, 2H), 5.30 – 5.26 (m, 1H), 4.18 (dq, *J* = 5.7, 2.7 Hz, 1H), 4.12 (d, *J* = 6.9 Hz, 1H), 3.57 (s, 3H), 3.44 (q, 4H), 3.30 – 3.17 (m, 2H), 3.08 (s, 1H), 3.02 (d, *J* = 5.0 Hz, 1H), 2.85 (d, *J* = 4.7 Hz, 2H), 2.81 – 2.72 (m, 1H), 2.36 – 2.26 (m, 1H), 1.19 (t, *J* = 7.1 Hz, 6H). ^{13}C-NMR (101 MHz, DMSO-d_6) δ 160.76, 155.78, 151.57, 147.67, 139.92, 134.89, 129.81, 125.78, 125.38, 125.09, 119.34, 116.79, 105.63, 91.08, 66.73, 65.84, 59.33, 46.14, 44.10, 42.47, 41.36, 40.40, 37.52, 32.45, 21.05, 12.29. HPLC-PDA-MS (using method A) RT: 2.59 min, λ_{max} = 214, 246, 317, 389 nm; purity > 98% (254 nm). HRMS (m/z): $[M+H]^+$ calcd. for $C_{31}H_{34}N_2O_5$, 515.2546; found, 515.2537.

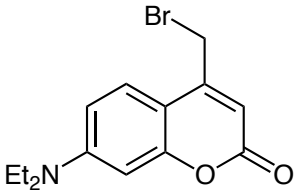

4-(bromomethyl)-7-(diethylamino)-2*H*-chromen-2-one (**140**): A solution of 7-(diethylamino)-4-(hydroxymethyl)-2*H*-chromen-2-one (**128b**) (358 mg, 1.45 mmol) and triethylamine (0.40 mL, 2.9 mmol) in DCM (12 mL) was cooled to 0°C, methanesulfonyl chloride (0.17 mL, 2.1 mmol) was added dropwise and the reaction mixture was stirred 2 hours at 0°C. The mixture was quenched with cold saturated $NaHCO_3$ (50 mL) and DCM (20 mL) was added. The organic layer was separated, washed with brine (2x50 mL) dried over Na_sSO_4, filtered off and concentrated under reduced pressure. Afterwards, the crude was solved in THF (12 mL) and LiBr (503 mg, 5.8 mmol) was added and the reaction mixture was stirred 2.5 hours. The mixture was concentrated, DCM (30 mL) was added, washed with brine (2x30 mL), dried over Na_2SO_4 and the solvent was removed under reduced pressure. The crude was purified through *flash* silica column chromatography using DCM/AcOEt 99:1 as mobile phase, affording the title compound (**140**) (200 mg, 44%) as a yellow solid[10]. ^{1}H-NMR (400 MHz, Chloroform-d) δ 7.49 (d, *J* = 9.0 Hz, 1H), 6.62 (dd, *J* = 9.0, 2.6 Hz, 1H), 6.51 (d, *J* = 2.6 Hz, 1H), 6.13 (s, 1H), 4.40 (d, *J* = 0.7 Hz, 2H), 3.42 (q, *J* = 7.1 Hz, 4H), 1.21 (t, *J* = 7.1 Hz, 6H).

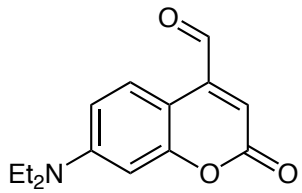

7-(diethylamino)-2-oxo-2*H*-chromene-4-carbaldehyde (**142**): A solution of 7-(diethylamino)-4-methyl-2*H*-chromen-2-one (**141**) (10 g, 43.2 mmol) and selenium oxide (13.91 g, 125 mmol) in xylene (200 mL), was stirred and refluxed 3 days. The solvent was removed under reduced pressure and purified through *flash* silica column chromatography using DCM/Acetone 95:5 as mobile phase to afford the desired title compound (**142**) (2 g, 19%) as red oil[9]. ^{1}H-NMR (400 MHz, Chloroform-d) δ 10.03 (d, *J* = 0.7 Hz, 1H), 8.32 (d, *J* = 9.2 Hz, 1H), 6.67 (dd, *J* = 9.2, 2.6 Hz, 1H), 6.57 (d, *J* = 2.6 Hz, 1H), 6.47 (s, 1H), 3.43 (q, *J* = 7.1 Hz, 4H), 1.22 (t, *J* = 7.1 Hz, 6H).

Photochemical characterization

Materials and methods

Light source

The light source used to measure the photochemical properties of azo compounds was carried out by single or dual wavelength LED plates (*FCTecnics*) at a distance of 2-3 cm, laser pointers (*Tor·laser*) of 405 nm (blue), 532 nm (green) and 100 mW each one irradiating and UVA lamps for cage compounds. To evaluate the isomerization of the azo compounds or the un-caging of caged compounds samples spectrophotometrically, 2 minutes of continuous illumination were applied placed in 10-mm Quartz *Suprasil* cells (*Hellma Analytics*).

UV-Visible absorption spectra

A solution of photoisomerisable compounds (100 µM) or cage compounds (25 µM) in DMSO and in PBS (1% DMSO) respectively, were displaced at *Varian Cary 300* UV-Vis spectrophotometer to obtain the absorption spectra scanning betwwen 650 nm and 275 nm with an average time of 33 ms at 1-nm intervals for full absorption spectra. To achieve UV-Visible spectra after

illumination, we performed the measure immediately after illuminating for a minimum of two minutes in both cases.

To determine the photoisomerisation of azo compounds, from *trans* to *cis* configuration, the UV-Vis spectra were recorded after illumination at defined wavelengths extracted the maximal absorbance values around 380 nm and plotted versus the illumination wavelength. The reverse isomerisation, from *cis* to *trans* isomers we recorded UV-Vis spectra after illumination at defined wavelength and plotted them versus the last illumination wavelength.

To determine the un-caging of cage compounds (**129a**, **129b**, **129c**, **129d**, **133**, **135** and **139**), we recorded the UV-Vis spectra in comparison with its corresponding actives compounds, recording after illumination at defined wavelength laser at several times (10, 20, 30, 60, 90, 300 seconds for compounds **129c** and **133** at 405 nm), (15, 30, 45, 90, 300 seconds for compounds **129a** and **129b** at 300-350 nm), (30, 60, 90, 150, 300 for compounds **139** and **135** at 405 nm), (30, 120, 300, 900, 2700 seconds for compound **129d** at 532 nm).

The quantum yield, was quantified by the slope between the mols of the released active specie and the absorbed mols of photons during the time applied before.

The mols of released active specie was measured doing a straight calibration of this active compounds with known concentrations (5 µM, 1 µM, 500 nM, 250 nM, 100 nM, 50 nM and 25 nM) and the samples of the caged compounds irradiated for un-caging at UV spectra were measured at HPLC-MS to extrapolate the concentration and obtaining the mols due the known volume of the original aliquote used (3,5 mL).

For measuring the mols of photons absorbed by the sample, an optic fibre was used to quantify the potency with and without sample given by the source of light in W/m^2. The mols absorbed were measured following the *formulae 1*.

$$\mathbf{n_{abs} = n_{tot} - n_{no\text{-}abs}}$$

Formulae 1: Formulae for determination the mols of photons absorbed given in W/m^2, being n_{tot} the quantified number mols of the source of light measured without the sample, and $n_{no\text{-}abs}$ the quantified number of mols of the source of light measured with the sample.

Once we measured the absorbed mols of photons in W/m^2, a calibration correction (10/11.8) and the area previously measured in photographic paper, was applied to obtain the potency based in this conversion factor (*formulae 2*):

Potency = n_{abs} W/m^2 x (10/11.8) x (1000 mW /1 W) x (1 m^2 / 10000 cm^2) x Area cm^2

Formulae 2: Potency obtained from the absorbed mols and the area of un-caging of light source with a calibration correction.

Afterwards, the energy for a mol of photon of certain wavelength was calculated by *formulae 3* and the energy used at each time by the *formulae 4*, obtaining the energy for all time of un-caging performed before.

$$E = hc/\lambda$$

Formulae 3: Formulae of energy of a photon at certain wavelength, being h the planck constant, c the velocity of light at vacuum and λ the corresponding wavelength.

$$E = P \cdot t$$

Formulae 4: Formulae for energy depending on the potency (P) and the time (t).

Finally the mols of photons absorbed for every time of un-caging, was calculated dividing the energy used each time of un-caging (*formulae 4*) by the calculated energy of one photon (*formulae 3*).

As we exposed previously, the slope representation *a*, from the equation exposed in *figure 92*) between the photon mols and the released active specie mols provide the quantum yield.

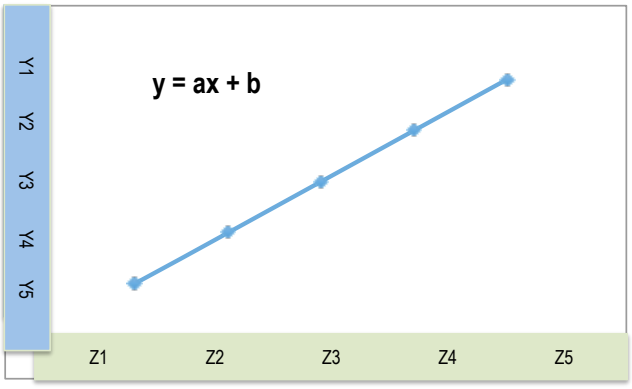

Time	Mols of released active specie	Mols of photons
X1	Y1	Z1
X2	Y2	Z2
X3	Y3	Z3
X4	Y4	Z4
X5	Y5	Z5

Figure 93: Representation between the mols of compound and the mols of photons giving the quantum yield, *a* form the equation.

Molar absorptivity was calculated from *formulae 5*, considering L as 1 cm of longitude, and the knowing concentration (C) for each cage compound of 25 µM.

$$\varepsilon = \frac{A}{C} \cdot L$$

Formulae 5: Formulae obtained from Lambert-Beer equation.

A summary of the obtained results from caged compounds of quantum yields, molar absorptivity and maximum absorption was exposed in *table 9.*

	129a	**129b**	**129c**	**129d**	**133**	**135**	**139**
ε **(M^{-1} cm^{-1})**	10.000	6.800	21.200	11.440	8.256	11.280	16.800
λ_{abs} **(nm)**	305	310	385	490	385	325-350	395
ϕ	0.032	0.005	0.180	0.063	0.03	0.034	0.035

Table 12: Summarize of photochemical properties of caged compounds studied.

Un-caging assisted by HPLC

Preliminary un-caging experiments for compounds **129a**, **129b**, **129c** and **129d** were done performing a straight calibration of corresponding active compounds in DMSO first and for compound **129c** in PBS (1% DMSO) after, with cross concentrations from 1 mM to 1 µM, injected to HPLC plotting the area readings versus the corresponding concentration and fitting the obtained schuss function (*formulae 5*) with *GraphPad Prism 6* software.

$$\mathbf{y = ax + b}$$

Formulae 5: Formulae of straight calibration depending of its slope (a) and its constant (b)

Four solutions of the corresponding cage-compounds in PBS (1% DMSO) (25 µL of 1 mM concentration) were irradiated at the corresponding wavelength respectively and they were diluted 10 times (final volume = 250 µL), injected to HPLC and the resulting area of released active compound was extrapolated from the previous schuss function undoing the 10 times dilution.

Pharmacological characterization

Functional cell-based assays

Cell culture and transfection

Materials and methods

HEK293 cells were cultured and transfected by electroporation for expression of all rat mGlu receptors as explained in the procedure section. Cultures were performed in Dulbecco's modified Eagle's medium (*Gibco* DMEM; *Thermo Fisher Scientific*) supplemented with 10% fetal calf serum (DMEM, *Thermo Fisher Scientific*). For those mGlu receptors that are not naturally linked to the phospholipase C (PLC) signalling pathway (all except $mGlu_{1/5}$), we co-transfected a chimeric $G_{q/i}$-protein (G_q top) to couple receptor activation to the PLC pathway and obtain IP production[12]. To maintain ambient glutamate at minimal concentrations, we co-transfected the excitatory amino acid transporter 1 (EAAC1). All receptors contained an HA tag in their *N*-terminus to monitor their cell surface expression by ELISA. Once transfected, cells were seeded in black (for cage-compounds) or clear (for azo-compounds) bottom 96-well plates at a concentration of 1.5 x 10^5 cells/well. At least 4 hours later, we changed the medium to glutamate-free DMEM *GlutaMAX-I* (*Thermo Fisher Scientific*).

Procedure

We prepared the DNA mixes in a different eppendorf tubes, as the following table shows for each one of the mGlu receptors corresponding a 20 million cells. The plasmid solution concentration was generally 1 µg/µL.

After that, the black 96-well plates with opaque-bottom (for a classic IP accumulation experiment of cage-compounds) or with transparent bottom (for IP accumulation with illumination for azo-compound) were filled with 50 µL of poly-L-ornitine 1x (PLO), and they were left in the incubator at 37°C and 5% CO_2 for 30 minutes minimum. We selected dishes with HEK293 cells with a 70% of confluence and removed the medium of the dishes. Then the cells were washed with 3-5 mL of PBS and 3 mL of trypsin were added in each dish and then were left in the incubator at 37°C and 5% CO_2 for 5-10 minutes.

	mGlu1	mGlu2	mGlu3	mGlu4
mGlu	4 µL (4 µg)	8 µL (8 µg)	8 µL (8 µg)	7 µL (7 µg)
EAAC1	4 µL (4 µg)	4 µL (4 µg)	4 µL (4 µg)	4 µL (4 µg)
Gq top	0 µL	4 µL (4 µg)	4 µL (4 µg)	4 µL (4 µg)
H_2O	296 µL	288 µL	288 µL	289 µL
EB5x	80 µL	80 µL	80 µL	80 µL
$MgSO_4$	16 µL	16 µL	16 µL	16 µL

	mGlu5	mGlu6	mGlu7	mGlu8
mGlu	1.2 µL (1.2 µg)	12 µL (12 µg)	10 µL (10 µg)	6 µL (6 µg)
EAAC1	4 µL (4 µg)	4 µL (4 µg)	4 µL (4 µg)	3 µL (3 µg)
Gq top	0 µL	4 µL (4 µg)	6 µL (4 µg)	3 µL (4 µg)
H_2O	298.8 µL	284 µL	284 µL	292 µL
EB5x	80 µL	80 µL	80 µL	80 µL
$MgSO_4$	16 µL	16 µL	16 µL	16 µL

Table 13: Proportions of DNA mixes used in transfection of HEK293 cells per mGlu receptor subtype.

Afterwards, we added 7 mL of DMEM to each dish with trypsin, homogenised the cell suspensions and placed in two *falcon* tubes. Then we counted the amount of cells in the suspension taking a 20 µL with the aid of a Malasez chamber.

We centrifuge the falcon tube with the cell suspension in 5 minutes at 1000 rpm. After that, the supernatant was aspired and we added the corresponding volume of electroporation buffer (EB1x) to obtain the cell suspension of 10 million cells per 100 µL.

We added 200 µL of a freshly prepared cell suspension to each *eppendorf* tube with the corresponding DNA mix and we placed the obtained suspensions in an electroporation cuvette and were electroporated with the programme of 10 million cells. The obtained Tc should be between 16 and 24 ms.

Then, we placed the living cells of each cuvette in a falcon tube with 19-20 mL of DMEM. The tubes with the same transfected cells were joined and homogenised.
Afterwards, the PLO solution was aspired from the plates, washed every well with 100 µL of PBS and 150 µL of each cell solution was added to every well of the corresponding plate. Then the plates were kept in the incubator at 37°C and 5% CO_2. Between 4 hours before the experiment, we removed the medium and added 100 µL of *Glutamax* medium and the plates were kept in the incubator at 37°C and 5% CO_2.

IP accumulation assays

General material and methods

We estimated IP accumulation using the *IP-One HTRF* kit (*Cisbio Bioassays*) according to the manufacturer's instructions. Cells were stimulated to induce IP accumulations while being treated with test compound for 30 min, at 37°C and 5% CO_2. For azo-compounds experiments with illumination, the plates placed over a LED plate (*FCTecnics*) at a distance of 2-3 cm with continuous illumination during the stimulation with the compounds. To allow stimulation in both dark conditions and violet light illumination, one-half of the 96-well plate clear-bottom was covered with aluminium foil. On the other hand, for cage-compounds experiments, the compound was previously irradiated over 2-5 minutes (depending on the compound) and then displaced at the black-bottom plates for stimulation time. To avoid effects derived from the fast relaxation in case of azo-compounds in aquous solution and the quenching of the FRET in case of the cage-compounds after the 30 minutes stimulation, we washed cells once in stimulation buffer alone before continuing with the lysis step of the assay protocol. For fluorescence readings with *RUBY*star *HTRF HTS* microplate reader (*BMG Labtech*), we transferred cell lysates to a black dark-bottom 96-well plates (just for azo-compounds). Data was analysed, dose-response curves were fitted to the corresponding sigmoidal curve and variance analysis was done with *GraphPad Prism* 6.

HTRF IP-One basis

The IP accumulation assay that we used is based on a time resolved FRET, using a terbium cryptate donor, which emits fluorescence at 620 nm, and an acceptor that emits at 665 nm upon

Förster resonance energy transfer. Additionally, this fluorescence is characteristically long-lived and introducing a time delay of approximately 50 to 150 µs between the system extraction and fluorescence measurement allows the signal to be cleared of all non-specific short-lived emissions. Particulary, in HTRF IP-One assay we used a specific inositol phosphate (IP) antibody labelled with the terbium cryptate (FRET donor) and IP labelled with the FRET acceptor (d2).

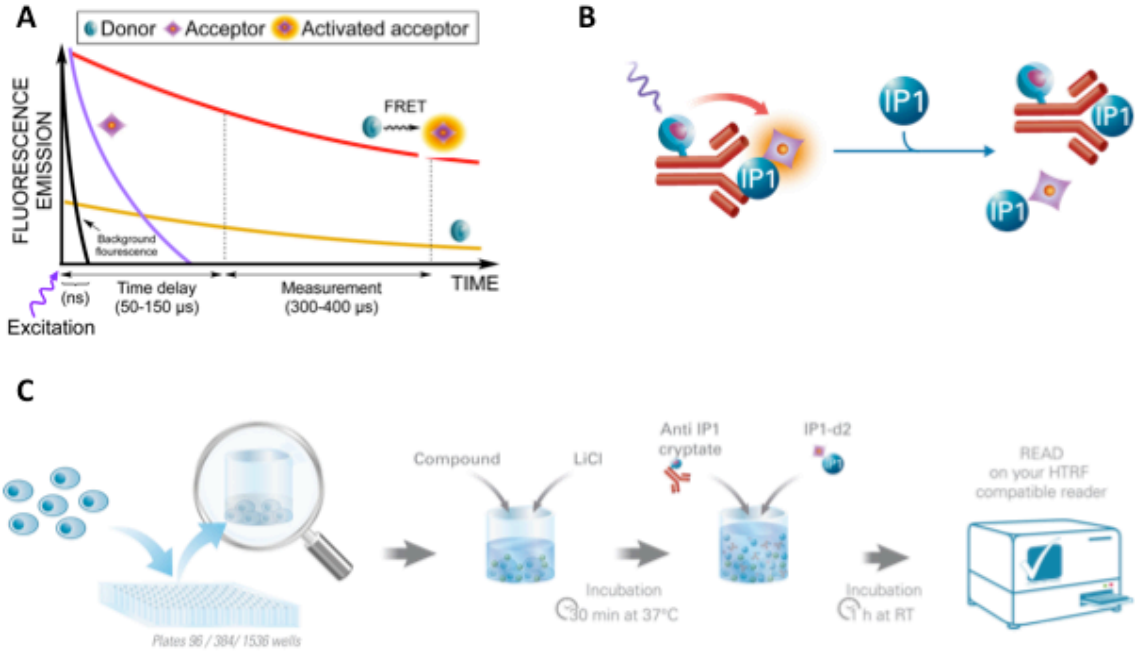

Figure 94: Basis of IP-One HTRF assay. (A) HTRF emission is time-delayed and avoids interferences with conventional fluorescence at the measurement point. (B) A terbium-cryptate-labelled antibody and a d2-labelled IP are used, which produce FRET upon recognition. Cell-production of IP induces a competition with the introduced d2-labelled IP for the recognition of the antibody, leading a single donor emission or FRET emission. (C) Diagram of the procedure of *IP-One*assay.

The procedure of the assay begins with 30 minutes of incubation of the compounds to be tested dissolved IP-One HTRF stimulation buffer (*Cisbio Bioassays*) in cells previously cultured and overexpressing the receptor we want stimulate. This buffer contains lithium chloride, that inhibits the degradation of intracellular inositol phosphate (IP) to *myo*-inositol, leading to a IP accumulation in the cytosol. Subsequent addition of the labelled antibody and d2-IP in a lysis buffer, produces rupture of the membranes of the cells and the competition of the introduced d2-labelled IP and the cell-produced IP for the recognition of the antibody, leading to FRET emission or a single donor emission respectively. Therefore, the fluorescence emissions could be read to obtain the results as a ratio of fluorescence detection at 665 nm and 620 nm. Afterwards we normalised the top and the bottom values between 0 and 100% of the receptor activation with the

values of a control compound with well defined standardised pharmacology.

Procedure for single dose screening

The solution of the compounds to be tested was prepared according with *table 11* in IP-One stimulation buffer. We removed the medium from the 96-well plate and 70 µL of the corresponding solution were displaced in every well. Every compound was tested with 2 replicates inside the plates. Then the plates were incubated at 37°C and 5% CO_2 for 30 minutes. After that, we removed the cellular medium with the compound and added 70 µL of stimulation buffer per well and 15 µL of solution of d2 and 15 µL of solution of terbium cryptate in HTRS lysis buffer (*Cisbio Bioassays*). We left the plate protected against light incubating a minimum of 1 hour at room temperature and the fluorescence was read with *RUBYstar HTRF HTS* microplate reader (*BMG Labtech*).

	mGlu4	**mGlu5**
Compound to test	50 µM	50 µM
Orthosteric Agonist	3 nM (L-AP4) (for PAM) 300 nM (L-AP4) (for NAM)	1 nM Quis (for PAM) 100 nM Quis (for NAM)

Table 14: Concentrations of agonists and compounds to test for single-dose-screening.

Procedure for dose-response curves without illumination

First we prepared eight intermediate solutions of each compound to be tested with *IP-One stimulation buffer* (*Cisbio Bioassays*) and we added another solution of the corresponding orthosteric agonist (L-AP_4 10 nM for $mGlu_4$ PAM evaluation, quisqualate 300 nM for $mGlu_5$ NAM evaluation), also in the same buffer, obtain a constant dilution for all the points of the dose-response curve.

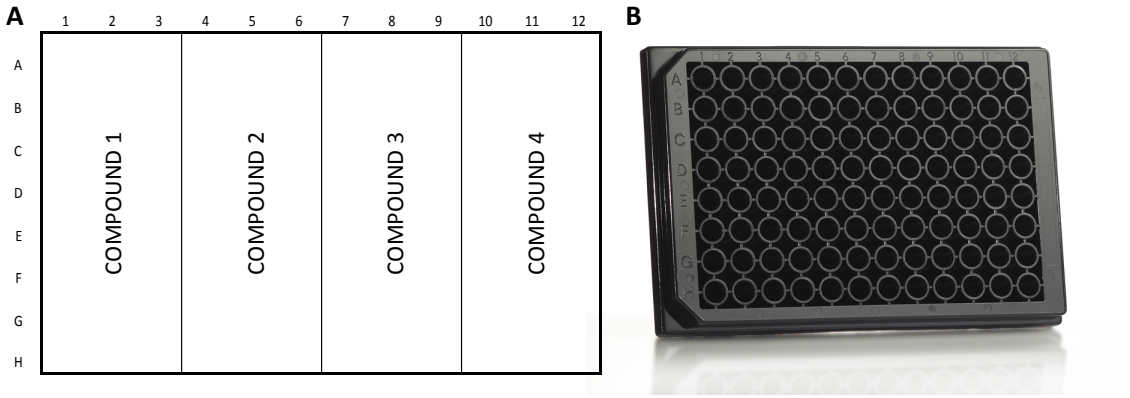

Figure 95: Plates used for dose-response without illumination. (A) Disposition of the compounds on the plates with three replicates per point of the resulting curve. (B) Black bottom 96-well plate used in these experiment.

We removed the medium in a dark opaque-bottom 96-well plate with HEK293 cells expressing the corresponding receptor and added 70 µL of the corresponding solution in every well. For each compound, we generated a dose response curve with eight points with three replicates per point. Then the plates were left incubating the compounds at 37°C and 5% CO_2 for 30 minutes. After that, we removed the cellular medium with the compounds and added 70 µL of stimulation buffer per well and 15 µL of solution of d2 and 15 µL of solution of terbium cryptate in *HTRF lysis buffer* (*Cisbio Bioassays*). The plates were protected from light and incubated a minimum of 1 hour at room temperature and the fluorescence was read with a *RUBYstar HTRF HTS* microplate reader (*BMG Labtech*).

Dose-response curves with illumination

Incase of azocompounds the procedure was the same for the dose-response curves without illumination with little variations to be able to evaluate photoswitching. We generated eight-point-dose-response curves, corresponding to eight concentrations of compound tested. We removed the medium from the black 96-well plate with transfected HEK293 cells, and added 70 µL of the corresponding solution in every well. We located two of the replicates in the six first columns of the plate and the two resting on the six last last columns (*figure 96A*) and we covered the bottom part of the six first columns with aluminium foil and the paper strips to affix it *(Figure 96BC).*

For the stimulation, we placed the plate over a LED-plate with the desired photoswitching wavelength (figure 96D) and we stimulated the cells with the compounds at 37°C and 5% CO_2 for 30 minutes in the dark conditions (located in the covered half of the plate) and under illumination (located in the uncovered half of the plate) in parallel. After the incubation, we removed the

cellular medium with the compounds and added 70 µL of stimulation buffer per well and 15 µL of solution of d2 and 15 µL of solution of terbium cryptate in HTRS lysis buffer (*Cisbio Bioassays*). We left the plates protected from light incubating a minimum of 1 hour at room temperature and the fluorescence was read with a *RUBYstar HTRF HTS* microplate reader (*BMG Labtech*).

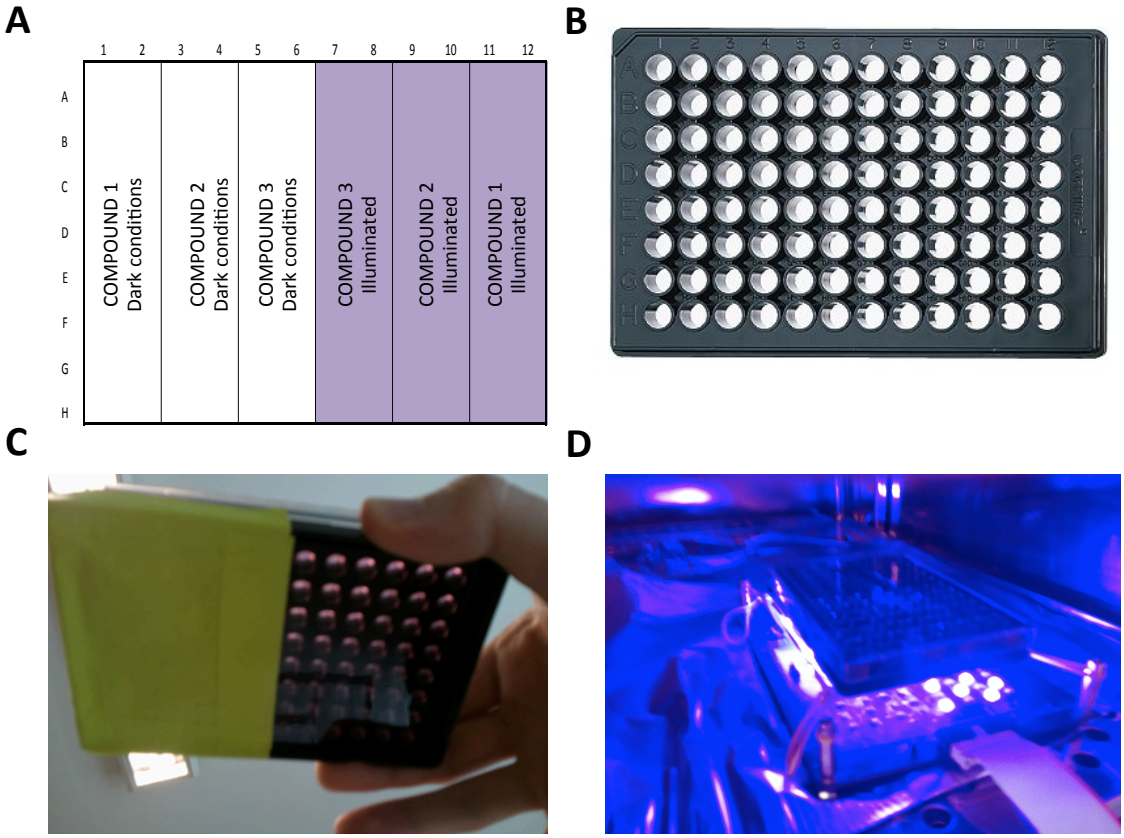

Figure 96: Plates used for dose-response curves with illumination for azocompounds. (A) Arrangement of the compounds on the plates with two replicates per point of the resulting curve. Violet background corresponds to the solutions illuminated during the incubation of the compounds and withe backgrounds to those compounds protected from light. (B) Transparent bottom 96-well plate used in these experiments from the top. (C) Transparent bottom 96-well plate used in these experiments from the bottom. Half of the bottom of the plate was covered with aluminium foil and strips to protect the cells and compounds solutions from light. (D) Incubation of the compounds with the cells with illumination from the bottom with a LED-plate with half of the plate protected from the light.

On the other hand, the procedure for cage-compounds was the same for the dose-reponse curves without illumination generating eight points corresponding to eight concentrations of compound tested with 3 replicates per point. A sample solution of the corresponding cage-compound was irradiated the required time before placing it on the 96-well black-bottom plate (*figure 97*).

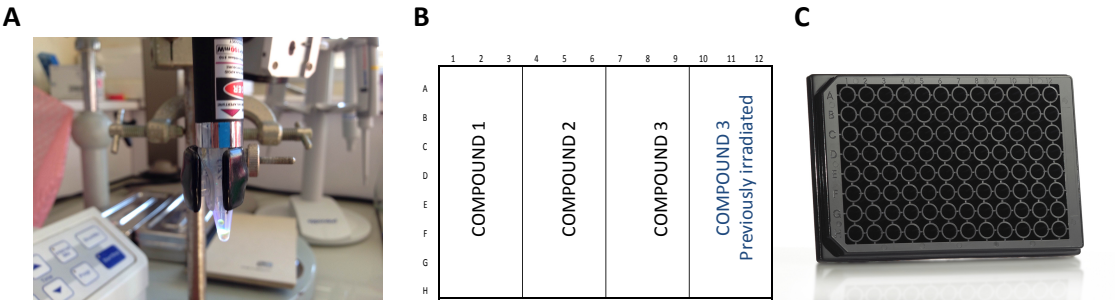

Figure 97: Plates used for dose-response curves with illumination for cage-compounds. (A) Sample of the cage compound during the irradiation before displacing it at the 96-well plate. (B) Arrangement of the compounds on the plate with three replicates per point of the resulting curve. Compounds 1 and 2 were an orthosteric agonist and the reference active compound. Compound 3 was the cage compound related to compound 2 with and without illumination. (C) Black bottom 96-well plate used in these experiment.

For the stimulation, we placed the plate in the incubator and we stimulated the cells with the compounds at 37°C and 5% CO_2 for 30 minutes in the dark conditions. After the incubation, we removed the cellular medium with the compounds and added 70 µL of stimulation buffer per well and 15 µL of solution of d2 and 15 µL of solution of terbium cryptate in HTRS lysis buffer (*Cisbio Bioassays*). We left the plates protected from light incubating a minimum of 1 hour at room temperature and the fluorescence was read with a *RUBYstar HTRF HTS* microplate reader (*BMG Labtech*).

In all of those dose-response protocols, the tips of the pipette were changed after every dilution points due the unspecific adhesion of compounds which we could observe a slight coloration of the tips, with this we could avoid undesired amounts of compounds into the most diluted dissolutions.

Procedure for selectivity assays

The selectivity assays procedure is very similar to the single-dose screening. We used it to test a single dose of a compound on the eight subtypes of mGlu receptors, as PAMs and NAMs. To do that we used two dark-bottom plates with HEK293 cells overexpressing a single mGlu subtype every two rows (*figure 98A*).

The solutions to stimulate the cells were prepared with *HTRF IP-One stimulation buffer* (*Cisbio Bioassays*), with the corresponding orthosteric agonists specific for each mGlu subtype, as depicted in *table 12*, and with the testing concentration of the photochromic compound under

evaluation. We did two replicates for each dilution. *(figure 98B).*

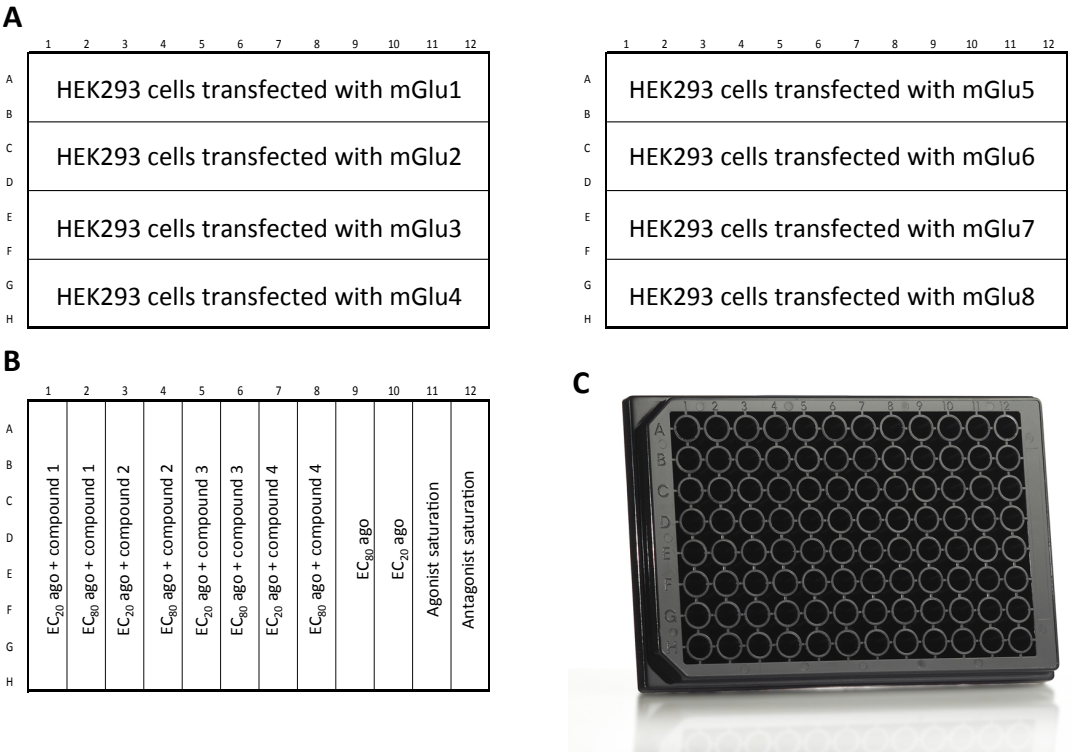

Figure 98: Plates used for selectivity assays. (A) Disposition of the different HEK293 cells transfected with different mGlu subtypes on two 96-well plates. (B) Disposition of the compounds on the plates with two replicates per point. (C) Black bottom 96-well plate used in these experiment.

Group	Subtype	Orthosteric agonist	Low dose (EC_{20})	High dose (EC_{80})	Saturating dose
I	$mGlu_1$ $mGlu_5$	Quisqualate	20 nM 0.5 nM	2 µM 100 nM	200 µM 10 µM*
II	$mGlu_2$ $mGlu_3$	LY354740	1 nM 2 nM*	100 nM 200 nM	10 µM 20 µM
III	$mGlu_4$ $mGlu_6$ $mGlu_7$ $mGlu_8$	L-AP4	3 nM 100 nM 5 µM 10 mM	300 nM 10 µM 500 µM 1 µM	30 µM 1 mM 10 mM 100 µM

Table 15: Doses used for every receptor for the study of the selectivity. Low doses were used to evaluate PAM effects, high doses to evaluate NAM effects, saturating doses as an agonist control and a concentration of LY341495 200 µM for every subtype as an antagonist control. * An additional 100 nM of LY341495 was added to the low dose and the high doses for $mGlu_3$ to decrease its constitutive activity.

We removed the medium from the 96-well plate with transfected HEK293 cells, and added 70 µL

of the corresponding solution in every well. For the stimulation, we placed the plate in the incubator and we stimulated the cells with the compounds at 37°C and 5% CO_2 for 30 minutes in the dark conditions. After the incubation, we removed the cellular medium with the compounds and added 70 µL of stimulation buffer per well and 15 µL of solution of d2 and 15 µL of solution of terbium cryptate in HTRS lysis buffer (*Cisbio Bioassays*). We left the plates protected from light incubating a minimum of 1 hour at room temperature and the fluorescence was read with a *RUBYstar HTRF HTS* microplate reader (*BMG Labtech*).

Bibliography

1. Schonberger, M.; Althaus, M.; Fronius, M.; Clauss, W.; Trauner, D., Controlling epithelial sodium channels with light using photoswitchable amilorides. *Nature chemistry* **2014,** *6* (8), 712-9.
2. Luminita Wagner, V. R., Alina Raditoiu, Monica Florentina Raduly, Functionalized Azobenzenes Chromogens with Aromatic Amino Primary Groups. *Revista de Chimie* **2009,** *60* (5), 444-449.
3. Carreno, M. C.; Mudarra, G. F.; Merino, E.; Ribagorda, M., Synthesis of azobenzenes from quinone acetals and arylhydrazines. *The Journal of organic chemistry* **2004,** *69* (10), 3413-6.
4. Havlik, I. C., C.; Toth, A.; Bacaloglu, R. , Synthesis and characterization of some 4'-substituted 4-aminoazobenzenes. Determination of basicity constants. *Revue Roumaine de Chimie* **1983,** *28* (9-10), 903-913.
5. Bolea, C., Mutel, V., Rocher, J.-P., Bessis, A.-S.; Le Poul, E. Novel aminopyridine derivatives as mGluR5 antagonists. 2004.
6. Li Xiaoleng, B. T. Synthetic method of 1,3-cycloheptanedione. 19/02/2014, 2014.
7. Hong, S. P.; Liu, K. G.; Ma, G.; Sabio, M.; Uberti, M. A.; Bacolod, M. D.; Peterson, J.; Zou, Z. Z.; Robichaud, A. J.; Doller, D., Tricyclic thiazolopyrazole derivatives as metabotropic glutamate receptor 4 positive allosteric modulators. *Journal of medicinal chemistry* **2011,** *54* (14), 5070-81.
8. Hayashibe, S. I., H. Okada, M. Kohara, A. Maeno, K. Yahiro, K. Shimada, I. Tanabe, K. Negoro, K. Kamikuba, T. Sakamoto, S. Novel Thiazolobenzimidazole Derivates. 2002.
9. Fournier, L.; Aujard, I.; Le Saux, T.; Maurin, S.; Beaupierre, S.; Baudin, J. B.; Jullien, L., Coumarinylmethyl caging groups with redshifted absorption. *Chemistry (Weinheim an der Bergstrasse, Germany)* **2013,** *19* (51), 17494-507.
10. Seven, I.; Weinrich, T.; Gränz, M.; Grünewald, C.; Brüß, S.; Krstić, I.; Prisner, T. F.; Heckel, A.; Göbel, M. W., Photolabile Protecting Groups for Nitroxide Spin Labels. *European Journal of Organic Chemistry* **2014,** *2014* (19), 4037-4043.
11. Feng, L.; Lv, K.; Liu, M.; Wang, S.; Zhao, J.; You, X.; Li, S.; Cao, J.; Guo, H., Synthesis and in vitro antibacterial activity of gemifloxacin derivatives containing a substituted benzyloxime moiety. *European journal of medicinal chemistry* **2012,** *55*, 125-36.

12. Gomeza, J.; Mary, S.; Brabet, I.; Parmentier, M. L.; Restituito, S.; Bockaert, J.; Pin, J. P., Coupling of metabotropic glutamate receptors 2 and 4 to G alpha 15, G alpha 16, and chimeric G alpha q/i proteins: characterization of new antagonists. *Molecular pharmacology* **1996,** *50* (4), 923-30.

Resum en Català

Introducció

Receptors metabotropic del glutamat (mGluRs)

Els receptors metabotròpics de glutamat (mGluRs) són receptors clau en la modulació de la transmissió sinàptica excitatória i estan àmpliament distribuïts en el sistema nerviós central (SNC) i el sistema nerviós perifèric (PNS). Pertanyen a la classe C dels receptors de proteïna-G, que s'activen per el seu neurotransmissor més comú: El glutamat.

Estructura i mecanismes d'activació

Els receptors de glutamat metabotròpics son receptors que formen obligatòriament dímers, i cada protomer esta constituït per tres dominis: el domini extracel·lular (VFT), un domini ric en cisteïna (CRD) i el domini transmembrana (TMD).

El domini extracel·lular (VFT), coexisteix en dos estats: en estat obert en absència de lligand i estabilitzat per antagonistes, o bé en estat tancat estabilitzat per agonistes necessaris per a l'activació del receptor.

Els dominis extracel·lulars del dímer estan en equilibri conformacional depenent de si estan en estat obert o tancat un o ambdós protomers. En absència de lligant, o en presència d'antagonistes, s'obren les dues VFTs. La unió d'un o dos agonistes provoca el tancament d'una o dues VFTs del dímer, donant com a resultat l'activació del receptor.

Després de l'activació del receptor, el tancament de les dues VFTs del dímer comporta a un gran canvi en l'orientació relativa d'aquestes passant d'una orientació de repòs a una d'activa. La principal conseqüència d'aquesta reorientació és un acostament dels lòbuls de les VFTs, obtenint una conformació activa que estabilitza el domini transmembrana (*Figura 1*).

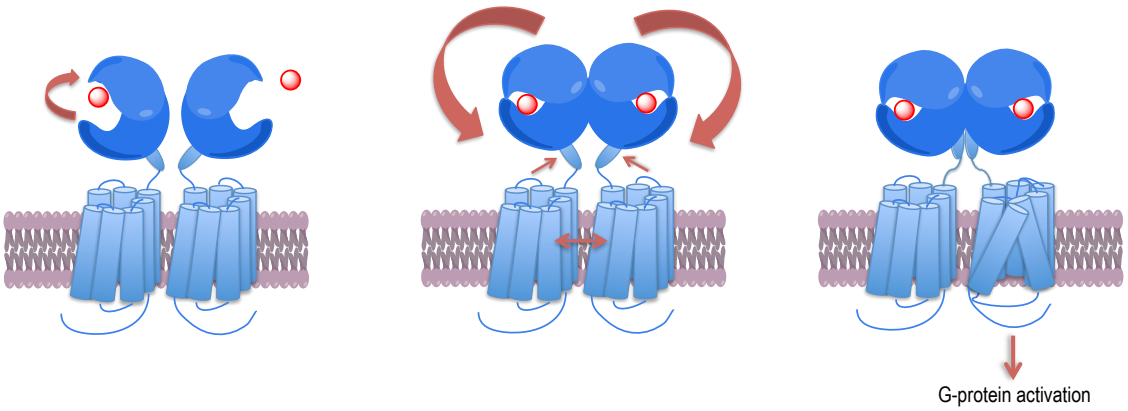

Figura 1: Etapes d'activació dels mGluRs[1]

El domini ric en cisteïna (CRD) uneix el domini extracel·lular i el domini transmembrana. Esta constituït per nou cisteïnes, que ofereixen quatre ponts disulfur dins del domini i la novena cisteïna esta lligada a la VFT mitjançant un pont disulfur addicional. El paper que desenvolupa la CRD és crucial i ambdós dominis del dímer estan en contacte quan hi ha l'activació del receptor.
El domini transmembrana (TMD), pot adoptar diferents conformacions i són les responsables de l'activació de les proteïnes G. Un cop activat el receptor, el domini transmembrana d'un protomer canvia d'un estat en repòs a una conformació activa, mentre que l'altre roman en repòs. El protomer actiu és el responsable de la transducció del senyal del lligant ortoestèric o endogen de la VFT a la proteïna G.

Classificació dels mGluRs

La majoria de les accions produïdes pel glutamat en el sistema nerviós central estan involucrats amb l'activació dels receptors metabotropics del glutamat. Existeixen vuit subtipus de mGluRs, que s'expressen en tot el sistema nerviós central i perifèric, excepte el receptor metabotropic subtipus 6 que només s'expressa en la retina. Aquests subtipus es classifiquen en tres grups generals en funció de la seva seqüencia i farmacologia (*Taula 1*).

Grup	Subtipus	Gen	Glu EC_{50}	Orth. ago	EC_{50}	Prot-G. (principal senyalització)
I	$mGlu_1$	GRM1	9-13	Quisqualic acid (**2**)	0.1-1	Gq (+IP3, + Ca^{2+} intracel·lular, +DAG, activació de PKC)
	$mGlu_5$	GRM5	3-10		0.03-0.3	
II	$mGlu_2$	GRM2	4-20	LY 354740 (**3**)	0.005	Gi/o (-cAMP, inhibeix canals de Ca^{2+}, activació de canals de K^+, activació vies de MAPK i PtdIns-3-K)
	$mGlu_3$	GRM3	4-5		0.0034	
III	$mGlu_4$	GRM4	3-20	L-AP_4 (**4**)	0.2-1.2	Gi/o (-cAMP, inhibeix canals de Ca^{2+}, activació de canals de K^+, activació vies de MAPK i PtdIns-3-K)
	$mGlu_7$	GRM7	1000		0.9	
	$mGlu_8$	GRM8	16		160-500	
	$mGlu_6$	GRM6	2.5-11		0.06-0.6	Go (inhibeix canal TrpM1 Ca^{2+})

Taula 1: Classificació dels receptors de mGlu, amb el receptor endogen (glutamat) per cada subtipus EC_{50} en unitats μM^2, el lligand comú per cada grup (*Figura2*), amb la corresponen potencia EC_{50} en unitats μM i les principals proteïnes-G i les seves senyalitzacions principals[3].

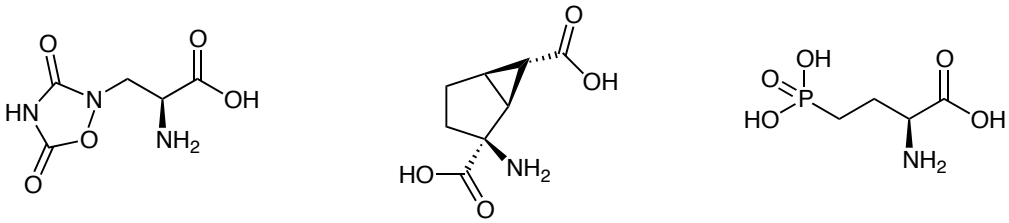

Quisqualic acid (**2**) LY 354740 (**3**) L-AP_4 (**4**)

Figura 2: Estructures dels agonistes ortoestèrics dels diferents grups.

Grup I

El grup I està constituït per els receptors metabotropics subtipus 1, 5 i estan expressats al llarg de tot el CNS en neurones. Aquests receptors es troben predominantment a la post sinapsis on es produeix un augment en l'excitament neuronal, no obstant, el grup I localitzat en la pre sinapsis pot incrementar o disminuir l'alliberament del neurotransmissor.

Grup II

El grup II dels mGluRs, comprenen els receptors tipus 2 i 3, àmpliament distribuïts al sistema nerviós central i perifèric. Generalment estan expressats en la pre sinapsis on es controla l'alliberament de neurotransmissor. També s'ha trobat en posicions post sinàptiques on, a diferencia amb el grup I, en aquest cas indueixen la hiperpolarització.

Grup III

El grup III del mGluRs (subtipus 4, 6, 7 i 8), estan expressats presinàpticament en neurones i distribuït en tot el CNS, a excepció del subtipus 6, el qual esta localitzat en la post sinapsis del retinal.

Classificació dels lligands en els mGluRs

A pesar de l'existència de diferents eines per modular l'activitat dels mGluRs com els nanobodies o els anticossos, una de les aproximacions clàssiques respecte aquesta modulació són molècules petites que s'uneixen al receptor.

Aquests lligands poden ser classificats en dos classes en dependència d'on tenen la capacitat d'unir-se dins el receptor: Lligands que actuen al domini extracel·lular o la VFT, també anomenats lligands competitius del glutamat o ortoestérics, i lligands que actuen a la TMD, anomenats lligands al·lostèrics o lligands no competitius.

Lligands de la VFT

Els lligands que actuen en la VFT estan basats en el glutamat (el lligand endogen). Aquests poden tenir diferents comportaments, poden ésser agonistes totals, parcials i antagonistes o agonistes inversos (que competeixen en el mateix centre d'unió que el agonista endogen).

És bastant complex dissenyar lligands competitius selectius, ja que la VFT de tots els receptors són modulats per el mateix receptor endògen. No obstant, alguns agonistes selectius varen ser dissenyats per cada grup de mGlu com per exemple el quisqualat (**2**) (grup I), LY 354740 (**3**) (grup II), o L-AP_4 (**4**) (grup III) (*Taula 1, Figura 2*).

Tanmateix, altres lligands també han estat desenvolupats com antagonistes a la VFT, els quals s'uneixen ortoestéricament al centre actiu i eviten el tancament de la VFT, com per exemple el LY 341495 (**5**) (*Figura3*). Recentment, un centre d'unió addicional de la VFT ha estat descobert gràcies a un nou agonista del grup III LSP4-2022 (**6**) (*Figura 3*), aquest descobriment a fet possible nous moduladors al·lostèrics que s'uneixen al domini extracel·lular (EDAM).

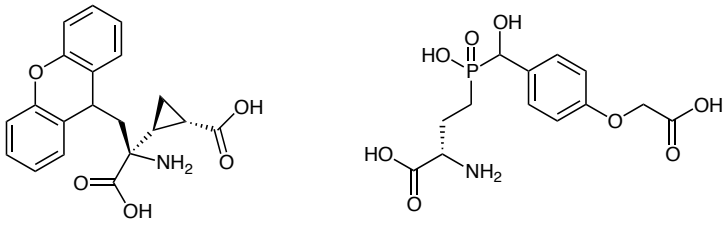

LY 341495 (**5**) LSP4-2022 (**6**)

Figura 3: Estructures del antagonista LY 341495 (**5**) i del LSP4-2022 (**6**).

Lligands de la TMD

La falta de selectivitat dels lligands desenvolupats fins ara dintre del mateix grup que actuen en la VFT, va promoure la cerca de noves molècules que actuessin en centres al·lostèrics del TMD. Aquest nou centre d'unió va ser un gran avanç en termes de selectivitat degut a que el lligand endogen a diferencia d'altres classes de GPCRs, s'uneix en l'espai extracel·lular i no en la transmembrana, deixant buida una cavitat on només es veurà modificada per un lligand selectiu del corresponent subgrup.

Aquests lligands poden tenir diferents tipus de comportament en dependència a la modulació de la part transmembrana.

Aquells lligands que potencien la resposta d'un protòmer del dimer per l'unió primer del agonista en la VFT estabilitzant la seva conformació activa s'anomenen PAMs (moduladors al·lostèric positius), d'altre banda aquells lligands que estabilitzen la conformació inactiva dels dos protòmers de la TMD inhibint la funció del receptor s'anomenen NAMs (moduladors al·lostèric negatius. Existeixen també altres moduladors al·lostèrics que s'uneixen fortament al receptor però en canvi no indueixen una funcionalitat al receptor anomenats SAMs (moduladors al·lostèrics silenciós), o també moduladors positius que tenen una activitat agonista intrínseca donant lloc a una activitat funcional, aquests moduladors s'anomenen ago-PAMs.

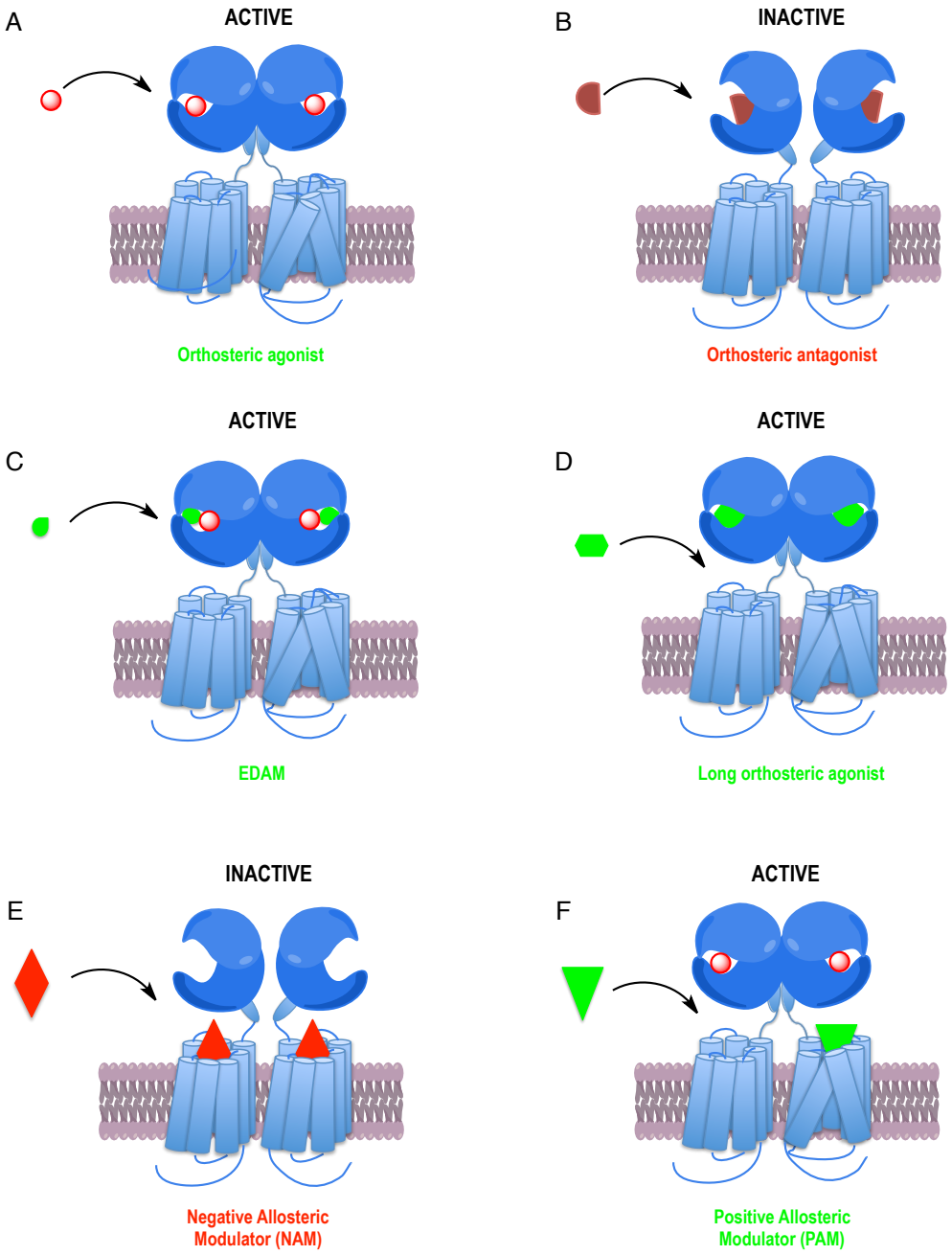

Figura 4: Models general de unió dels diferents moduladors en els mGluRs: A) Agonistes ortoestèrics, B) Antagonistes ortoestèrics, C) Moduladors allosterics del domini extracel·lular (EDAM), D) Agonista ortoestèric llarg, E) Modulador al·lostèric negatiu (NAM), F) Modulador al·lostèric positiu (PAM) [4].

Potencial terapèutic dels receptors metabotropics del glutamat.

Com ja hem dit abans, el fet que els receptors metabotropics del glutamat estiguin distribuïts per tot el sistema nerviós central i perifèric, i que cada un dels subgrups de mGlu tingui un rol dins aquesta xarxa, ja que la seva modulació pogui ser clau pel tractament de malalties amb clara contribució neurològica.

NAMs de $mGlu_1$ i $mGlu_5$ per dolor

Diferents estudis han demostrat l'eficàcia de NAMs de $mGlu_1$ en diferents models d'analgèsia[5], en alguns casos en dependència de la dosi s'ha demostrat que es pot revertir la sensibilització induïda per capsaïcina en tractaments talàmic-espinal, demostrant el potencial pel tractament de dolor persistent associat a sensibilització en espina dorsal.
Els NAMs de $mGlu_5$ també s'han demostrat com a bons inhibidors de dolor arribant en molts casos a fases clíniques pel tractament induït de hiperalgèsia[6].

NAMs de $mGlu_5$ per ansietat, depressió i síndrome de fràgil X

Diferents estudis[7]suggereixen els NAMs de $mGlu_5$ com una bona aproximació terapèutica pel tractament de l'ansietat demostrant activitats ansiolítiques en diferents models animals, també existeix una relació d'antagonisme de $mGlu_5$ amb l'activitat antidepressiva. Altres desordres han estat estudiats en models animals per lligands negatius de $mGlu_5$ en malalties com addicció, dolor crònic, migranya, Parkinson i també per síndrome de fràgil X.

PAMs de $mGlu_5$ per esquizofrènia

Els moduladors positius al·lostèrics de $mGlu_5$ a sorgit com una nova aproximació terapèutica pel tractament d'esquizofrènia i desordres cognitius.
Nombrosos estudis[8] conclouen que el receptor $mGlu_5$ està molt associat a la senyalització produïda pel receptor NMDA el qual juga un paper clau en varies zones del cervell implicades en el desenvolupament de l'esquizofrènia. L'activació de $mGlu_5$ i la subseqüent millora en l'activació del receptor de NMDA constitueix una bona aproximació.

PAMs de $mGlu_2$ per esquizofrènia i ansietat.

Apart de PAMs de $mGlu_5$, altres subtipus de receptors del glutamat juguen un paper important en el tractament d'enfermetats com l'esquizofrènia i l'ansietat. Moltes regions del cervell involucrades en ambdós malalties, expressen receptors de $mGlu_2$ on els seus agonistes poden reduir la neurotransmissió en aquestes regions[9].

PAMs de $mGlu_3$ per neuroprotecció

Els mGluRs també han estat descrits com una bona diana per diferents malalties neurodegeneratives[10]. En particular, els agonistes del grup II dels mGlus son considerats neuroprotectors, ja que en estudis amb ratolins KO de $mGlu_2$ i $mGlu_3$ es va demostrar que el subtipus 3 era necessari en els astròcits per obtenir un efecte en el mecanisme del factor de creixement ß, que en absència de $mGlu_3$, la activació neuronal amb $mGlu_2$ contribuïa a una excitotoxicitat.

PAMs de $mGlu_4$ per Parkinson

El receptor $mGlu_4$ està expressat en les fibres GABAergiques, i que és una etapa indirecta pel control motor. L'activació d'aquests receptors fan disminuir l'alliberament de GABA en la sinapsis de l'estriat, el qual està sobre activat degut a la pèrdua de dopamina en les neurones en la malaltia de Parkinson demostrant que aquests receptors poden arribar a ser claus en la disminució dels efectes[11].

Modulació en la funció de proteïnes mitjançant llum

Hi han diverses maneres actualment per controlar la funció d'una proteïna o d'una via de senyalització utilitzant llum: Optogenètica, farmacologia optogenètica, optofarmacologia amb compostos fotoisomeritzables i optofarmacologia amb compostos gàbia.

Els cromòfors fotoisomeritzables poden ser trobats en la natura i poden commutar la seva funcionalitat proteica mitjançant l'irradiació amb llum de manera rapida i precisa. Un clar exemple es el retinal en les opsines o canalrodopsines o bacteriopsines (*Figura 5A*).

La farmacologia optogenètica és una aproximació que es basa en l'ús de lligands fotoisomeritzables ancorats covalentment en el mateix receptor (PTLs). Aquests lligands estan formats per la unió de varis fragments: un lligand terminal amb un fotocommutador intermedi, que alhora està unit a un grup reactiu per poder esser ancorat finalment a la proteïna de manera covalent (*Figura 5B*).

Ambdós casos descrits abans permeten el control de les funcions de la proteïna de manera precisa i amb un bon rang d'eficiència, però és necessària la introducció d'una modificació genètica fet que l'exclou per a teràpies en humans.

Una bona alternativa per un tractament terapèutic és, en canvi, l'optofarmacologia on no cal cap tipus de modificació genètica sent bons candidats com a fàrmacs per una aplicació terapèutica amb control de l'activitat regulada per llum.

Existeixen dos tipus de dissenys en l'optofarmacologia, els compostos fotoisomeritzables i els compostos gàbia.

Els compostos gàbia estan basats en la protecció de grups funcionals amb grups fotolàbils que s'enllacen de manera covalent a la molècula activa i que sota la irradiació amb llum és alliberada de manera irreversible. Aquest disseny permet un control espai-temporal en la seva alliberació però un cop es produeix la desprotecció es perd completament el control en la funció de la proteïna (*Figura 5C*).

En canvi, els compostos fotoisomeritzables (normalment azobenzenes) son modificacions estructurals de la mateixa molècula i que estan incloses en la mateixa estructura o bé a prop dels grups que interactuen en el receptor. La diferencia respectes els compostos gàbia esmentats abans, es que en aquest cas sota irradiació es produeix un canvi conformacional que un cop deixa de ser il·luminada pot tornar a la seva configuració més estable obtenint un control sobre la funció proteica que amb els compostos gàbia perdíem (*Figura 5D*).

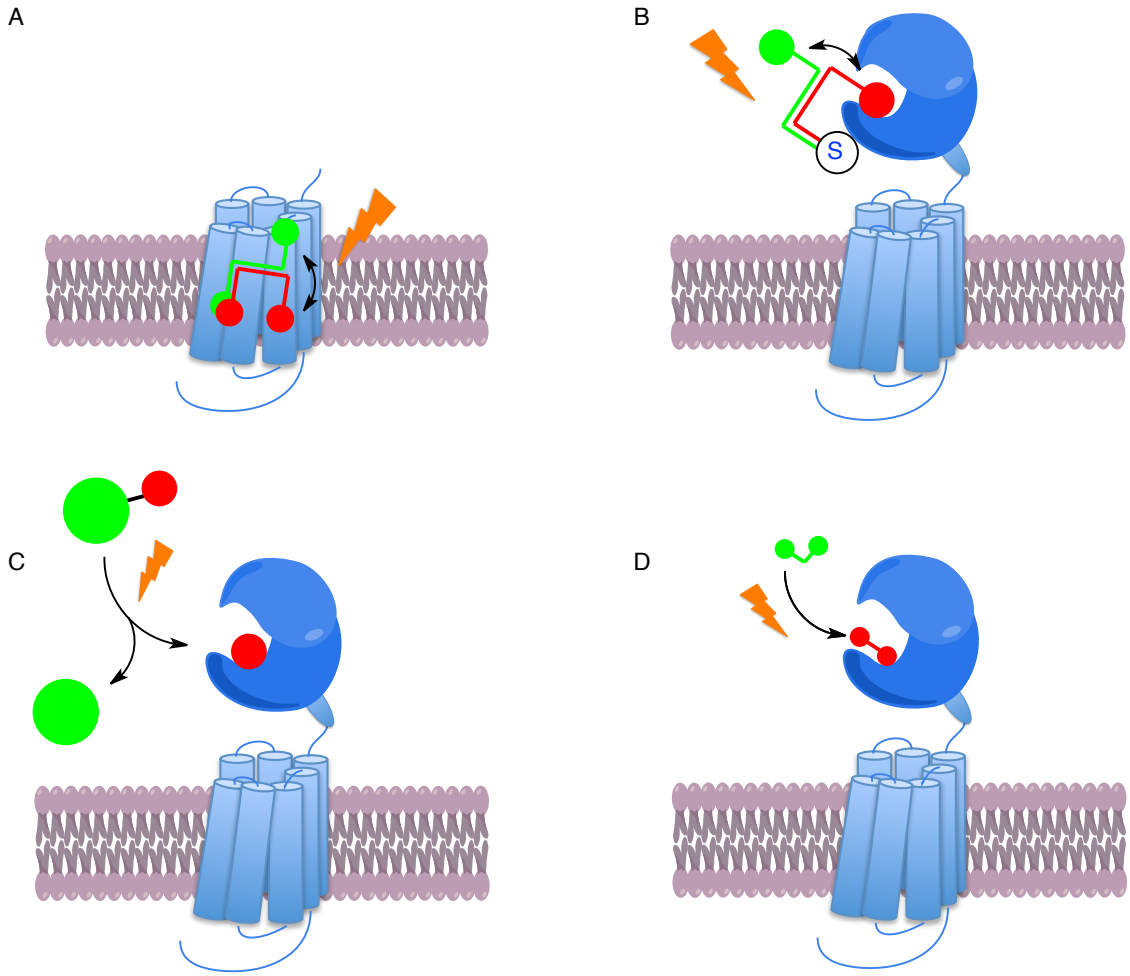

Figura 5: Representació de les quatre principals aproximacions en el control de l'activitat d'una proteïna amb llum: A) Optogenètica, B) farmacologia optogenetica, C) optofarmacologia amb compostos gàbia, D) optofarmacologia amb compostos fotoisomeritzables[12].

Objectius

Els objectius que ens vam marcar en aquesta tesi varen ser:

1) El disseny i síntesi de nous compostos fotocommutables com a moduladors al·lostèrics positius de $mGlu_4$ i moduladors al·lostèrics negatius de $mGlu_5$ (ja que estan indicats per dolor), basats en l'aproximació *cis*-on, que consisteix en produir un efecte bioactiu dins el receptor amb el lligand en una conformació *cis*, mentre que el isòmer *trans* corresponent roman inactiu. En

paral·lel, també avaluarem les propietats fotoquímiques i es farà una caracterització farmacològica.

2) El disseny i síntesis de nous lligands fotoactivables (compostos gàbia), basats en la modificació estructural de compostos ja coneguts com a NAMs de $mGlu_1$ i $mGlu_5$ i també com a PAMs de $mGlu_4$, tots implicats en la transmissió del dolor i que poden oferir certes avantatges respecte els lligands fotocommutables. També es caracteritzarà fotoquímica i farmacològicament per extrapolar l'aproximació desenvolupada a un fàrmac conegut i comercial que actua en receptors involucrats amb dolor com els μ-opiod.

Resultats i Discussió

Capítol 1: Compostos fotocommutables: aproximació *Cis-On*

Els objectius que ens vàrem marcar en aquests present capítol va ser el disseny i síntesis de nous compostos fotoisomeritzables com a PAMs de $mGlu_4$ o NAMs de $mGlu_5$ que tinguessin un comportament on en la configuració *cis* del azobenzè tingues una activitat biològica respecte la disposició *trans* que hauria de romandre inactiva.

En la tesi de Xavi Gòmez es varen descriure nous moduladors fotocommutables a partir d'un PAM de $mGlu_4$ de referencia VU0415374 (**33**)[13] on varien canviar en cada cas una de les dos amides per un grup azo, obtenint un compost fotocommutable potent com a NAM de $mGlu_5$ (Alloswitch-1 **34**)[14] i un altre com a PAM de $mGlu_4$ (Optogluram **59**)[4].

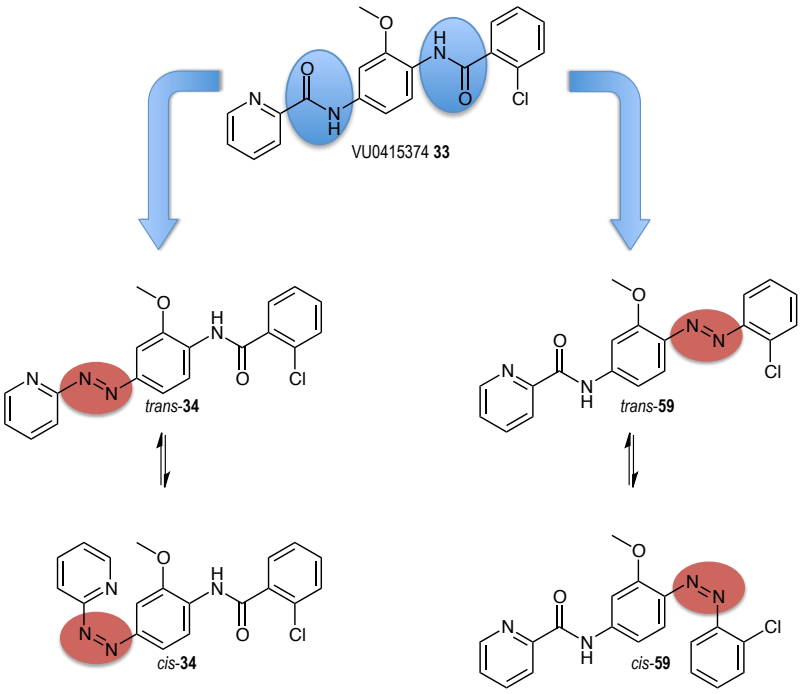

Figura 6: Disseny dels azobenzens **33** i **59** a partir del compost de referencia VU0415374 **33**.

Ambdós azobenzens varen constituir un avenç en el control de la funció de mGluRs, poden regular el control inclòs en sistemes vius tipus peixos zebra, ratolins o capgrossos.

Tot i això, el disseny no va ésser el més adient de cara un interès terapèutic degut a que els compostos varen ésser azobenzens on la disposició *trans* era la activa i, on només sota irradiació es podia desactivar.

Per a una aplicació terapèutica, era necessari el disseny de noves molècules on només actuessin en el lloc i el moment que es volgués romanen inactiva un cop no hi hagués irradiació, o dit d'una altre manera, l'obtenció d'un azobenzè on la disposició *cis* (termodinàmicament menys estable) fos la disposició activa.

Així doncs es varen dissenyar diferents azobenzens com a NAMs de $mGlu_5$ (*Figura 8*) i PAMs de $mGlu_4$ (*Figura 7*), basats en compostos de referencia on la addició de un anell de azobenzè en disposició *trans* no pogués entrar dins el receptor, mentre que isomeritzant a la conformació *cis* adoptés una estructura més lineal i pogués interactuar dins el lloc d'unió.

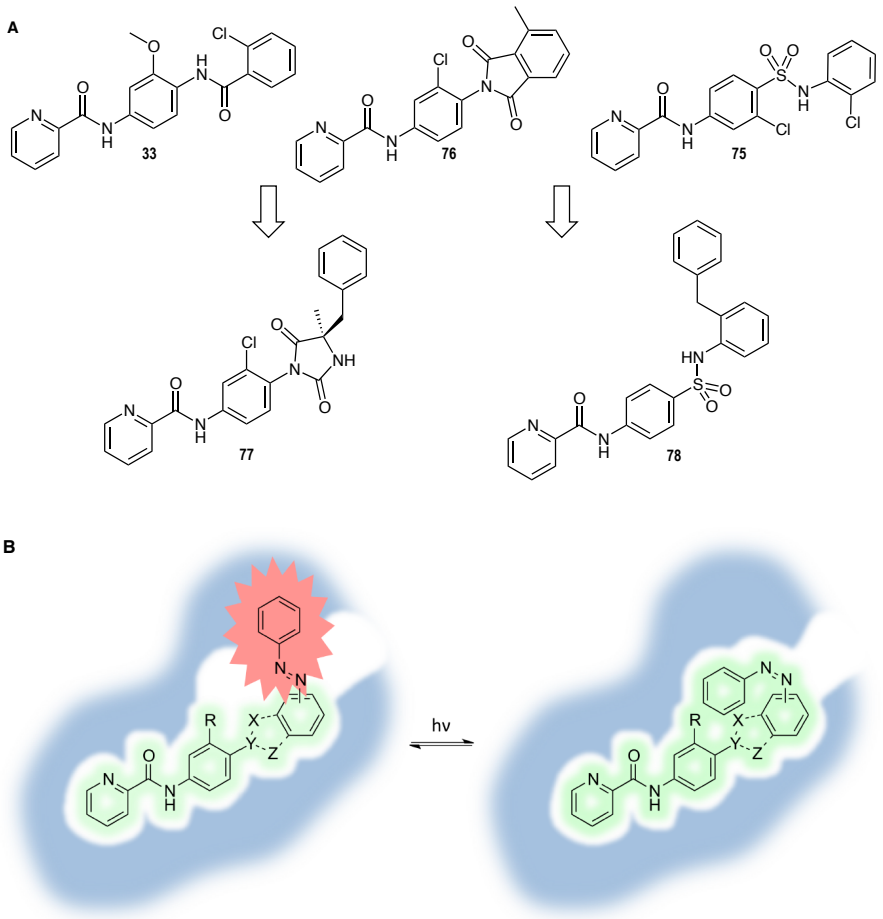

Figura 7: Disseny de compostos *cis-on* com a PAMs de $mGlu_4$. A) Compostos trobats a la literatura que podrien ser fàcilment mimetitzats per un azobenzè, B) Aproximació *cis-on* esperada.

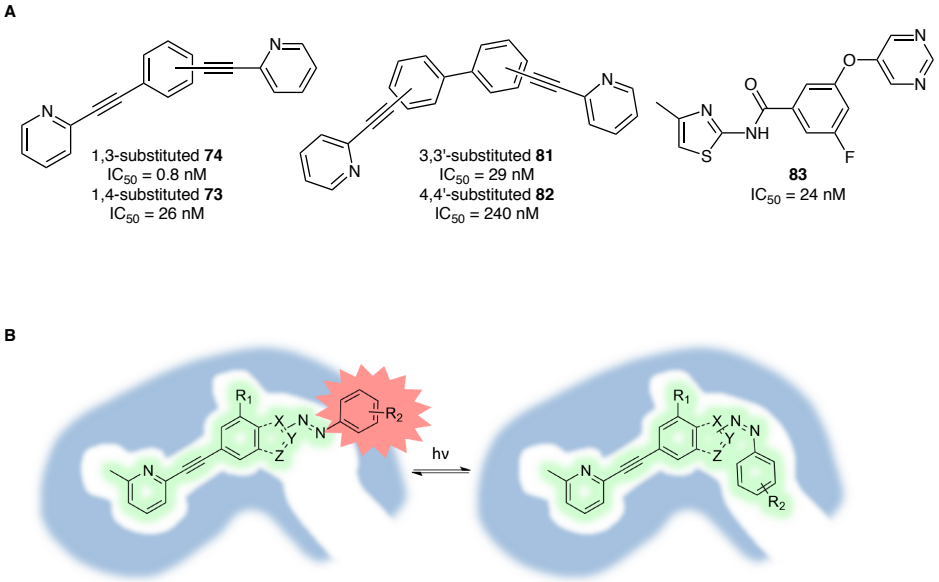

Figura 8: Disseny de compostos *cis-on* com a NAMs de $mGlu_5$. A) Compostos trobats a la literatura que podrien ser fàcilment mimetitzats per un azobenzè, B) Aproximació *cis-on* esperada.

Així doncs es varen sintetitzar cinc compostos (*Figura 9*) i es va fer una caracterització fotoquímica per tal de obtenir la longitud d'ona optima per isomeritzar de *trans* a *cis* i també de *cis* a *trans* (*Figura 10*).

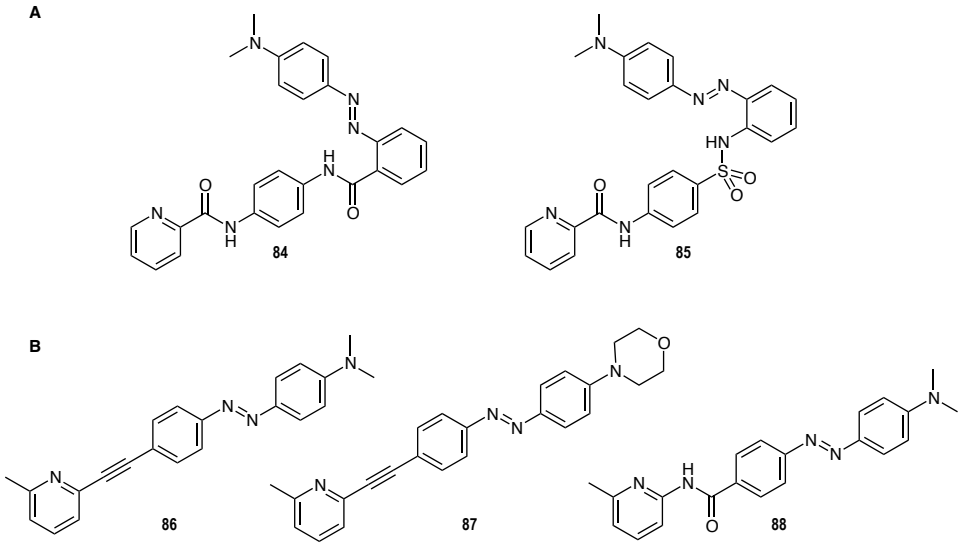

Figura 9: Estructures dissenyades i sintetitzades. A) Com a PAMs de $mGlu_4$, B) Com a NAMs de $mGlu_5$.

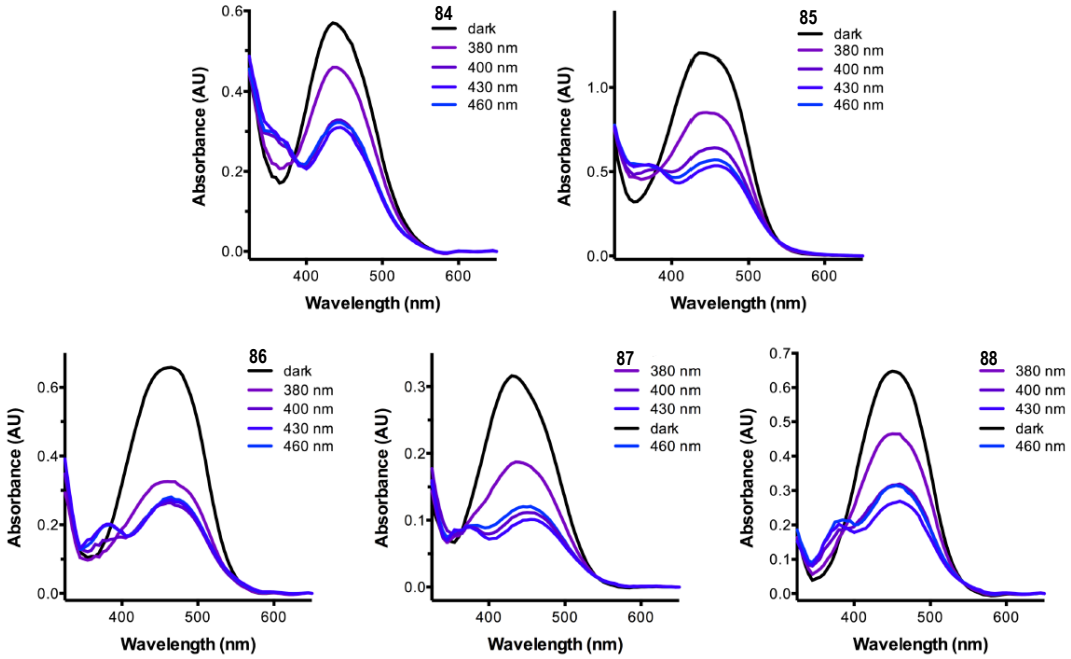

Figura 10: Espectres UV-Vis de tots els compostos dissenyats i sintetitzats amb i sense il·luminació.

A més, gràcies d'una banda a la incorporació de grups electro-donadors en el anell terminal del azobenzè, i grups electró-atractors a l'altre, en el disseny fet anteriorment, es va poder irradiar a longituds d'ona molt esteses dins el rang del visible.

Un cop establerta les condicions fotoquímiques, vàrem caracteritzar farmacològicament tots els compostos.

Per avaluar l'activitat farmacològica dels suposats PAMs de $mGlu_4$ o NAMs de $mGlu_5$ amb suposat comportament *cis-on*, primer els vam assajar a dosi única amb cèl·lules HEK293 sobrexpressant $mGlu_4$ o $mGlu_5$ amb l'assaig de IP-One. Vam assajar tots els compostos com a PAMs i NAMs de $mGlu_4$ i $mGlu_5$, independentment del propòsit en el seu disseny, i amb cada mesura realitzada tant en condicions fosques (sense il·luminar) com amb il·luminació (*Figura 11*)

.

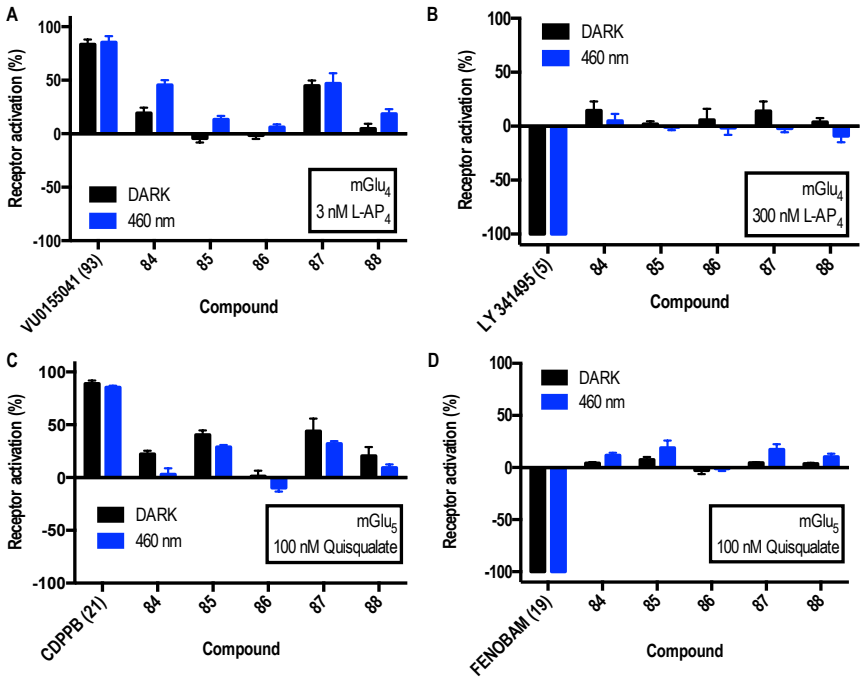

Figura 11: Experiments de dosi simple dels compostos **84**, **85**, **86**, **87** i **88**. A) Com a PAMs de $mGlu_4$, B) NAMs de $mGlu_4$, C) PAMs de $mGlu_5$ i D) NAMs de $mGlu_5$. La resposta de FRET es va normalitzar a 0%-100% entre l'efecte a concentració baixa d'agonista (EC_{20}) i l'efecte de saturació d'agonista per l'avaluació efecte de PAM . En canvi, per la del NAM, es va normalitzar a -100%-0% entre l'efecte de saturació de l'antagonista amb la concentració alta d'antagonista (EC_{80}). Cada barra correspon a la mitjana d'un mínim de dos replicats independents amb la SEM corresponent com a barres d'error.

Desafortunadament, no es varen trobar uns grans efectes sota irradiació com es pot observar en la *Figura11*, tampoc es varen observar grans diferencies entre l'activitat en condicions fosques respecte les il·luminades en cap compost. No obstant, en el cas **84**, **85** i **86** es van obtenir una diferencia petita entre ambdós condicions que ens va fer pensar en la possibilitat de tenir un mínim de comportament *cis-on*. El compost més prometedor va ser el **84** en el que es va observar més efecte tot i que sense suficient potencia. Els altres compostos varen mostrar un efecte PAM parcial en ambdues condicions d'il·luminació.

Així doncs, vàrem voler fer una avaluació més exhaustiva d'aquests compostos que van mostrar un comportament *cis-on* més notable, generant corbes dosi-resposta en assajos de acumulació de IP-One en cèl·lules HEK293 sobrexpressant $mGlu_4$ sota condicions fosques i de il·luminació (*Figura 12*).

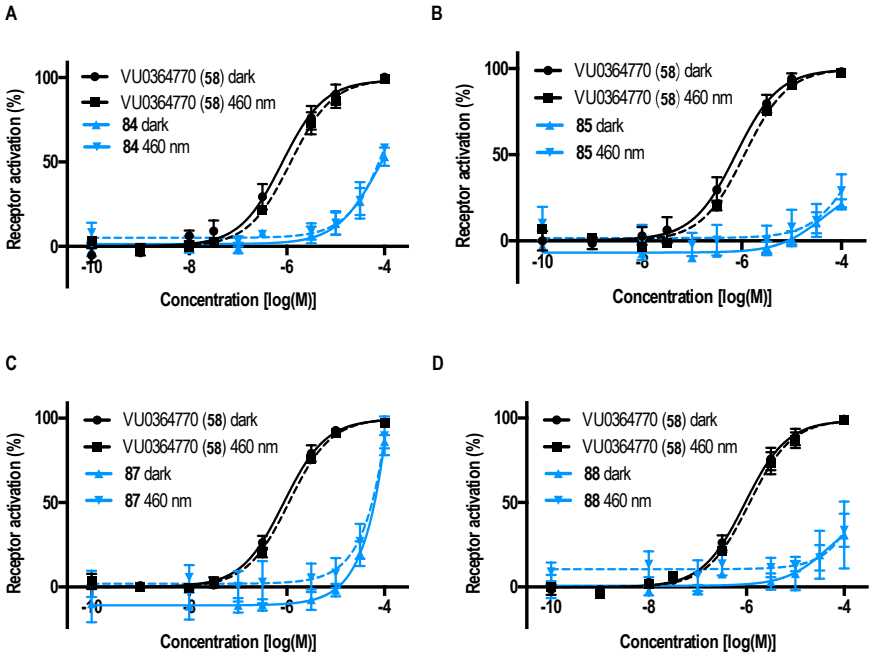

Figura 12: Corbes dosi-resposta en assajos de IP-One en cèl·lules HEK293 sobrexpressant $mGlu_4$ amb concentracions constants del agonista selectiu $L\text{-}AP_4$ (**4**) 3 nM. Línies continues son les mostres incubades en condicions fosques i les línies discontinues les il·luminades a 460 nm. Cada punt correspon a la mitjana d'un mínim de tres replicats independents amb la SEM corresponent com a barres d'error.

Desafortunadament, no vàrem poder veure un efecte clar on el compost il·luminat fos més potent que el compost en condicions fosques, de fet, aquests resultats no es corresponen amb el comportament observat anteriorment en els assajos a dosi simple (*Figura 11*), exceptuant el compost **87** en que no es veien diferencies entre ambdós condicions.

En aquest punt vàrem decidir canviar algunes condicions experimentals com a un últim intent per intentar reproduir l'efecte observat a dosi única.

Així doncs, es varen generar dos assajos més de dosi-resposta per els compostosmes prometedors (**84** i **85**).

Fins ara, el protocol utilitzat en la dilució dels compostos en la placa de 96 era canviant les puntes de les micropipetes degut a la hidrofobicitat dels azobenzenes, el quals resten enganxats a la punta. Aquest fet podia provocar un canvi de concentracions de cada pou. Així, en el nou protocol es va realitzar sense canvi de puntes de micro pipeta (WCT). A més, es va incloure un nou assaig on es van avaluar els compostos incubant 60 minuts enlloc de 30, variant així lleugerament el protocol inicial (LIT) (*Figura 13*).

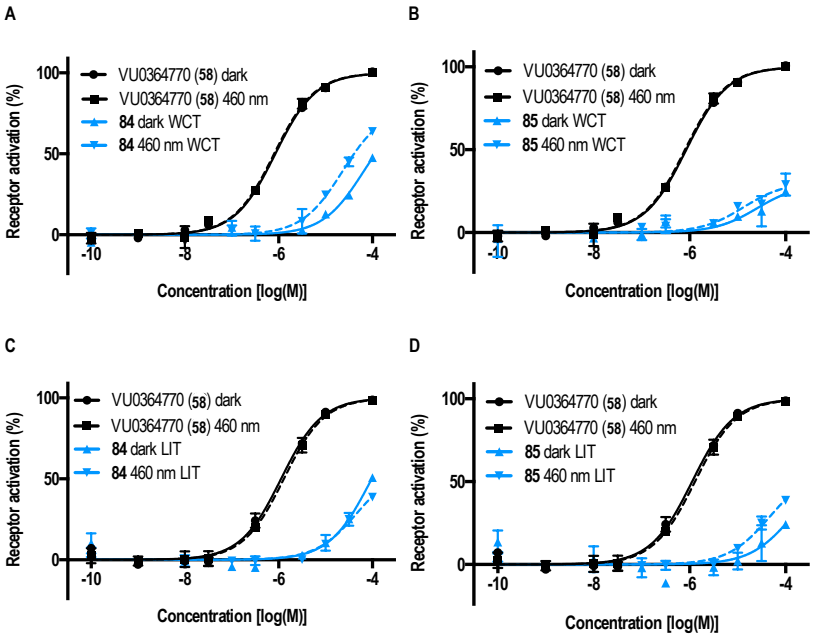

Figura 13: Corbes dosi-resposta dels compostos **84** i **85** utilitzant el protocol "sense canvi de puntes" (WCT) (A,B) i amb "temps llargs d'incubació" (LIT) (C,D) en assajos de IP-One en cèl·lules HEK293 sobrexpressant $mGlu_4$ amb una concentració constant de L-AP_4 (**4**) 3 nM. Línies contínues corresponen a les mostres incubades en condicions fosques i les línies discontinues a les incubades en condicions de irradiació a 460 nm. Cada punt correspont a la mitjana de mínim de 3 replicats independents amb el corresponent SEM com a barres d'error.

Ara sí, el canvi de protocol va permetre poder obtenir més diferencies entre ambdues condicions, especialment pel compost **84** (*Figura 13A*) en WCT i pel compost **84** en LIT (*Figura 13D*).

Ara bé, tot i que aquests compostos es podien considerar un bon punt de partida, la potencia obtinguda no va ser l'adient per tal de poder observar-n'he un efecte cis-on clar. Així doncs, es va fer un nou disseny basat en l'estructura del compost **84** i tenint en compte també altres compostos de referencia on bàsicament es varen fer incorporacions de diferents grups funcionals en un anell aromàtic per tal de potenciar-ne la diferencia entre condicions fosques i amb irradiació (*Figura 14*).

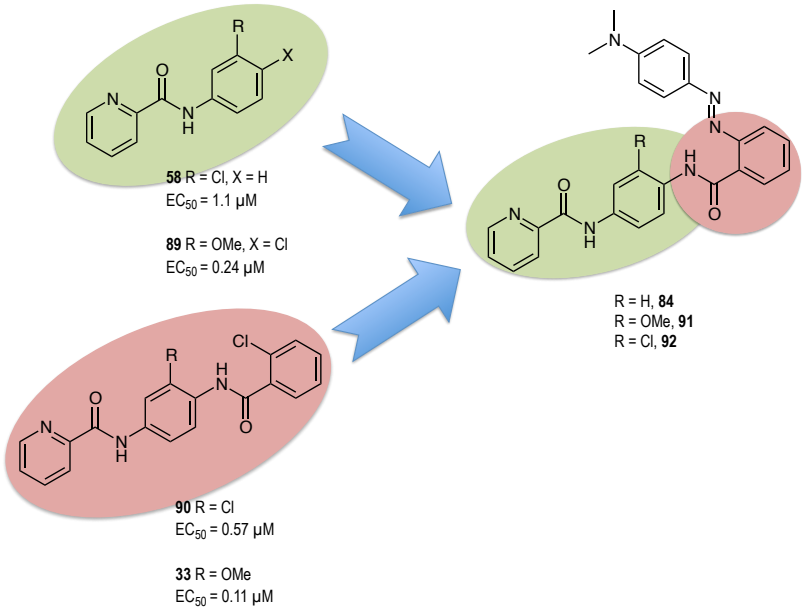

Figura14: Diseny de nous compostos *cis-on* com a PAMs de $mGlu_4$ basats en el compost **84** descrit anteriorment.

Així doncs, es van sintetitzar els compostos **91** i **92** i es va mesurar els màxims d'absorció dels dos compostos nous generats en comparació amb el compost ja descrit **84**. Com es pot observar en la *Figura 15*, els compostos sintetitzats presentaven bandes d'absorció sobre el rang del visible, al igual que el seu precursor **84**.

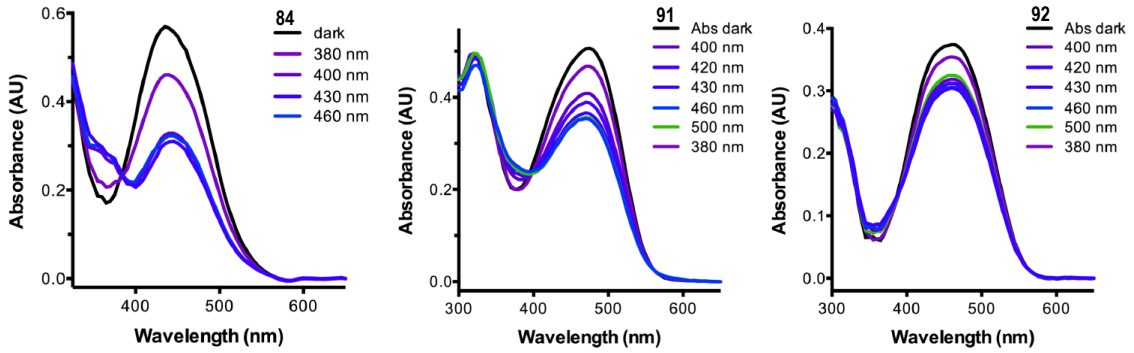

Figura 15: Espectre UV-Vis d'absorció dels compostos **84**, **91** i **92** en condicions fosques i amb diferents longituds d'ona.

Un cop caracteritzats fotoquímicament, es va avaluar la seva activitat en assajos d'acumulació de IP-One en cèl·lules HEK293 sobrexpressant $mGlu_4$, generant dosis-resposta per ambdós compostos en condicions fosques i d'il·luminació a 460 nm.

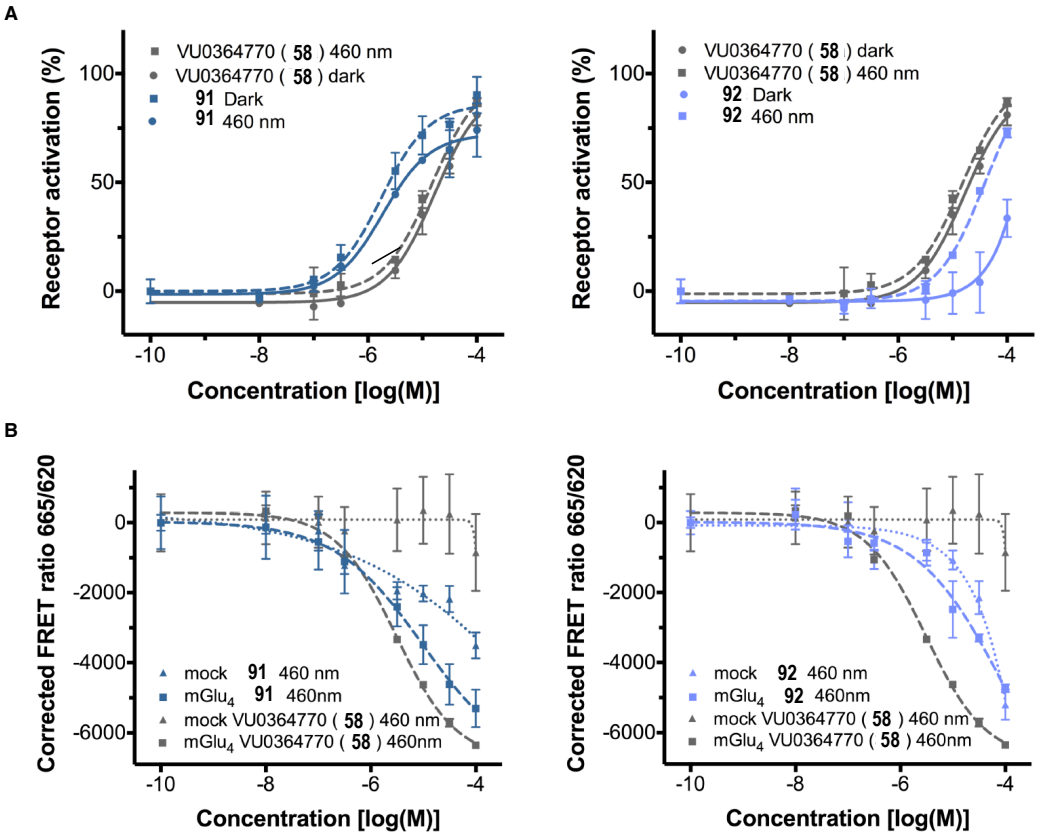

Figura 16: Corbes dosi-resposta en assajos de IP-One dels compostos **91** i **92**. A) Corbes dosi-resposta en assajos amb cèl·lules HEK293 sobrexpressant $mGlu_4$ amb concentracions constants del agonista selectiu L-AP_4 (**4**) 3 nM. Línies continues son les mostres incubades en condicions fosques i les línies discontinues les il·luminades a 460 nm. Cada punt correspon a la mitjana d'un mínim de tres replicats independents amb la SEM corresponent com a barres d'error. B) Corbes dosi-resposta en assajos amb cèl·lules HEK293 sense expressió de $mGlu_4$ amb concentracions constants del agonista selectiu L-AP_4 (**4**) 3 nM. Línies continues son les mostres incubades en condicions fosques i les línies discontinues les il·luminades a 460 nm. Cada punt correspon a la mitjana d'un mínim de tres replicats independents amb la SEM corresponent com a barres d'error.

En la *Figura 16A*, es va observar un increment en l'efecte *cis*-on en el dos compostos generats. Finalment, es varen fer uns assajos per descartar que els efectes observats no fossin produïts per efectes inespecífics (*Figura 16B*).

Desafortunadament, l'activitat observada va ser produïda per efectes inespecífics involucrats en la producció de IP.

Primera aproximació *cis-on* com a nous compostos terapèutics

La necessitat de síntesis de compostos fotocommutables, va fer replantejar-nos l'estratègia en el disseny per evitar els possibles efectes no específics obtinguts anteriorment.

En aquest cas vàrem canviar l'aproximació de l'azo-extensió pel canvi de grups funcionals a grups azo. Conseqüentment la potencia dels compostos es poden veure afectats degut aquest canvi, però a la vegada obtenint un nou punt de partida.

Així doncs, ens vàrem centrar en el disseny de nous PAMs de $mGlu_4$ o NAMs de $mGlu_5$ involucrats en el tractament del dolor basant-nos en altres compostos ja descrits en la literatura.

De tots els compostos analitzats, es va optar per agafar com a punt de partida un PAM de $mGlu_4$ anomenat CD2267-0368 (**94**)[15] (*Figura 17*), Aquest estava basat en el PAM VU0155041 (**93**), i es va escollir perquè presentava un grup difenil éter, remplaçable per un grup azo ja que en la seva disposició *cis* tenen propietats estructurals molt semblants en qüestió de distància i angles d'enllaç, poden així mimetitzar la seva activitat biològica (*Figura 18*).

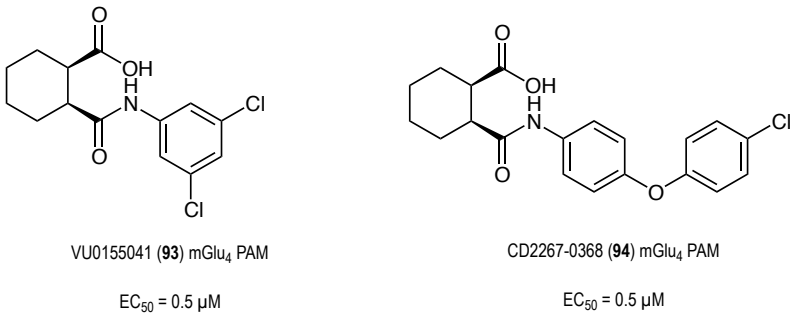

Figura 17: Estructures de PAMs selectius de $mGlu_4$

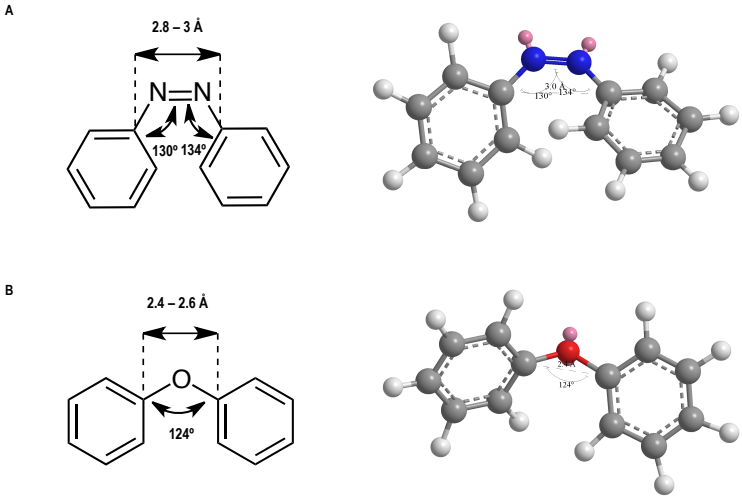

Figura 18: Estructura del azobenzè en disposició *cis* respecte estructura del difenil éter. A) Angle i distancia d'enllaç del azobenzè amb minimització d'energia MM2. B) Angle i distancia d'enllaç del difenil éter amb minimització d'energia MM2.

Així doncs, es varen dissenyar cinc compostos més, intercanviant els grups difenil éter per azobenzens.

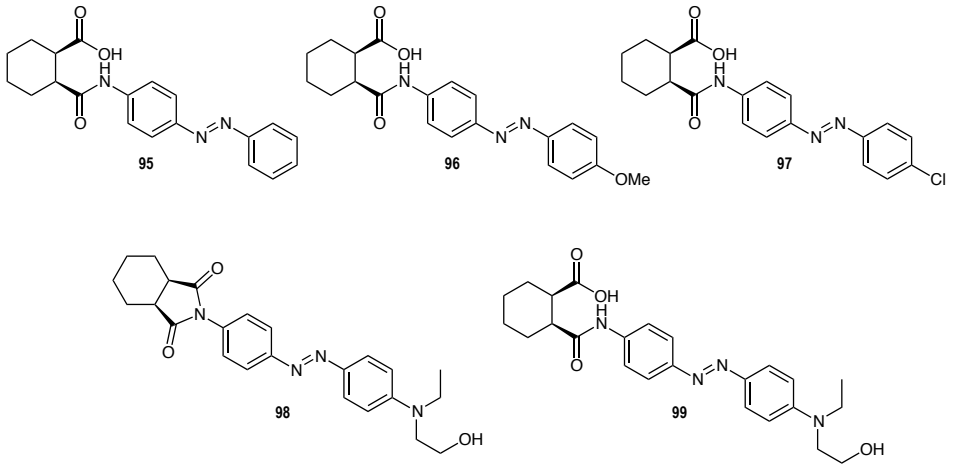

Figura19: Compostos dissenyats com a PAMs de $mGlu_4$ amb efectes *cis-on*.

Tots els compostos es van sintetitzar per obertura del anhídrid **100a** per part d'una azoanilina més o menys elaborada (*Esquemes 1*, *2*, *3* i *4*)

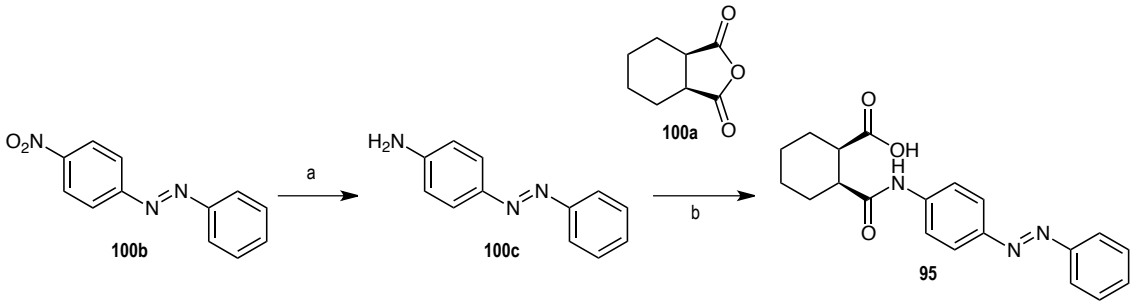

Esquema 1: Síntesis del compost **95**. Reactius i condicions: a) $Na_2S \cdot 9H_2O$, EtOH, reflux, 1h, 40%; b) **100a**, NEt_3, THF, reflux, 12 h, 41%.

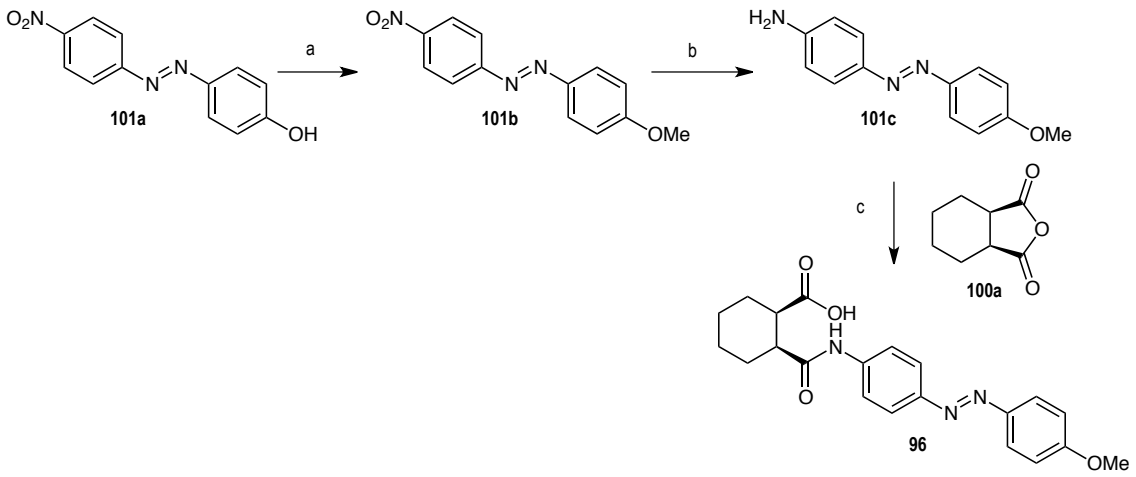

Esquema 2: Síntesis del compost **96**. Reactius i condicions: a) K_2CO_3, MeI, AcN, r.t., 12 h, 47%; b) $Na_2S \cdot 9H_2O$, EtOH, reflux, 1h, 37%; c) **100a**, NEt_3, THF, reflux, 12 h, 62%.

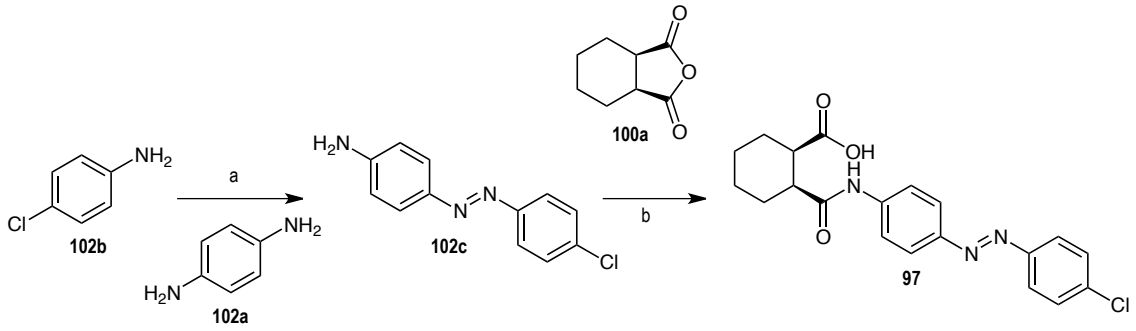

Esquema 3: Síntesis del compost **97**. Reactius i condicions: a) Oxone, DCM, AcOH, 24h, r.t., 45%; b) **100a**, NEt_3, THF, reflux, 12 h, 42%.

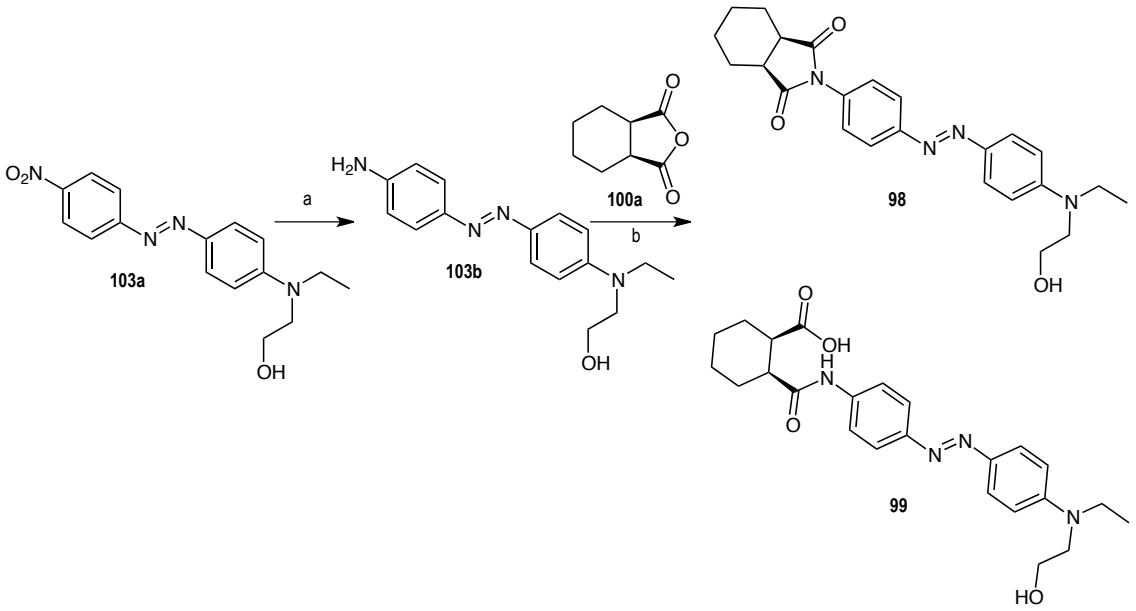

Esquema 4: Síntesis dels compostos **98** i **99**. Reactius i condicions: a) $Na_2S \cdot 9H_2O$, EtOH, reflux, 1h, 25%; b) **100a**, NEt_3, THF, reflux, 12 h, (**98**) - 7%, (**99**) - 45%.

Un cop es varen obtenir el compostos, vàrem avaluar la seva fotoquímica de isomerització en diferents condicions de llum, aplicant longituds d'ona de 380 nm per la isomerització de *trans* a *cis* i 500 nm per tornar a la configuració *trans*, en els compostos **95**, **96** i **97**, i longituds de 460 nm per isomeritzar de *trans* a *cis* i 380 nm per recuperar la disposició *trans* en els compostos **98** i **99** (*Figura 19*).

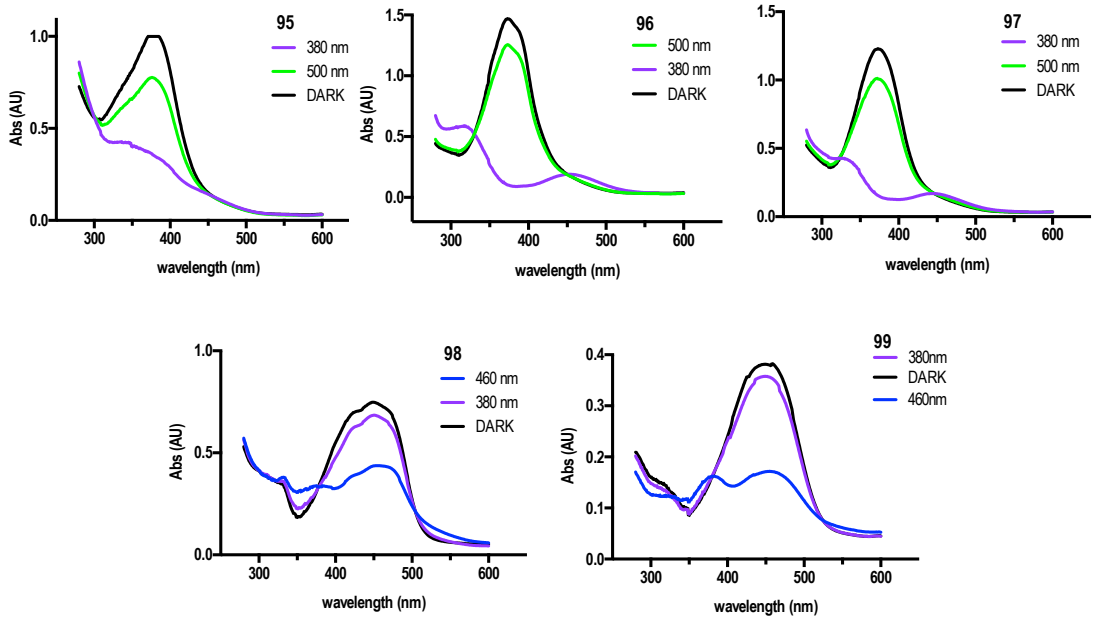

Figura 19: Caracterització fotoquímica dels compostos **95**, **96**, **97**,**98** i **99**. Espectre d'absorció UV-Vis en condicions fosques (línia negre), a 380 nm (línia violeta), a 500 nm (línia verda) per els compostos **95**, **96** i **97**. Espectre d'absorció UV-Vis en condicions fosques (línia negre), a 380 nm (línia violeta), a 460 nm (línia blava) per els compostos **98** i **99**.

Després de l'avaluació fotoquímica, es varen fer els assajos de dosi única mitjançant acumulació de IP-One amb cèl·lules HEK293 sobrexpressant $mGlu_4$ i $mGlu_5$ i mesurant l'activitat PAM i NAM per cadascun dels dos receptors en la corresponent longitud d'ona abans mesurada.

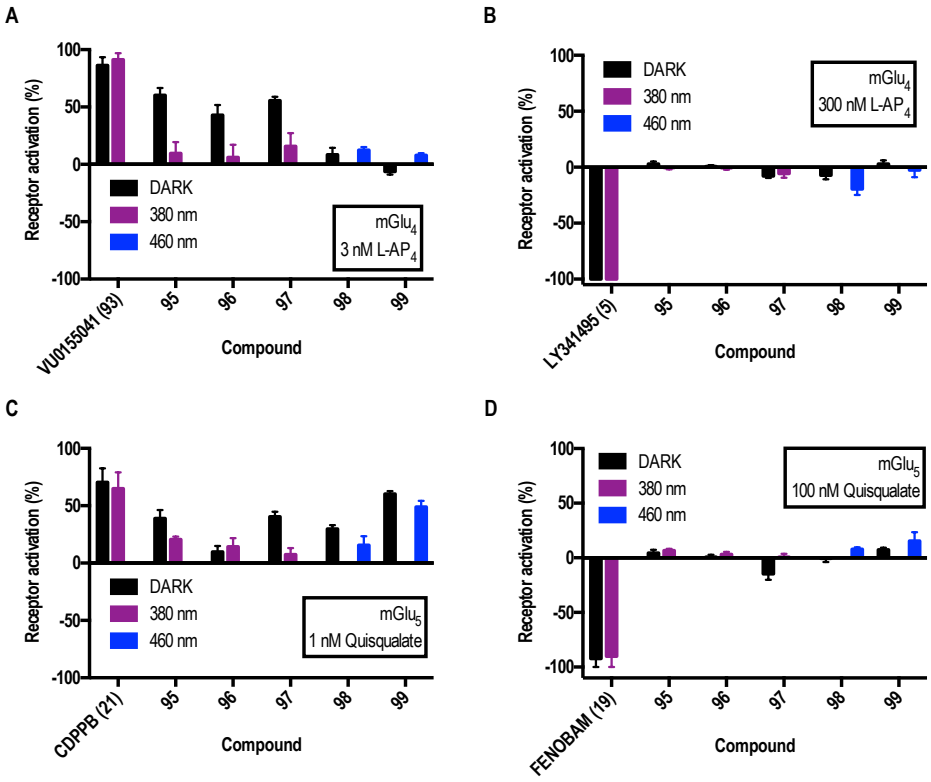

Figura 20: Experiments de dosi simple dels compostos **95**, **96**, **97**, **98** i **99**. A) Com a PAMs de $mGlu_4$, B) NAMs de $mGlu_4$, C) PAMs de $mGlu_5$ i D) NAMs de $mGlu_5$. La resposta de FRET es va normalitzar a 0%-100% entre l'efecte a concentració baixa d'agonista (EC_{20}) i l'efecte de saturació d'agonista per l'avaluació efecte de PAM . En canvi, per la del NAM, es va normalitzar a -100%-0% entre l'efecte de saturació de l'antagonista amb la concentració alta d'antagonista (EC_{80}). Cada barra correspon a la mitjana d'un mínim de dos replicats independents amb la SEM corresponent com a barres d'error.

Desafortunadament, un altre cop no vàrem obtenir un efecte prou significatiu entre ambdues condicions de irradiació. Tot i així, es va observar un efecte força moderat per els compostos **95**, **96** i **97** com a PAMs de $mGlu_4$ però amb un comportament *trans-on*. Encara que inicialment no era el que estàvem buscant, es van fer assajos de dosi-resposta dels tres compostos per comparar-n'he la seva activitat amb el compost de referencia VU0155041 (**93**) (*Figura 21*) i el descrit en la bibliografia CD2267-0368 (**94**).

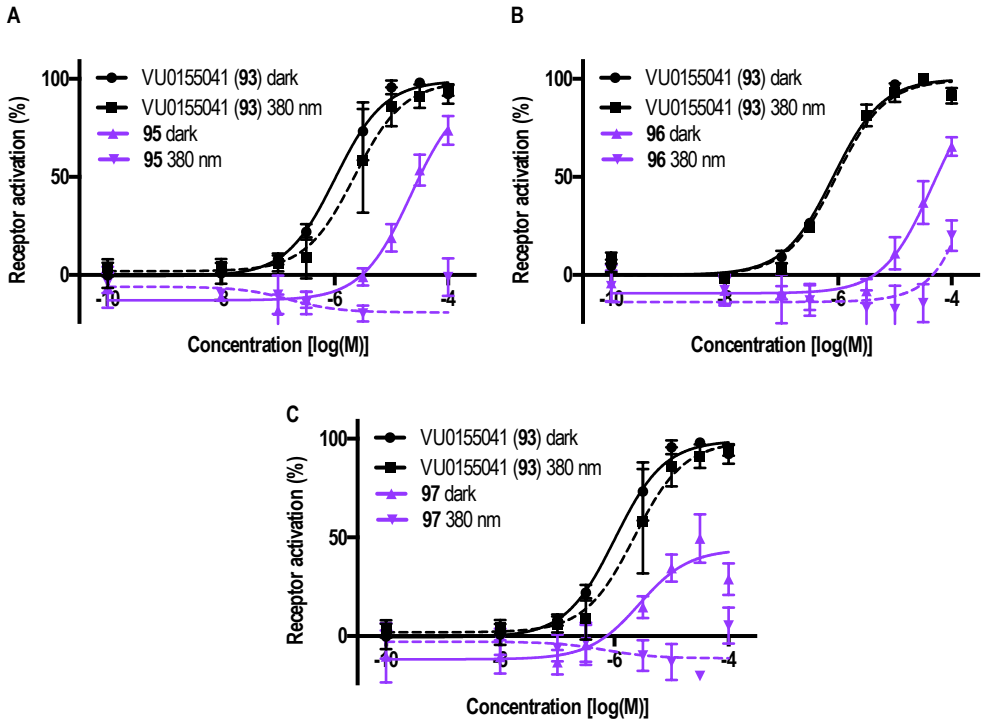

Figura 21: Corbes dosi-resposta en assajos de IP-One en cèl·lules HEK293 sobrexpressant $mGlu_4$ amb concentracions constants del agonista selectiu L-AP_4 (**4**) 3 nM. Línies continues son les mostres incubades en condicions fosques i les línies discontinues les il·luminades a 380 nm. Cada punt correspon a la mitjana d'un mínim de tres replicats independents amb la SEM corresponent com a barres d'error.

Els compostos **95** (EC_{50} = 22 μM) i **96** (EC_{50} = 46 μM) varen perdre quasi tota l'activitat respecte el compost de referència **94** (EC_{50} = 0.5 μM)[15] mostrant efectes importants en concentracions elevades probablement degut a efectes no específics. En canvi, el derivat **97** (EC_{50} = 2.7 μM) es va mantenir proper a la potencia del compost referencia, tot i que amb efecte parcial com a PAM de $mGlu_4$.

Malgrat que no es va poder obtenir azocompostos *cis*-on desitjats, els resultats obtinguts ens varen donar un coneixement de com haurien de estar constituïts els PAMs per presentar una bona interacció amb la proteïna. D'una banda, els substituent en posició *para* respecte el azobenzè sembla ser força important per la seva activitat, per tant, tant si és substituït per grups donadors, llargs o si simplement és eliminat, es perd d'activitat. D'altre banda, mantenint un clor en posició *para* al azobenzè, l'activitat es manté quasi bé en el mateix ordre que el compost referencia **94**, com ja s'esperava per homologia estructural on el difenil éter conté en posició para un grup clor.

En definitiva, la substitució dels azobenzens per grups de difenil éter sembla no fer perdre l'activitat, encara que el isòmer *trans* segueixin sent la disposició activa en la seva activitat funcional.

Finalment, en un últim intent de poder veure un efecte significatiu *cis*-on, vàrem seguir mantenint la teoria sobre el canvi funcional de un grup difenil éter basat en el compost de referència **94**, però explorant altres posicions dins l'anell aromàtic (*orto* **104**, *meta* **105**, i *para* **106**). D'aquesta forma, es pretén mimetitzar totes les possible disposicions del grup éter dins el receptor degut a la seva lliure mobilitat en la rotació del enllaç del oxigen respecte cada un dels anells aromàtics on amb el azobenzè queda més restringit, i d'aquesta manera veure alguna diferència (*Figura 22*).

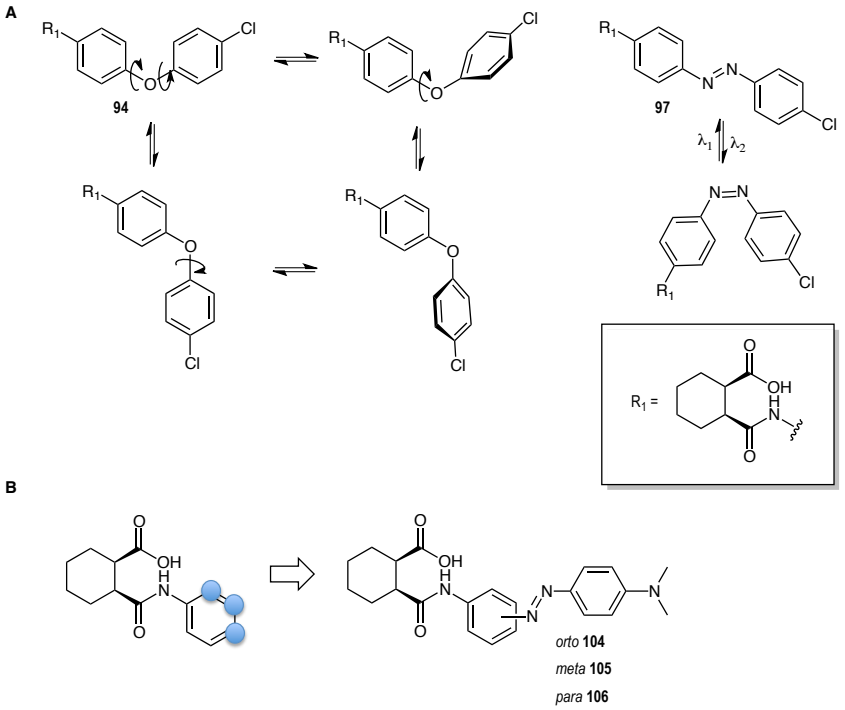

Figura 22: A) Possible mobilitat del compost **94** dins el receptor sobre el l'eix dels enllaços dels anells aromàtics amb el oxigen i en comparació amb el corresponent azoderivat **97**. B) Estructures dels nous azocompostos amb possibles efectes *cis-on* per estudiar les diferències entre les substitucions aromàtiques.

Al mateix temps, degut al gran nombre de intermitjos de azobenzens generats fins ara, vàrem pensar que podia ser interessant sintetitzar una llibreria de azocompostos com a PAMs de $mGlu_4$ basant-nos en altres compostos prèviament descrits en la literatura. Un grup altament estudiat en compostos PAM de $mGlu_4$ és l'amida del àcid picolínic (*Figura 23*) tal i com s'ha observat anteriorment en azobenzens com l'optogluram (**59**) descrit per Xavi Gomez.

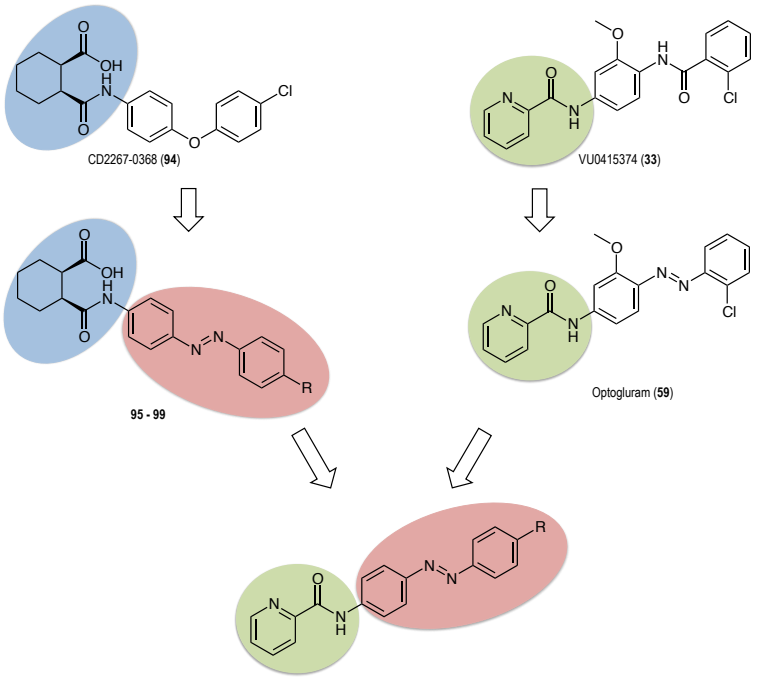

Figura 23: Nou disseny estructural en la llibreria de azocompostos com a PAMs de $mGlu_4$.

D'aquesta manera, es varen generar els azocompostos en exposats en la *Figura 24*.

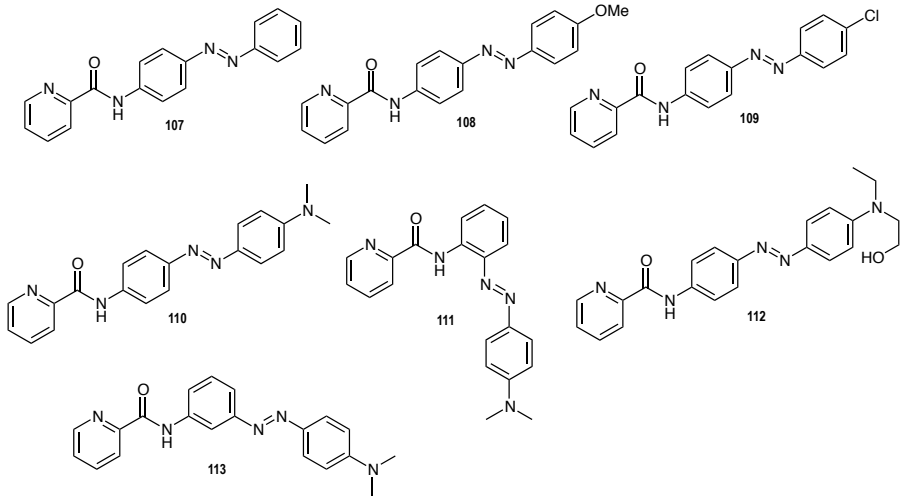

Figura 24: Estructures de la llibreria dels azocompostos com a PAMs de $mGlu_4$.

D'altre banda, també es va pensar en generar dos estructures més que fossin PAMs de $mGlu_5$ basant-nos novament en compostos descrits en la bibliografia, degut a la manca de azocompostos desenvolupant aquesta activitat funcional. Així, en el primer cas vàrem seguir utilitzant la mateixa aproximació utilitzada fins ara canviant l'amida per azobenzens (*Figura 25*). En el segon cas ens vàrem basar en l'alloswitch-1 (**34**) canviant una piridina per un anell fluorofenil esperant observar un canvi de NAM a PAM de $mGlu_5$.

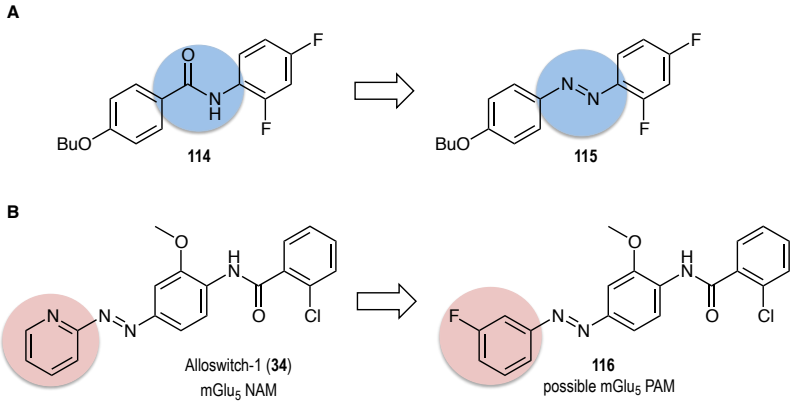

Figura 25: Estructures i disseny per la llibreria de azocompostos com a PAMs de $mGlu_5$.

Novament, els compostos **104**, **105** i **106** es van obtenir per l'obertura de l'anhídrid **100a** en azoanilines més o menys elaborades (*Esquemes 5* i *6*).

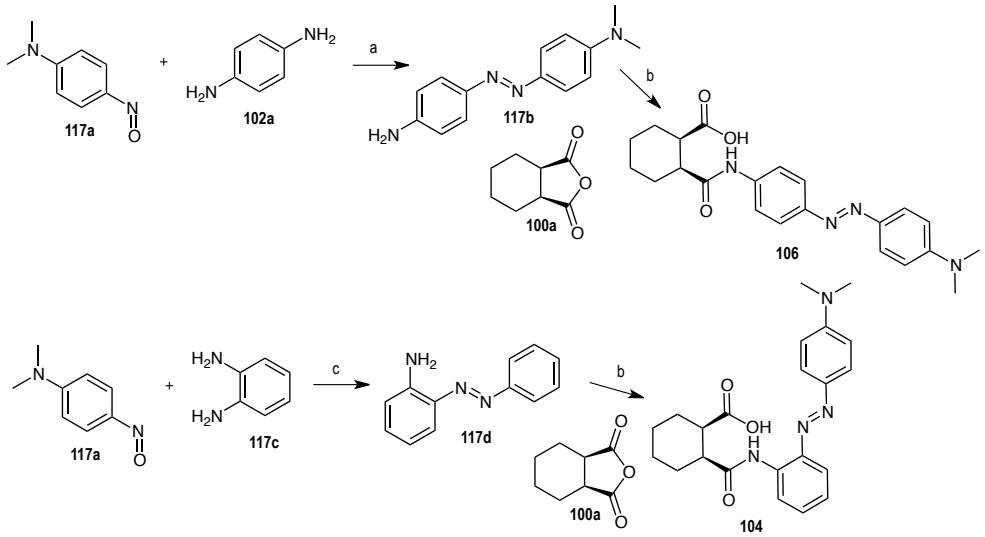

Esquema 5: Síntesis de **104** i **106**. Reactius i condicions: a) AcOH, DCM r.t., 24h, 20%; b) **100a**, NEt_3,THF, reflux, 12 h, (**104**)- 28%, (**106**)- 41%; c) (i) KOH (sense disolvent); (ii) toluene 90ºC, 1h, 57%.

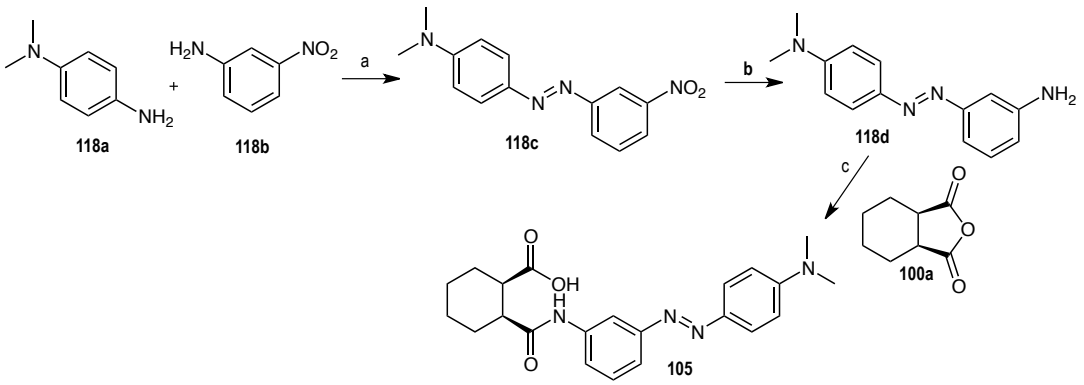

Esquema 6: Síntesis de **105**. Reactius i condicions: a) Oxone, DCM, AcOH, 24h, r.t. 45%; b) $Na_2S \cdot 9H_2O$, EtOH, reflux, 1h, 69%; c) **100a**, NEt_3, THF, reflux, 12 h, 35%.

Els compostos **107** fins **113** varen ser sintetitzats seguint el procediment descrit anteriorment en l'*esquema 7*. Tots els azobenzens intermitjos sintetitzats fins ara es van fer reaccionar amb clorur d'àcid picolínic obtenint tots els compostos entre un 10-26% de rendiment.

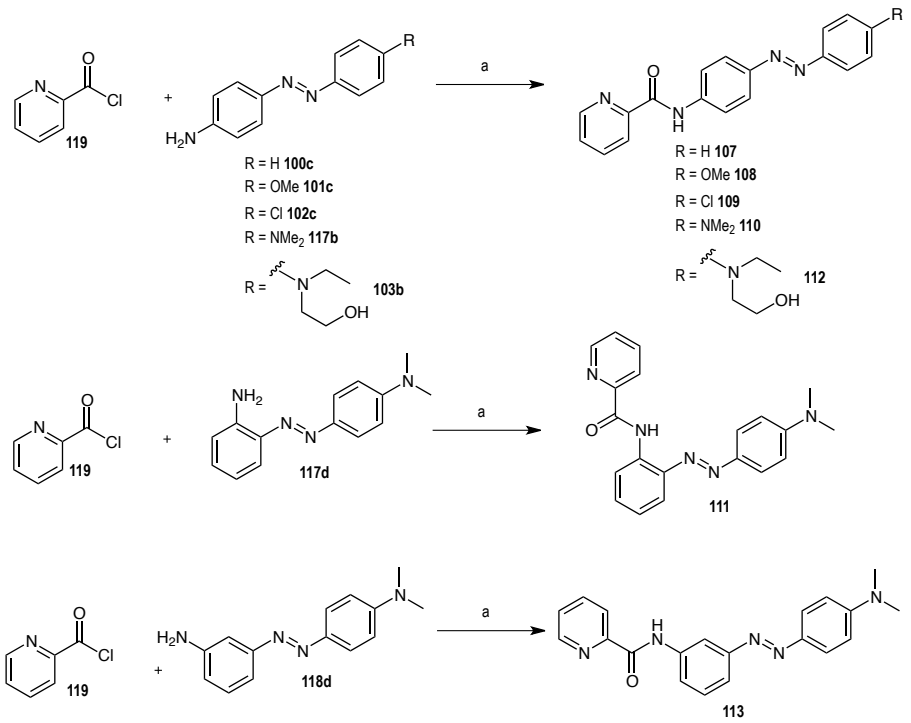

Esquema 7: Síntesis de **107**, **108**, **109**, **110**, **111**, **112** i **113**. Reactius i condicions: a) NEt_3, DCM 40ºC, 24h, (**107**)- 10%, (**108**)- 15%, (**109**)- 11%, (**110**)- 22%, (**111**)- 22%, (**112**)- 13%, (**113**)- 26%.

Finalment els compostos **115** i **116** varen ser preparats com es descriu en el *esquema 8*.

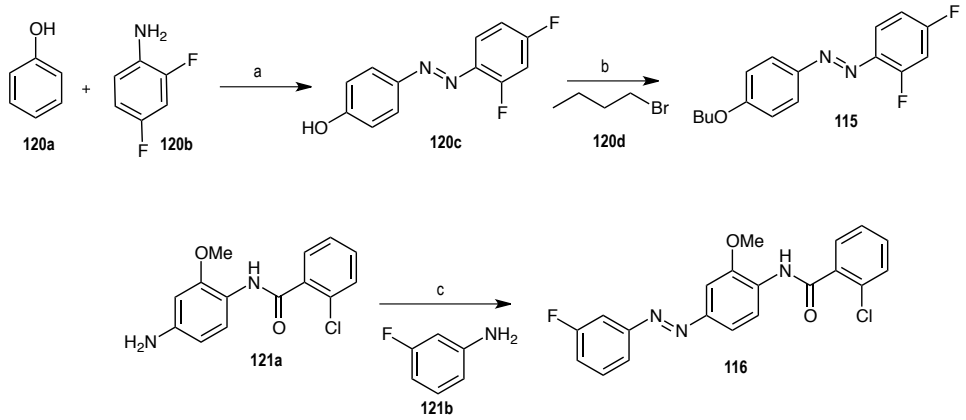

Esquema 8: Síntesis dels compostos **115** i **116**. Reactius i condicions: a) $NaNO_2$, NaOH, HCl, H_2O 0ºC, 2h, 41%; b) K_2CO_3, DMF r.t., 24h, 68%, c) Oxone, DCM, AcOH, 24h, r.t. 42%.

Després de tota la síntesis, es va tornar a caracteritzar els compostos fotoquímicament. En primer lloc es varen fer en condicions fosques i després es va analitzar la isomerització per cadascun d'ells havent-n'he d'irradiar a 460 nm per la transició *trans* a *cis* i a 380 nm per tornar a la disposició *trans* en els compostos amb propietats push-pull **104**, **105**, **106**, **110**, **112** i **113** (*Figura 26*).

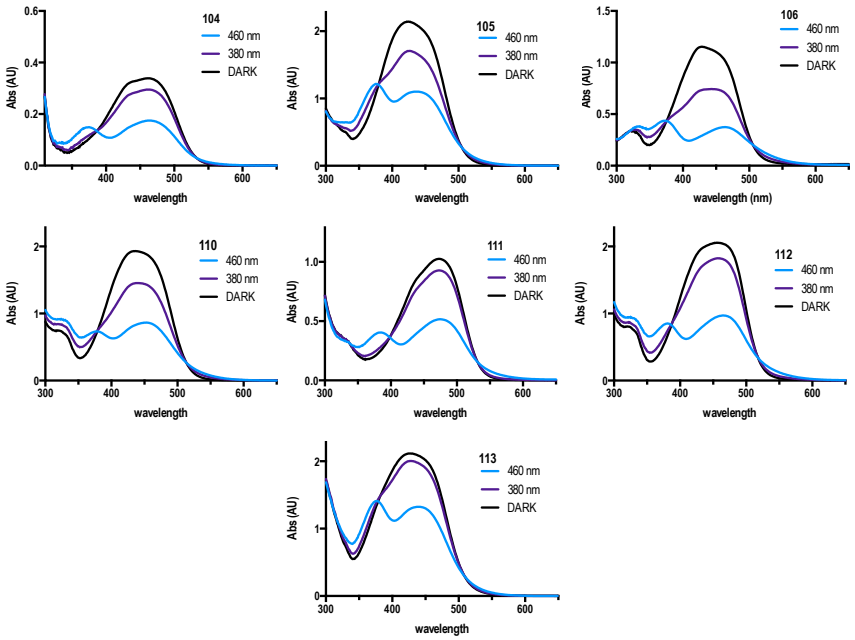

Figura 26: Caracterització fotoquímica dels compostos **104**, **105**, **106**, **110**, **112** i **113**. Espectre d'absorció UV-Vis en condicions fosques (línia negre), sota 460 nm (línia blava) i sota 380 nm (línia violeta).

D'altre banda, com va ser d'esperar en els compostos **107**, **108**, **109**, **115** i **116**, la transició de *trans* a *cis* es va fer irradiant a 380 nm mentre que per tornar a la configuració incial es va irradiar a 500 nm.

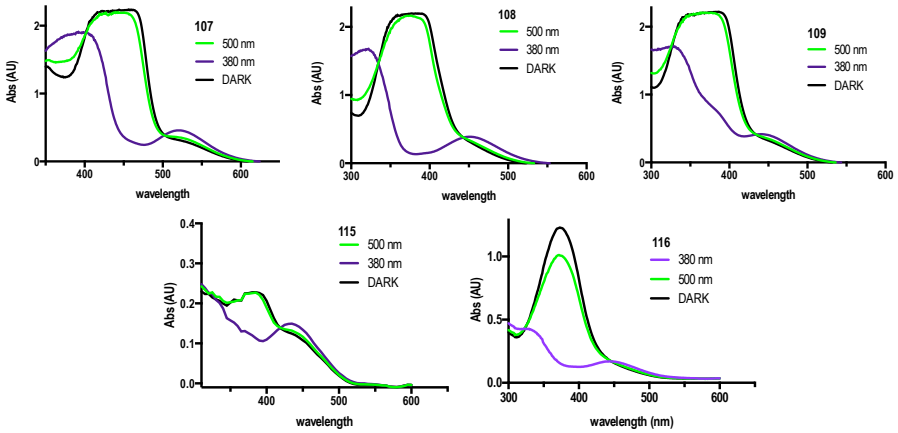

Figura 27: Caracterització fotoquímica dels compostos **107**, **108**, **109**, **115** i **116**. Espectre d'absorció UV-Vis en condicions fosques (línia negre), sota 380 nm (línia violeta) i sota 500 nm (línia verda).

Després de la caracterització fotoquímica, es van realitzar els assajos farmacològics a dosi simple mitjançant acumulació de IP-One en cèl·lules HEK293 sobrexpressant $mGlu_4$ i $mGlu_5$ com a PAMs i NAMs de cada un dels receptors i a la longitud d'ona corresponent de cada compost (*Figura 28*).

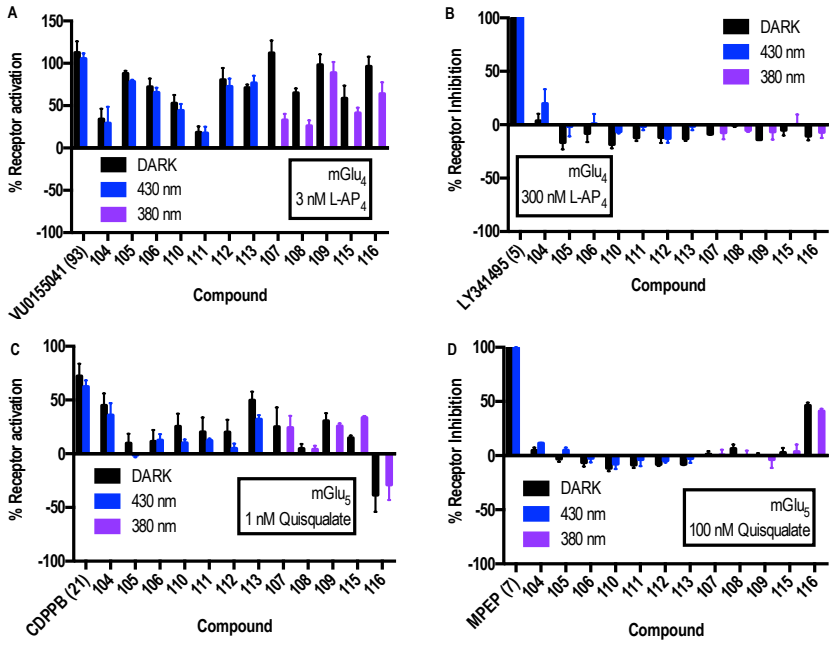

Figura 28: Experiments de dosi simple dels compostos **104** a **116**. A) Com a PAMs de $mGlu_4$, B) NAMs de $mGlu_4$, C) PAMs de $mGlu_5$ i D) NAMs de $mGlu_5$. La resposta de FRET es va normalitzar a 0%-100% entre l'efecte a concentració baixa d'agonista (EC_{20}) i l'efecte de saturació d'agonista per l'avaluació efecte de PAM . En canvi, per la del NAM, es va normalitzar a 0%-100% entre l'efecte de saturació de l'antagonista amb la concentració alta d'antagonista (EC_{80}). Cada barra correspon a la mitjana d'un mínim de dos replicats independents amb la SEM corresponent com a barres d'error.

Desafortunadament, un altre cop no es varen observar activitats *cis-on* excepte pels compostos **104** com a NAM de $mGlu_4$ i **115** com a PAM de $mGlu_5$, on es va poder veure una mica de tendència encara que no significativa per l'augment d'activitat del isòmer *cis* respecte el *trans*. També es va poder comprovar que alguns compostos de la llibreria com **107**, **109** i **116** varen ésser compostos amb bona activitat i d'altres com **112** i **113** amb una activitat moderada com a PAMs de $mGlu_4$, però amb activitat *trans-on* en algun d'ells o sense diferencia. Sorprenentment, el compost com el **116** va mostrar una bona activitat no tan sols com a NAM de $mGlu_5$ sinó

també com a PAM de $mGlu_4$ tot i que va ser dissenyat com a PAM de $mGlu_5$, aquesta activitat dual poden donar lloc a estudis com un neuroprotector.

Tots i els bons resultats en la llibreria, ens vàrem centrar en caracteritzar per dosi resposta els compostos que vàrem obtenir una tendència *cis-on* amb assajos de acumulació de IP-One amb cèl·lules HEK293 transfectades amb $mGlu_4$ pel compost **104** i amb $mGlu_5$ pel compost **115** com a NAM i PAM respectivament (*Figura 29A*) . A la vegada també es van fer per tots dos casos experiments de control negatiu per comprovar si son efectes inespecífics (control MOCK) (*Figura 29B*).

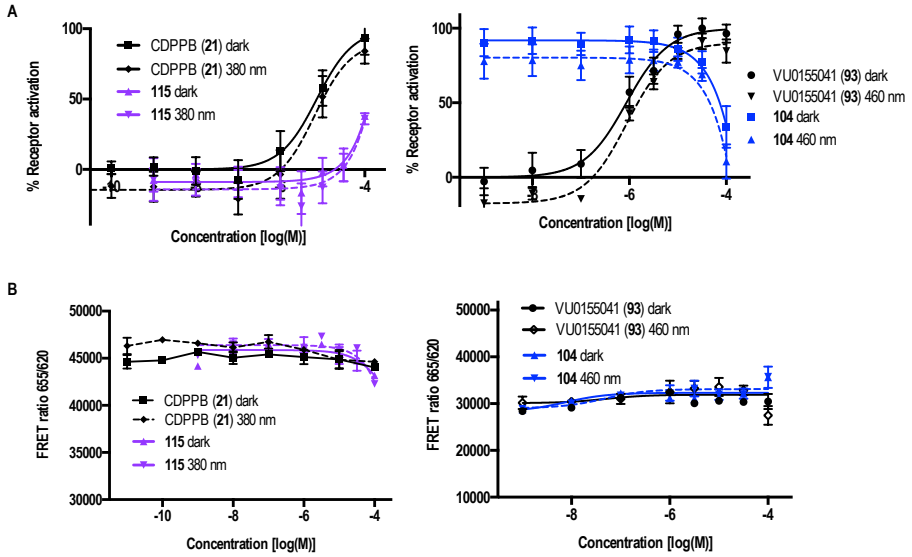

Figura 29: Corbes dosi resposta amb assaig de IP-One en cèl·lules HEK293 amb els compostos **104** i **115** utilitzant VU0155041 (**93**) com a referència de $mGlu_4$ i CDPPB (**21**) com referència de $mGlu_5$. A) Dosi-resposta utilitzant cèl·lules HEK293 sobrexpressant $mGlu_5$ per **115** amb concentració constant d'agonista selectiu quisqualat (**2**) 100 nM i cèl·lules HEK293 sobrexpressant $mGlu_4$ per **104** amb concentració constant d'agonista selectiu L-AP_4 (**4**) 300 nM i 3 nM per el compost de referència **93**. Línies continues son les mostres incubades en condicions fosques i les línies discontinues les il·luminades a 460 nm per **104** i 380 nm per **115**. Cada punt correspon a la mitjana d'un mínim de tres replicats independents amb la SEM corresponent com a barres d'error. B) Dosi-resposta utilitzant cèl·lules HEK293 sense sobrexpressió de $mGlu_5$ per **115** amb concentració constant d'agonista selectiu quisqualat (**2**) 100 nM i cèl·lules HEK293 sense sobrexpressió de $mGlu_4$ per **104** amb concentració constant d'agonista selectiu L-AP_4 (**4**) 300 nM i 3 nM per el compost de referència **93**. Línies continues son les mostres incubades en condicions fosques i les línies discontinues les il·luminades a 460 nm per **104** i 380 nm per **115**. Cada punt correspon a la mitjana d'un mínim de tres replicats independents amb la SEM corresponent com a barres d'error.

En ambdós casos, no es va poder tornar a observar la diferència entre els assajos en condicions fosques i les irradiades. Les avaluacions fetes per els efectes inespecífics en cèl·lules HEK293 amb transfecció de plàsmid de DNA buit però, van mostrar algun efecte en altes concentracions,

significant doncs un altre cop que el efectes observat a dosi única es degut probablement a un altre receptor que esta involucrat amb la producció de IP.

Conclusions

Es van avaluar mitjançant assajos de dosi única en $mGlu_4$ i $mGlu_5$ pels compostos **84**, **85**, **86**, **87** i **88** en condicions fosques i d'il·luminació, amb suposat comportament *cis*-on per aquests receptors obtenint dos compostos prometedors (**84** i **85**) com a PAMs de $mGlu_4$ mostrant un increment en l'activitat en il·luminació. Ambdós compostos es van assajar mitjançant corbes dosi resposta, on no es va poder observar un efecte *cis*-on clar.

Es van dissenyar, sintetitzar i avaluar en dosi resposta dos compostos nous (**91** i **92**) com a PAMs de $mGlu_4$ obtenint resultats positius com a *cis*-on. Aquests bons resultats no varen ser confirmats en el control negatiu utilitzant assajos de IPone sense sobrexpressar el receptor, on es va obtenir resultats semblants als mostrats amb cèl·lules expressant $mGlu_4$. Així doncs, l'activitat *cis*-on va ser atribuït a efectes no específics induint una resposta en l'assaig de IPone.

Vam dissenyar i sintetitzar els compostos **95**, **96**, **97**, **98** i **99** amb suposat comportament *cis*-on com a PAMs de $mGlu_4$. Varen ser caracteritzats les seves propietats fotoquímiques i les farmacològiques mitjançant assajos de dosi única primer, i corbes dosi resposta després, per avaluar-ne el comportament però, desafortunadament, tots els compostos varen mostra una activitat *trans*-on.

Vàrem dissenyar i sintetitzar els compostos **104**, **105** i **106** per obtenir un comportament *cis*-on com a PAMs de $mGlu_4$. A més, els compostos de **107** fins a **116** varen ser dissenyats i sintetitzats per una llibreria de compostos fotocommutables com a PAMs de $mGlu_4$ i $mGlu_5$. Tots els compostos varen ser caracteritzats fotoquímicament i també la seves propietats farmacològiques en receptors de $mGlu_4$ i $mGlu_5$. Els compostos **104** i **115** van ser avaluats amb corbes dosi resposta degut a la petita tendència en l'activitat *cis*-on. Aquests resultats no varen ser confirmats en controls negatius en absència del receptor corresponent. Així doncs l'activitat observada es va atribuir a efectes inespecífics.

Capítol 2: Compostos gàbia per moduladors al·lostèrics del Glutamat.

Els objectius marcats per aquest capítol van ser dissenyar i sintetitzar nous compostos gàbia com a NAMs i PAMs per a receptors metabotròpics dels glutamat subtipus 5, 1 i 4 respectivament, involucrats en el tractament contra el dolor.

Els compostos gàbia són molècules en les quals la seva activitat biològica està controlada per llum per conversió fotolítica de forma inactiva a forma activa.

Es basen en els conceptes següents: o bé són molècules actives atrapades en complexos estructurals que són oberts o destruïts per llum (*Figura 30A*) o bé són molècules actives unides covalentment a un residu obtenint-se un compost inactiu que es destrueix lliberant la molècula activa per efecte de la llum (*Figura 30B*)[16].

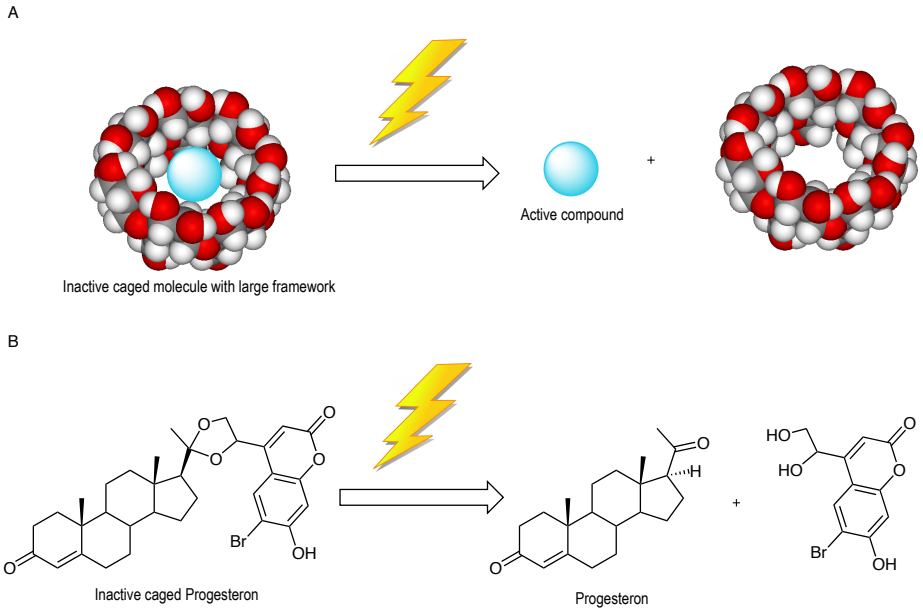

Figura30: Exemples dels dos tipus de compostos gàbia. A) Compostos actius atrapats en un gran complex molecular. B) Compostos gàbia atrapats per un enllaç covalent.

Els compostos gàbia són molt útils des del punt de vista biològic ja que poden ser alliberats amb un control de temps, espai i amplitud.

Per la utilització d'aquests tipus de compostos a nivell biològic han de complir un compost de condicions: El compost gàbia ha de romandre inerta en el sistema biològic, la fotòlisis ha de tenir un bon rendiment d'alliberament en longituds d'ona no perilloses pel sistema i els residus fotoquímics del alliberament no han de interferir o interactuar amb el sistema biològic.

Com bé sabem la llum UV profunda (250-300 nm) a pesar de ser la més energètica, és també la més perillosa podent afectar altres biomolècules esteses per l'organisme. Així doncs l'importància de fer alliberament al rang del visible és crucial (380 nm fins a 650 nm) per tal de no veures afectat, i a més podem obtenir ones més penetrants en teixits (*Figura 32*).

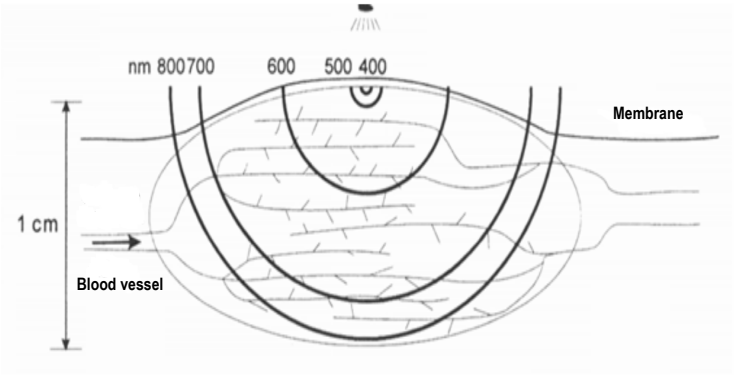

Figura32: Representació de diferents longituds d'one respecta la seva penetració en teixits.

Per aquests fets, avui dia diferents tipus de molècules per fer atrapaments sobre biomolècules s'han desenvolupat al llarg dels anys. A pesar de l'existència de múltiples molècules fotolàbils en la present tesis ens hem centrat en dos: Els derivats de nitrobenzil i de coumarina[17].

Els derivats de nitrobenzyl (*Figura33*), varen ser desenvolupats per l'alliberament de lligands biològicament actius a prop del rang del UV (de 300 a 400 nm) com per exemple fosfats, àcids carboxílics, amides, alcohols i carbonils com també ions metàl·lics. Aquesta família al ser hidrofòbica, mostra poca estabilitat. Per aquest fet normalment s'uneixen als compostos actius via carbamat amb aminoàcids, tot i que la seva cinètica de fragmentació restringeix la seva aplicació al ús de senyalització de bioprocessos[18].

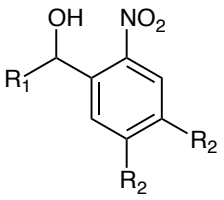

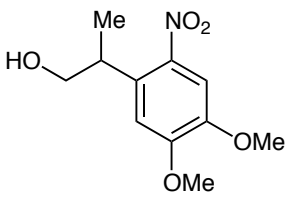

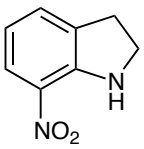

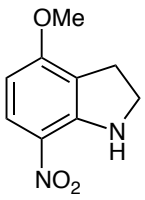

122a R_1 = H; R_2 = H (NB-OH)
122b R_1 = COOH; R_2 = H (CNB-OH)
122c R_1 = Me; R_2 = H (NPE-OH)
122d R_1 = H; R_2 = OMe (DMNB-OH)
122e R_1 = Me; R_2 = OMe (DMNPE-OH)

122f

124a NI

124b MNI

Figura33: Alguns exemples de molècules fotolàbils que pertanyen a la família de nitrobenzils.

D'altre banda, la família de coumarines (*Figura 34*) va ser desenvolupats per el atrapament de molts compostos biològics amb grups tals com fosfats, carboxilats, amines, alcohols, fenols i carbonils. A diferència de la família dels nitrobenzils, en aquest cas es poden assolir fàcilment longituds d'ona molt més properes al visible. Dins d'aquesta família podem distingir-ne quatre grups amb diferents propietats fisiològiques i fotoquímiques[17].

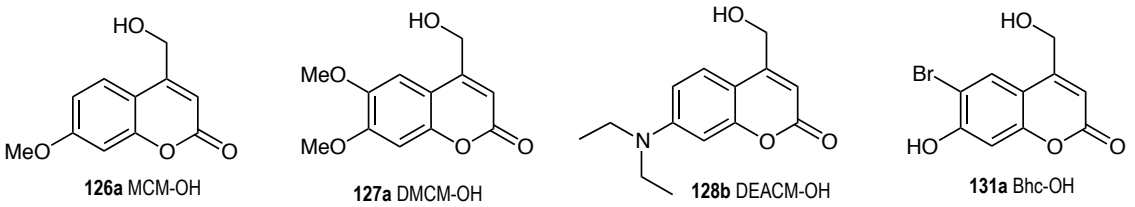

Figura34: Alguns exemples de molècules fotolàbils que pertanyen a la família de les coumarines.

Així doncs, primer de tot vàrem fer una recerca bibliogràfica per trobar un modulador al·lostèric negatiu de $mGlu_5$ degut a la funcionalitat analgèsica per el tractament del dolor prèviament esmentat.

El compost s'hauria de modificar un enllaç covalent per emmascarar-n'he la seva activitat biològica, per aquesta raó hi havia algunes condicions farmacològiques i estructurals tals com tenir una activitat funcional important (del ordre nanomolar), ser inert en presencia de llum i la més important tenir un grup funcional modificable per enllaçar amb la nostre molècula gàbia.

Sota aquests requeriments, finalment vàrem optar per el compost ADX10059 o també anomenat Raseglurant (**18**), complia tots els punts descrits anteriorment, sent un potent NAM de $mGlu_5$ (IC_{50} = 10 nM), ningun efecte descrit sota irradiació i la presencia de una aminopiridina que podia ser fàcilment modificada per unir-la al grup fotolàbil.

El disseny es va fer per a quatre compostos gàbia que estiguessin repartits al llarg del espectre del UV-Visible generant el compost gàbia inactiu mitjançant un carbamat com a pont d'unió per la seva bona cinètica d'alliberament en medis fisiològics.

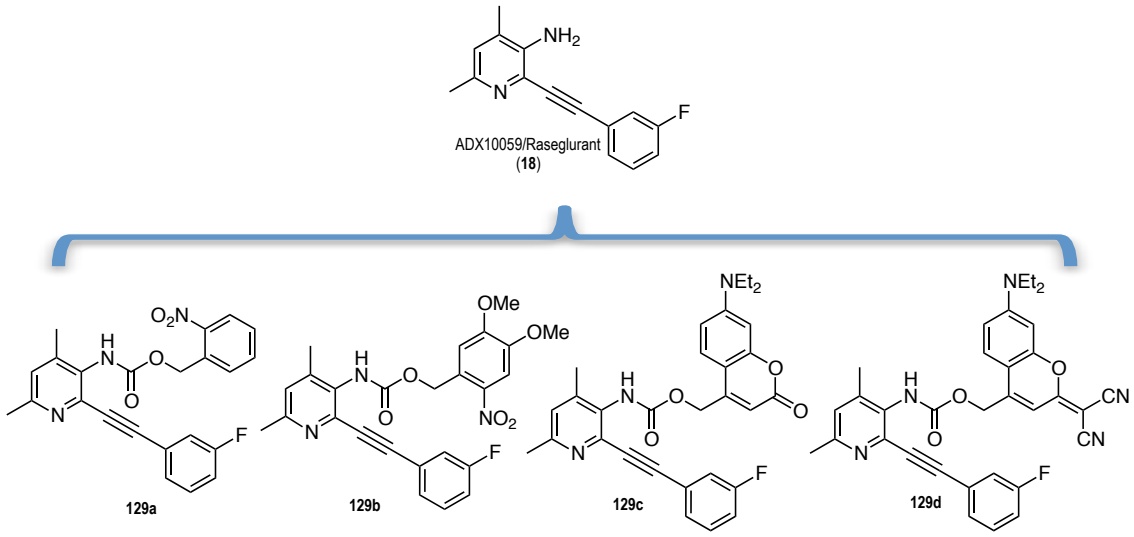

Figura35: Estructures dels compostos gàbia dissenyats basats en el NAM de $mGlu_5$ Raseglurant.

El Raseglurant (**18**) i els seus derivats (**129a-d**) es van sintetitzar tal i com es mostra en l'*Esquema 9*.

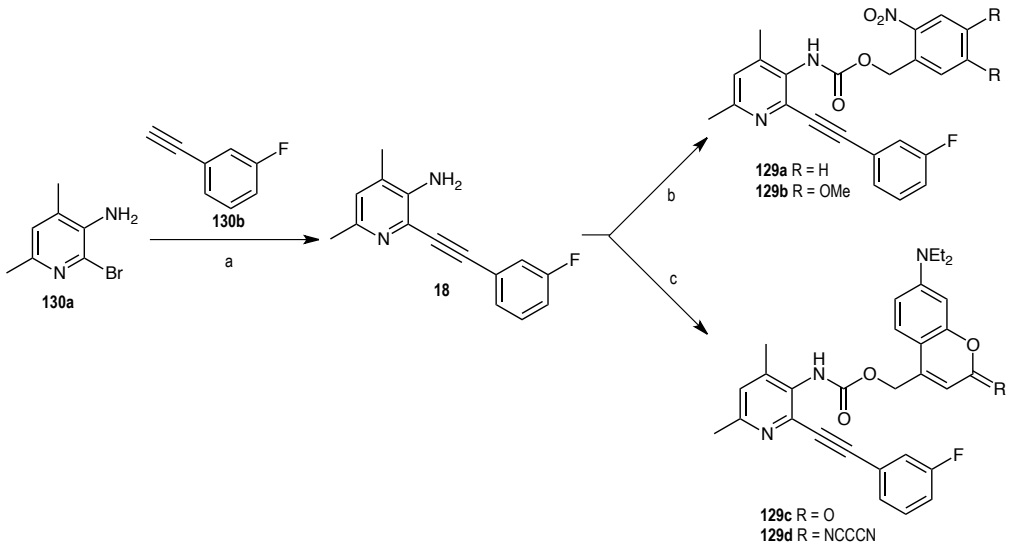

Esquema 9: Síntesis dels compostos **18**, **129a**, **129b**, **129c** i **129d**. a) $Pd(PPh_3)_2Cl_2$, CuI, NEt_3, DMF, 40ºC, 8h, 83%; b) **122a** or **122d**, triphosgene, NEt_3, toluene, 100ºC, 12 h, 70% for **129a** and 65% for **129b**; c) **128b** or **132**, triphosgene, NEt_3, NaH, toluene, THF, 90ºC, 12 h, 55% for **129c** and 20% for **129b**.

Tots els compostos varen ser caracteritzats fotoquímicament, mesurant primer els espectres d'absorció del raseglurant i dels respectius compostos gàbia (*Figura 36A*) i de l'alliberament a diferents temps de cadascun d'ells (*Figura 36B*).

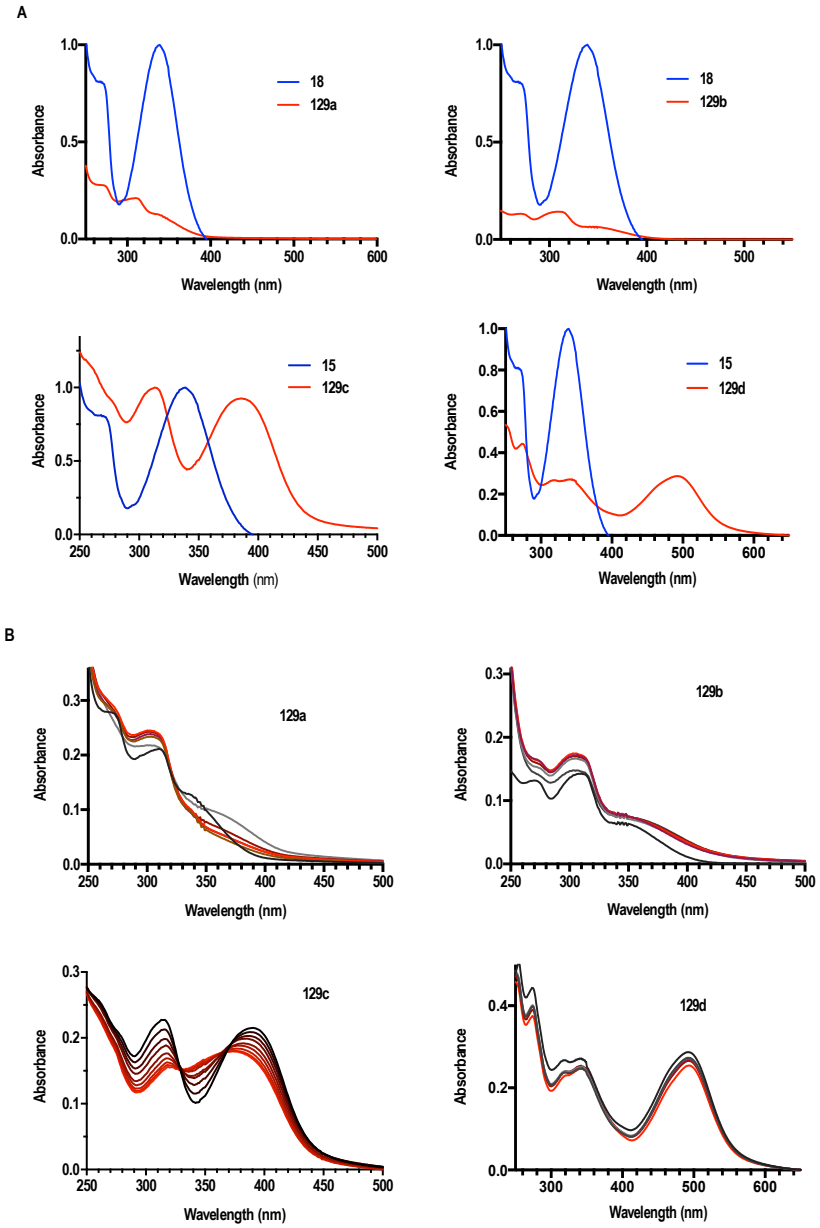

Figura36: Espectres UV-Vis del compostos gàbia **129a-d** i del raseglurant **18**. A) Espectra UV-Visible en condicions fosques dels compostos gàbia en comparació amb el Raseglurant. B) Alliberament a la longitud d'ona corresponent per cadascun dels compostos. La línia negre correspon en condicions fosques (sense irradiar) i les línies vermelles a diferents temps (*veure part experimental*)

Els compostos **129a** i **129b** varen tenir una absorció dins el UV profund (300-350 nm), així doncs aquests compostos quedaven exclosos per a aplicacions en sistemes vius. Contràriament, els compostos **129c** i **129d** van absorbir en rangs dels visible 390-405 nm (llum blava) i 480-490 nm (llum verda) respectivament.

Es van obtenir rendiments quàntics pobres per a quasi tots ells excepte per el compost **129c** el qual a la seva longitud d'ona es va registrar un rendiment quàntic del 0.18 (sobre 1).

A pesar d'aquests primers resultats on només es va obtenir un compost molt làbil, també es varen fer experiments preliminars d'alliberament també per HPLC en DMSO (*Figura 37*)irradiant els compostos en les seves corresponents longituds d'ona, excepte els dos compostos **129a** i **129b** que es varen irradiar a 405 nm degut a la perillositat de irradiar al UV.

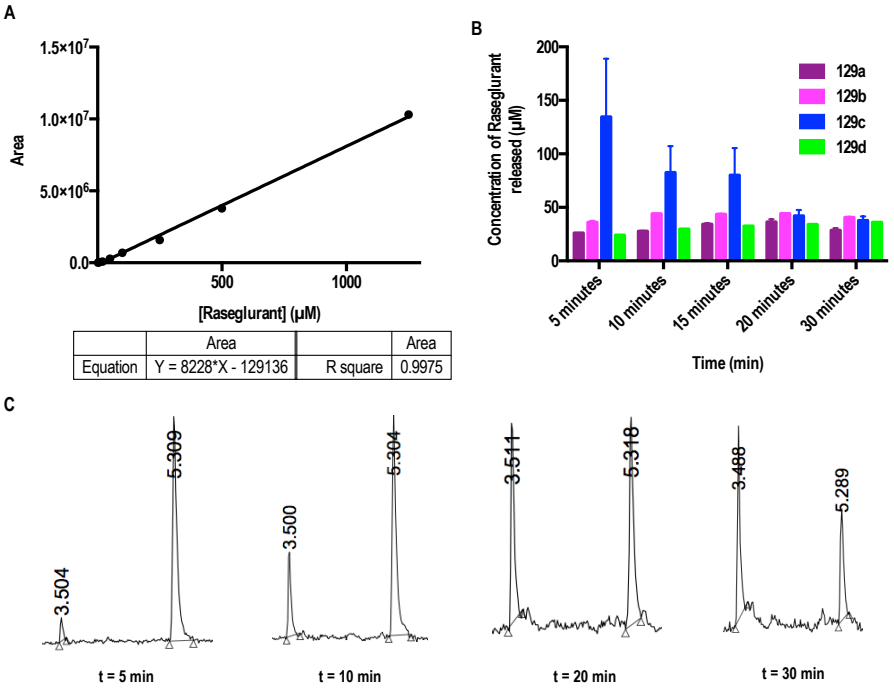

Figura 37: Experiments preliminars d'alliberament per HPLC. A) Recta de calibratge per quantificació de Raseglurant utilitzant dilucions creuades. B) Concentració de Raseglurant alliberat per cada compost gàbia a diferents temps de irradiació. Cada barra correspon a la mitjana de 2 replicats independents amb el corresponent SEM com barres d'error. C) Exemple del cromatograma de HPLC obtingut en l'alliberament del compost gàbia **129b** a 405 nm, filtrat per PDA a 380 nm (màxim d'absorció del Raseglurant), mostrant un temps de retenció de 3.50 pel Raseglurant i de 5.30 per el compost gàbia **129b**.

En els experiments preliminars es va poder observar un bon alliberament pel compost **129c** als 5 minuts com era d'esperar, degut al seu alt rendiment quàntic, en canvi va ser moderat per el compost **129d** i bastant pobre pels compostos amb màxim d'absorció al UV al ser irradiats a 405 nm.

Malgrat que els resultats estan en concordança amb els experiments inicials, sorprenentment vàrem observar una degradació de Raseglurant després de 5 minuts en el experiment corresponent al compost **129c** (a la *Figura 37B* es veu com disminueix la concentració de **18**

amb el temps). Això suposava un problema perquè el compost fos testat *in-vitro* o *in-vivo*. Vàrem pensar que un fet que podria haver promogut aquesta degradació era la utilització de DMSO com a dissolvent, i que poder amb condicions fisiològiques podria estabilitzar-se més degut al canvi de solvatació. Així doncs, es va assajar el compost en condicions fisiològiques amb un 1% de DMSO i una concentració de Raseglurant de 1 mM no observant-n'he més degradació (*Figura 38*).

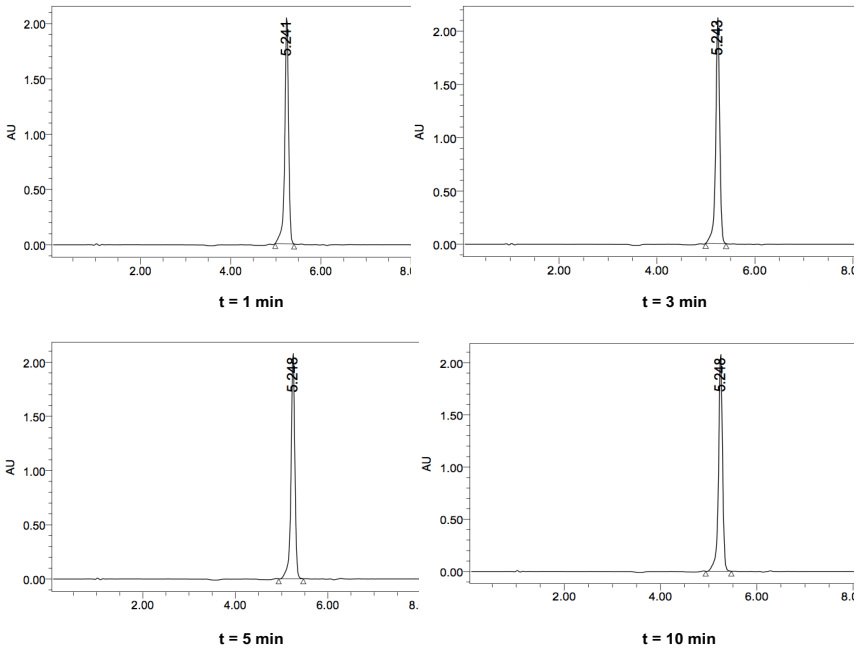

Figura 38: Cromatograma de HPLC després d'irradiar a diferents en condicions fisiològiques.

Així doncs, vàrem poder evitar la degradació del compost actiu canviant-n'he simplement el medi a l'hora de fer-n'he l'alliberament.

Després de la caracterització fotoquímica, es varen realitzar assajos de farmacologia amb experiments d'acumulació de IP-One. Primer de tot, degut a la degradació de Raseglurant abans esmentada, vàrem comprovar amb assajos de dosi-resposta irradiant-l'ho a 405 nm en DMSO i en medi fisiològic (*Figura 39*).

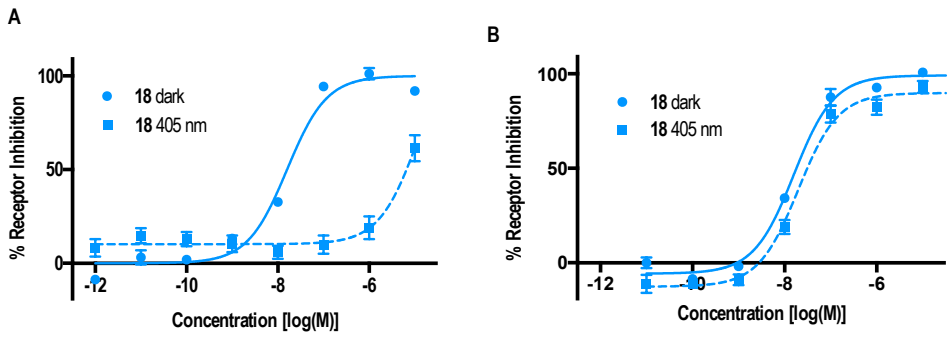

Figura 39: Activitat biològica del raseglurant sota irradiació en diferents medis durant 5 minuts. A) Il·luminació a 405 nm en condicions de DMSO. B) Il·luminació a 405 nm en condicions fisiològiques. Cada punt correspont a la mitjana del tres replicats independents amb les corresponent SEM com a barres d'error.

Un cop demostrat, que el nostre compost actiu sota les condicions apropiades (medi fisiològic) no degradava, vàrem realitzar assajos de dosi-resposta per tots els compostos gàbia dissenyats (*Figura 40*) en les mateixes condicions.

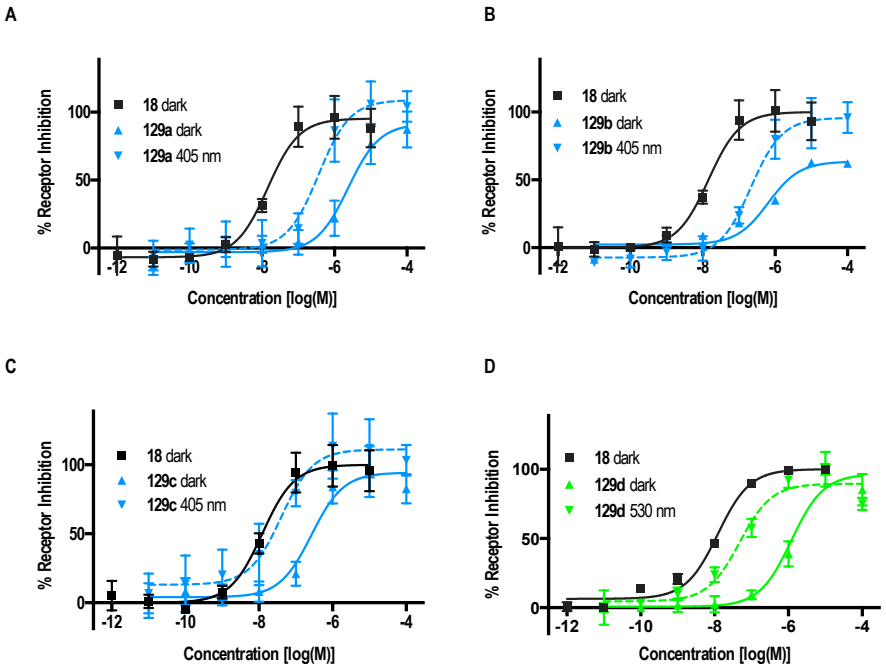

Figura 40: Corbes dosi-resposta d'alliberament de raseglurant per cadascun dels compostos gàbia amb assajos de IP-One en cèl·lules HEK293 sobrexpressant $mGlu_5$ amb concentració constant de quisqualat (**2**) 100 nM. Línies continues corresponen a les mostres incubades en condicions fosques i les línies discontinues a les mostres irradiades a 405 nm (blau) i 530 (verd). Cada punt correspon a la mitjana de mínim tres replicats independents amb la corresponen SEM com barres d'error.

Inesperadament, en tots els casos es va observar una activitat força important dels compostos gàbia, especialment pel compost més làbil **129c**, en el qual la seva activitat va ser només 10 cops menys potent que el Raseglurant. Això suposava un problema alhora de realitzar altres experiments i sobretot per a l'aplicació *in-vivo* d'aquest compost ja que, tal i com hem comentat abans, idealment el compost gàbia hauria de ser inactiu.

Malgrat els resultats obtinguts, ens va semblar molt poc probable que el compost gàbia tingués una activitat associada ja que el lloc d'unió en el $mGlu_5$ es un espai molt estret. Per això, vam decidir explorar altres possibles explicacions: O bé la coumarina **128b** sigues activa en $mGlu_5$, o

bé que es tractes, com ja es va observar en el capítol anterior, de efectes inespecífics, o bé que la puresa del nostre compost gàbia no fos l'adient i vingués acompanyat de petites quantitats de Raseglurant.

Per descarta les dues primeres opcions, vàrem assajar en les condicions anteriors per una banda la coumarina **128b** en condicions fosques i d'irradiació a 405 nm (*Figura 41A*), i per l'altre banda es va assajar el raseglurant, el compost gàbia **129c** i la coumarina **128b** en condicions fosques fent dosis-resposta en cèl·lules HEK293 sense sobrexpressió de $mGlu_5$ amb un plàsmid buit per veure'n els efectes inespecífics (*Figura 41B*).

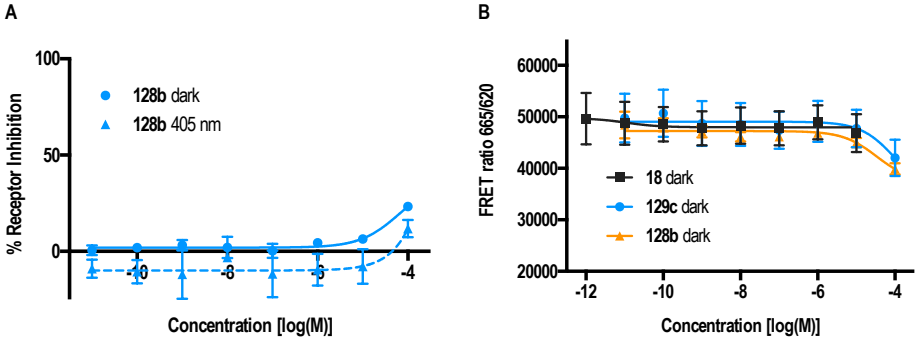

Figura 41: Corbes dosi-resposta d'alliberament de raseglurant per cadascun dels compostos gàbia amb assajos de IP-One. A) Amb cèl·lules HEK293 sobrexpressant $mGlu_5$ amb concentració constant de quisqualat (**2**) 100 nM. Línies continues corresponen a les mostres incubades en condicions fosques i les línies discontinues a les mostres irradiades a 405 nm (blau). B) Amb cèl·lules HEK293 sense sobrexpressió de $mGlu_5$ amb un plàsmid de DNA buit. Cada punt correspon a la mitjana de mínim tres replicats independents amb la corresponen SEM com barres d'error.

Com es va poder observar en la *Figura 41* no es va obtenir cap efecte per part del residu corresponent al alliberament del compost gàbia, i no es varen observar tampoc efectes inespecífics en cadascun dels compostos involucrats en el alliberament del compost.

Així doncs, descartades les dues primeres opcions, es va fer un anàlisis profund sobre la puresa del compost **129c**, mitjançant rectes de calibratge del raseglurant analitzat per HPLC-MS i mostres del compost. D'aquesta forma que el compost **129c** tenia com a impuresa prop de 1% de raseglurant. Aquest fet podia estar afectant als nostres assajos funcionals ja que el Raseglurant és molt potent. Així doncs es va fer una purificació del producte més exhaustiva fins a obtenir un 0.15% de raseglurant en la mostra per tenir una proporció de raseglurant 1000 cops menys que el compost **129c**.

Un cop purificat, vàrem tornar a repetir la dosi resposta pel compost gàbia **129c** obtenint aquest cop la inactivitat completa del compost gàbia (*Figura 42*).

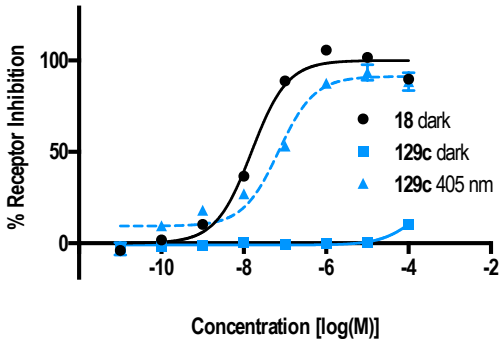

Figura 42: Dosi-resposta d'alliberament del compost **129c** purificat amb assajos de IP-One en cèl·lules HEK293 sobrexpressant $mGlu_5$ amb concentració constant de quisqualat (**2**) 100 nM. Línies continues corresponen a les mostres incubades en condicions fosques i les línies discontinues a les mostres irradiades a 405 nm (blau) i 530 (verd). Cada punt correspon a la mitjana de mínim tres replicats independents amb la corresponen SEM com barres d'error.

Seguidament es varen realitzar altres assajos d'activitat funcionals del compost **129c**, **18** i **128b** (*Figura 43*) com a PAM i NAM per a tots els receptors metabotropics del glutamat (del 1 al 8).

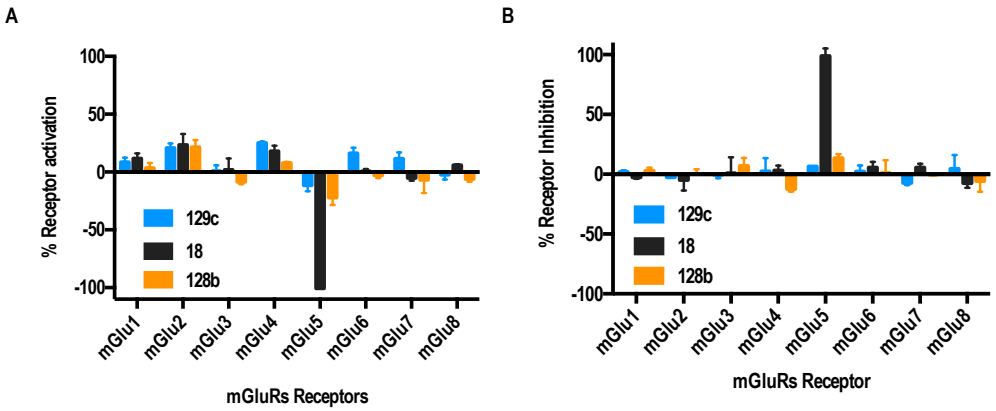

Figura 43: Activitat dels compostos **18**, **129c** i **128b** en tots els subtipus de mGlus com a PAM (A) i NAM (B) tot en condicions fosques. Dades normalitzades per l'activació del receptor respecte els PAMs i per l'inhibició respecte els NAMs d'una mitjana de mínim tres replicats independents, fets en duplicat amb la corresponent SEM com a barres d'error.

Aquests mostren que tant **129c** com **128b** són inactius en tots els receptors, i **18** és selectiu pel subtipus 5, tal i com estava descrit per la literatura.

Els bons resultats obtinguts en els assajos *in-vitro* ens van portar a evaluar el compost gàbia **129c** en dos models de dolor: model de lesió per constricció crònica (CCI) i test de formalina (*Figura 44A*).

La injecció sistèmica de raseglurant (10 mg/kg) incrementava el llindar del dolor en CCI sense tenir en compte la irradiació amb llum (*Figura 44B*). Contràriament, tal i com esperàvem la injecció sistèmica del **129c** (10 mg/kg) incrementava significativament el llindar del dolor en el CCI dels ratolins només després de la irradiació a 405 nm (*Figura 44B*).

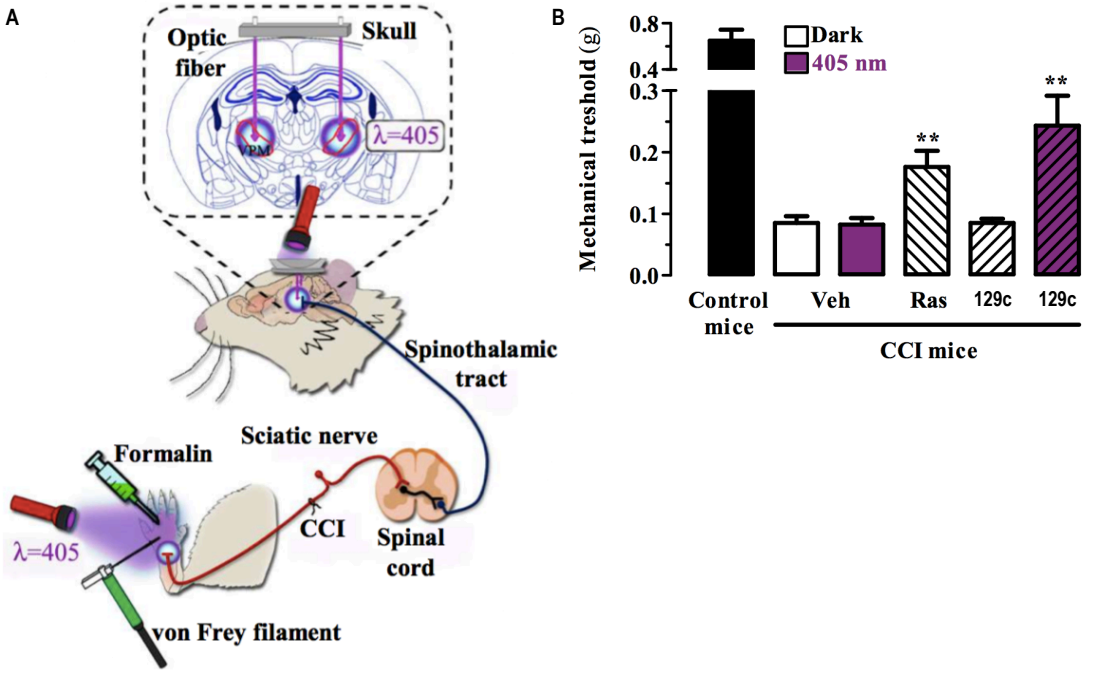

Figura 44: A) Esquema de inducció de lesió de constricció crònica (CCI) i sistema d'alliberament del fàrmac amb irradiació *in-vivo*. B) Llindar del dolor mecànic mitjançant filaments de von Frey amb ($P < 0.01$) de nivell de significació.

El test de formalina, els quals permet un anàlisis objectiu del dolor basats en un comportament de desconfort dels animals, esta constituït per una primera fase de dolor (5 minuts després de injecció de formalina) basat en el dolor inflamatori i una segona fase (20-30 minuts després de la injecció de formalina) basat en el dolor crònic i que en conjunt reflexa els desenvolupament de la sensibilitat central[19].

Així doncs, mentre el compost gàbia **129c** (10 mg/kg) no promovia l'efecte antinociceptiu en condicions fosques, en condicions d'irradiació a 405 nm es varen veure efectes antinociceptius notables en ambdós fases, 54±5% (fase I) i 34±5% (fase II) (*Figura 45A*) demostrant que el nostre compost gàbia podia ser foto-activat perifèricament.

També vàrem comprovar els efectes de **129c** alliberant amb llum aplicant-l'ho al tàlem. Mentre que el nostre compost (10 mg/kg) va ser inactiu en condicions basals, sota irradiació va causar analgèsia tant en fase I (45±9%) i en fase II (90±4%) en resposta al test de formalina (*Figura 45B).*

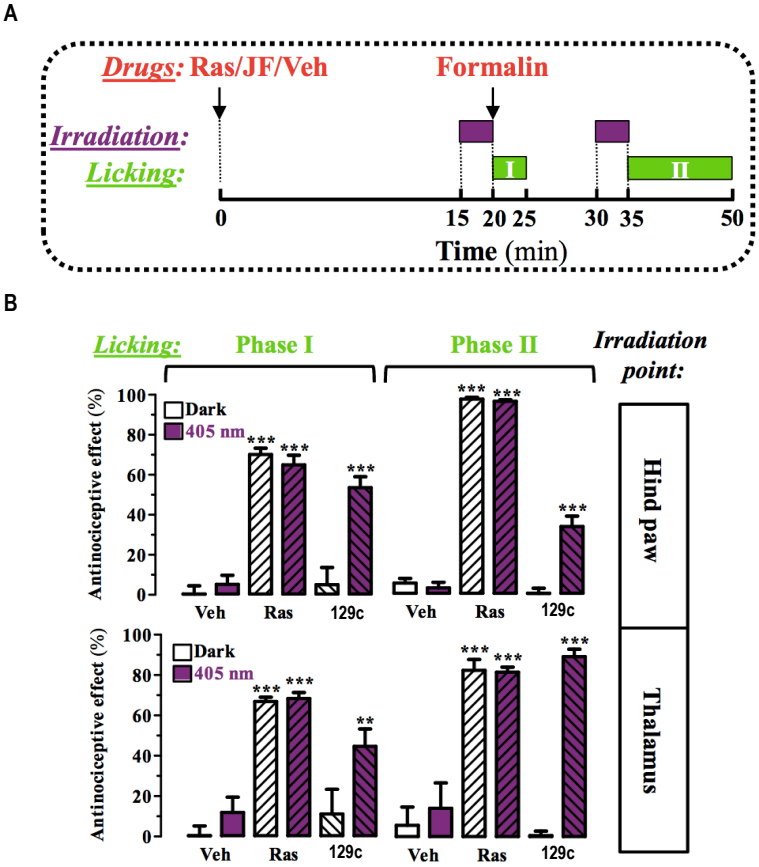

Figura 45: A) Esquema del test de formalina aplicat a nivell tant de sistema neviós perifèric com central. B) Normalitzat del efecte antinoceptiu calculat per el temps de llepada dels ratolins amb ($P < 0.001$) de nivell de significació.

Els bons resultats obtinguts amb el compost **129c** ens varen fer intentar validar l'aproximació amb altres subtipus de mGlus com el $mGlu_1$ o $mGlu_4$ que estan presents a la post sinapsis i presinàptiques respectivament i que estan involucrats en el tractament del dolor.

Respecte el NAM de $mGlu_1$ vàrem optar per el compost YM298198 (**15**) degut a que aquest cop no contenia el grup acetilè amb tendència a poder ser degradat per la llum i per l'anilina que pot ser fàcilment modificada (*Figura 46*).

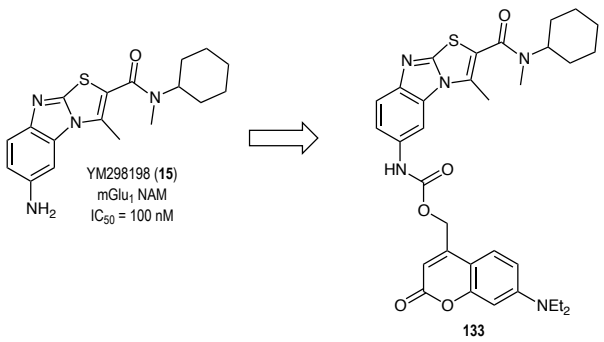

Figura 46: Estructures químiques de YM298198 i el disseny del seu respectiu compost gàbia **133**.

Respecte el compost dissenyat per $mGlu_4$, es va optar per un compost assumint la mateixes condicions buscades per el NAM de $mGlu_1$ dissenyat abans, escollint el compost referència TCN-22A (**134**) (*Figura 47*).

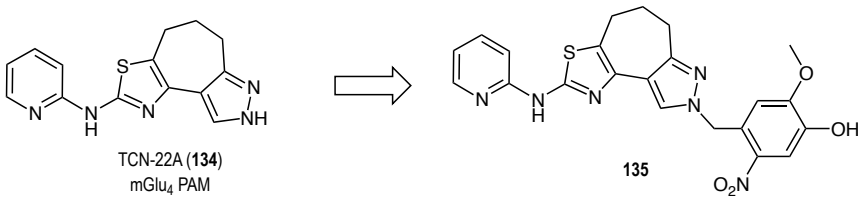

Figura 47: Estructures químiques de TCN-22A i el disseny del seu respectiu compost gàbia **135**

Així doncs, el compost gàbia **133** es va sintetitzar seguint l'estratègia sintètica mostrada en l'*esquema 14*.

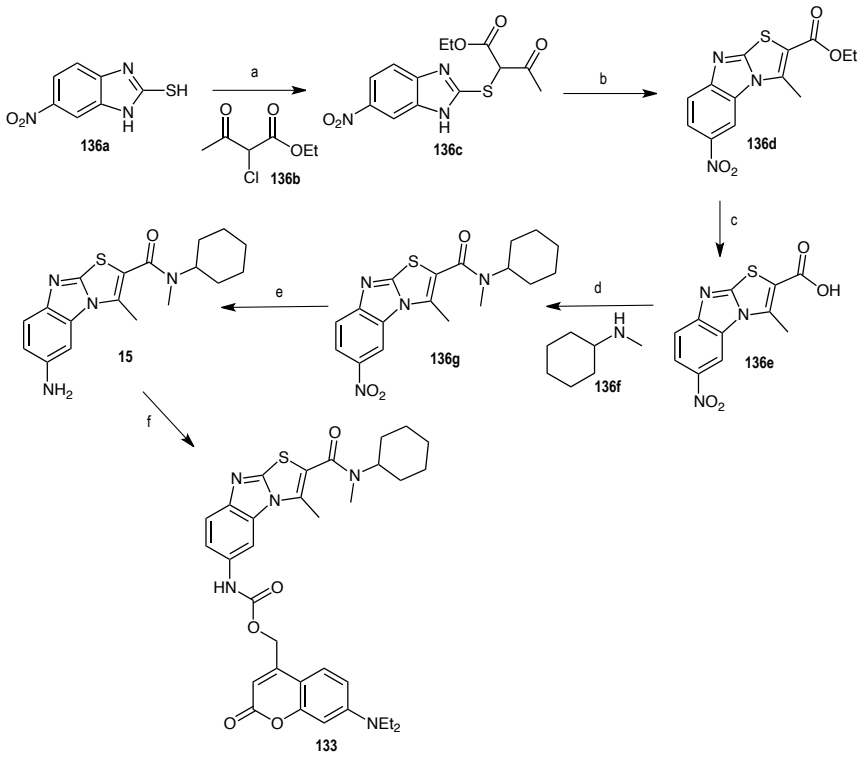

Esquema 14: Sintesis dels compostos **133** i **15**. Reactius i condicions: a) KOH, EtOH, 80ºC, 18h; b) Pyridine/Acetic anhydride 3:1, 100ºC, 3 h, 40% (over two steps a and b); c) NaOH, EtOH/Dioxane 1:1, r.t., 6 h, 94%; d) Tionyl chloride, DCM, r.t., overnight, 21%; e) $Na_2S_2O_3$, HCl, THF/MeOH 1:1, r.t., 39%; f) **128b**, triphosgene, NaH, toluene, THF, 100ºC, overnight, 10%.

El compost gàbia **135** va ser sintetitzat seguint l'estratègia sintètica mostrada en l'*esquema 15*.

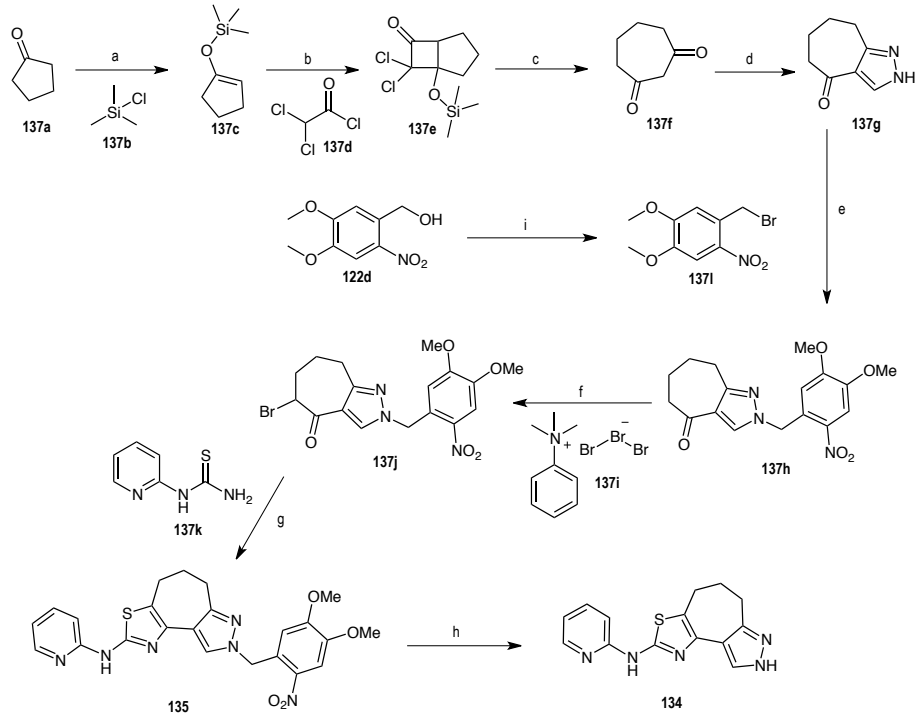

Esquema 15: Síntesi dels compostos **134** i **135**. Reactius i condicions: a) NaI, NEt_3, can, r.t., overnight, 56%; b) NEt_3, Hexane, r.t., 18 h, 80%; c) 2-propanol, water, Zn, AcOH, -10ºC, 30 min, 96%; d) DMF-DMA, Hydrazine, 0ºC, 1 hour, 46%; e) K_2CO_3, can, 60ºC, 3 days, 30%; f) DCM, reflux, 1.5 h, 98%; g) EtOH, reflux, overnight, 70%; h) TFA, MW, 30 min, 100ºC, 84%; i) PBr_3, DCM, reflux, 3 h, 62%.

Un cop sintetitzats els compostos gàbia desitjats, es va tornar a mesurar el seus màxims d'absorció en comparació al seu compost actiu (*Figura 48A*) i l'alliberament a diferents temps seguit per espectre de UV-Vis (*Figura 48B*) per calcular els paràmetres fotoquímics (*taula 9, part experimental*).

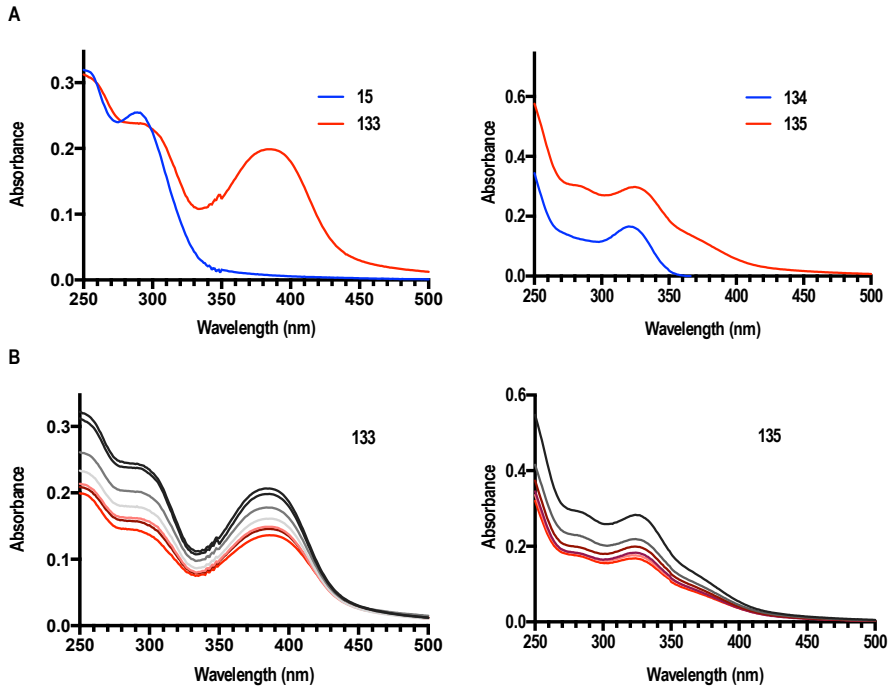

Figura 48: Espectres UV-Vis pels compostos gàbia **133** i **135**. A) Espectra UV-Vis sense irradiació de cada compost gàbia en comparació amb el compost actiu corresponent. B) L'alliberament a la longitud d'ona corresponent de cada compost gàbia a diferents temps. La línia negre correspon en condicions fosques (sense irradiar) i les línies vermelles a diferents temps (*veure part experimental*)

Com era d'esperar, el compost **133** va enregistrar un màxim d'absorció molt similar al compost **129c** ja que està unit a la mateixa coumarina DEACM **128b**, la qual promou una absorció prop del rang del blau. Tot i així, aquest cop el seu rendiment quàntic no va ser l'esperat sent 5 cops menys làbil que el compost **129c** (*Taula 9, part experimental*). Per una altre banda, el compost gàbia **135** va mostrar el seu màxim al UV però mantenia certa absorció a 405 nm. Per aquest

motiu es va poder irradiar aquesta longitud d'ona alhora de fer-n'he l'alliberament però òbviament rendiments d'alliberament pobres.

Un cop van ser caracteritzats fotoquímicament, malgrat els seus pobres resultats, es van caracteritzar farmacològicament de la mateixa manera que es van realitzar els assajos de IP-One pels compostos gàbia del raseglurant. Aquest cop les cèl·lules HEK293 sobrexpressaven el corresponent receptor per cadascun dels compostos ($mGlu_1$ per **133** i $mGlu_4$ per **135**) il·luminant ambdós a 405 nm (*Figura 49*) en els dos casos.

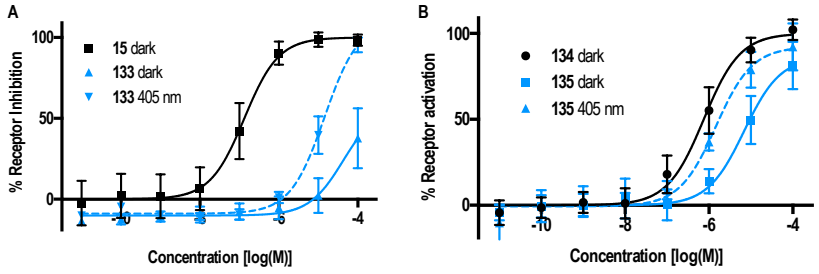

Figura 49: Dosi-resposta d'alliberament del compost **133** i **135** amb assajos de IP-One amb irradiació de 5 minuts. A) Amb cèl·lules HEK293 sobrexpressant $mGlu_1$ amb concentració constant de quisqualat (**2**) 100 nM. B) Amb cèl·lules HEK293 sobrexpressant $mGlu_4$ amb concentració constant de L-AP_4 (**4**) 3 nM Línies continues corresponen a les mostres incubades en condicions fosques i les línies discontinues a les mostres irradiades a 405 nm (blau). Cada punt correspon a la mitjana de mínim tres replicats independents amb la corresponen SEM com barres d'error.

El compost **133** va resultar ser un bon compost gàbia degut a la seva inactivitat abans de ser activat mitjançant irradiació. Com hem comentat el caracterització fotoquímica, degut al seu poc rendiment quàntic podem observar que no es va poder assolir l'activitat respecte al compost actiu **15**, no obstant, el compost pot ser objecte d'estudis de comportament en sistemes vius com rates però amb irradiacions selectives a altres zones del cervell amb expressió alta de $mGlu_1$.

En canvi, el compost gàbia **135** va presentar una activitat sense irradiació quan idealment hauria de ser inactiu. Això podia ser degut a un error en el disseny, on el nitrobenzil unit al pirazol podia no estar molestant suficient per fer-ne caure completament l'activitat. Un bon disseny alternatiu a ser considerat podria ser la unió d'aquest grup a l'amina pont entre el tiazol i la piridina obstruint-ne l'entrada al lloc d'unió.

Alternativament als receptors metabotròpics del glutamat, altres GPCRs són presents al llarg del sistema nerviós central i perifèric. Un dels receptors més comuns i estudiats de la família de rodopsina (classe A), són els receptors μ-opiods, pels quals la morfina és el lligant més conegut actuant en aquest receptor per el tractament del dolor tant crònic com inflamatori.

El gran problema d'aquest fàrmac són els seu efectes secundaris altament coneguts com per exemple la disminució de pressió sanguínia i d'esforç respiratòria, l'addicció, o vòmits.

Així doncs, pot ser una bon compost a engabiar, per tal de prevenir tots aquests efectes secundaris.

En aquest cas, l'estructura química presentava dos grups funcionals (fenol i alcohol al·lílic) on es podien unir amb compostos fotolàbils. No obstant, Thompson i col·laboradors[20], varen estudiar les diferents activitats biològiques de la morfina i els seus derivats, i van comprovar que l'única modificació estructural que feia decaure'n l'activitat quasi bé 100 cops, era la substitució en el fenol.

Davant d'aquestes evidències, es va voler modificar aquest grup amb la coumarina utilitzada anteriorment **128b**, tot i que en aquest cas, la generació de un carbonat podia arribar a ser un problema alhora de la metabolització o l'estabilitat d'aquest en condicions fisiològiques. Això va fer que ens plantegessin la unió directe entre l'enllaç oxigen-carboni, on fotoquímicament podia presentar més problemes d'alliberament però podíem evitar-n'he tots aquests problemes (*Figura 50).*

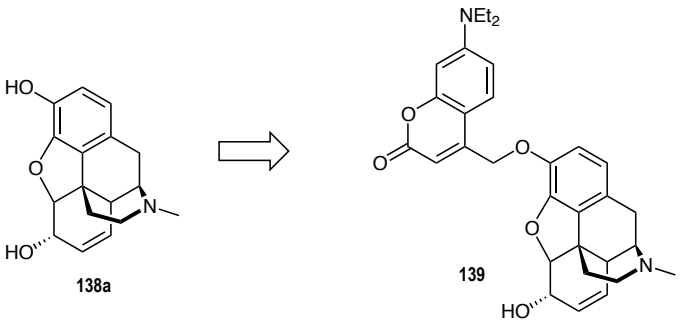

Figura 50: Disseny estructural de la morfina gàbia **139**.

Així doncs, es va sintetitzar el compost gàbia **139** fàcilment en dues etapes com es mostra en l'*esquema 16*. La Morfina va ser alquilada amb la coumarina **140** prèviament sintetitzada a partir de la coumarina **128b** (etapa b), per obtenir **139** com sal d'hidroclorur.

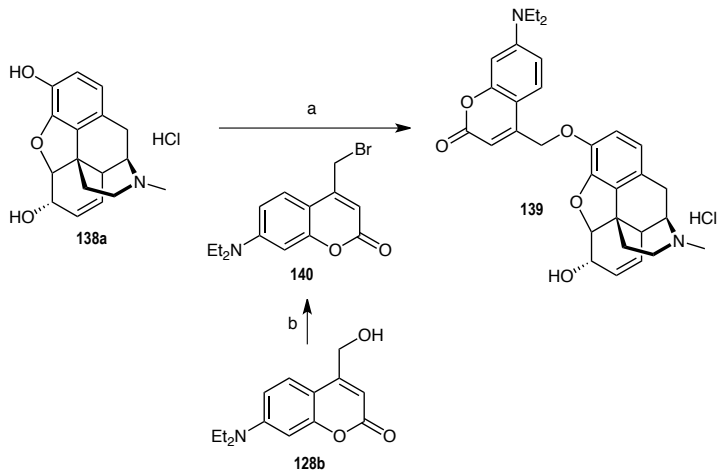

Esquema 16: Síntesi del compost **139**. Reactius i condicions: a) K_2CO_3, DMF, r.t., 4 days, 47%; b) NEt_3, MsCl, LiBr, DCM, THF, r.t., 3 h, 44%.

Un cop es va obtenir el compost gàbia **139**, es van realitzar els experiments de fotoquímica prèviament descrits per els altres compostos gàbia, obtenint primer el espectre sense irradiar de **139** en comparació amb la morfina, i després enregistrant-n'he els espectres de UV-Vis d'alliberament a diferents temps i calculant-n'he els paràmetres fotoquímics.

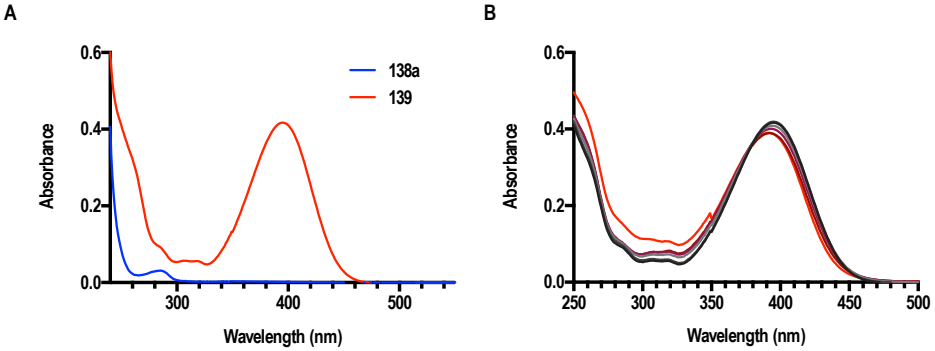

Figura 51: A) Espectre UV-Vis sense irradiació i en comparació a la morfina. B) Alliberament a diferents temps del compost gàbia **139**. La línia negre correspon en condicions fosques (sense irradiar) i les línies vermelles a diferents temps (*veure part experimental*)

Tot i que l'alliberament no va ser molt bo, probablement degut aquesta unió entre la coumarina **128b** i la morfina, es va obtenir rendiments quàntics de 0.03 observant també un desplaçament en el espectre de UV-Vis.

Considerant aquest pobre alliberament es va voler verificar per HPLC la quantitat obtinguda de morfina durant el temps (*Figura 52*).

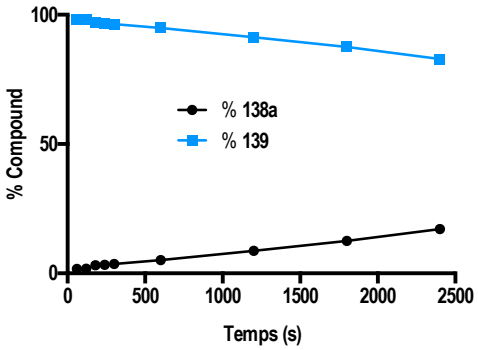

Figura 52: % de compostos **138a** i **139** després de l'alliberació a diferents temps.

Com era d'esperar, l'alliberament va ser molt lent i en els primers 60 segons només vàrem observar un 1.7% de Morfina.

La pobre alliberació pot ser interesant en la aplicabilitat d'aquesta molècula gàbia per obtenir-n'he un efecte notable evitant tots els efectes no desitjats descrits anteriorment.

Aquest compost serà objecte d'estudi en assajos biològics futurs, sobretot en aplicacions perifèriques del sistema nerviós.

Conclusions

S'han sintetitzat diferents compostos gàbies com a NAM de $mGlu_1$ (**133**) utilitzant **15** i DEACM (**128b**), com a NAMs de $mGlu_5$ utilitzant Raseglurant (**18**) amb **122a** (**129a**), **122d** (**129b**), DEACM (**129c**) i **132** (**129d**). També es va sintetitzar com a PAM de $mGlu_4$ (**135**) utilitzant **134** i **137I**. A més, es va sintetitzar un compost gàbia de morfina utilitzant DEACM (**128b**) com agonista per a receptors μ-opiod.

Els compostos gàbia va ser caracteritzats fotoquímicament determinant-ne els rendiments quàntics 0.03 per **133**, 0.032 per **129a**, 0.005 **129b**, 0.063 per **129d**, 0.034 de **135** i 0.035 per **139**. El compost **129c** va resultar ser el més efectiu obtenint un rendiment quàntic de 0.18.

Tots els compostos varen ser caracteritzats farmacològicament emprant assajos de IP-One per a cada receptor, sent inactius per a gairebé tots els compostos en forma de gàbia, excepte pel compost **135** que va tenir activitat com a PAM de $mGlu_4$. Després d'irradiar a la corresponent longitud d'ona compatibles amb els experiments biològics, vàrem obtenir activitat associada al alliberament del compost actiu. De nou, el compost **129c** va presentar la millor efectivitat obtenint la mateixa activitat que el raseglurant.

El compost **129c** va ser assajat *in-vivo* en models de dolor agut, crònic i neuropàtic en ratolins. Els resultats obtinguts varen mostrar un efecte analgèsic dependent de il·luminació en teixits rellevants per a la transmissió del dolor i que contenen receptors de $mGlu_5$, mentre que no es va obtenir efecte il·luminant teixits contenint receptors de $mGlu_5$ però sense estar involucrats en la transmissió del dolor.

Bibliografia

1. Rondard, P.; Goudet, C.; Kniazeff, J.; Pin, J. P.; Prezeau, L., The complexity of their activation mechanism opens new possibilities for the modulation of mGlu and GABAB class C G protein-coupled receptors. *Neuropharmacology* **2011,** *60* (1), 82-92.
2. Pin, J. P.; De Colle, C.; Bessis, A. S.; Acher, F., New perspectives for the development of selective metabotropic glutamate receptor ligands. *European journal of pharmacology* **1999,** *375* (1-3), 277-94.
3. Nicoletti, F.; Bockaert, J.; Collingridge, G. L.; Conn, P. J.; Ferraguti, F.; Schoepp, D. D.; Wroblewski, J. T.; Pin, J. P., Metabotropic glutamate receptors: from the workbench to the bedside. *Neuropharmacology* **2011,** *60* (7-8), 1017-41.
4. Santacana, X. G. Design, synthesis and characterisation of photoswitchable allosteric modullators of metabotropic glutamate receptors. Universitat de Barcelona, 2016.
5. Neugebauer, V.; Chen, P. S.; Willis, W. D., Role of metabotropic glutamate receptor subtype mGluR1 in brief nociception and central sensitization of primate STT cells. *Journal of neurophysiology* **1999,** *82* (1), 272-82.
6. Cavallone, L., Fenobam on Heat/Capsaicin Induced Hyperalgesia in Healthy Volunteers.
7. Spooren, W.; Gasparini, F., mGlu5 receptor antagonists: a novel class of anxiolytics? *Drug news & perspectives* **2004,** *17* (4), 251-7.
8. Homayoun, H.; Stefani, M. R.; Adams, B. W.; Tamagan, G. D.; Moghaddam, B., Functional Interaction Between NMDA and mGlu5 Receptors: Effects on Working Memory, Instrumental Learning, Motor Behaviors, and Dopamine Release. *Neuropsychopharmacology : official publication of the American College of Neuropsychopharmacology* **2004,** *29* (7), 1259-69.
9. Doherty, J. J.; Alagarsamy, S.; Bough, K. J.; Conn, P. J.; Dingledine, R.; Mott, D. D., Metabotropic glutamate receptors modulate feedback inhibition in a developmentally regulated manner in rat dentate gyrus. *The Journal of physiology* **2004,** *561* (Pt 2), 395-401.
10. Nicoletti, F.; Bruno, V.; Copani, A.; Casabona, G.; Knopfel, T., Metabotropic glutamate receptors: a new target for the therapy of neurodegenerative disorders? *Trends in neurosciences* **1996,** *19* (7), 267-71.
11. Macinnes, N.; Duty, S., Group III metabotropic glutamate receptors act as hetero-receptors modulating evoked GABA release in the globus pallidus in vivo. *European journal of pharmacology* **2008,** *580* (1-2), 95-9.

12. Kramer, R. H.; Mourot, A.; Adesnik, H., Optogenetic pharmacology for control of native neuronal signaling proteins. *Nature neuroscience* **2013,** *16* (7), 816-23.

13. East, S. P.; Bamford, S.; Dietz, M. G.; Eickmeier, C.; Flegg, A.; Ferger, B.; Gemkow, M. J.; Heilker, R.; Hengerer, B.; Kotey, A.; Loke, P.; Schanzle, G.; Schubert, H. D.; Scott, J.; Whittaker, M.; Williams, M.; Zawadzki, P.; Gerlach, K., An orally bioavailable positive allosteric modulator of the mGlu4 receptor with efficacy in an animal model of motor dysfunction. *Bioorganic & medicinal chemistry letters* **2010,** *20* (16), 4901-5.

14. Pittolo, S.; Gomez-Santacana, X.; Eckelt, K.; Rovira, X.; Dalton, J.; Goudet, C.; Pin, J. P.; Llobet, A.; Giraldo, J.; Llebaria, A.; Gorostiza, P., An allosteric modulator to control endogenous G protein-coupled receptors with light. **2014,** *10* (10), 813-5.

15. Engers, D. W.; Field, J. R.; Le, U.; Zhou, Y.; Bolinger, J. D.; Zamorano, R.; Blobaum, A. L.; Jones, C. K.; Jadhav, S.; Weaver, C. D.; Conn, P. J.; Lindsley, C. W.; Niswender, C. M.; Hopkins, C. R., Discovery, synthesis, and structure-activity relationship development of a series of N-(4-acetamido)phenylpicolinamides as positive allosteric modulators of metabotropic glutamate receptor 4 (mGlu(4)) with CNS exposure in rats. *Journal of medicinal chemistry* **2011,** *54* (4), 1106-10.

16. Adams, S. R.; Tsien, R. Y., Controlling cell chemistry with caged compounds. *Annual review of physiology* **1993,** *55*, 755-84.

17. Maurice Goeldner, R. G., *Dynamic Studies in Biology*. WILEY-VCH: 2005.

18. Bort, G.; Gallavardin, T.; Ogden, D.; Dalko, P. I., From one-photon to two-photon probes: "caged" compounds, actuators, and photoswitches. *Angewandte Chemie (International ed. in English)* **2013,** *52* (17), 4526-37.

19. Mogil, J. S., Animal models of pain: progress and challenges. *Nature reviews. Neuroscience* **2009,** *10* (4), 283-94.

20. Thompson, C. M.; Wojno, H.; Greiner, E.; May, E. L.; Rice, K. C.; Selley, D. E., Activation of G-proteins by morphine and codeine congeners: insights to the relevance of O- and N-demethylated metabolites at mu- and delta-opioid receptors. *The Journal of pharmacology and experimental therapeutics* **2004,** *308* (2), 547-54.